Final Report MoM-Liner Group 10

V. Badal	4458605
Q. Booster	4358023
J. De Bont	4268598
M. Korzelius	4304578
N. Suard	4490932
G. Van Dekken	4447425
T. Van den Berg	4441354
D. Van der Horst	4464540
N. Wahler	4446976

Project Duration: April 23, 2018 – July 5, 2018

Tutors:

Dr. S. Hartjes	TU Delft, supervisor
S. Tambe	TU Delft
R. Li	TU Delft

July 3, 2018

Version 2.0

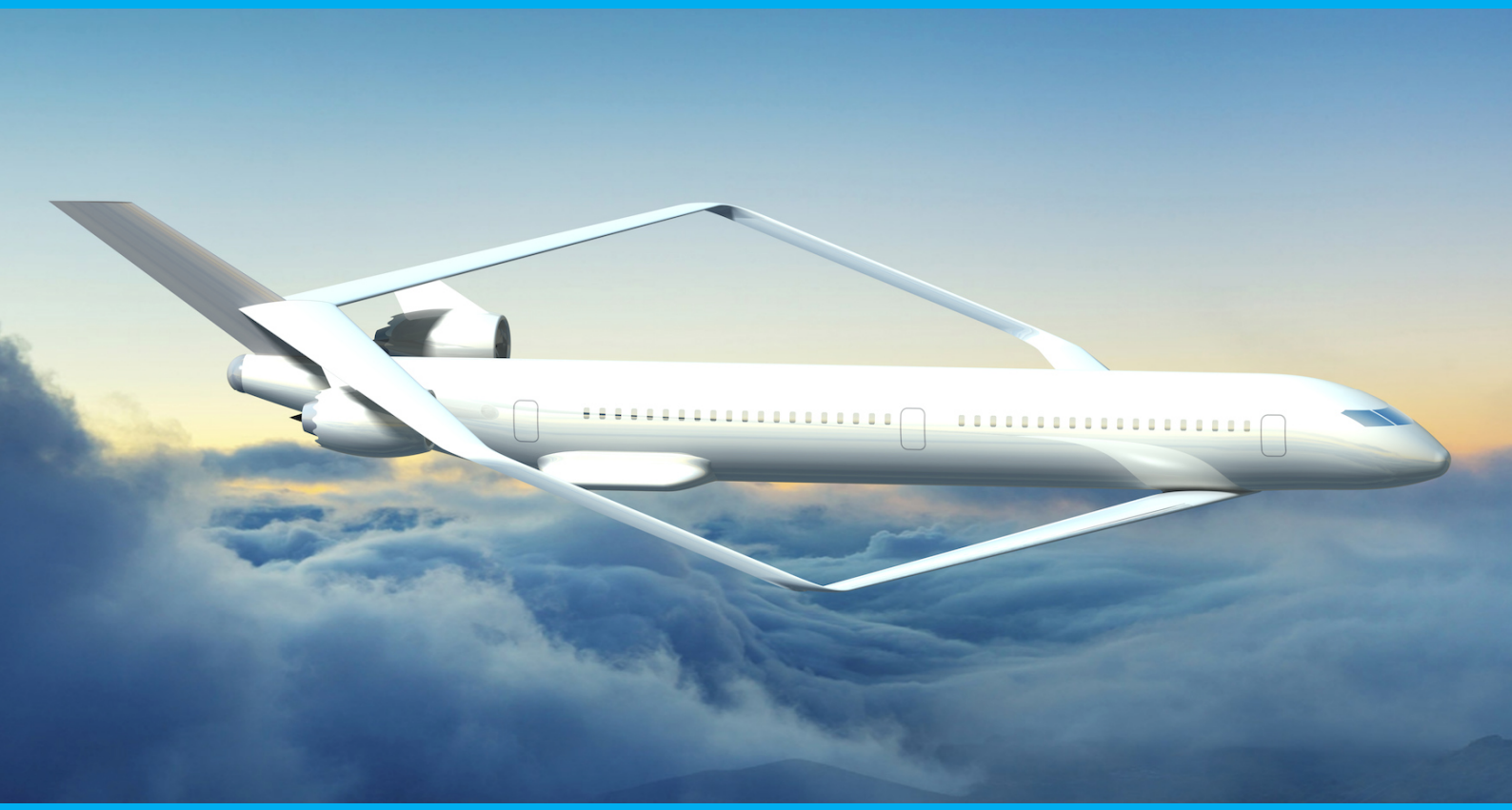

TU Delft

MoM Liner

Executive Overview

Project Objectives

A middle-of-the-market jet will be designed to fill the growing gap in the aviation market. This aircraft will be designed by nine students in ten weeks.

Market Analysis

A market analysis was performed to predict the potential future MoM-liner sales. Two potential functions of the MoM-liner were analyzed: replacing the current fleet and filling the market gap. Considering replacing the current fleet, the Boeing 757-200, 767-200 and Airbus A310 were identified as aircraft which could possibly be replaced by the MoM-liner. Of these aircraft there are currently 756 in service. The current development of smaller jets operating in the middle-of-the-market range also indicate that airlines are very interested in smaller, long range aircraft: Of the Boeing 737 MAX 10, B787-8 and Airbus A321neo 2756 orders are placed already.

In order to get a better insight into the potential MoM-liner operators, airline business strategy drivers were analyzed. A further analysis of the market gap showed that there is a strong case for developing a new aircraft in the 5,000-6,000 NM range. The smaller passenger number of the MoM-liner allows airlines to operate more flights on a particular route rather than flying one larger aircraft. This way airliners can offer their passengers more flexibility. Research of Low-Cost Carriers showed that there is also a strong demand for cheap and efficient aircraft capable of operating on long-haul routes under these type of airlines. Additionally, the MoM-liner can play a role in the transition from the Hub-and-Spoke model to a Point-to-Point model.

Finally, a market share estimation was performed. This is necessary to estimate the unit cost of the aircraft. It is estimated that 50% of the current legacy MoM-liner fleet will be replaced by the new MoM-liner. This equates to approximately 380 aircraft. In the Low-Cost Long-Haul market, it is estimated that 240 units of the MoM-liner will be ordered. An additional 200 aircraft are expected to be ordered by some major global carriers to be used as Point-to-Point aircraft. To summarize, in total 820 units of the MoM-liner are expected to be ordered.

Requirement Analysis

Before the final design of the MoM-liner was started, the system requirements were analyzed. The identified user requirements, which will supposedly have a high impact on the final design have been identified and documented. Also, additional requirements were obtained using a requirements discovery tree. The requirements were assigned with a priority index, indicating the impact of the requirement on the design. Finally, the function of the MoM-liner system was analyzed using a functional flow diagram. This diagram, together with the functional breakdown can be found in section 4.2.

Preliminary Design

From a previously conducted baseline research three distinct aircraft concepts were defined: A Box wing aircraft, a strut-braced high wing aircraft and an optimized conventional aircraft. These design options were analyzed and designed in further detail. Afterwards, an extensive trade-off was performed. The trade-off criteria considered were: Maintainability, performance, ground operations, sustainability, cost, comfort and risk. During the trade-off it was recognized that the most optimal design would be a hybrid between the box wing and the conventional configuration. The final hybrid design uses the wing configuration of the box wing aircraft with high bypass ratio turbofans.

Preliminary Sizing Methodology

As a first step in the preliminary sizing of the MoM-liner, a class-I weight estimation was performed. The class-I weight estimation is mainly based on an initial guess of the MTOW and the mission profile of the aircraft. The output of the class-I weight estimation was subsequently used in a class-II weight estimation. As the class-II weight estimation is only valid for conventional aircraft, a factor was obtained for both the fuselage and wing structure.

This allowed the MoM-liner design team to estimate the weight of the box wing configuration MoM-liner with a sufficient degree of accuracy. After the initial weight estimation was performed, the design space diagram was generated. From this diagram, the wing surface area and thrust were deduced. The design space diagram was generated by sizing the aircraft for the following criteria: Stall speed, take-off, landing distance, climb rate, climb gradient and cruise speed.

Aerodynamic Analysis

After the preliminary sizing of the aircraft, detailed design was started. The aerodynamic analysis was performed using Tornado Vortex Lattice Methods (VLM) software. The objective of the aerodynamic analysis was to obtain the most optimal aerodynamic design. This was done by designing for minimum cruise drag, thus optimizing for $\left(\frac{L}{D}\right)_{cruise}$.

The lift of the MoM-liner can be accurately calculated using the assumption of inviscid flow by using the Kutta condition at the trailing edge. The drag, however, cannot be calculated this way. The drag is calculated by taking into account viscosity, which causes drag through the following two mechanisms: Introducing skin-friction drag due to shear acting on the wing surface and introducing pressure drag due to flow separation. As the Tornado VLM uses techniques which doesn't estimate the drag properly, additional measures were taken to get a more accurate drag estimation. Also, some drag components, such as the interference drag, are hard to estimate. One can account for this drag component by applying the component drag build-up method, which takes into account the pressure-, skin-friction-, fuselage-, wing-, tail- and pylon drag.

Having done an analysis of all drag components acting on the aircraft, the general wing planform design could be set-up. In the general planform design, a value was set for the sweep angle, dihedral and taper. The value for sweep was obtained using the drag divergence Mach number, which was set 0.03 above the cruise Mach number. A value of 33 degrees was obtained. The dihedral was estimated using a method from Raymer [1]. Raymer recommends starting off with a default dihedral of 3 degrees, then remove 1 degree per 10 degrees sweep, and lastly add 2 degrees for low-mounted wings or remove 2 degrees for top-mounted wings. Using this method a dihedral of 2 degrees is obtained for the front wing, and an anhedral of -2 degrees is obtained for the aft wing. For the taper a program was written to compute the most optimal value for $\frac{L}{D}$. An optimization was performed, using the method of steepest descent. The method was said to have converged if the change in $\frac{L}{D}$ between two iterations is less than 0.01 or if the taper ratio drops below 0.2 as the wing would not be structurally sound anymore. Using the optimization, a taper ratio of 0.433 was obtained.

The airfoil profile was selected prior to the optimization of the design. The selection was done using a method described in Gudmundsson, which defined a set of characteristics such as the thickness ratio, C_L at 0 angle of attack, $C_{L_{max}}$ and $C_{D_{min}}$. The resulting airfoil profile selected is the NASA SSC(2)-1010.

Structural Analysis

In the preliminary design of the MoM-liner, a structural analysis was performed for the fuselage- and wing structure. Both the fuselage and wing were modeled using the principle of structural idealization. The structural analysis method states that all stringers are replaced by booms. The remaining skin is lumped into the boom areas. The skin in between booms if made zero thickness. Main assumptions of the structural idealization method are that the booms carry only normal stress, while the skin is only effective in carrying shear. The fuselage was modeled as an elliptical cylinder with a floor just below the horizontal symmetry line and a fixed stringer and frame spacing. The nose and tail cone are not considered. For the wing, only the wing box structure was analyzed. It was assumed that the vertical connection between the front and rear wing is unloaded. This assumption was deemed valid after consulting experts in the field of Prandtl plane designs.

Analyzing the load case of a structure is a very important aspect when performing a structural analysis. For both the wing and the fuselage the most critical load case was determined to be a 2.5g maneuver. For the fuselage, the loading diagram was obtained by modelling the structure as two cantilever beams. This was necessary because modeling the structure as one beam would make the problem indeterminate. The loading diagram of the wing structure could be obtained by modelling the wing as a cantilever beam.

After the loading of both models was obtained, the stresses in the structural models were analyzed. For both models, the normal and shear stresses due to bending and shear were calculated. For the fuselage structure the stress induced by the pressurization was also taken into account.

An initial material analysis showed that aluminum was the most optimal material for both structural models. The use of composites was investigated for the fuselage model. However, it was concluded that composites were not

feasible for the MoM-liner fuselage. The reason for this is that composites need a certain thickness to resist damage. This minimum thickness might add up to a considerable thickness, meaning that probably no weight saving can be achieved at all. The weight savings induced by the use of composites mainly come into play when designing large wide body aircraft. Also, the cost of composites is significantly higher than the cost of aluminum. Aluminum Al 7074 T6 was used in the preliminary structural analysis of the MoM-liner.

Three main failure modes were considered in the fuselage and wing structure: Compression buckling, shear buckling and tensile yield failure. These failure modes were used to optimize the structural models. For the wing, the optimized variables are the skin thickness and the number of stringers. For the fuselage, the optimized variables are the skin thickness and the stringer flange, web and cap thickness. The optimization works as follows: First the structure is discretized over the length of the structure, generating an n amount of cross-sections. A minimum gauge is set for each section. This means that a minimum skin thickness is set for the structure. This way the structure can never return a thickness that is too thin to be manufactured. Constraints are then defined using the previously mentioned failure modes such that the program is aware of the modes it is sizing for. Finally, an objective function is written for each model. The goal of the objective function is to minimize the weight of the structure, thereby achieving the optimal design.

After the optimization of the models, a preliminary window cut-out analysis was performed for the fuselage structure. The analysis calculated the additional shear flow in the panels surrounding a cut-out. This could then be used to get an estimate of the weight penalty of a window cut-out.

Stability & Control

For a passenger aircraft design it is important that the aircraft is both stable and controllable. Static stability describes the reaction of an aircraft in steady flight to a disturbance in the air affecting its angle of attack. The static stability of the MoM-liner was analyzed using a method described by Torenbeek. The controllability is determined using a similar method to the stability analysis. The stability and control analysis resulted in a most front and most aft location of the center of gravity at which the aircraft would still be stable and controllable. This c.g. range was subsequently taken into account when creating the loading diagram of the aircraft.

High lift devices were selected based on the required $\Delta C_{L_{max}}$, which was obtained using methods described by Torenbeek. The wing control surfaces were designed using conventional methods. The positioning of the control surfaces could not be determined using a conventional method, since the MoM-liner uses a box wing configuration. It was concluded that the MoM-liner would need two sets of ailerons and elevators, one set on each wing. Spoilers were implemented in the wing design to assist with the descent and braking of the aircraft.

The vertical tail was designed keeping lateral and directional stability in mind. The rudder design was tightly connected to the vertical design. Considerations in the rudder design were losing an engine and crosswind landings, as for these conditions the rudder must be able to provide a counteracting moment to the disturbance. The MoM-liner was designed to safely fly in crosswinds up to 40kts.

Engine Sizing

The MoM-liner uses high bypass ratio turbofan engines. The engine of the MoM-liner was designed using rubberizing scaling. This is a method which scales existing engines to meet certain performance requirements. The main parameters affecting the engine sizing are: takeoff thrust, cruise drag, engine placement and thrust settings. In order to scale an engine to fit the MoM-liner's performance needs an analysis of the current generation and next-gen engines was performed. Using all data collected on the engines, a couple of correlations were made were used to estimate what the performance of a totally new engine would be. A correlation between engine diameter/cruise thrust, weight/take-off thrust, and specific fuel consumption/bypass ratio was performed. The mission fuel burn of the engine was estimated using the fuel fractions method, using a SFC obtained from the correlation graphs.

Next to performance, sustainability was also taken into account in the selection of the engine. The main aspects taken into account were the fuel burn and noise of the engine.

Performance Analysis

After the final design parameters had been determined, a performance analysis was performed. It was done in a more refined and detailed manner than for the design space diagram and was aimed to verify that the initial requirements and sizing constraints were still accounted for. Both the minimum and maximum speed of the MoM-liner were determined. The climb performance, which includes the minimum and maximum glide angle and rate of climb, was subsequently analyzed. Finally, the airfield performance of the MoM-liner was examined. This included an analysis of the take-off performance and the landing performance.

Results

This section discusses the results obtained from the preliminary design of the MoM-liner.

Preliminary Sizing Results

The preliminary sizing results include the maximum takeoff weight and the thrust. The results can be found in Table 1.

Table 1: Preliminary Sizing Results

Parameter	Value
MTOW [kg]	149,831
Thrust [N]	223,951

Aerodynamic Analysis Results

This section shows the results of the aerodynamic analysis. The first output of the aerodynamic analysis is the wing planform layout. The final values for the wing planform geometry can be found in Table 2.

Table 2: Final Box Wing Planfrom

		Front Wing	Aft Wing	Connecting Strut
Area	[m^2]	132.95	132.95	N/A
Span	[m]	40	40	6.103
Sweep	[degree]	33	-33	70
Dihedral	[degree]	2	-2	N/A
Root Chord	[m]	4.55	4.76	2.02
Tip Chord	[m]	2.02	2.11	2.11
Taper Ratio	[-]	0.433	0.433	1.045
Incidence Angle	[degree]	-1.4	-2.4	N/A
Local C_L	[-]	0.292	0.181	N/A

After the wing planform had been designed, the aerodynamic characteristics of the MoM-liner, such as the L/D and the cruise speed and altitude were calculated. These results can be found in Table 3. Finally, the loading of the front and aft wing, the C_{l_α} curve and drag polar were obtained. These graphs can be found in section 12.3.

Table 3: Aerodynamic Analysis results

Parameter	Value
$C_{L_{cruise}}$	0.474
$C_{D_{cruise}}$	0.0200
L/D	23.61
V_{cruise} [m/s]	236
h_{cruise} [km]	11

Structural Analysis Results

In the structural analysis chapter, two different models were analyzed: A fuselage model and a wing model. First, the loading and stress of the models were analyzed. The resulting shear and moment diagrams and stress plots can be found in section 12.4. The fuselage structure was optimized for skin and stringer flange thickness. The wing structure was optimized for skin thickness and stringer pitch. Figure 1 shows the final optimized skin thickness distribution around the fuselage cross-section. Table 4 shows the results for the optimized wing box structure.

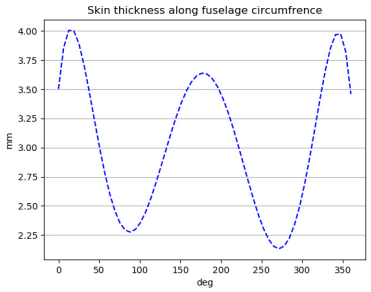

Figure 1: Final Optimized Skin Thickness Distribution

Table 4: Final Wing Box Configurations

Parameter	Front Wing	Rear Wing
Number of Stringers Upper Skin [-]	59	18
Number of Stringers Lower Skin [-]	56	10
Skin Thickness [mm]	3.6	2.0
Number of Spars [-]	4	4
Spar Thickness [mm]	10.0	10.0
Spar Locations [%c]	0.20, 0.45, 0.6, 0.75	0.20, 0.45, 0.6, 0.75

Finally, a preliminary window cut-out analysis was performed for the fuselage structure. This yielded a weight penalty of 2.42kg per window.

Engine Sizing Results

The conclusion of the engine analysis was that there are a two options which would meet the MoM-liner's requirements:

RR XWB-84: A 45% smaller version of the existing engine, with an increased bypass ratio (9.6 -> 15).

PW 1100G: A 27% larger version, with an increased bypass ratio (12.5->15). To boost the thrust ratio, an electrically boosted turbofan will be necessary.

The fuel volume required for a flight of 5,000 NM with max payload can be seen in Table 5.

Table 5: Fuel Requirements MoM-liner

Parameter	Value
Fuel weight [kg]	49,894
Fuel volume [m^3]	62.37

Static Stability & Control Results

The static stability and control analysis was necessary to check whether the MoM-liner design was stable and controllable. To check the stability, the most front and aft c.g. location was determined using a loading diagram. The diagram can be found in section 12.7. Table 6 shows the most front and aft c.g. location obtained. The conclusion from the static stability and control analysis was that that the aircraft was both stable and controllable.
The results of the control surfaces, high lift device and vertical tail and rudder sizing can be found in section 12.7.

Performance Results

This section shows the results of the performance analysis. The results from the performance analysis of the final design can be found in Table 7. The results of the take-off and landing performance analysis can be found in Table 8 and Table 9.

Internal and External Layout

The internal and external layout of the MoM-liner were analyzed. For the design of the cabin layout the main aspects which were taken into account are: The layout of doors, emergency exits and windows, the layout of galleys

Table 6: Static Stability and Control Results

Parameter	Value	Value
Most Forward c.g. Location	287 % MAC	33.6 m from nose
Most Aft c.g. Location	328 % MAC	36.4 m from nose
Static Margin	41 % MAC	2.82 m

Table 7: Results from Performance Analysis of Final Design

Parameter	Value at Sea Level	Speed at Sea Level	Value at 35,000 ft	Speed at 35,000 ft
Min. Speed (Take-off)	-	62.99 m/s	-	113.15 m/s
Min. Speed (Landing)	-	56.86 m/s	-	102.1 m/s
Max. Speed	-	304.0 m/s	-	376.0 m/s
Max. Angle of Climb (AEO)	0.27 rad	96.4 m/s	0.09 rad	173.1 m/s
Max. Angle of Climb (OEI)	0.12 rad	96.4 m/s	0.03 rad	173.1 m/s
Min. Angle of Descend	-0.03 rad	96.4 m/s	-0.03	173.1 m/s
Max. Rate of Climb	47.2 m/s	263.5 m/s	21.16	279.5 m/s
Min. Rate of descend	-2.88 m	68.14 m/s	-5.21 m/s	122.4 m/s
Max. Angle of Climb @ V_2 (AEO)	0.247 rad	75.6 m/s	0.0665 rad	135.8 m/s
Max. Angle of Climb @ V_2 (OEI)	0.0924 rad	75.6 m/s	0.00314 rad	135.8 m/s
Max. Rate of Climb @ V_2 (AEO)	18.49 m/s	75.6 m/s	9.02 m/s	135.8 m/s
Max. Rate of Climb @ V_2 (OEI)	6.973 m/s	75.6 m/s	0.427 m/s	135.8 m/s

Table 8: Take-off Maneuver Analysis Results

Parameter	Value
x_{ground}	990.7 m
x_{air}	315.4 m
$x_{total,take-off}$	1,306.1 m
$x_{take-off,CS-25}$	1,502.0 m

Table 9: Landing Maneuver Analysis Results

Parameter	Value
x_{air}	436.7 m
x_{trans}	147.8 m
x_{brake}	796.2 m
$x_{total,landing}$	1,353.7 m
$x_{landing,CS-25}$	2,256.1 m

and lavatories, the layout of cargo and baggage holds and inspection, maintenance and servicing considerations and finally, the passenger comfort. Images of the internal and external layout can be found in section 12.9 and section 12.10.

Sensitivity Analysis

A sensitivity analysis was performed for the main design aspects to look at which parameters affect the design the most. A sensitivity analysis was performed for the maximum take-off weight, aerodynamics, fuselage structure, wingbox structure and engine sizing.

For the MTOW sensitivity analysis, the most critical aspects which would increase the MTOW were the range and SFC, which would increase the MTOW by 12 and 14 % respectively after a 30% mutation.

For the aerodynamic analysis, a sensitivity analysis was performed regarding the spacing between the front and aft wing. The result of this analysis was that a larger separation between the two wings is advantageous.

For the fuselage structure, the effect of the geometry, loading and material properties of the structure on the structural weight were analyzed. Table 10 shows the result of this sensitivity analysis. It could be concluded that the parameters which have the largest influence on the design are: The stringer spacing, lift force of the front wing and the yield stress of the material.

For the wingbox structure the approach taken was similar to the fuselage. The effect of aerodynamic loads, stringer dimensions, stringer thickness, spar thickness and E-modulus on the structural weight were analyzed. The results can be found in Table 11. From these results it could be observed that the aerodynamic loads have the most impact on the structural weight of the fuselage.

Finally, for the engine sizing sensitivity analysis, the effect of changing the bypass ratio on the fuel volume and cruise SFC. It showed that decreasing the bypass ratio of an engine didn't significantly increase the fuel consumption of the engine.

Table 10: Sensitivity Analysis on the Fuselage Structure, Showing the Percentage Change in Structural Weight when Implementing a ±25% Change in Input Parameter

		+25%	-25%
User Defined Geometry	Stringer Spacing	+11.27%	-6.3%
	Frame Spacing	+4.0%	-3.2%
	Stringer Geometry	+1.6%	-0.9%
	y Distance Floor	-2.5%	+1.1%
Loads	Lift Front Wing	+22.3%	-21.7%
	Lift Back Wing	+4.3%	-1.1%
	Pressure Difference	+4.2%	-1.2%
	Load Factor	+16.9%	-14.8%
Material Properties	Young's Modulus	-4.4%	+3.5%
	Poisson Ratio	-1.4%	+0.06%
	Yield Stress	-18.8%	+14.7

Table 11: Table Indicating the Change in Wing Weight as a Result of a 25% Increase in Input Factors

Factor Changed	Front Wing Weight Change [%]	Rear Wing Weight Change [%]	Total Wing Weight Change [%]
Aerodynamic Loads	+23.6	+16.6	+21.3
Stringer Dimensions	+4.7	+10.1	+6.4
Stringer Thickness	-0.0	+0.5	+0.2
Spar Thickness	+6.54	+7.3	+6.8
E-modulus	-10.7	-7.5	-9.6

Aircraft Systems Analysis

The four main systems in an aircraft are the fuel system, hydraulic system, electrical system and environmental control system, each designed accordingly.

The fuel system consists of various components all with their own guidelines and regulations. The MoM-liner will have 20.80 m^3 fuel tanks in the front wing, 22.80 m^3 fuel tanks in the rear wing and a fuel tank of 18.77 m^3 will be located in the tail cone of the fuselage. The pumps have a designed throughput of of 28,576 kg/hr and must be able to deliver 34 m^3/hr. These will then pump fuel to the engines and pump fuel through the aircraft to maintain stability.

Flight controls, landing gear and braking systems are all power by the hydraulic system. This system consists out of a fluid reservoir, the hydraulic pumps, accumulators, lines, valves and cockpit controls. A hydraulic system will be used for the back wing power by the engines. An additional redundant electrical system will be used for the rear wing as safety measure. The front wing will be fully powered by electrical pumps, including back-up pumps.

An electrical system provides electricity for almost all subsystems. The primary power generation consists of an electrical generator on each engine. An auxiliary power unit (APU) will take over in case of engine failure or when the engines are not running during ground operations. The APU will be located in the tail cone of the fuselage. Additional batteries are stored here as well, as a redundancy measure.

Pressurization system, pneumatic system, air-conditioning system and oxygen system are all covered by the environmental control system. This all ties into the comfort level of the passengers. As the MoM-liner engines do not have bleed air systems the health concerns of passengers is at a lower level. An emergency oxygen generator is located in the aircraft above the seats.

The data handling system processes data on board. It consists out of three types of buses; address buses, data buses and control buses. All three play a major role in processing the operators' inputs. These types on buses each have their own components, each essential for the operation of a different part of the aircraft.

Risk Assessment

Identifying technical risk is an important step in mitigating potential risks and assuring that the system meets all requirements. The main technical risks associated with the MoM-liner design are: Electrical failure, Anti-/De-Icing Failure, manufacturing risks and structural failure. Additional risk might come in the form of business risk and financial risk.

Contingency margins were used to ensure that the final design still meets the requirements. These contingency margins can be reduced as the design becomes more mature. Contingency margins were set for the aircraft mass, loads, SFC and size. Additionally, budget monitoring was performed for the aircraft mass, SFC and cost to make sure that all resources stay within predefined bounds.

Sustainable Development Strategy

Sustainability was an integral part in the MoM-liner design. Sustainability has three aspects: Economical, environmental and societal. There are three categories where sustainability should be considered, inputs, operations and products. Inputs cover the raw material selection, operations cover the process of going from raw materials to a finished product A few of the considerations that are taken into account are: noise, material selection, fuel consumption, manufacturing techniques, end-of-life solutions and aircraft operations. It is very important to design an aircraft with an as high as possible recyclability percentage, the MoM-liner is at least 75% recyclable and probably more. This figure is obtained primarily by selecting aluminum as the main material, this metal is highly recyclable and is therefore a great choice for the MoM-liner. Furthermore engine selection has a big impact on sustainability, not just with fuel consumption but also with noise production. The engines on the MoM-liner are market-leading in terms of fuel consumption and noise production, which was necessary to meet the requirements set for the propulsion system.
In terms of manufacturing, the MoM-liner will use a state of the art Gigafactory. This factory runs on renewable energy, and uses a modern manufacturing technique called lean manufacturing. This technique ensures the most efficient processes are used, in terms of use of material, transportation distances, etc.
As the MoM-liner will be a very modern aircraft, designed and built in the 21st century, it will be way ahead of it's competition in terms of environmental impact, operational cost and societal impact. This positions the MoM-liner as one of the most promising aircraft of the next 50 years.

Post DSE Considerations

Multiple processes can happen after DSE and provide additional information on the options for the aircraft. One being autonomous flight, where a autopilot controls the whole flight and a human pilot only takes over in case of emergency. This would improve overall flight efficiency while maintaining safety. However, it is for further investigation whether this is truly feasible.
After the DSE a final design phase can be started, in which a technical design phase and organizational operation phase form the key points of the project design and development logic. Other major aspects of post DSE considerations are the manufacturing, assembly and integration plan. Finally the reliability, availability, maintainability and safety characteristics of the aircraft should be considered. This will ensure that the design functions optimally and can be used in commercially.

Cost Analysis

The total cost of the MoM-liner can be broken down into two main contributions: Direct operating cost and indirect operating cost. Direct operating cost are the expenses directly related with flying and maintenance of an aircraft. Examples of indirect operating cost are: public relation cost expenses, facility maintenance costs, administrative costs, facility leasing costs.

After an analysis of the direct and indirect operating cost was performed, a return on investment was computed. This takes into account aspects such as the research and development cost and manufacturing cost. Table 18.8 shows the resulting expected profit values using different profit margins.

Conclusion

The box-wing, MoM-liner concept is a high efficiency, small, long range aircraft that is designed to fill the gap in the middle of the market. Design studies were performed to evaluate the feasibility of the concept and to ensure that it is able to meet the market requirements. The aerodynamic, structural and performance parameters were optimized using a MDO approach. The optimal maximum take off weight after optimization was found to be 149,831 kg and it was found that The MoM-liner will have a cruise C_D of 0.02 and an L/D of 23.61. Also, the specific fuel consumption is substantially better than current generation aircraft. The minimum required runway length of 2600m means that the MoM-liner can operate from smaller airports that are essential to fill the point to point market. In short, the MoM-liner meets all requirements that were set out for it and will be able to fill the gap in the market that was defined at the beginning of the project.

Contents

Nomenclature

α	Angle of attack	$[rad]$
$\bar{x}$	x location of centroid	$[m]$
$\bar{y}$	y location of centroid	$[m]$
δa_{max}	Maximum aileron deflection angle	$[rad]$
$\Delta C_{L_{max}}$	Difference in maximum lift coefficient of the wing	$[-]$
$\Delta C_{l_{max}}$	Difference in maximum lift coefficient of the airfoil	$[-]$
ΔC_{L_S}	Spoiler lift coefficient derivative	$[-]$
Δp	Pressure differential	$[-]$
δ_S	Spoiler deflection angle	$[rad]$
ϵ	Downwash	$[deg]$
η_h	Dynamic pressure ratio	$[-]$
η_p	Propeller efficiency	$[-]$
γ	Pitch angle	$[rad]$
Λ	Sweep angle	$[rad]$
$\Lambda_{c/4}$	Quarter chord sweep	$[rad]$
μ_B	Brake pad friction coefficient	$[-]$
μ_G	Tire friction coefficient	$[-]$
ρ	Air density	$[kg/m^3]$
σ	Altitude correction factor	$[-]$
σ_{cc}	Cripling stress in stringer	$[Pa]$
σ_{circ}	Circular stresses due to pressure	$[Pa]$
σ_{long}	Transverse stresses due to pressure	$[Pa]$
σ_N	Normal stress	$[Pa]$
σ_y	Maximum yield stress	$[Pa]$
τ	Effectiveness	$[-]$
τ_{cr}	Critical shear stress	$[Pa]$
τ_{xy}	Shear stress	$[Pa]$
θ	Twist	$[deg]$
A	Aspect ratio	$[-]$
A_{max}	Maximum cross section	$[m^2]$
A_{panel}	Area of panel	$[m^2]$
B	Boom area	$[m^2]$
b	Boom separation	$[m]$
b	Wing span	$[m]$
b_E	Elevator span	$[m]$
b_h	Tail span	$[m]$
b_s	Spoiler span	$[m]$
C	Cost	[$]
c	Chord	$[m]$
$c(y)$	Chord at y position	$[m]$
$c.g.$	Center of gravity	$[m]$
C_D	Drag coefficient	$[-]$
C_f	Skin friction coefficient	$[-]$
c_j	Thrust specific fuel consumption	$[kg/s/N]$
C_L	Lift coefficient	$[-]$
c_p	Power specific fuel consumption	$[kg/J]$
c_r	Root chord	$[m]$
C_S	Spoiler chord	$[m]$
c_t	Tip chord	$[m]$
C_{D_0}	Zero lift drag coefficient	$[-]$
c_{d_0}	Airfoil zero-lift drag coefficient	$[-]$
c_j	Specific fuel consumption	$[(kg/hr)/N]$
c_{l_α}	Airfoil lift curve slope	$[-]$
C_{l_P}	Roll damping derivative	$[-]$
C_{L_α}	Lift curve slope	$[1/rad]$
$C_{l_{\delta a}}$	Aileron control derivative	$[-]$
$C_{L_{\Delta E}}$	Elevator lift coefficient derivative	$[-]$
$C_{m_{ac}}$	Moment coefficient around the aerodynamic center	$[-]$
c_p	Specific heat of air	$[J/K]$
D	Drag	$[N]$
d_{fuse}	Part of wing inside fuselage	$[m]$
E	Endurance	$[hr]$
E	Young's modulus	[Pa]
e	Oswald efficiency factor	$[-]$
f	Landing weight/take-off weight	$[-]$
FC	Fuel consumptions	$[liter/km]$
FF	Form factor	$[-]$
G	Shear modulus	$[Pa]$
g	Gravitational acceleration	$[m/s^2]$
h	Altitude	$[m]$
h	Height	$[m]$
I_{xx}	Second moment of area about the x axis	$[m^4]$
I_{zz}	Second moment of area about the z axis	$[m^4]$
IF	Interference factor	$[-]$
k_1	Brake power ratio	$[-]$
L	Lift	$[N]$
l_h	Tail arm	$[m]$
LCN	Number of nose gear wheels	$[-]$
M	Mach number	$[-]$
m or $MTOW$	Maximum take-off weight	$[kg]$
M_x	Moment around x axis	$[Nm]$
M_y	Moment around y axis	$[Nm]$
M_{ff}	Mass fuel fraction	$[-]$
MAC	Mean aerodynamic chord	$[m]$
N_{mw}	Number of main gear wheels	$[-]$
N_{nw}	Number of nose gear wheels	$[-]$
P	Roll rate	$[rad/s]$
p	Air pressure	$[Pa]$
q_s	Shear flow	$[N/m]$
R	Radius	$[m]$
R	Range	$[m]$
Re	Reynolds number	$[-]$
ROC	Rate of climbs	$[m/s]$
S	Wing area	$[m^2]$
S_h	Tail area	$[m^2]$
S_S	Spoiler area	$[m^2]$
S_x	Shear force in x direction	$[N]$
S_y	Shear force in y direction	$[N]$
S_{land}	Landing distance	$[m]$
S_{ref}	Aileron area	$[m^2]$
S_{wet}	Wetted area	$[m^2]$
S_{wf}	Wing flapped area	$[m^2]$
SF	Safety factor	$[-]$
SFC	Specific fuel consumption	$[(kg/hr)/N]$
SM	Stability margin	$[m/m]$
T	Thrust	$[N]$
t	Skin thickness	$[m]$
$TMCT$	Maximum Continous Thrust	[N]
$TMTO$	Maximum Takeoff Thrust	[N]
TOP	Take-off parameter	$[N]$
V	Speed	$[m/s]$
v	Poisson ratio	$[-]$
W_F	Fuel weight	$[kg]$
W_{crew}	Crew weight	$[N]$
W_{land}	Landing weight	$[N]$
W_{MZF}	Zero fuel weight	$[kg]$
W_{OE}	Operational empty weight	$[N]$
W_{PL}	Payload weight	$[kg]$
W_{tfo}	Weight of trapped fuel and oil	$[N]$
W_{TO}	Take-off weight	$[kg]$
y	Spanwise position	$[m]$
y	y distance to structures centroid	$[m]$

1 Introduction

With an annual growth rate forecast of 3.6%, air transport passengers will nearly double to 7.8 billion by 2036 [1]. This growth is accompanied by rapid innovation in the aeronautic industry - new aircraft are being developed to meet the high demand. However, taking a close look at the current aircraft dominating the aviation market, it can be concluded that there is a gap in the market. This gap is due to the absence of new, innovative small long-haul aircraft, as the current aircraft in this category (Boeing 757-200 and Airbus A310) are old and out of production. A new middle-of-the-market (MoM) airliner will be designed to fill this gap.

The demand for such small long-haul aircraft is strengthened by multiple market segments, both low-cost carriers as well as legacy carriers would benefit from a small long-haul aircraft. To elaborate further, the industry is moving away from the traditional hub-and-spoke system to a more versatile model: the point-to-point system (P2P). The P2P system itself is already being implemented for short-haul routes, however, this market is still under development for the long-haul routes. Among the main benefits of the long-haul P2P system is the ability to directly connect smaller airports, thus opening up intercontinental route possibilities that were untouched by the hub-and-spoke market. For this task, operating small long-haul aircraft is highly beneficial, as passenger demand may not be high enough to fill current, larger long-haul aircraft. With the introduction of a truly efficient MoM aircraft, it would become possible for legacy and low-cost carriers to profitably execute a long-range P2P system. In general, the complete industry tends to smaller aircraft as these are deemed more versatile.

As briefly stated earlier, a new airliner will be designed to fill the existing gap. To specify, the mission is to design a small long-haul airliner to replace the aging fleet of comparable aircraft and fill the growing gap in this emerging market, while having better efficiency, reliability and sustainability than comparable existing aircraft, such as mainly the B757-200. This report is part of a series of four, where this is the fourth and final report in this series, after the Project Plan, the Baseline report and the Midterm report [2][3][4]. The previous parts elaborated on the project planning and organization, as well as the decision making in the Midterm report, following an elaborate trade-off, to design a box wing aircraft. The main purpose of this part (part IV) is to provide a more detailed design compared to the preliminary design presented in the Midterm report. This includes an aerodynamic, structural, performance and stability and control analysis. However, also the system as a whole has to be properly understood and future planning has to be taken into consideration.

In order to adequately do this, this report is structured as follows. First, in chapter 2, the project objectives are discussed. Then, in chapter 3, a revised market analysis is presented, adding an estimate for the amount of units which will be sold. Next, in chapter 4, the requirements from previous reports are revised and some have been updated. In chapter 5, a summary of the trade-off between three design concepts made in the Midterm report is provided. A first preliminary sizing method is explained in chapter 6. Then, in chapter 7, chapter 8, chapter 9, chapter 10 and chapter 11 the methodologies for performing a more detailed analysis for aerodynamics, structural analysis, stability & control, propulsion and performance are outlined and performed. In chapter 12, the results and optimization are illustrated. Then, a sensitivity analysis is performed in chapter 13. Next, aircraft system characteristics are explained, analyzed and designed in chapter 14. A risk analysis is then performed in chapter 15 where risks are identified and measures to mitigate them are given. Furthermore, in chapter 16, a sustainable development strategy is outlined to analyze how the MoM-liner will be as sustainable as possible. Then, in chapter 17, considerations for the post DSE (Design Synthesis Exercise) phase are analyzed as to explain what actions can be taken after the DSE. One of the more important aspects for the customer, the cost, is then analyzed and calculated in chapter 18. Then, a compliance matrix is given in chapter 19 to see whether the design at hand meets the given requirements. This all is concluded in chapter 20. Finally, recommendations for further design stages and further research are outlined in chapter 21.

[1] URL `http://www.iata.org/pressroom/pr/Pages/2016-10-18-02.aspx` [cited 31 May 2018]

2
Project Objectives

In this project nine students from the Delft University of Technology will design a Middle-of-the-Market aircraft in a ten week period. The main objective for the students is to show their gained knowledge throughout their studies, but also to improve their communication and team-working skills. As outlined in chapter 16, sustainability is an increasingly important factor for the aerospace industry, as manufacturers strive to decrease the environmental impact of their project as much as possible. Therefore, sustainability plays a vital role in the design process of this aircraft. Thus, sustainability is one of the key objectives of the project that will be explored further.

The objective of the prospective aircraft is to close the growing gap in the current aircraft market. Around 1983, both Airbus and Boeing introduced small medium- to long-haul aircraft. At the time, these designs were only a moderate successes as demand for such missions was low. However, a substantial number of Boeing 757-200's are still used for low-density trans-Atlantic routes as well as cross-continental flights in the United States. As time goes by, this fleet is aging and in need of replacement. In addition to replacing existing legacy carrier fleets, a new Middle-of-the-Market airliner should allow low-cost carriers to expand their network by allowing them to serve point-to-point service to more distant destinations.

Furthermore, next to replacing the current fleet, the MoM-liner must also provide large improvements in comparison to the older aircraft, especially concerning fuel efficiency, noise pollution and passenger comfort. The main objective of the project regarding sustainability is to assure at least 75% of the material used in the aircraft's construction is re-usable. Additionally, the design needs to have lower operating costs than comparable existing aircraft. Besides, the unit cost must not exceed 160 million USD, including amortization of development costs. The unit cost is allowed to exceed 160 million, as long as the increase in price can be covered by the reduction on operational cost. Additional requirements defined for the aircraft can be found in the Baseline Report [3].

With these project objectives the following mission need statement has been set up:
Design a small long-haul airliner to replace the aging fleet of comparable aircraft and fill the growing gap in this emerging market, while having better efficiency, reliability and sustainability.

Also, the following project objective statement was formulated:
Designing a sustainable, efficient and small long-haul airliner to demonstrate the skills acquired during the Bachelor's program of Aerospace Engineering by nine students over a ten week period.

3
Market Analysis

Market analysis is an important tool, aircraft manufacturers use market analysis to determine in which direction the industry is going and what potential aircraft design, or services, the customers might need in the future. The next 20-30 years are going to be an interesting time in the aviation industry, the exponential growth of passenger demand combined with new emerging markets mean there is a need for a new type of aircraft. Combining this with the introduction of new super-efficient engines, as well as a couple of new experimental aircraft designs, could lead to a big leap forward in aviation efficiency. This chapter will analyze where the MoM-liner fits into the market, what the demand is and which aircraft it could potentially replace or compete against. Section 3.1 analyzes one of the two potential functions of the MoM-liner: replacing current fleet. Section 3.2 discusses the other function: filling the market gap. Then, in section 3.3, some business strategy drivers for the MoM-liner are elaborated upon. Lastly, in section 3.4, a market share analysis is performed.

3.1. Replacing Current Fleet

Currently there are two main middle-of-the-market aircraft in service with airlines around the world that were identified in the initial project description. These are the Boeing B757-200 and Airbus A310. These two aircraft entered service in the 1980s and are in desperate need of replacement. In addition to these two aircraft, other aircraft that fall within the target market for the new MoM-liner were identified. The Boeing 767-200 which is now out of production and is reaching the end of its useful life has a comparable range and maximum passenger capacity to the aforementioned aircraft.

Table 3.1 gives an overview of all the aircraft that can be considered to be MoM-aircraft, indicating their passenger capacity and range. From this it is clear that there is a significant market demand for aircraft in this class with a total of 756 aircraft currently in service.

Table 3.1: Current Middle-of-the-Market Fleet

Aircraft	**Number of Passengers** [-] [5]	**Range** [NM] [5]	**Number in Service** [-] [6]
Boeing 757-200	239	3,812	633
Airbus A310	280	3,645	47
Boeing 767-200	255	3,150	76
Total	-	-	**756**

The aforementioned aircraft are old, inefficient and no longer in production, making obtaining spare parts difficult. Airlines, however, keep these aircraft to their unique position in the market, they allow airlines to service long-haul routes that would not be profitable to operate with wide-body aircraft [7]. If a new aircraft in this category were to be developed, it seems likely that demand among the operators of the B757-200, A310 and B767-200 would be strong as they seek to replace the more inefficient, older aircraft. It is important to note that not all carriers using these older aircraft will want to replace their aging fleet, some of these older aircraft are now used for cargo. Since cargo carriers utilize their aircraft far less than passenger carriers, it might not make sense to buy new aircraft for this task.

The majority of the current operators of MoM-aircraft are legacy carriers. The aircraft are operated extensively in the US with 498 of the 756 being operated by North American carriers [8]. The B757-200 in particular is operated on both low demand intercontinental routes such as Charlotte to Dublin and domestic routes with high demand like New York to California [7]. Another use case that is specifically mentioned is that the B757-200 has been found to be ideal for flying to ski resorts [7]. The high thrust-to-weight ratio of the B757-200 allows it to operate efficiently

even at relatively low air densities. While the MoM-liner should not necessarily be similarly overpowered, as this is inefficient, high altitude take-off and landing performance should be considered to allow it to take over the Boeing 757-200's market share.

3.2. Market Gap

Although currently there is no direct competitor for the MoM-liner, both Boeing and Airbus are encroaching into this market from below and above. Boeing announced the new B737 MAX 10 and Airbus is releasing the A321neo. These aircraft seek to fill the gap in the market with a larger, longer range version of smaller aircraft. In addition, some effort has been made to fill this gap in the market by building smaller versions of larger aircraft like the Boeing 787-8.

Only few of these aircraft have actually been delivered. It is, hence, not yet clear exactly how they will be used by airlines some indication of the demand for the middle-of-the-market aircraft can be found by looking at the orders[1][2][3]. The orders for the aforementioned aircraft are summarized in Table 3.2.

Table 3.2: Specifications and Orders of Aircraft Approaching the Middle-of-Market from Above and Below [9][10][11]

Airliner	**Number of Passengers** [-]	**Range** [NM]	**Orders**
Boeing B737 MAX 10	230	3,850	407
Airbus A321neo	244	4,000	1,930
Boeing 787-8	359	7,355	419
Total	-	-	**2,756**

From this it is clear that there is significant demand for the aircraft that fall either side of the proposed MoM-liner. This seems to indicate that airlines are very interested in smaller, longer range aircraft.

3.3. Airline Business Strategy Drivers

The airline industry is a constantly evolving and improving industry. There are some key drivers that encourage airlines to adapt, and perhaps expand their existing services. These drivers can range from passenger demand to new technologies, maybe even to seasonal demand for some routes. An aircraft like the MoM-liner, with its long-haul capability, while still being relatively small, could fit these new needs exactly.

3.3.1. Range

From Table 3.1 it can be seen that for the aging aircraft in the MoM-liner category their range is still fairly low. Introducing a longer range MoM-liner would likely open up new opportunities and markets that the B757-200, A310 and B767-200 cannot currently operate. This is something that has been extensively discussed by aerospace manufacturers like Boeing. Boeing's Commercial Marketing Vice President Randy Tinseth said on the 11th February 2015 on the subject of simply creating an upgraded version of the B757: "The fact is, there's absolutely no business case to support that. We're very happy with our B737 and 787 product lineups. So we're studying the space in between them. Customer feedback has led us to look at an airplane that is larger than today's B737 and has greater range than the B757." [12]. This seems to indicate that based on analysis by manufacturers at least the future of the MoM-liner market will be longer range than the current aging generation of small long range aircraft and that simply updating these aircraft is not a viable option. There is, therefore, a strong market case for developing a new longer range aircraft. A range of 5,000-6,000 NM would improve access to emerging markets as well as provide the opportunity to create a point-to-point network. The MoM-liner requirement state a range of 5,000 NM needs to be achieved. Figure 3.1 shows the area of the Earth this aircraft could fly from Amsterdam, this range represents the MAX fuel range of the aircraft[4]. However, it should be noted that to replace the current fleet the MoM-liner should also be profitable and efficient operating smaller ranges, like the B757 does now.

[1] URL `http://active.boeing.com/commercial/orders/displaystandardreport.cfm?cboCurrentModel=737&optReportType=AllModels&cboAllModel=737&ViewReportF=View+Report` [cited 2 May 2018]

[2] URL `http://www.airbus.com/aircraft/market/orders-deliveries.html` [cited 2 May 2018]

[3] URL `http://active.boeing.com/commercial/orders/displaystandardreport.cfm?cboCurrentModel=787&optReportType=AllModels&cboAllModel=787&ViewReportF=View+Report` [cited 2 May 2018]

[4] URL `https://wallpapercave.com/wp/8oy3pFs.jpg` [cited 4 May 2018]

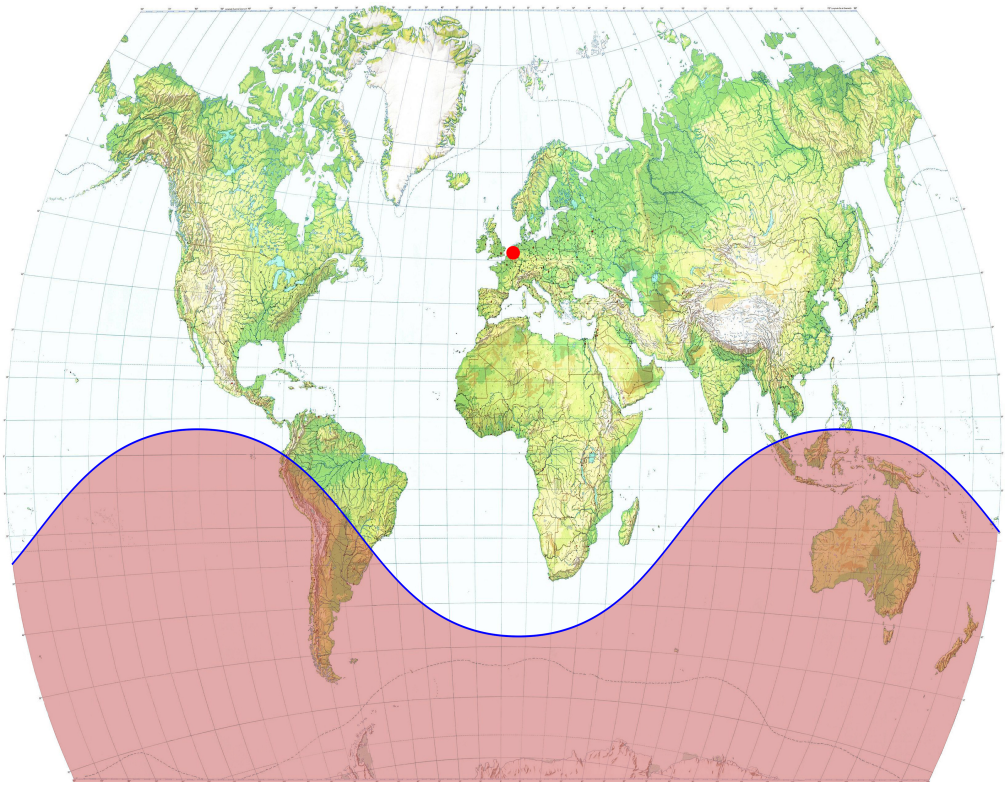

Figure 3.1: 6,000 NM Range from Amsterdam

3.3.2. Flight Frequency

In addition to replacing comparable aircraft and opening new routes, the introduction of an efficient small long range airliner may even replace larger aircraft. Airlines may choose to operate more flights on a particular route rather than one larger aircraft, as this offers passengers more flexibility. This is, of course, not possible at many busy airports such as Schiphol or Heathrow which are more or less operating at their maximum capacity. However, for less busy routes more flights per day may be an attractive option for airlines who are able to accommodate passengers' travel plans better.

3.3.3. Low-Cost Long-Haul

The success of Low-Cost Carriers (LCC) in the last couple of years has been proven, they have expanded into every major international market and are the fastest growing business in the segment [13]. Establishing a Low-Cost Long-Haul (LCLH) service, though, has been very challenging in the past, but this market seems to be emerging right now. Especially in the European market the rise of LCLH has been significant in the last couple of years [13].

The reason LCLH has been so difficult to start is because long-haul flights are inherently expensive. First of all, the total cost of a long-haul flight is higher, and with the added fuel, taxes and surcharges, the price is significantly higher than short-haul LCC flights. As of 2013 no LCLH carrier has survived for more than one economic cycle, this shows that either the market conditions are not ready for LCLH or the technology is not sufficient yet [14]. However, in recent years carriers like Norwegian have proven that the LCLH can be successful and has its place in the market [15].

Comparing the Airbus and Boeing market outlooks for 2017-2036, the market conditions are now right for a LCLH carrier [13][16]. The traffic flows from Europe-USA, Europe-Middle East are expected to grow by almost 100% in the next 20 years [16]. Furthermore, flights to and from Asia will also increase drastically, combined with the increase in traffic in Europe this could lead to a huge increase in the demand for long-haul flights.

An airline like Southwest Airlines is the perfect example of how a LCC can expand into LCLH. Long-haul flights are the fastest growing market in the US, and Southwest is in a position to undercut the legacy carriers if they get the right plane for the job. The need for a cheap, efficient, aircraft capable of long-haul transport is more apparent than ever [17].

3.3.4. Business Passengers

The business travelers market is huge, and getting bigger every year. Nine out of the ten largest LCC's target business travelers, and ten out of the thirty largest airlines have an LCC in their group [16]. Long-haul business travelers are the most lucrative passengers, and airlines earn the most per seat for these passengers[5]. Aircraft manufacturers do not control how airlines arrange seats in their fleet, or what the distribution over classes will be. Airlines can choose to operate flights with only business class seats, but as of now this has not been feasible due to the demand for this service only being high enough on a handful of routes. This might change in the future, with the increase of business travel, and a small point-to-point long-haul aircraft could be the aircraft airlines need to start flying these very lucrative services in the future.

3.3.5. Point-to-Point vs. Hub-and-Spoke Model

The benefits of point-to-point (P2P) versus hub-and-spoke (H&S) models have been a hot topic of debate. The success of the B787, and the 'failure' of the A380 clearly shows the market moving toward a P2P system. The benefits are a lower travel time at a slightly higher cost, but passengers seem to be okay with the slightly higher price in order to get to the destination quicker. In the past the carriers that use H&S system have been able to provide slightly lower prices on their long-haul flights, this is partly due to economy of scales and increased load factors [18]. Nevertheless, the introduction of the B787-series has proven that P2P works on long-haul flights, and the MoM-liner would be able to suit the 5,000 NM P2P flights perfectly.

Airlines like Southwest and Ryanair have proven the viability of P2P LCC flights for short-haul, and they would be prime candidates to expand their services to provide LCLH flights. Ryanair's recent purchase of 110 B737 MAX 200s shows its intention to expand into the 'semi' long-haul routes, and for that reason a true long-haul aircraft like the MoM-liner could be a great success in the current and future market [18][19]. A carrier like Norwegian that uses the Boeing 787 on most of its routes right now, might also want to use a small long-haul aircraft that can be used on routes that the B787 provides too much capacity for.

A small remark about flights between the existing hubs, and how a small long-haul aircraft would not necessarily only be usable for P2P to smaller destinations. Having multiple smaller aircraft flying the same route, at different times, could actually be beneficial for an airline. As being able to provide an array of departure and arrival times could help attract passengers. Also maximizing the load factor on these relatively smaller aircraft is easier to do than on a much larger aircraft. Furthermore, with fluctuating seasonal demand, extra aircraft can be added to these routes during high demand. During the low season, these extra aircraft can be used on other, smaller, P2P routes.

To summarize, the advantages of P2P are lower fuel burn and shorter travel times due to direct flights. The market has been moving towards a P2P system in the last couple of years, and the introduction of aircraft like the B787 and A350 confirm this. The MoM-liner will bring P2P transport to the middle of the market, making LCLH accessible to LCCs. This could open new routes for legacy carriers, and make LCLH routes attractive for LCCs.

3.3.6. Cabin

Aircraft cabin layouts are becoming increasingly denser. The overall market trend towards cheaper flights has encouraged airlines to optimize cabin usage, which in turn allows airlines to offer consumers cheaper flights. The low cost market is rapidly growing, particularly as the low cost carrier model has been increasingly adopted in South-East Asia [13]. The aircraft cabin should be optimized for single class, dense configuration, to be able to provide the cheapest seats. Another trend that has been identified by aircraft manufacturers is the trend towards increased connectivity, a significant portion of the aircraft are equipped with on board broadband [16].

3.3.7. Environment

The aviation industry, just like any other industry, has to meet new environmental regulations. Boeing wants to meet emission reductions in a three step program, with their final step being a 50% reduction of the aviation net CO2 emissions in 2050, Airbus did unfortunately not include any environmental targets in their market outlook [13]. Boeing has a very ambitious target, and this might prove difficult to meet, unless significant improvements are made in the propulsion, aerodynamic and material departments.

[5] URL `https://www.youtube.com/watch?v=BzB5xtGGsTc` [cited 26 April 2018]

3.4. Market Share Estimation

In order to accurately estimate the unit cost of the aircraft it is important to obtain an estimate of the number of aircraft that will be sold. The demand by market sector must be considered and an approximation of the number of orders per airline created.

3.4.1. Legacy Aircraft Replacement

Currently there is no aircraft currently being produced that can compete with the MoM-liner directly. Airlines seeking to replace their current fleet would have no real alternative. Approximately 25% of B757-200s, B767-200s and A310s are in cargo service [6] where due to low flight hours they are unlikely to replace the fleet with new aircraft as they would not benefit substantially from the increased efficiency. Moreover, it is possible that many airlines may not replace these aircraft with comparable aircraft due to changes in business model. However, it seems logical that about 50% of the current legacy MoM-liner fleet would be replaced with the new MoM-liner, this equates to approximately 380 aircraft.

3.4.2. Low-Cost Long-Haul

It is more difficult to quantify the number of aircraft orders from low cost carriers as this market is reliant of these carriers modifying their business models and perhaps even entirely new carriers being created. Currently the only low cost carrier that has a substantial presence in the long haul market is Norwegian, which has purchased 29 Boeing 787-8s and is seeking to further expand its fleet[6]. Low cost carriers rely on having large fleets to allow for flexibility and tend to order aircraft of a single model in large volumes. Therefore, this market has the potential to be very lucrative with airlines like Easyjet and Ryanair purchasing A320s and B737s in batches of over 100 aircraft [6]. The MoM-liner is a larger aircraft, thus it is unlikely that airlines would order these aircraft in as large numbers as short range single aisle aircraft. However, an approximate order of 40 does not seem unreasonable. The number of airlines that would be willing to adapt their business model is also a relative unknown. Currently Norwegian Air, Wizz Air, AirAsiaX and Eurowings all operate LCLH services. Assuming all these acquire the MoM-liner and are perhaps joined by new LCLH carriers such as LEVEL (IAGs LCLH venture), it seems reasonable that somewhere in the region of 6-7 airlines could order the MoM-liner. The minimum estimate for orders in this market is hence taken to be 240 units.

3.4.3. Point-to-Point

Once again it is difficult to predict the growth of the P2P market as it is heavily dependent on airlines changing their strategies. The success of the B787, A321neo and B737 MAX have shown that there certainly is demand for longer range small aircraft. However, given that there is significant demand for new smaller long haul aircraft from legacy carriers. This market is perhaps not as substantial as that of low cost long haul. B787 orders from legacy carriers have generally averaged about 20 units [6]. There has been significant interest and enthusiasm among current Boeing customers for the proposed B797 concept[7]. It is difficult to determine how this interest will translate into orders, but it will be assumed ten of the major global carriers will place substantial orders, around 200 aircraft. This estimate is perhaps a little conservative, however, given the significant uncertainty this is the value that will be used for cost estimation purposes.

3.4.4. Summary

The predicted values by market and total predicted orders are presented in Table 3.3. Conservative values were selected in all cases to ensure that it is still possible to make a profit. Moreover, an important consideration is that the MoM-liner is being developed by an unknown company, so companies may be more reluctant to place orders.

Table 3.3: MoM-liner Order Forecast

Market Sector	Predicted Orders
Legacy Aircraft Replacement	380
Low-Cost Long-Haul	240
P2P	200
Total	**820**

[6] URL `https://www.norwegian.com/en/about/our-story/our-aircraft/` [cited 18 June 2018]
[7] URL `http://money.cnn.com/2017/06/20/news/companies/boeing-797-paris-first-peek/index.html` [cited 18 June 2018]

4

Requirement Analysis

This chapter establishes the requirements that the system shall be designed for. In the baseline report [3] these requirements were established by defining the mission profile leading to the functional flow diagram, a functional breakdown structure and a requirement discovery tree. The mission profile was already established earlier and will simply be presented again in section 4.1. An updated functional flow diagram and functional breakdown structure is presented in section 4.2. Followed by an updated list of requirements as presented in section 4.3.

4.1. Mission Profile

The mission profile of the MoM-liner is the standard mission profile for a commercial aircraft certified under CS-25. The aircraft starts up its engines, takes off and then climbs to cruise altitude. During cruise, the aircraft will perform step-climbs, as the aircraft burns fuel it will become lighter and can therefore fly at a higher, more efficient, altitude. The aircraft will then descend and attempt to land. The aircraft has some loitering time, in case it needs to wait before it can land, for the MoM-liner this is 30 minutes. In case of bad weather or some other inconvenience due to which the aircraft will not be able to land, the aircraft will climb back to a lower "loiter" cruise altitude and fly to an alternative airport. The fuel reserve to fly to an alternative airport allows for up to an hour of flight [20]. After landing, the aircraft will taxi to the gate and shut down its engines, this concludes a typical commercial mission profile with the option to loiter or even divert to an alternative airport. The mission profile is shown in Figure 4.1.

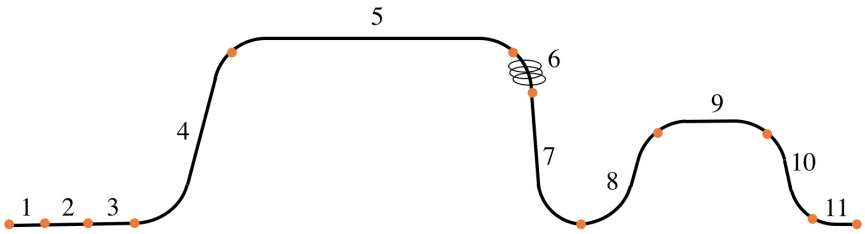

Figure 4.1: Mission Profile

Table 4.1: Mission Profile

Mission			
1	Engine start and warm-up	7	Descent 1
2	Taxi	8	Climb 2
3	Take-off	9	Cruise 2
4	Climb 1	10	Descent 2
5	Cruise 1	11	Landing
6	Loiter	12	Taxi, engine shutdown

4.2. Functional Flow Diagram

To find out what functions a system has to perform, it is useful to set up a functional flow diagram. The function flow diagram shows all the functions the system has to perform and has been used to derive the sub-system requirements, which are presented in section 4.3. The functional flow diagram has guided the tough process of setting up requirements, by knowing what needs to be done. The mission profile itself has been broken down in eleven phases, with all its functional components as seen in Figure 4.2. The function flow indicates the flow of the system functions, however for requirement synthesis, it is more useful to break the flow down into a so-called functional breakdown structure. The functional break down structure is presented in Figure 4.3.

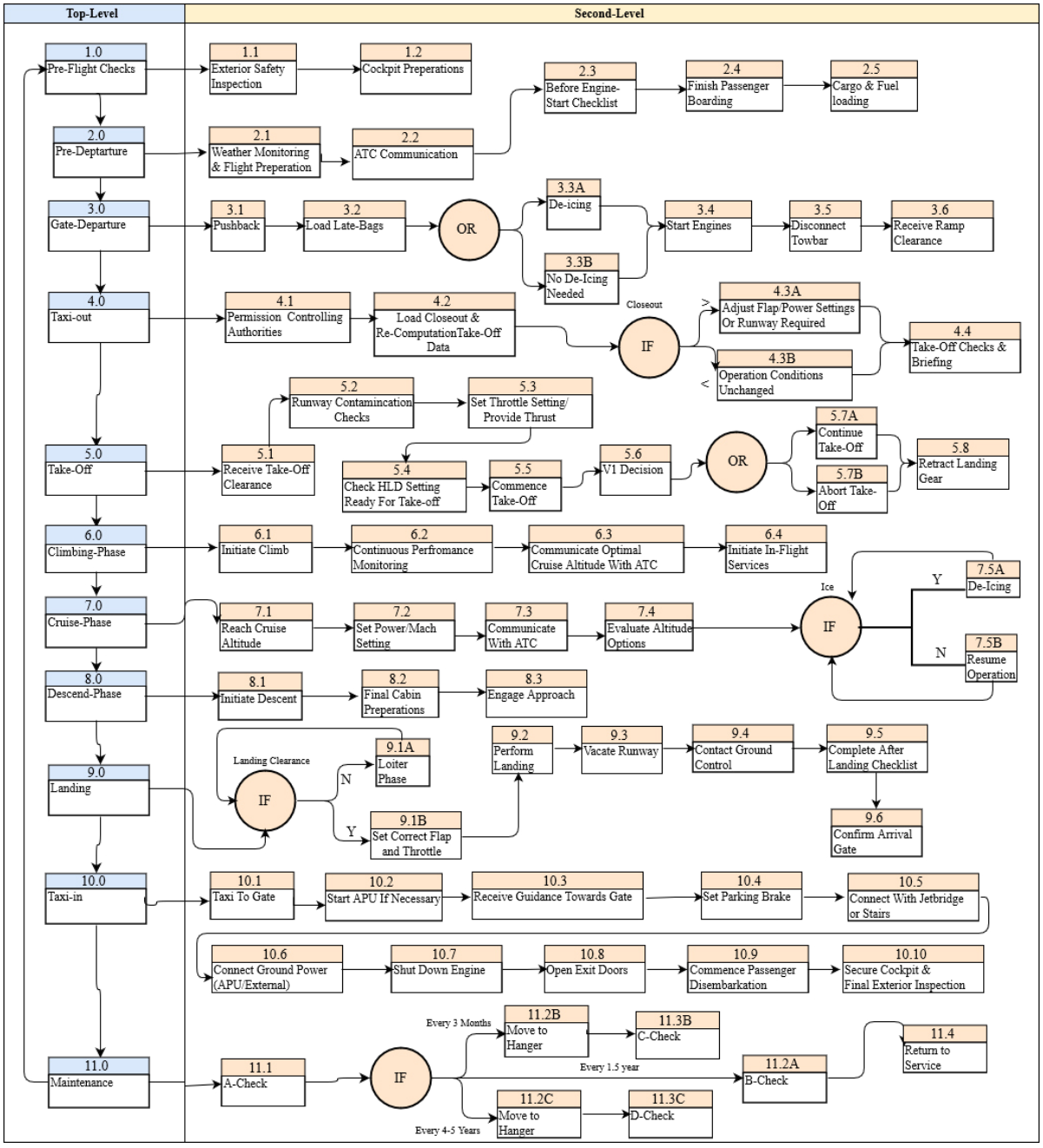

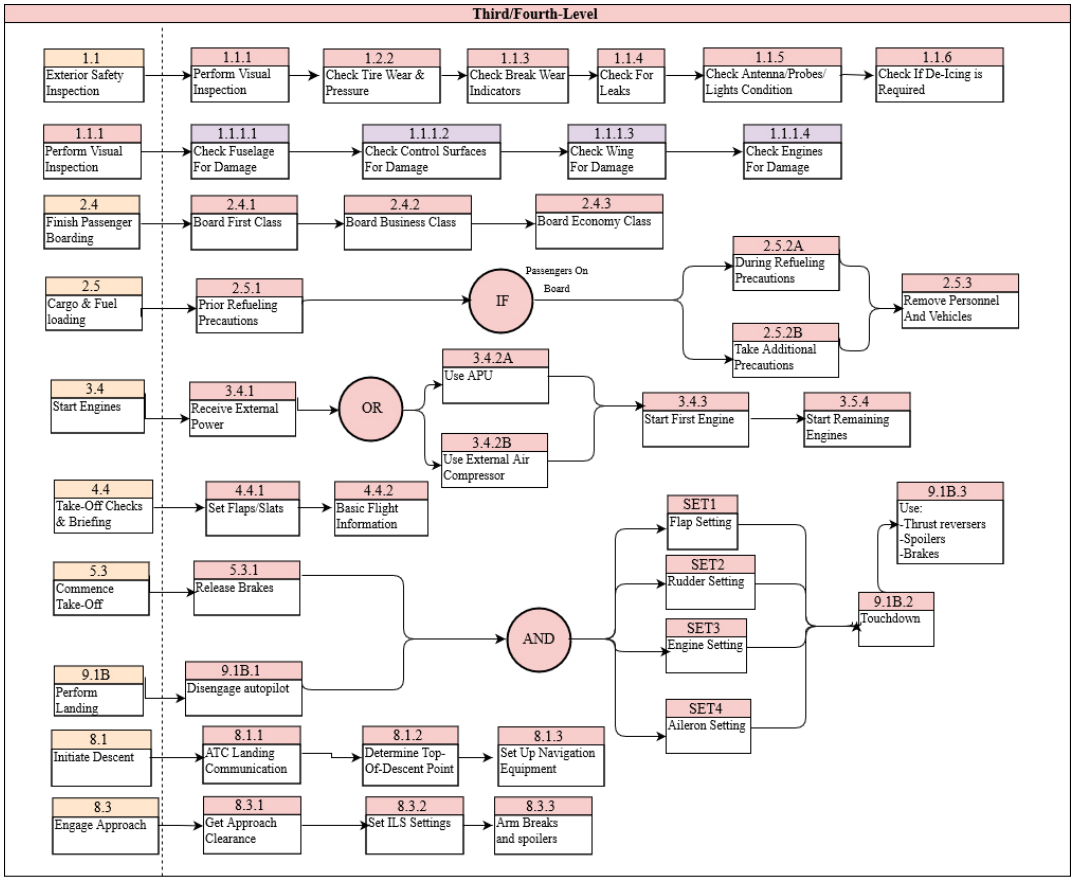

Figure 4.2: Functional Flow Diagram

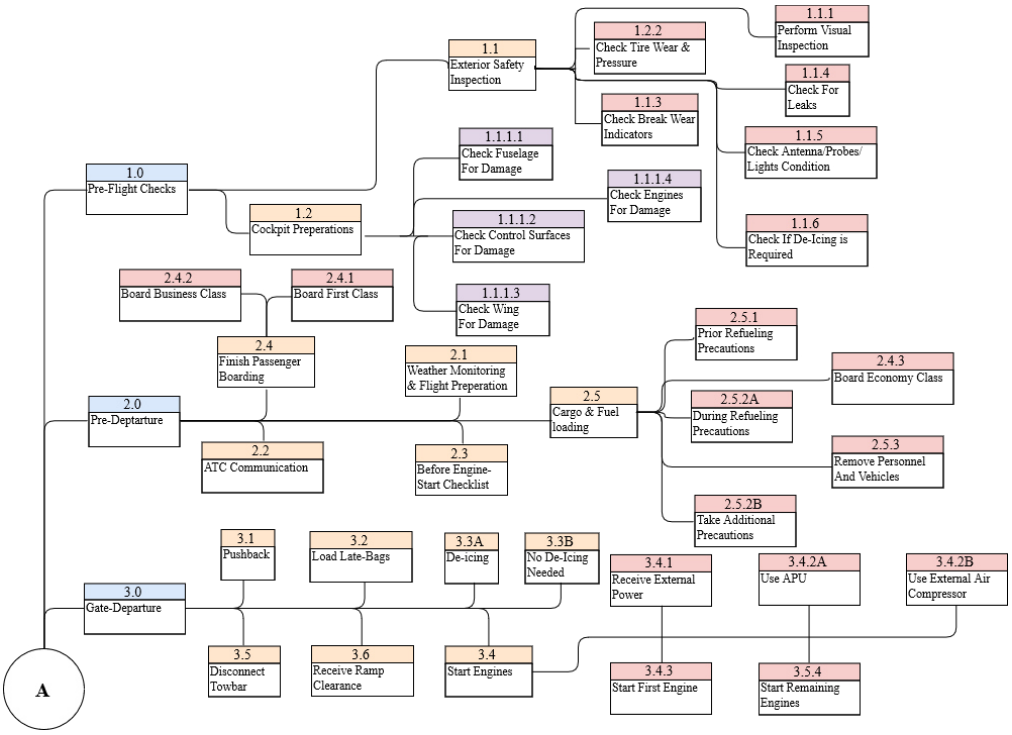

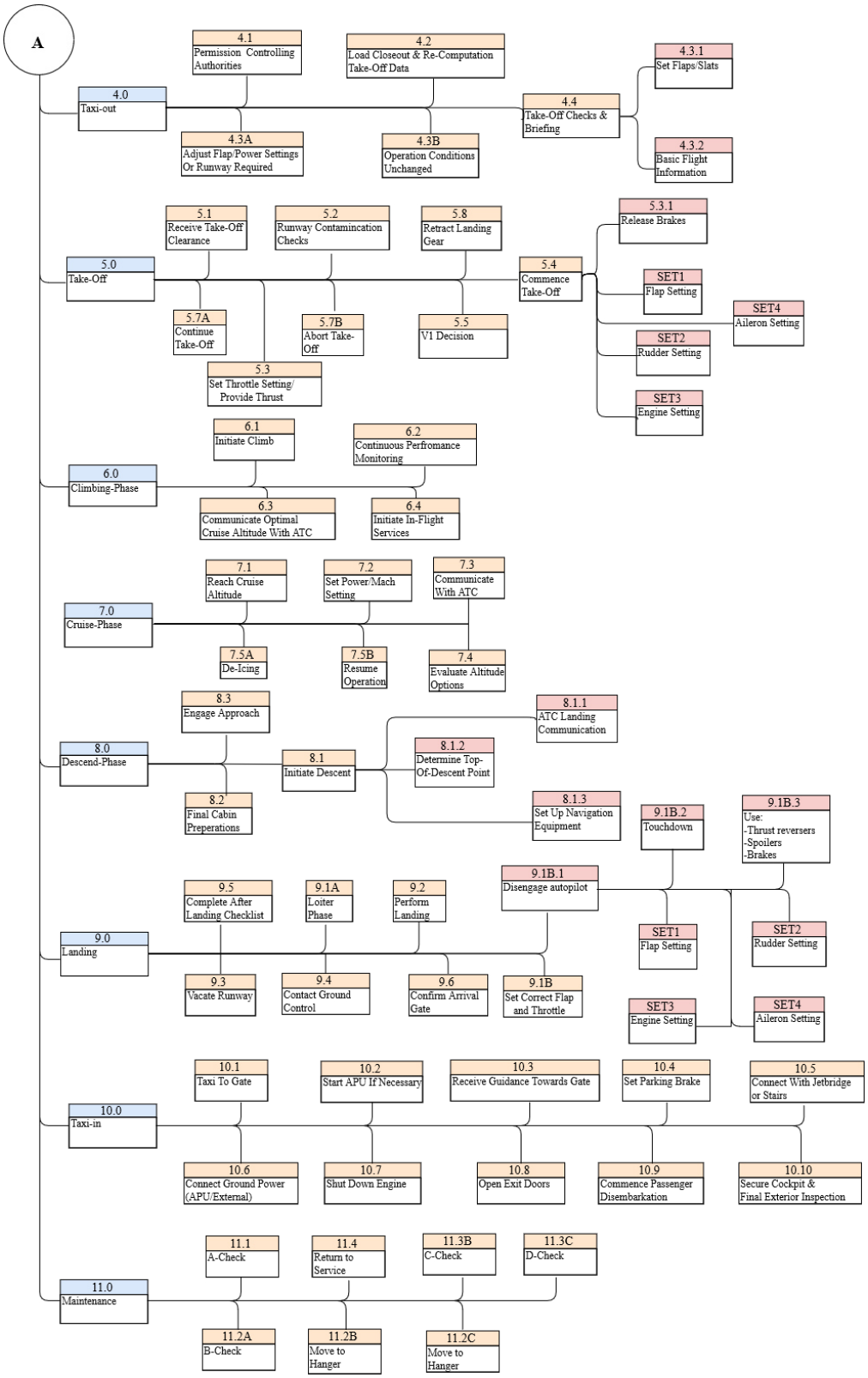

Figure 4.3: Functional Breakdown Diagram

4.3. Mission Requirements

In the project plan the user requirements were established [2]. Some of these requirements were considered killing requirements to the feasibility and the efficiency of the final design. These have therefore been discussed through client communication and some of them have been adjusted accordingly. The specified user requirements for this design project are:

- MOM-UREQ-1: Maximum range at maximum payload shall exceed 5,000 NM.
- MOM-UREQ-2: Cruise speed shall be 0.8 M.
- MOM-UREQ-3: Required runway length for take-off shall not exceed 2,600 m at maximum take-off mass in ISA conditions.
- MOM-UREQ-4: Aircraft shall be compliant with EASA CS-25 airworthiness regulations.
- MOM-UREQ-5: Aircraft shall be at least 40% more fuel efficient than the Boeing 757-200 per seat-km.
- MOM-UREQ-6: At least 75% of materials used on the aircraft shall be reusable.
- MOM-UREQ-7: Maximum passenger capacity shall be more than 229 passengers in a single class configuration.
- MOM-UREQ-8: Total unit cost shall not exceed 160 MUSD.
- MOM-UREQ-9: Operational cost shall be at least 30% lower than the Boeing 757-200.
- MOM-UREQ-10: Passenger comfort levels shall be comparable to the Airbus 350 and Boeing 787.

Some user requirements would pose a threat to the design process and the final design have been analyzed and adjusted in previous reports, resulting in a more feasible set of requirements to design for. Requirements have been assigned a priority, for which the priority identifier meaning has been presented in Table 4.2.

Table 4.2: Requirement Priority Definitions

Priority	Implication
3	The requirement is a "must have" as outlined by policy or law
2	The requirement is needed for improved processing, and the fulfillment of the requirement will create immediate benefits
1	The requirement is a "nice to have" which may include new functionality

The identified user requirements, which will supposedly have a high impact on the final design have been identified and documented, as represented along with the requirement updates achieved through client discussions in Table 4.3.

Table 4.3: Driving Requirements with Client Updates

Identifier	Requirement	Priority	Update Log
MOM-PERF-01	The operational range of the aircraft shall exceed ~~6,000~~ 5,000 nautical miles.	2	Allows for lower MTOW
MOM-PERF-03	Required runway length for take-off shall be less than ~~2,000~~ 2,600 m at MTOW in ISA conditions.	2	Allows for smaller engines and more efficient cruise performance.
MOM-SUST-01	At least 75% of the material used on the aircraft shall be reusable.	2	Not Updated
MOM-SUST-02	Aircraft shall be 40% more more fuel efficient than the Boeing 757-200 per seat-km	2	Not updated
MOM-EC-01	The operational cost per block hour shall not exceed 3,000 USD.	2	Not updated
MOM-EC-02	The unit cost shall not exceed ~~100~~ 160 MUSD~~, which includes amortization of development costs~~.	2	The initial cost price was impossible to meet for this mission

Justification for choosing these requirements as driving requirements will be provided below.

- The operational range requirement was provided by the customer. Other aircraft within the middle-of-the-market category have ranges around 3,100-3,800 NM [5]. This leads to almost double the range for the new aircraft compared to currently available designs in this category. Therefore, investigation has been performed, what a potential lower range would yield. Through a statistical analysis at first and later an analysis based on class-I and class-II methods, it was shown that decreasing the range would yield a signification reduction in MTOW. When the client was confronted with this data, a range of 5,000 NM was accepted upon.

- The minimum take-off runway length of the closest competitor, the Boeing 757, is up to 2,360 m [21]; the new aircraft is required to reduce this distance to only 2,000 m. This requirement will significantly affect the size of the engines and wings in order to ensure the required acceleration and performance for this short take-off distance is obtained. This poses difficulties, since for take-off large engines are required, there may be an extreme excess in thrust in cruise. Especially for the box wing design this poses a threat, since this design should have a lower cruise drag. After discussion with the client, a take-off runway of about 2,600 meters, as it does not limit the market for available operating airports, it was decided to increase the runway length.
- The re-usability requirement will likely limit the choice in materials significantly; certain types of composites are very limited in their recyclability and thus might be excluded from being used in the design.
- The fuel burn per seat-km should be at least 40% more fuel efficient than the Boeing 757 [21]. It is an ambitious requirement that also ties in with the range requirement. It will mostly influence considerations about the drag, the airframe and the efficiency of the engines. This thus ties back to, for example, the runway requirements. If the engine thrust needed for take-off is reduced, more efficient cruise performance can be attained, therefore lowering operating costs. Ambitious as it is, it is hard to put an exact number on what currently is possible.
- The operational cost of the Boeing 757-200 ranges from $4,000 to $4,500 [22]. The new aircraft shall be 30% cheaper to operate than the B757-200 which brings the cost down to about $3,000. This is a considerable reduction and thus was one of the most important factors in the trade-off. However, the reduced drag over long range flight should make this possible.
- Lastly, the fact that the initial unit cost was required to be 100 MUSD would drive the design to an unreasonable extend. Modern aircraft like the Boeing 787 cost around 239-325 MUSD[1]. Especially considering the other requirements, a lot of new technologies will need to be incorporated into the design to adhere to the limitations. Some of these requirements might drive the design beyond reasonable margins.

In order to be able to effectively translate the user requirements into technical requirements, the motivations of the user should be thoroughly understood. Airlines want to reach their destination as fast as possible to reduce operational costs; the minimum speed of Mach 0.8 is derived from this need. The speed to which that Mach number corresponds is a function of the temperature, therefore the cruising altitude influences the Mach number corresponding to a certain speed. If the aircraft is able to efficiently fly at a lower cruising altitude, thus a lower Mach number yet the same actual cruise speed, this might still satisfy the customer. Additionally, the airline wants to ensure that their passengers have a comfortable experience on board in order to effectively compete with the latest generation of aircraft. The passenger experience is a factor of multiple elements, meaning the cabin specifications of the B787 or A350 do not have to be perfectly replicated to meet comfort requirements. The more detailed subsystem requirements derived from user required by use of a requirement discovery tree as presented in the baseline report [3] and have been presented in Table 4.4. The respective updated requirements have been updated.

Identifier	Requirement	Priority
Aiport		
MOM-AIRP-01	The aircraft shall be able to land on tarmac runways	3
MOM-AIRP-02	The aircraft shall be able to land on concrete runways	3
MOM-AIRP-03	The aircraft shall comply with ICAO Aerodrome Reference code IV-D	2
MOM-AIRP-04	The landing gear shall be positioned such that no tip-over will occur during any phase of operation	3
MOM-AIRP-05	The landing gear shall be able to carry the aircraft weight at Maximum Ramp Weight	3
MOM-AIRP-06	The aircraft shall be steerable on the ground for all loading conditions	3
MOM-AIRP-07	The aircraft shall have at least one fuel interface	3
MOM-AIRP-08	The aircraft shall be able to communicate with ground staff	3
MOM-AIRP-09	The aircraft shall be able to configure with jet-bridge interfaces	3
MOM-AIRP-10	The aircraft shall be able to receive pushback	3
MOM-AIRP-11	The aircraft shall be able to load passengers	3
MOM-AIRP-12	The aircraft shall be able to load cargo	3
MOM-AIRP-13	The aircraft shall be able to communicate with Air Traffic Control	3
MOM-AIRP-14	The aircraft shall be able to use current de-icing installations	2
Certification		
MOM-CERT-01	The aircraft shall comply with CS-25 regulations	3
MOM-CERT-02	The aircraft shall meet the climb gradient specified in CS-25.121	3
MOM-CERT-07	In accordance with CS-25.143(a), the aircraft shall be safely controllable and maneuverable in climb, level flight, descent and landing	3

[1] URL `http://www.boeing.com/company/about-bca/#/prices` [cited 3 May 2018]

MOM-CERT-19	In accordance with CS-25.231(a), the aircraft shall have no uncontrollable tendency to nose over in any reasonably expected operating condition or when rebound occurs during landing or take-off	3
MOM-CERT-20	In accordance with CS-25.341, the aircraft shall be able to withstand a positive load factor of 2.5	3
MOM-CERT-21	In accordance with CS-25.783(a), each cabin shall have at least one easily accessible external door	3
MOM-CERT-28	The aircraft shall have a sufficient amount of emergency exits	3
Comfort		
MOM-COMF-01	The aircraft shall have a pressure higher than 0.8 bar	2
MOM-COMF-02	The aircraft shall have a comparable humidity to the Boeing 787 and Airbus A350	2
MOM-COMF-03	The seating area per passenger shall be comparable to the Boeing 787 and Airbus A350	2
MOM-COMF-04	The aircraft overhead compartment shall be able to contain at least one standard size carry-on bag per passenger	1
MOM-COMF-05	The aircraft shall have an in-flight entertainment system	1
MOM-COMF-06	The aircraft shall have a TBD amount of passengers per lavatory	2
MOM-COMF–07	The aircraft aisle shall be able to contain a service trolley	3
MOM-COMF-08	The aircraft cabin noise shall be comparable to the Boeing 787 and Airbus A350	2
Performance		
MOM-PERF-01	The aircraft shall have an operational range of at least 5,000 NM	2
MOM-PERF-02	The aircraft shall have an operational long range cruise speed of 0.8 Mach	2
MOM-PERF-03	Required runway length for take-off shall be less than 2,600 m at MTOW in ISA conditions	2
MOM-PERF-04	Maximum passenger capacity shall be greater than or equal to 230 in a single-class configuration	2
Sustainability		
MOM-SUST-01	At least 75% of the material used on the aircraft shall be reusable	2
MOM-SUST-02	Aircraft shall burn no more than 0.0114 kg of fuel per seat kilometer (in single class configuration)	2
MOM-SUST-03	The aircraft shall comply with airport noise regulations	3
Economic		
MOM-EC-01	The operational cost per block hour shall not exceed 3,000 USD	2
MOM-EC-02	The unit cost shall not exceed 160 MUSD, which includes amortization of development costs	2
MOM-EC-03	The aircraft shall enter into service before 2035	1

5
Preliminary Design

This chapter provides a brief overview of the work done and decisions made. In section 5.1 the decisions made in previous reports with regards to the design concept are revised and briefly explained. Then, in section 5.2, the trade-off results and summary is provided, showing the final concept decision made in the midterm report [4]. Next, the hybrid concept, which in this report will be further designed for, will be presented in section 5.3. Lastly, the final result is then given in section 5.4.

5.1. Design Concepts

From a previously conducted baseline research and extensive design option evaluation [3], three distinct concepts were defined using an extensive design option tree. The design option tree aimed at discovering all possible design options for the different aircraft subsystems. These options were then evaluated, the unfeasible ones eliminated and from the remainders three promising concepts were assembled. The three concepts were deliberately designed with feasible, yet differing wing configurations and propulsion systems, so hybrid designs would be possible when conducting a trade-off in order to establish an optimal configuration for this design.

5.1.1. Concept I - Box Wing Aircraft

The box wing aircraft, commonly referred to as 'Prandtl plane', makes use of two wings. The front wing, placed on the lower end of the fuselage, is swept backwards while the back wing, located at the high end of the fuselage, is swept forward. The tips of these two wings are then connected by a vertical structure creating a box-like look, hence the name. The box wing configuration is said to improve the induced drag in comparison with conventional aircraft. As propulsion system a turbo-electric system was selected. This system makes use of a turbo-generator (turbine) providing electrical energy for a set of distributed propellers, providing the necessary thrust.

5.1.2. Concept II - Strut-Braced High-Wing Aircraft

The strut-braced high-wing aircraft has its wing mounted above the fuselage, reinforced by a strut connected to the bottom of the fuselage. This strut generates a bending relief in the wing, making it possible to significantly increase the aspect ratio, which in turn reduces the induced drag of the aircraft. The configuration is powered by two fuselage-mounted open rotor engines (propfans). Open rotor engines feature two sets of counter-rotating fans on the outside of the engine. These engines offer a vast increase in efficiency compared to even the most modern high-bypass turbofans.

5.1.3. Concept III - Optimized Conventional Aircraft

This concept consists of a standard low-wing conventional configuration aircraft, powered by two of the latest generation turbofan engines. The design will be improved compared to aircraft like the B757-200 by using new aerodynamic techniques. It will feature an improved nose design to decrease form drag and winglets to reduce induced drag. The modern turbofan engines will also be equipped with chevrons to reduce noise. This concept uses technology that has already been successfully deployed and has extensive flight

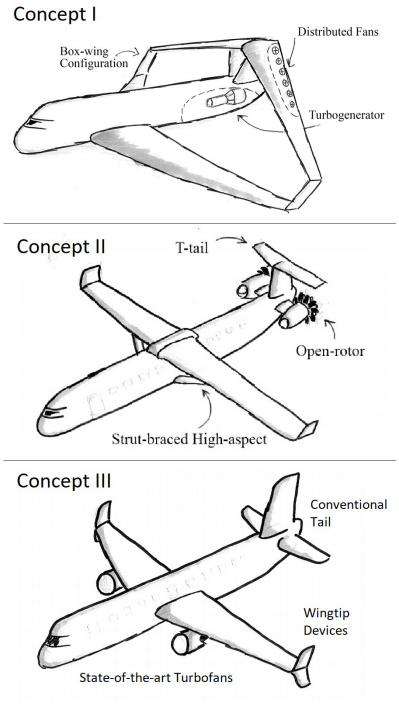

Figure 5.1: Visualization of the Three Concepts

heritage, it will therefore have a lower technical risk and development cost.

5.2. Design Trade-Off Summary

Out of these three concepts one final concept was chosen to analyze and design in further detail. This was done on the basis of a trade-off which will be summarized in this section. However, these concepts and their systems are chosen as to have diversity in subsystems, like the wing locations and propulsion systems. This is done to analyze the most different systems and thus room is left open for hybrid concepts in the end of the trade-off, if it is seen one concept is losing out just because of one system. For example, the propulsion system of concept II can be put on concept III or concept I, or vice versa.

In this section, first the weighting system, trade-off criteria, and scoring system are outlined. Then, a justification to the given scores is given. Next, the results of the trade-off between the three concepts is shortly explained. Then, a hybrid concept is taken into account accompanied by the results of the trade-off with this hybrid concept included.

5.2.1. Weighting System

First, a weighting system for the trade-off is set up. The weighting is done on a scale from 1 to 5. Where 5 is a critical criterion and 1 is still an important consideration, however less important than criteria with higher weights. A scale from 1 to 5 was chosen to lessen the gap between some criteria. Although, weights 1 and 2 are not really apparent in the final trade-off, they were present in a first draft of the trade-off, and therefore it was chosen to keep the weighting scale the same to keep the relative gaps the same, and not switch to, for example, a 1-3 scale.

5.2.2. Trade-off Criteria

Then, the trade-off criteria were set up. Seven main categories became apparent during the brainstorm session of the criteria. These, together with their sub criteria, are:

1. **Maintainability**
    - Accessibility
    - Complexity
2. **Performance**
    - Lift-to-drag ratio in cruise
    - Cruise speed
    - Weight
    - Cruise drag
    - Specific fuel consumption
    - $\Delta C_{L_{max}}$
3. **Ground Operations**
    - Airport accessibility
    - Ground accessibility
4. **Sustainability**
    - Emissions
    - Environmental noise
5. **Costs**
    - Unit cost
    - Operational cost
6. **Comfort**
    - Boarding
    - Seating
    - Cabin noise
7. **Risk**
    - Development risk
    - Operational risk
    - Manufacturing risk.

These sub-criteria all have their respective weighting, and the main criteria also have a weight. Together they lead to a final score, as shown in Table 5.1. An explanation on the scoring and results will be given after Table 5.1. In Table 5.1, the last column with the scoring for a "hybrid concept" can be ignored for now; this will be explained later on in this section.

5.2.3. Scoring System

The scoring was, just as the weighting system, done on a scale from 1 to 5. A score of 1 is given for performance highly below average or even impossibility of the design, a score of 5 for the best possible performance in a criterion. Most of the trade-off was performed qualitatively, since it was hard to quantify some parameters for the more novel concepts. The main aspect of this trade-off, though, is that the three concepts are scored against each other, so they are each others baseline and compared to each other.

To reduce bias the group of nine students is split up into three groups of three. Each group consists of one person per concept, so there is adequate knowledge of all concepts within a group, and there should be no favoritism

Table 5.1: Total Scoring

Parameter	Weight	Concept I	Concept II	Concept III	Hybrid Concept
Maintainability	4.0	1.8	2.3	4.3	3.5
Performance	5.0	4.4	3.4	3.3	4.1
Ground Operations	4.0	4.1	3.6	3.9	4.1
Sustainability	5.0	4.6	3.4	3.0	3.8
Costs	4.0	2.6	3.5	3.7	3.8
Comfort	3.0	3.6	2.6	3.3	3.5
Risk	3.0	1.9	3.4	4.5	4.1
Total Weighted Average	-	3.41	3.19	3.67	3.84

towards a concept. Moreover, this rules out the risk that people will score their own concept higher than the others (bias). Furthermore, this helps with individual decision making, instead of being lead into following other person's opinions in the scoring. For example, if one person scores something a 4, the next person is automatically more drawn towards scoring it a 4, too. Besides, the scores of three group members are well thought out, and the three groups each give their scores. In the end, these scores are averaged to reduce bias even further, so that a fair trade-off can be performed.

5.2.4. Justification of Scores

Now that the scoring system has been explained, the actual scores can be explained. This will be done per main criterion.

Maintainability

- **Accessibility**: High wings and engine position in concept I and II make accessibility worse. Concept III can be a problem in terms of accessibility because it is going to be high off the ground if high-bypass engines are used. Yet, overall accessibility is best as most parts can be accessed from ground level.
- **Complexity**: Concept I and II's more novel nature make them more complex as they make use of unproven technology, and are thus harder to maintain. Concept I has more outlandish systems - like the turbo-electric propulsion system - and is thus more complex than concept II. Furthermore, concept II calls for folding wings if it wants to operate from the same airports as concept I and III, this raises its complexity. Concept III is still complex, however it is a well proven design with established procedures, lowering its complexity.

Performance

- **Lift-to-drag ratio**: Concept I has the best lift-to-drag ratio; concepts II and III lie rather close together, but concept III performs slightly better in cruise.
- **Cruise speed**: Concept I and III can easily meet the 0.8 Mach requirement. Concept II, however, cannot. Due to shockwave interaction between strut and wing, it can only reach 0.72 Mach. Thus, it has to fly at a lower altitude to retain a similar ground speed as the other concepts.
- **Weight**: In terms of weight, concept I and CII are very close to each other, concept II is only 1,500 kg heavier, whereas concept III is a whole 30,000 kg heavier. However, it is not unacceptably heavy as comparable aircraft are not that much lighter.
- **Cruise drag**: Concept II has a considerably higher drag, because it has to fly at a lower altitude.
- **Fuel consumption**: Regarding the fuel consumption, concept II yields the best SFC. Concept III already pushes today's limits. A lot of uncertainty occurs for concept I's turbo-electric propulsion system, i.e. estimates go as either 25% lower or higher than concept III.
- $\Delta C_{L_{max}}$: A last criterion for the performance is the $\Delta C_{L_{max}}$, as a high value calls for more and more complex high-lift devices. All concept call for around the same $\Delta C_{L_{max}}$. During preliminary calculations, concept III needed only a $\Delta C_{L_{max}}$ of 0.7, which seemed low, so it was assumed a calculation error was made and thus concept III was given a similar score to concepts I and II.
- In Table 5.1, it can be seen that concept I is the clear winner with respect to performance.

Ground Operations

- **Airport accessibility**: When looking at airport accessibility, concept II lacks behind, because of its aforementioned larger wing span. Concept II would be an ICAO Aerodrome Reference Code E aircraft, whereas the other concept, as well as the B757 are code D aircraft[1]. This implies it can operate from a lot less airports, which conflicts highly with the purpose of the MoM-liner. The other concepts are both easily able to meet the requirement.
- **Ground accessibility**: For ground accessibility the complete opposite is true, concept II scores best there. This for the fact that it has a high-wing and the engines are located high, so it can have short landing gear, and thus the aircraft will be low to the ground. The one thing that can cause a difficulty is the strut, which trucks need to be wary about. On the other hand, however, the strut is approximately placed where the engine is placed for conventional aircraft, so not that much changes. Therefore, accessibility when the aircraft is on the ground is quite well for concept II. Concept I and III score lower, as they both have a low wing, concept III even has an engine mounted under the wing, which calls for longer landing gear, and thus the aircraft will be higher off the ground. Furthermore, for concept I connecting a second jet bridge may cause problems because of the box wing structure, i.e. a wing will be in the way.

Sustainability

- **Emissions:**: Emissions are closely related to the specific fuel consumption, however, also the type of propulsion system and types of exhaust gases are important. The turbo-electric propulsion system of concept I is a very green system in this respect, so it scores best in this category. The open rotor propulsion of concept II also has less NO_x emissions than concept III.
- **Environmental noise**: The open rotor system nowadays is dramatic in terms of noise, mainly due to the second (counter-rotating) rotor. The turbofan engines also produce significant noise, even if implementing the most current technology, such as chevrons. The turbo-electric propulsion system produces less noise, and thus scores best in this criterion.

Costs

- **Unit cost**: Due to the novel nature of concepts I and II, they will have more research and development cost and thus a higher unit cost; concept I more than concept II.
- **Operational cost**: The three concepts are projected to be 39.5, 25.0, and 18.5%, respectively, cheaper in operational cost than the B757. However, it should be noted there is a lot of uncertainty regarding concept I.
- It can be seen, in Table 5.1, concept I is really losing out in the cost criteria.

Comfort

- **Cabin noise & Boarding**: Concept II can be significantly worse for comfort, mainly due to the cabin noise from the open rotor propulsion. Besides, it has the potential inability to connect jet bridges, since it is so low to the ground. Concept I and III are comparable in terms of comfort, only concept I will have less cabin noise due to the quieter propulsion system.
- **Seating**: The same seats will be used in all three concepts, so there is no distinction to be made in this category.

Risk

- **Development, Operational & Manufacturing risk**: For concept III the risk is seen as low, as it is a proven design. All risks increase for concept II due to the novelty of the configuration for transport aircraft. Concept I has the highest values by a margin, mostly due to the very low technology readiness level of the propulsion system but also the unproven box-wing configuration. This is reflected in the high uncertainty for most of the performance figures for this concept.
- Again, this category, together with costs, is the criteria where concept I performs exceptionally poorly.

[1] URL `https://www.skybrary.aero/index.php/ICAO_Aerodrome_Reference_Code` [cited 20 June 2018]

5.2.5. Results

The final weighted scores can be seen in Table 5.1, with one more significant digit than the scores, for clarity's sake. Concept III is the winner of the trade-off between these three concepts. However, as also explained in the previous reports and previously in this section, room is left open to come up with a hybrid concept. Researching these three concepts, and after performing the trade-off, it was observed that a hybrid concept is actually relevant for this design. This will be elaborated upon in the next subsection.

5.3. Hybrid Concept

As explained, assembling a hybrid design was deemed very relevant. During the trade-off, it was recognized that concept I was performing poorly because of its outlandish turbo-electric propulsion system, while it had promising results for the airframe alone. Therefore, it was chosen to replace the propulsion system on concept I with that of concept III. The open rotor engines from concept II still show some drawbacks, and high-bypass turbofans can be efficient and less noisy. Hence it was chosen to opt for turbofan engines instead of open rotor engines to replace the turbo-electric propulsion system of concept I. With this change implemented, this new hybrid concept was also included in the trade-off. The results can be seen in the last column of Table 5.1. It can furthermore be seen that the hybrid design actually outperforms the other concepts. A box wing turbofan representation can be found in 5.2.

Figure 5.2: Artistic Illustration of Generic Box Wing Concept [23]

5.4. Final Result

After the final trade-off, it could be seen the hybrid design is the winner, and thus, according to these criteria, the most optimal design choice. The hybrid concept is not winning by a great margin, with the conventional aircraft closely behind it with a margin of 0.17. However, choosing the conventional aircraft, while having lower technical risk, has an increased risk of not being able to meet the efficiency requirements. Choosing a new and promising concept opens the option to have vast improvements in efficiency. For example, the hybrid concept can have extremely high bypass ratio turbofans with an even larger bypass ratio than the turbofans on concept III, because of ground clearance issues. Furthermore, control surfaces on this aircraft can be a lot smaller, and this aircraft can descend and ascend steeper. Therefore, due to the extra potential, the hybrid design was chosen for further investigation in the next phase, presented in this report. Thus, the box wing aircraft with high-bypass turbofan engines was selected to be the final design.

6
Preliminary Sizing Methodology

Once the general concept selection is finished, now the winning concept needs to be analyzed further to generate specific inputs that will be used by all other specialized departments. The preliminary sizing methods are similar to the ones used in the midterm report [4]. First, the class-I weight estimation is outlined in section 6.1. This report also discusses the class-II weight estimation as described by Torenbeek [24], with updated weight estimation equations specifically for the box wing design. Finally, the design space is presented in section 6.3 to determine the necessary wing area and thrust.

6.1. Class-I Weight Estimation

Using the design mission profile from the previous report [4], an initial weight estimation can be performed to get a first estimation of the take-off weight (W_{TO}), operational empty weight (W_{OE}) and fuel weight (W_F) of the aircraft. The class-I weight estimation is based on the concept of fuel fractions. The general outline is described in this section and based on a methodology described by Roskam [25].

The takeoff weight can be broken down into the sum of the operational empty weight (W_{OE}), the fuel weight (W_F) and the payload weight (W_{PL}), as depicted in Equation 6.1.

$$W_{TO} = W_{OE} + W_F + W_{PL} \tag{6.1}$$

The first step in the class-I weight estimation is estimating the mission payload weight. This is done based on average weights of passenger and crew and the average luggage weight that is brought along on a flight. In Table 6.1 the inputs used to compute the payload weight is depicted. These inputs are determined from statistics [25].

Table 6.1: Input Parameters

Payload Masses [kg]	
Passenger Mass	88
Passenger luggage Mass (per person)	16.8
Crew luggage Mass (per person)	13.6
Number of Passengers	234

After obtaining the mission payload weight, the needs to be initiated by guessing a likely value for the take-off weight $W_{TO_{guess}}$. This value is always based on statistical data and will be changed as the iterative process runs.

The fuel weight is determined through the fuel fraction method. For the less fuel intensive phases of the flight, the fuel used during each phase is obtained from statistical data. This is done for the engine start-up, taxi, take-off, climb and acceleration, descent, landing and shut-down phase. For the more fuel intensive phases, the fuel used during the respective phase is estimated using the Breguet equations. For the cruise phase, the fuel used is estimated using Equation 6.2 for propeller aircraft and Equation 6.3 for jet aircraft. In these equations, the important parameters include the range of the cruise phase, the $\frac{L}{D}$ during the cruise phase and specific engine characteristics.

$$R_{cr} = 375 \cdot \left(\frac{\eta_p}{c_p}\right)_{cr} \left(\frac{L}{D}\right)_{cr} ln\left(\frac{W_4}{W_5}\right)_{prop} \tag{6.2}$$

$$R_{cr} = \left(\frac{V}{c_j}\right)_{cr} \left(\frac{L}{D}\right)_{cr} ln\left(\frac{W_4}{W_5}\right)_{jet} \tag{6.3}$$

Equation 6.4 and Equation 6.5 are used to calculate the fuel used during the loiter phase for propeller aircraft and jet aircraft respectively. The fuel used during this phase is mainly dependent on the same parameters as for the

cruise phase. Only the speed and engine performance during the loitering phase differ as now the objective is to minimize total power requirements, not to cover distance.

$$E_{ltr} = 375 \cdot \left(\frac{1}{V_{ltr}}\right)\left(\frac{\eta_p}{c_p}\right)_{ltr}\left(\frac{L}{D}\right)_{ltr} ln\left(\frac{W_5}{W_6}\right)_{prop} \quad (6.4) \qquad E_{ltr} = \left(\frac{1}{c_j}\right)_{ltr}\left(\frac{L}{D}\right)_{ltr} ln\left(\frac{W_5}{W_6}\right)_{jet} \quad (6.5)$$

Once the fuel used during every phase is determined, the mission fuel fraction is determined using Equation 6.6.

$$M_{ff} = \left(\frac{W_1}{W_{TO}}\right)\sum_{i=1}^{i=n}\left(\frac{W_{i+1}}{W_i}\right) \quad (6.6)$$

The total fuel weight can then be determined using Equation 6.7, also taking into account the reserve fuel $W_{F_{res}}$.

$$W_F = \left(1 - M_{ff}\right) W_{TO} + W_{F_{res}} \quad (6.7)$$

Using the estimated take-off weight, fuel weight and payload weight, a tentative value for the operational empty weight can now be determined using Equation 6.8.

$$W_{OE_{tent}} = W_{TO_{guess}} - W_F - W_{PL} \quad (6.8)$$

A value for the empty weight of the aircraft is then obtained by subtracting the weight of the crew and trapped fuel & oil (W_{tfo}) from $W_{OE_{tent}}$ (Equation 6.9).

$$W_{E_{tent}} = W_{OE_{tent}} - W_{tfo} - W_{crew} \quad (6.9)$$

The tentative value for the empty weight $W_{E_{tent}}$ is subsequently compared to an 'allowable value' for W_E. This allowable value for W_E can be obtained from linear relations between $log_{10}W_E$ and $log_{10}W_{TO}$, which are based on statistical data and can be found for many different aircraft types. Once an allowable value for W_E is obtained, this value is compared to the tentative value for the empty weight $W_{E_{tent}}$. The final step is to compare W_E and $W_{E_{tent}}$. Usually, these initial values lay quite far apart. If W_E and $W_{E_{tent}}$ differ more than 0.5%, an adjustment is made to the estimated take-off weight $W_{TO_{guess}}$. Once W_E and $W_{E_{tent}}$ lie within the required 0.5% margin, the final value for the take-off weight is obtained.

6.2. Class-II Weight Estimation

Once the class-I weight estimation gives convergent values for the take-off weight, and the conceptual layout of wing, fuselage and engines has advanced, a class-II weight estimation can be performed. The class-II weight estimation is much more refined as it splits the aircraft up into many different subcomponents and computes weights per subcomponent. This allows for a more refined input, based on the actual design parameters instead of pure statistical values, and thus gives more accurate results when all contributions are summed up. For this design, the method and equations used follow from Troenbeek [26]. The only adjustments that were done are concerning the wing and the fuselage weight, as for those two parameters the box wing design has special implications and thus needs different formulas not included in Torenbeek's method.

Adjustment for Fuselage and Wing Weight

The class-II weight estimation method is based on the assumption that the wing is a cantilever beam, which in the case of the box wing is not applicable. There are two ways to solve this problem. The first solution is to generate a model which uses a physics based approach in order to size (and estimate) the weight of the wing and fuselage. Considering the scope of this project, and the limited time, this option was deemed too time intensive. The second option is to perform a literature study and consult experts, to determine a factor that the results of the class-II can be multiplied with to resemble the weights of the box wing components.

Fuselage Weight

Schmidt and Vos [27], show a 21% reduction in fuselage weight for a box wing compared to a conventional design due to additional support from the second wing. Their analysis uses a physics based approach and is therefore considered quite accurate.
Another comparison done by Zohlandt [28] determined that the weight of the fuselage for a Prandtl plane and a conventional aircraft with identical missions differ by about 15% . This was determined using a design software package setup by the FPP department at the TU Delft[1]. This software uses the mentioned method by Schmidt and Vos. This design software has been update recently, and therefore the 15% reduction needs to be adjusted. According to Rousseau [29], the fuselage weight estimation should be improved by a further 6% . This brings the total fuselage weight reduction, compared to a similar conventional aircraft, to 15.9%. This factor will be used to adjust the outcome of the Class-II fuselage weight estimation.
Taking these two values into account a reduction of 16-21% is expected for the fuselage weight. A value very close to 15.9% is expected, as this is the most up to date value. To incorporate this reduction, the class-II weight estimation will be run, after which this factor will be applied to determine the final fuselage weight.

Wing Weight

Conventional class-II weight estimations do not take into account the additional weight difference due to the Prandtl-plane wing configuration. Multiple weight estimations for Prandtl-plane wings have been researched. The most common correction for box wings from normal wings is based on a weight estimation method by Howe [30]. The correction factor employed to account for the addition of the vertical struts connecting the wings has a value of 0.11 [28, 31]. However, as other class-II weight estimations have been performed using Torenbeek's methods, it is necessary to stick to this method for the wing weight estimations. It is assumed that the 0.11 weight factor still holds for the vertical connectors, but the weight of the separate wings is estimated with Equation 6.10 from Torenbeek.

$$W_{wing} = 0.0017 W_{MZF} \left(\frac{b}{cos(\Lambda_{c/2})}\right)^{0.75} \left(1 + \left(6.3 \frac{cos(\Lambda_{c/2})}{b}\right)^{0.50}\right) n_{ult}^{0.55} \left(\frac{bS}{\tau W_{MZF}} \frac{1}{cos(\Lambda_{c/2})}\right)^{0.30} \tag{6.10}$$

6.3. Design Space Diagram

After the initial weight estimation has been performed, the design space diagram can be generated. From this diagram, the wing surface area and the thrust/power can be deduced. These parameters are of essence in further analysis of chosen concepts. The analysis of the propulsion system can only be continued in more detail once the thrust/power is known and the aerodynamic analysis can only be further continued once the wing surface area is known. Both these parameters can be obtained by the combination of the design space diagram and the initial weight estimation.

The design space is generated by sizing the aircraft for the criteria depicted below. For each criteria the sizing is done by expressing the $\frac{T}{W}$ as a function of $\frac{W}{S}$. The obtained functions are then combined to yield a plot from which the desired $\frac{T}{W}$ and $\frac{W}{S}$ can be read. The equations implemented for each criteria are depicted as well as the inputs required. The methods presented in this section follow the methods as shown in [32].

1. **Sizing to stall speed requirements:** the stall speed can become limiting in three situations - cruise, takeoff and landing. For each situation the limits are found by using Equation 6.11.

$$\frac{W}{S} = \frac{1}{2} \rho V^2 C_{L_{MAX}} \tag{6.11}$$

2. **Sizing to takeoff requirements:** these requirements are sized by Equation 6.12. An important parameter in this equation in the takeoff parameter (TOP). This parameter is determined by statistical values. Furthermore it can also be seen that a correction factor for altitude effects ($\sigma_{airport}^{0.75}$) is included to account for atmospheric properties.

$$\frac{T}{W} = \frac{\frac{W}{S}}{TOP} \frac{1}{C_{L_{TO}} \sigma_{airport}^{0.75}} \tag{6.12}$$

[1] URL https://www.tudelft.nl/en/ae/organisation/departments/aerodynamics-wind-energy-flight-performance-and-propulsion/flight-performance-and-propulsion/flight-performance/research/aircraft-design-design-methodologies/ [cited 11 June 2018]

3. **Sizing to landing distance requirements:** the landing requirements are sized with the use of Equation 6.13.

$$\frac{W}{S} = \frac{C_{L_{MAX}} \rho V_{s_{land}}^2}{2f} \tag{6.13}$$

Where the landing stall velocity is derived by a statistical relation shown in Equation 6.14 and f is derived from Equation 6.15 [32].

$$V_{s_{land}}^2 = \frac{S_{land}}{0.5915} \tag{6.14}$$

$$f = \frac{W_{land}}{W_{TO}} \tag{6.15}$$

4. **Sizing to climb rate requirements:** the climb rate sizing criteria is determined by Equation 6.16. The minimum ROC in specific configurations is given by CS-25 and should be considered in sizing.

$$\frac{T}{W} = \frac{1}{\sigma_{cruise}}^{0.75} \frac{ROC}{\sqrt{\frac{W}{S}}\sqrt{\frac{2}{\rho C_{L_{TO}}}}} + \frac{C_D}{C_L} \tag{6.16}$$

The ROC is determined by the CS-25 requirements [20]. The lift and drag coefficient are determined by Equation 6.17 and Equation 6.18.

$$C_L = \sqrt{3 C_{D_0} \pi A e} \tag{6.17}$$

$$C_D = 4 C_{D_0} \tag{6.18}$$

5. **Sizing to climb gradient requirements:** when sizing for the climb gradient an extra factor must be taken into account. That is the fact that an engine should still be able to reach the required climb gradient with one engine inoperative (OEI). The minimum required climb gradients for different configurations is specified in the CS-25 regulations [20]. To take this into account the sizing to climb gradient was coded such that both the case with all engines operative and the case with OEI is computed. From these two situation the most restricting situation is limiting. The climb gradient is defined as $\frac{c}{V}$.

In the case that a single engine fails, Equation 6.19 is scaled by the first fraction in the equation. This fraction should only be taken into account when there is one engine inoperative.

$$\frac{T}{W} = \frac{N}{N-1}\left(\frac{c}{V} + 2\frac{C_{D_0}}{\pi A e}\right) \tag{6.19}$$

6. **Sizing to cruise speed requirements:** To size for the cruise speed requirements Equation 6.20 was used.

$$\frac{T}{W} = \frac{z}{k}(\sigma_{cruise})^{0.75} \cdot \left[\left(\frac{0.5 C_{D_0} \rho V^3}{k\frac{W}{S}} + k\frac{W}{S}\frac{1}{0.5\pi A e \rho V}\right)\right] \tag{6.20}$$

where k is the percentage of the MTOW and z is the power setting of the engines in cruise.

Now, all lines should be plotted together in a graph, and the unfeasible design space (W/P too high; T/W too low) should be marked. In the case of a propeller driven aircraft the optimal design point would lie in the uppermost right corner. In the case of jet driven aircraft the optimal design point would lie in the right lower corner of the acceptable design space.
Together with the initial weight estimation and the $\frac{W}{S}$ and $\frac{T}{W}$ the wing reference area and the required thrust are derived. The design space diagram can be found in section 12.2.

$$S_{ref} = W_{TO} \cdot \left(\frac{W}{S}\right)^{-1}, \quad T_{req} = W_{TO} \cdot \frac{T}{W}$$

7
Aerodynamic Analysis

In this chapter the aerodynamic analysis methodology is outlined. First an overall summary is presented in section 7.1 on the aerodynamic methodology. Then in section 7.2 the method of the aerodynamic analysis is presented, outlining the path followed to compute aerodynamic outputs. Lastly, section 7.3 gives more detail on the verification and validation of the used tools and the obtained results.

7.1. Summary Methodology

To obtain an optimal aerodynamic design and the lowest cruise drag possible, the aircraft has to be optimized for a high $\frac{L}{D}$ in cruise. The computations are done using Tornado Vortex Lattice Methods (VLM), an open source software. Since the class-II weight estimation uses an estimated $\frac{L}{D}$ obtained from statistics, and interactive loop is introduced to feed the $\frac{L}{D}$ obtained from Tornado VLM back into the weight estimation code. This is done until convergence is met as can be seen in Figure 7.1. Chronologically, data is received from the weight estimations & preliminary sizing, which is then passed on to the $\frac{L}{D}$ optimizer, after which the wing optimizer provides a complete wing planform. This is passed on the VLM program to obtain aerodynamic coefficients. At this point the difference between the class-II estimation and the VLM are compared and fed back if not within 1% margin to obtain the optimal component weight distribution. If this condition is met, the data is stored in the aircraft object, which is then passed on to stability, structures and performance.

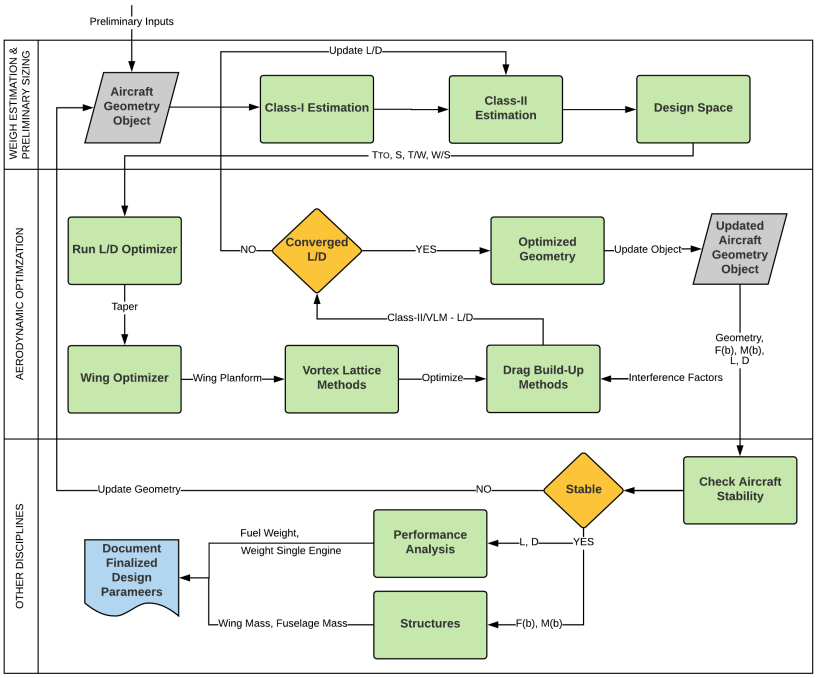

Figure 7.1: General Data Flow Within the Aerodynamic Analysis

7.2. Methodology

7.2.1. Drag Components

The lift of an airfoil can be accurately calculated using the assumption of invicid flow by use of the Kutta condition at the trailing edge, but using the same approach to approximate the drag however, yields zero drag, also known as d'Alembert's Paradox [33]. This paradox is removed when viscosity is taken into account, which causes drag through imploring two mechanisms:

- Introducing skin-friction drag due to shear acting on the wing surface
- Introducing pressure drag due to flow separation

It is important to understand the implications and the limitations when using software which uses techniques which do not estimate the drag properly. This is required to be able to account for these effects to provide a more accurate representation. Besides the inaccurate airfoil based estimations, other drag components are not directly accounted for, mainly the interference drag is hard to estimate. The interference drag is the drag caused by bringing two bodies in close proximity to each other, the bodies interaction changes the properties obtained. One can account for this drag component by applying the component drag build-up method [34]. In this method the subsonic parasite drag can be estimated by using the skin friction coefficient (C_f), the component form factor (FF) and the the interference factor (IF) by using Equation 7.1.

$$C_{D_0} = \frac{1}{S_{ref}} \sum_c C_{f_c} FF_c IF_c S_{wet_c} + C_{D_{misc}} \tag{7.1}$$

The drag terms that will be taken into account by the build-up method are: pressure-, skin-friction-. fuselage-, wing-, tail-, and pylon drag. The drag terms will be discussed shortly. A clear drag break down is provided in Figure 7.2.

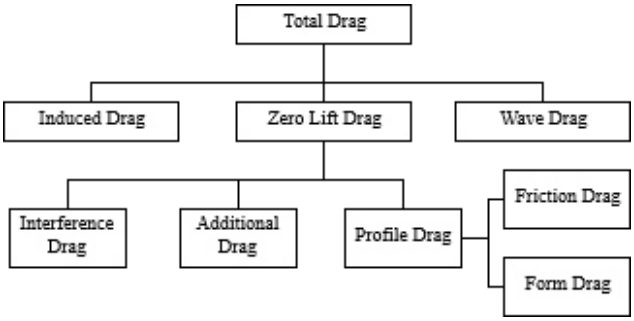

Figure 7.2: Total Drag Component Breakdown

7.2.2. Profile Drag

One can simply approximate the skin friction of an airfoil at zero angle of attack as a flat plate. This is a very rough estimate, however, in combination with other estimations it will yield reasonable values which can be used for further design. The skin-friction is built up from two components: the laminar skin-friction and the turbulent skin-friction. It is difficult to estimate the transition point and thus the critical Reynolds number with numerical methods, this is mostly done using data obtained from previous wind tunnel testing. Therefore, Anderson states that a critical Reynolds number, on average, lies around $5 \cdot 10^5$ At this point a transition region can be observed, converting laminar to turbulent flow.

Laminar Skin-Friction

The flat plate skin-friction estimation for laminar flow provides an estimation for a flat plate at zero angle of attack. This approximation will be more accurate for thinner wings, however this estimation can still be used for engineering prediction of skin-friction drag on thin airfoils [33]. The flow characteristics are highly dependent on the Reynolds number at some discrete location x along the chord. The Reynolds number at any discrete location x along the chord can be obtained by using Equation 7.2.

$$Re_x = \frac{\rho_\infty V_\infty x}{\mu_\infty} \tag{7.2}$$

Then the skin-friction coefficient can be obtained as a function of the Reynolds number by using Equation 7.3.

$$C_f = \frac{1.328}{\sqrt{Re_c}} \tag{7.3}$$

Turbulent Skin-Friction

The estimation of turbulent flow is difficult and requires empirical data. One can obtain the skin-friction coefficient C_f by using Equation 7.4.

$$C_f = \frac{0.455}{\left(log_{10}Re\right)^{2.58}\left(1+0.144M^2\right)^{0.65}} \tag{7.4}$$

The respective Reynolds number can be obtained by Equation 7.2.

Transition Region

Now that both the definitions of the laminar- and turbulent skin-friction have been specified, they can be used to find the total skin-friction over the wing. The flow transition has been graphically represented in Figure 7.3.

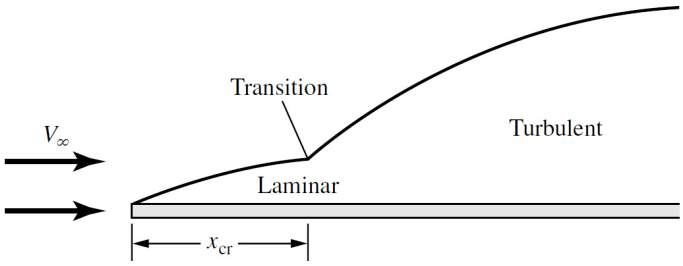

Figure 7.3: Flow Transition Region Representation [33]

Wings with a rough surface will have higher turbulent drag than given from Equation 7.4. This can be accounted for by applying a condition to the Reynolds number as provided in Equation 7.5. Here, the so-called cut-off Reynolds number is compared to account for roughness [33]. A lower Reynolds number will result in a higher skin-friction.

$$Re = min\left(\frac{\rho V l}{\mu}, 38.21\left(\frac{l}{k}\right)^{1.053}\right) \tag{7.5}$$

After taking the cut-off Reynolds number into account, the skin-friction coefficient can be found by integrating the laminar- and turbulent flow segments over the thin plate. This can be expressed as:

$$C_f = \frac{x_{cr}}{c}\left(C_f\right)_{laminar} + \left(C_f\right)_{turbulent} - \frac{x_{cr}}{c}\left(C_f\right)_{turbulent} \tag{7.6}$$

7.2.3. Interference Drag

To compute the drag per component, the FF and IF were introduced. The FF estimates the pressure drag due to viscous separation, where the IF estimates the effect on the drag induced by close proximity bodies. Before these entities can be computed or obtained, the wetted area of the above mentioned components have to be estimated. The wetted areas for the wing, horizontal tail, vertical tail and fuselage can be found through the respective relations described below [1]:

$$\begin{aligned}
S_{W_{wet}} &= 1.07 \cdot 2 \cdot S_{W_{exp}} \\
S_{HT_{wet}} &= 1.05 \cdot 2 \cdot S_{HT_{exp}} \\
S_{VT_{wet}} &= 1.05 \cdot 2 \cdot S_{VT_{exp}} \\
S_{F_{wet}} &= \frac{\pi D}{4}\left(\frac{1}{3L_1^2}\left[\left(4L_1^2+\frac{D^2}{4}\right)^{1.5} - \frac{D^3}{8}\right] - D + 4L_2 + 2\sqrt{L_3^2+\frac{D^2}{4}}\right)
\end{aligned}$$

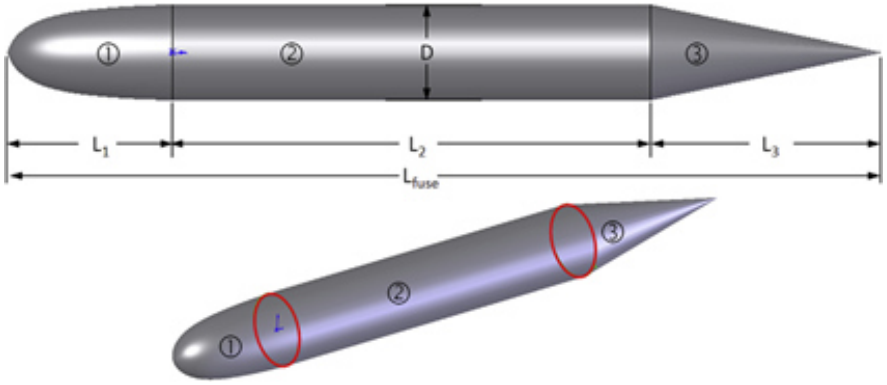

Figure 7.4: Fuselage Geometry Definitions

The definitions of the fuselage geometry have been included in Figure 7.4.
With these entities established, the IF can be obtained from literature, where the FF can be computed. The FF for the wing, tail and pylon is given in Equation 7.7, the fuselage skin-friction is estimated from Equation 7.8 and the nacelle from Equation 7.9.

$$FF = \left(1 + \frac{0.6}{\left(\frac{x}{c}\right)_m}\left(\frac{t}{c}\right) + 100\left(\frac{t}{c}\right)^4\right)\left(1.34M^{0.18}cos\left(\lambda_m\right)^{0.28}\right) \tag{7.7}$$

$$FF = \left(1 + \frac{60}{\left(\sqrt{\left(\frac{4}{\pi}\right)A_{max}}\right)^3} + \frac{\sqrt{\left(\frac{4}{\pi}\right)A_{max}}}{400}\right) \tag{7.8}$$

$$FF = 1 + \frac{0.35}{\sqrt{\left(\frac{4}{\pi}\right)A_{max}}} \tag{7.9}$$

The IF can be obtained from literature and other research. The IF for the connector can be taken as 1.25, the large turbofan engines causes a nacelle IF of 1.3 [34], all other components can be assumed 1 for the box wing [28].

7.2.4. Wave Drag

Like most modern airliners the MoM-liner is designed to fly in the transonic region. This introduces several issues with shock waves on the wing, which will generate additional drag on the aircraft. At the drag divergence Mach number the aircraft experiences a sudden increase in drag; this Mach number can be estimated using Equation 7.10. The term k_a is the technology factor of the airfoil, which is 0.935 for supercritical airfoils, and 0.87 for NACA 6-series airfoils.

$$M_{DD} = \frac{k_a}{cos\Lambda} - \frac{[t/c]_{streamwise}}{cos^2\Lambda} - \frac{C_L}{10cos^3\Lambda} \tag{7.10}$$

When the aircraft is flying above its critical Mach number but below the drag divergence Mach number the wave drag component can be estimated using Equation 7.11.

$$\Delta C_D = 0.002\left(1 - 2.5\frac{M_{DD} - M}{0.05}\right)^{-1} \tag{7.11}$$

7.2.5. General Wing Planform Design

The general size of the planform is set using the Class-I and Class-II weight estimation in combination with the span of the wings and the taper ratio, this will yield the general wing planform shape. The root and tip chord can be computed as functions of the wing area and the taper ratio, given in Equation 7.13.

$$\lambda = \frac{c_t}{c_r} \tag{7.12}$$

$$S_{\text{wing 1}} = c_r \left(\frac{(1+\lambda_1)\left(b - d_{fuse}\right)}{2} + d_{fuse} \right)$$
$$S_{\text{wing 2}} = c_r \frac{(1+\lambda_2) \cdot b}{2} \tag{7.13}$$

In order to mitigate the the effect of wave drag, sweep is added to the wing. The sweep of the wing reduces the velocity component of the air in chord-wise direction over the airfoil, effectively reducing the airspeed the airfoil sees and thus reducing the local Mach number. However, the span wise velocity component promotes the thickening of the boundary layer, making it more difficult for the flow to stay attached [35]. This effect significantly increases the possibility of tip stall in backward swept wings. The box wing design uses two different wings: the front wing is swept back, the back wing is swept forward. The front wing will thus experience tip stall earlier whereas the back wing will have root stall first, ensuring that the aircraft is still maneuverable around stall. The front wing also carries more load than the back wing, thus the front wing will always be the first to stall. This behavior is inherently stable and one of the main benefits of the box wing design, the main wing acts similar to a canard stability wise. The quarter chord sweep can be estimated using the empirical formula given in Equation 7.14.

$$\Lambda_{c/4} = \arccos 0.75 \frac{M^\dagger}{M_{dd}} \tag{7.14}$$

Here $M^\dagger$ = 0.935 is the technology factor for supercritcal airfoils. Torenbeek suggests setting the Mach drag divergence at 0.03 above the cruise Mach, yielding a M_{dd} of 0.83 [26]. Using these numbers, a quarter chord wing sweep of 33 degrees is obtained. This sweep is applied to the front wing as backward sweep, and the rear wing as forward sweep.

Furthermore, having a wing dihedral has major implications for aircraft stability. Introducing dihedral or anhedral can have several implications as discussed below. Usually the dihedral range is limited by the ground clearance between the engines [35]. However, the box wing concept will not encounter any difficulties here, since the wings are mounted under the aft wing, providing no clearance constrains. Also dihedral plays a large role in the lateral stability of the aircraft. In low-wing configurations, positive dihedral increases the stability whereas an anhedral negatively impacts the lateral stability. For wings with dihedral, the sideslip the aircraft experiences during a turn will lead to an increase in lift on the wing that faces into the sideslip, acting like a damping moment on the rolling motion [35]. For an aircraft with anhedral the opposite effect occurs, where the wing facing into the sideslip experiences a decrease in lift, making the aircraft roll even further. Swept wings have an inherent effective dihedral even if the geometrical dihedral is zero. The sideslip will increase the flow over the chord wise direction thus increasing the lift on that wing. For high-wing aircraft, this effect is exactly is exactly opposite. Although the rear wing is not mounted on the fuselage, but rather on the vertical tail it will still experience this effect.

In order to make a good first estimate of the dihedral, Raymer [1] recommends starting off with a default dihedral of 3 degrees, then remove 1 degree per 10 degrees of sweep, and lastly add 2 degrees for low-mounted wings or remove 2 degrees for top-mounted wings. Using this method a dihedral of 2 degrees is obtained for the front wing, and an anhedral of -2 degrees is obtained for the aft wing.

Table 7.1: Wing Planform Parameters

	Front Wing	**Aft Wing**
Sweep [deg]	33	-33
Dihedral [deg]	2	-2

The sweep in combination with the taper ratio influence the amount of lift induced drag the aircraft experiences. At the point of lowest induced drag, the lift distribution over the wing will have an elliptical shape. Varying the taper ratio is a way of obtaining such a lift distribution. On swept wings the flow component along the span increases the lift at the tips of the wings, thus deviating away from the elliptical lift distribution. To compensate, the taper ratio can be reduced. Small taper reduces the weight of the wing as the moment generated is low, however, a small taper means that the airfoil at the tip needs to operate at a higher lift coefficient due to the smaller chord, promoting tip stall. For the taper a program was written to compute the most optimal value for maximum lift over drag. That method is explained in the following sections.

7.2.6. Vortex Lattice Method

Aerodynamic analysis is usually a computationally expensive task. Vortex lattice methods offer a compromise between computation time and accuracy; these methods are mainly advantageous in the preliminary design phases [33]. In VLM the wing planform is modeled with a finite number of panels, on each of which a horseshoe vortex is applied. On each of these panels a point P is created on which a flow tangency condition is imposed, such that there is no flow into the wing. Now using the Biot-Savart law and the set of superimposed horseshoe vortices a system of equations can be set up, which can be solved for the unknown vorticity of each panel Γ_n. This method yields generally good results for the lift generated by the aircraft as well as its stability derivatives; this method does not yield accurate results for the drag as this method can only account for the lift induced drag.

To get a good estimate of the overall drag the additional contributions can be estimated. Using the methods described in the previous section, the wave drag, skin friction drag and form drag of various components can be estimated. These additional terms can then be added to the initial drag estimate obtained from the VLM.

Wing Optimization

In order to optimize the performance of the aircraft the lift over drag needs to be as low as possible. To minimize this as much as possible a numerical optimization program is created. The analysis is done using Tornado, a vlm program. Tornado was developed in 2000 by Tomas Melin for a master thesis [36]. The software is written in MATLAB, making it easy to adapt the code and to add additional components to it. Over the past decade several updates were added to the code, as well as a couple of additional modules. The adaptability makes this program perfect for integration into the optimization software.

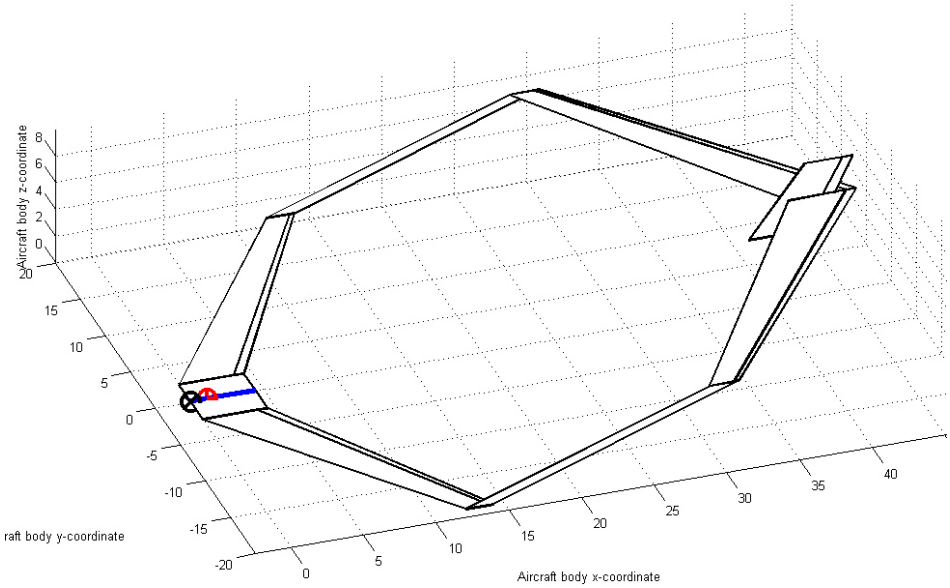

Figure 7.5: Wing Planform in Tornado

In order to incorporate tornado into the automatic sizing program, a python script was written to automatically generate box wings in the format that tornado can understand, Figure 7.5 depicts an example of a wing planform generated by this python module. This program takes the taper ratio of the main wings, surface area and sweep and outputs a wing planform including struts connecting the wings and a vertical tail. This geometry output is then passed to a specially written MATLAB script that acts like an interface between the python components and the tornado components. First this script finds the required angle of attack to obtain the required lift during cruise. After which tornado performs a full analysis and makes an estimate for the lift, drag and various stability coefficients. This data is then send back to the python optimizer program. This program adds the additional drag terms to obtain a more accurate drag estimate using the method described in the previous section. Now the lift over drag of the entire aircraft can easily be obtained. The taper ratio will then be varied such that the lift over drag is maximized, using a method described later in this section. This loop will continue till an optimum lift over drag is found.

Before Tornado can accurately compute the aerodynamic properties of the wing, a mesh spacing has to be determined. The smaller the mesh size, the more points on which computations have to be performed, and the longer it

takes to run. As the computational time scales with N^2, with N being the number of panels, the number should be kept as low as possible. The accuracy will, however, converge after at a specific spacing, so reducing the spacing will after a certain point not increase the accuracy. To find this point panels are added in both the chord wise direction (x) and the span wise direction (y); after adding 4 new panels the L/D is computed, the results of which are given in Figure 7.6a and Figure 7.6b. As can be seen from the figures, 17 panels in the cord and 50 panels in the span direction seem to yield good results.

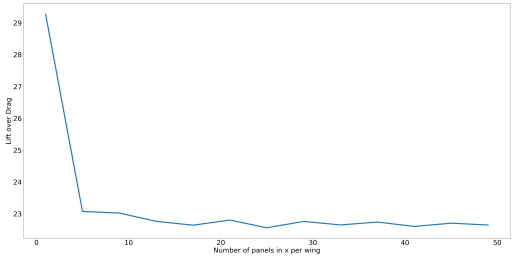

(a) Number of Panels in the Span Direction per Wing

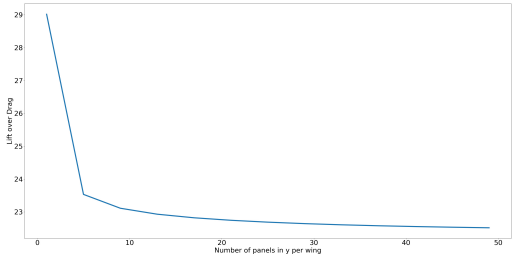

(b) Number of Panels in the Span Direction per Wing

Each iteration however still takes a considerable time, so instead of randomly guessing taper ratios or running through a set of values, the method of steepest decent is used, given in Equation 7.15. A new estimate for the taper ratio is made by multiplying the derivative of the L/D with respect to the taper ratio with a term α. α has to be chosen in such a way to ensure a fast convergence: if the value is too large this method will never converge; if it is too small the number of iterations before convergence is too high. A numerical approximation of the derivative of the drag can be made using Equation 7.16. The function is said to have converged if the change in L/D between two iterations is less than 0.01 or if the taper ratio drops below 0.2 as the wing would not be structurally sound anymore.

$$\lambda_{n+1} = \lambda_n - \alpha f'(\lambda_n) \tag{7.15}$$

$$f'_n(\lambda_n) = \frac{f_n - f_{n-1}}{\lambda_n - \lambda_{n-1}} \tag{7.16}$$

Limitations

Due to the VLM's limitations in estimating the drag, additional drag terms need to be added using empirical methods. However, drag is dependent on interactions between the different bodies that make up the plane. The semi-empirical methods are unable to model this accurately. Furthermore, the increase in weight due to the change in chord of the strut is not included in the model, changes in weight will have an effect on the lift in cruise and therefore also the L/D. The fact that the aircraft is in transonic flight also decreases the accuracy of the vortex lattice method. Lastly, the vortex lattice method is limited to small angles of attack as it cannot model separation accurately. In order to make a good estimate for the landing and takeoff lift, it is assumed that the wings will maintain the same ratio of lift as in cruise. In reality the wake of one wing is likely to hit the other wing at high angles of attack or with high lift devices deployed. Even with these shortfalls the accuracy is still sufficient for this stage in the design. For higher accuracy calculations a full CFD analysis needs to be made, after which wind-tunnel testing would aid in the more detailed design stages.

7.2.7. Airfoil Selection Process

To simplify the design process, it has been decided that an airfoil profile shall be selected prior to the optimization of the design. This can be done, since many mission aspects such as the lift coefficient in cruise etc. are already known through prior design phases. The goal of the airfoil selection is to obtain an airfoil with the overall best characteristics. The selection shall be done according to a method described in Gudmundsson [37], which defined a set of characteristics such as the thickness ratio, C_L at 0°angle of attack, $C_{C_{max}}$, $C_{D_{min}}$, and more characteristics such as described in Table 7.2. For the subsonic region of flight one tends to use super-critical airfoils. Six arbitrary supercritical airfoils have been selected, from different companies. Additionally, one airfoil which is not supercritical has been selected for comparison. The airfoils with the best characteristics for a parameter will receive the point, however it is possible that multiple airfoils receive a point.

Table 7.2: Airfoil Selection from Gudmundsson

Parameter	**Airfoil 1**	**Airfoil 2**	**Airfoil 3**	**Airfoil 4**	**Airfoil 5**	**Airfoil 6**	**Airfoil 7**	**Score**						
Name	NASA SC(2)-0412	HORST -MANN AND QUAST HQ-300	NASA SC(2)-0410	NASA /LAN-GLEY RC-SC2	NASA SC(2)-0612	NASA SC(2)-1010	NACA 2412	Score the airfoils by entering 1 to indicate the airfoil with the best characteristics. It is possible all the airfoils deserve a score.						
Thickness Ratio (higher is better)	12	16.6	10	10	12	10			1					
C_L at 0 Angle of Attack	0.2749	0.601	0.2443	0.0811	0.4615	0.8196	0.2442					1		
Angle of Attack for $C_L = 0$	-2.45	-4.66	-2.05	0.75	-3.9	-7.21	-2.25						1	
$C_{L_{max}}$	1.6283	1.6377	1.4554	1.2193	1.6581	1.6542	1.582					1	1	
Angle of Attack of $C_{L_{max}}$	15.25	12	12.75	13	14.5	11	16.5							1
$C_{D_{min}}$	0.0071	0.0067	0.0077	0.0083	0.0059	0.0056	0.0056						1	
Cl of $C_{D_{min}}$	-0.0119	0.3616	0.0769	0.1328	0.1784	0.4829	0.3469						1	
Cruise C_M	-0.0777	-0.11	-0.069	-0.011	-0.11	-0.15	-0.047				1			
$(\frac{C_L}{C_D})_{max}$	78.82	139.78	71.87	66.19	77.94	115.25	101.38		1					
C_L of $(\frac{C_L}{C_D})_{max}$	1.1039	1.2986	0.9336	0.85	1.1574	0.68	0.7624						1	
$C_{L_{cruise}}$ inside Drag Bucket	N	N	Y	N	Y	Y	Y			1		1	1	1
Sum								**0**	**2**	**1**	**1**	**3**	**6**	**2**

From Table 7.2 is can be found that the NASA SSC(2)-1010 airfoil wins the trade-off process. The profile of the NASA SC(2)-1010 airfoil is provided in Figure 7.7. The airfoil itself provides the highest C_L; furthermore it also allows for a low C_D in the drag bucket, around the cruise C_L. Also the C_L at $\left(\frac{L}{D}\right)_{max}$ lies, relative to the other airfoils, closest to the cruise C_L, which allows for a better $\left(\frac{L}{D}\right)$ during cruise.

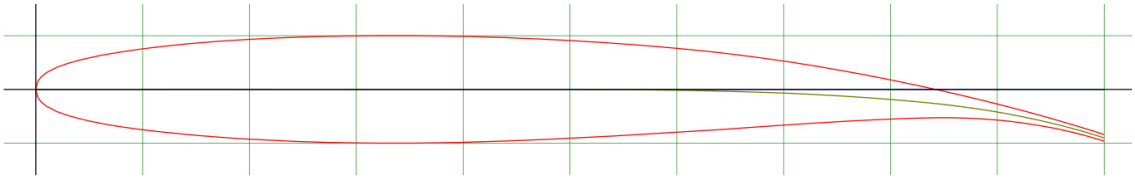

Figure 7.7: NASA SC(2)-1010 Airfoil Layout

The airfoil geometries and the data was obtained from an online airfoil database, which uses XFoil to simulate the data[1]. This was done at a Reynolds number of $1 \cdot 10^6$. Characteristic curves of the used airfoil are provided in Figure 7.8.

7.3. Aerodynamic Tools & Code Verification

7.3.1. Tornado VLM Validation

Tornado VLM is an established method that has been used for prolonged time by many instances, therefore validation processes have already been performed and can be found in literature. A validation of software for the calculation of aerodynamic coefficients has been performed by the Linköpings University [38]. Especially this validation is interesting, since multiple codes have been validated in this research, showing the accuracy of a wide range of VLM methods. The programs analyzed were Tornado, AVL, PANAIR, and a handbook-type estimation. Multiple aircraft have been looked at during the validation. Of these, the results for the Boeing 747-100 and the Boeing 777-300 are of special interest since they are long range aircraft with similar flight conditions.

[1] URL `https://www.airfoiltools.com` [cited 5 June 2018]

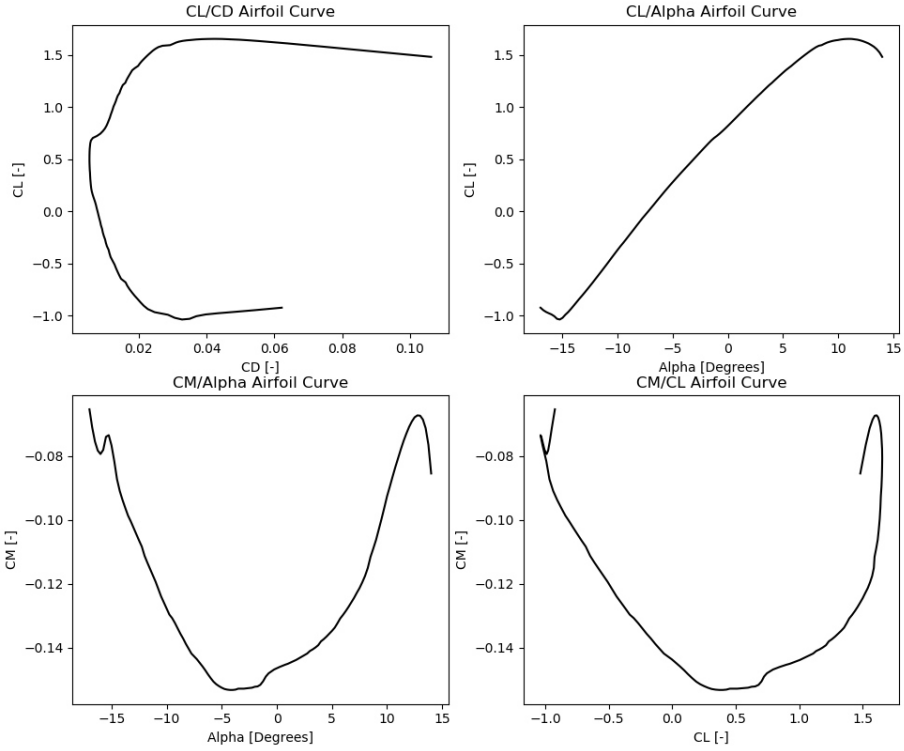

Figure 7.8: NASA SC(2)-1010 Airfoil Characteristic Curves

The validation has been done by performing calculations within all the respective methods; also a wind tunnel test has been performed. Given a good aircraft model, the wind tunnel testing should yield the closest result to the actual flight data. To allow for comparison, the root mean square error for drag and the root mean square error for lift will be analyzed.

Boeing 747-100 Validation

The validation data with regards to the C_L versus C_D has been presented in Figure 7.9a and the data representing the change in C_L versus AoA has been presented in Figure 7.10a. Their errors are presented in Figure 7.9b and Figure 7.10b respectively. Here it can be seen how and where the methods exactly deviate as a function of α and C_L. These results are condensed in Figure 7.10b, representing the root mean square values to observe method accuracy. The lowest error for drag is obtained from Tornado with a 4.5% RMS.

Table 7.3: Validation Results Boeing 747-100 [38]

Boeing 747-100				
Computation Model	C_{L_α}	C_{D_0}	RMS_{Lift}	RMS_{Drag}
Experimental	5.1	0.019	2.8%	3.7%
Tornado	5.0	0.018	4.6%	4.5%
Preliminary	6.1	0.016	32%	7.5%
AVL	5.1	0.017	4.0%	6.7%
PANAIR	5.0	0.017	3.4%	6.0%

Boeing 777-300 Validation

The validation data with regards to the C_L versus C_D has been presented in Figure 7.11a and the data representing the change in C_L versus AoA has been presented in Figure 7.12a. These results are condensed in Figure 7.12b, representing the root mean square values to observe method accuracy.

Table 7.4: Validation Results Boeing 777-300 [38]

Boeing 777-300				
Computation Model	C_{L_α}	C_{D_0}	RMS_{Lift}	RMS_{Drag}
Experimental	5.1	0.013	1%	3.3%
Tornado	5.3	0.011	6%	6.7%
Preliminary	5.9	0.011	14%	7.2%
AVL	5.1	0.011	2%	7.2%
PANAIR	5.2	0.011	3%	8.1%

Their errors are presented in Figure 7.11b and Figure 7.12b respectively. Here can be seen how and where the methods exactly deviate as a function of α and C_L.

Aerodynamic Validation & Verification: Result Discussion

Boeing 747-100: As can be seen from Table 7.3, Tornado provides accurate results for both lift and drag (RMS values of 4.6% and 4.5% respectively). However, one can observe that it fails to remain accurate as the C_L increases, as seen in Figure 7.9b. Thus, the error when estimating take-off and landing performance may be higher than desired. This said, it overestimates drag, which is obviously not desirable, but is preferred over underestimation. As compared to other models, slightly better estimations can be obtained for the lift by using AVL or PANAIR.

Boeing 777-300: It can be seen in Table 7.4 that the root mean square values are slightly higher than the case of the 747-100, however still within a respectable 6% root mean square for lift and 6.7% root mean square for drag. Similar to the 747-100 validation, AVL and PANAIR can obtain better lift estimations. Although Tornado is best at estimating the lift characteristics, it is still 'high'. The main source of error comes from the the negative angles of attack as seen in Figure 7.11b. All codes seem to perform poorly at the negative angles of attack up until about -1 degrees, all models underestimate the lift performance by more than 10%.

These two cases show the validation of high capacity, long-range aircraft. The main point of interest is that the above mentioned models provide a quite accurate representation with exception to high C_L values, thus using these methods to estimate the cruise performance should yield rather accurate results within limited time.

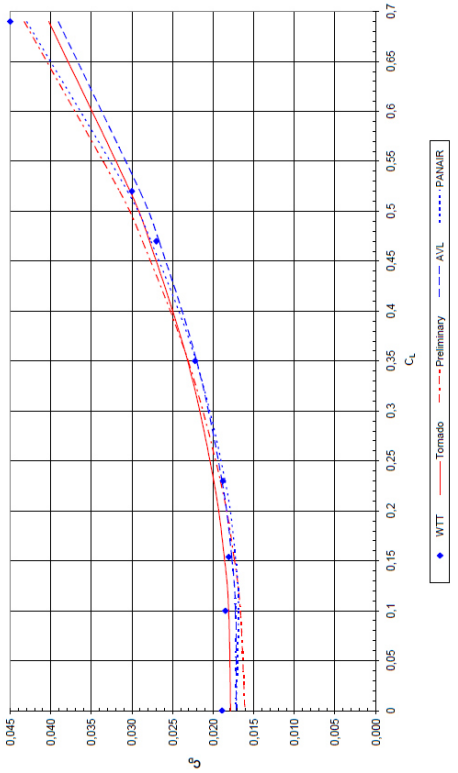

(a) Validation Data B747-100 Drag Polar Error Representation

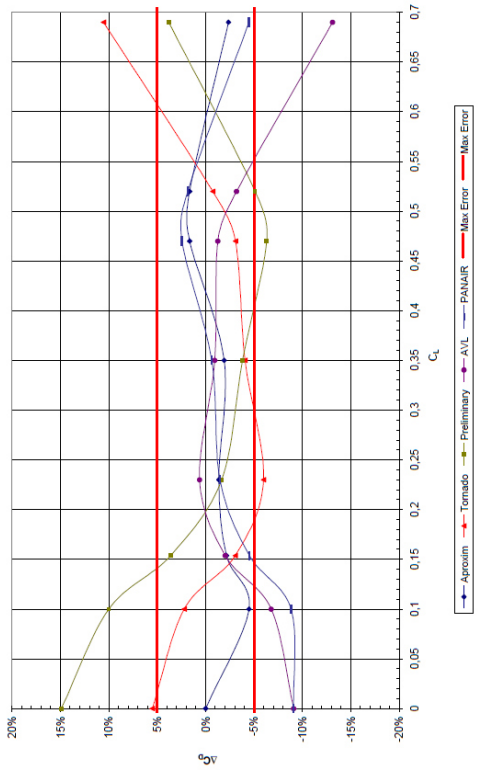

(b) Validation Data B747-100 Drag Polar Error Representation

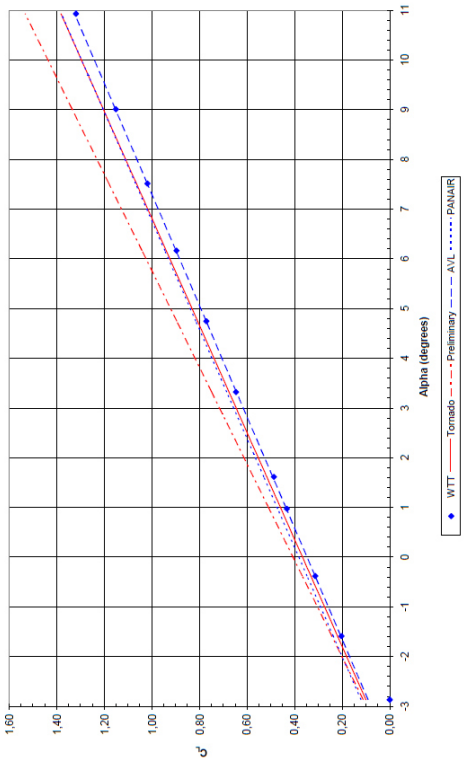

(a) Validation Data B747-100 Lift versus Angle of Attack

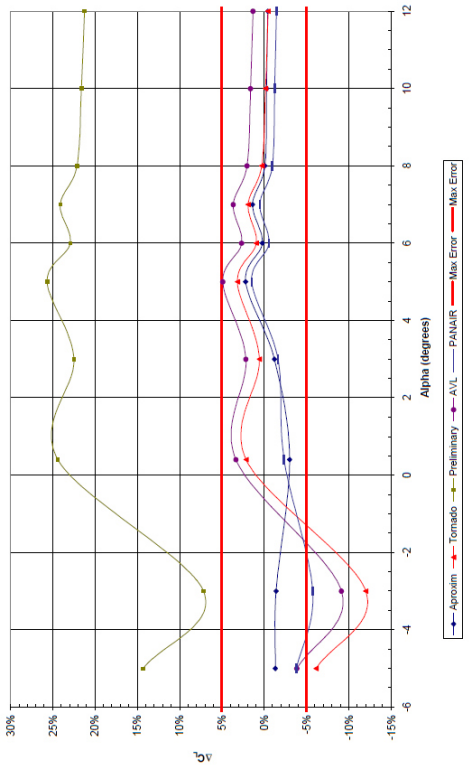

(b) Validation Data 747-100 Lift versus Angle of Attack Error Representation

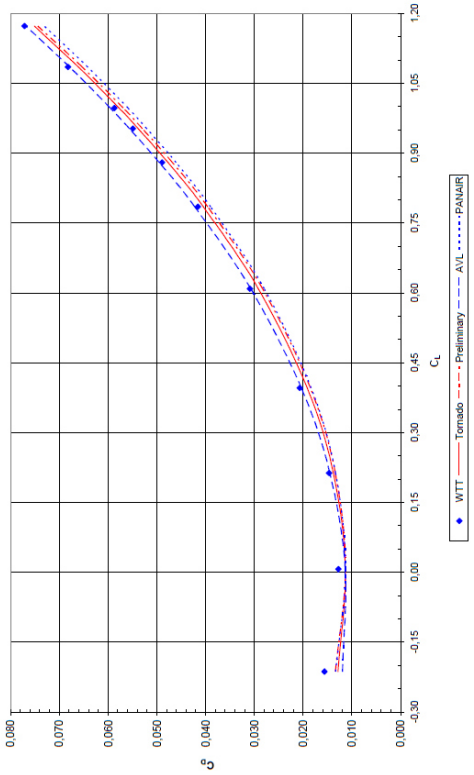

(a) Validation Data B777-300 Drag Polar

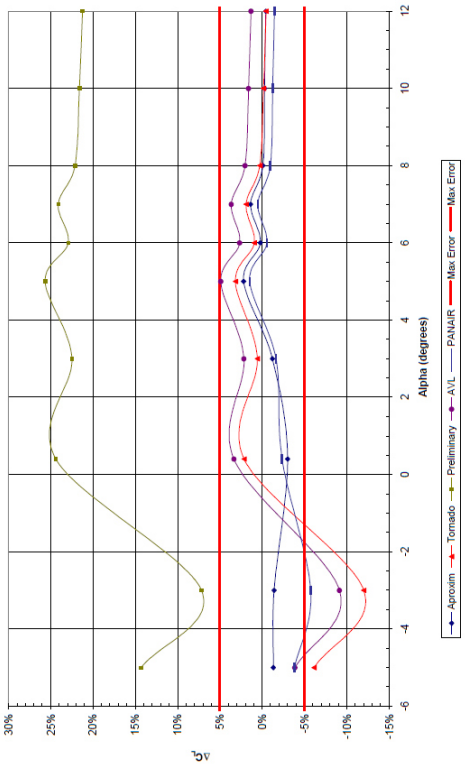

(b) Validation Data B777-300 Drag Polar Error Representation

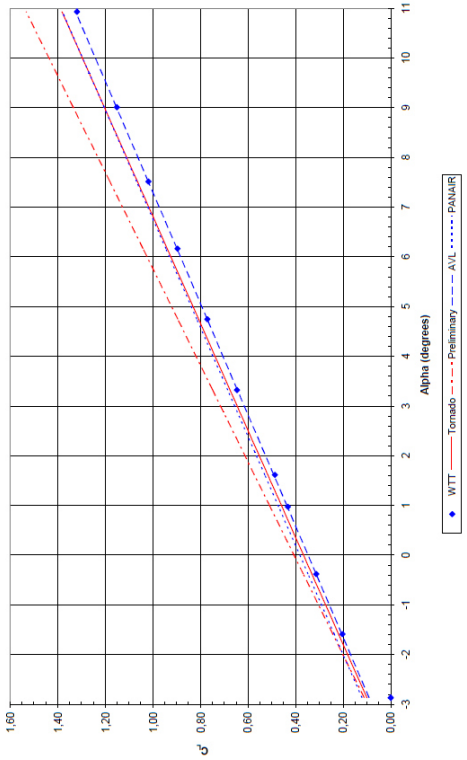

(a) Validation Data B777-300 Lift versus Angle of Attack

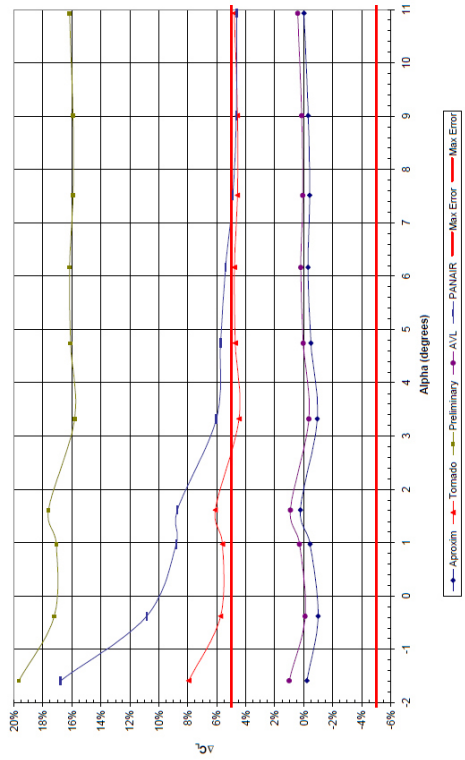

(b) Validation Data B777-300 Lift versus Angle of Attack Error Representation

8

Structural Analysis

This chapter details on the structural analysis that was performed. This analysis was both executed for both the fuselage and the wing of the aircraft. First the methodology will be presented, of which a short summary is given below. The results will be presented in a separate chapter, namely chapter 12.

8.1. Summary Methodology

The structural analysis for the wing and fuselage both rely on the structural idealization of the geometry. This idealization relies on modelling the longitudinal stiffeners as simple booms, and lumping the adjacent skin area into the area of that boom. After defining the geometry of the fuselage and wing separately, the internal stresses are computed to investigate the stress distribution throughout the structure. Failure modes for buckling and yielding are defined, from which the most critical is selected. Using the internal stresses and the most critical failure mode, an optimization is run to size the structure. For the wing structure the optimization is used to size the skin thickness and the number of stringers used, while for the fuselage the skin thickness and the web, flange, and cap thickness of the stringer is optimized.

8.2. Methodology

The methodology of the structural analysis will touch upon every step taken to perform a solid analysis. The method used for the wing and fuselage are quite similar and for each step the difference between wing and fuselage is presented clearly.

8.2.1. Assumptions

The assumptions used throughout the analysis are presented. First, the general assumptions both holding for the wing and fuselage is shown, where after assumption specific to each structure are elaborated.

General

- ***Discretization in longitudinal direction:*** both the wing and fuselage are discretized in longitudinal direction. Generating n amount of cross sections, over which the computations are performed. The larger the number of discretizations, the more accurate the analysis will become. In the wing analysis the discretization spacing will be $0.2m$ and in the fuselage analysis the discretization spacing will be $0.38m$. This is deemed sufficient to generate accurate results.

- ***Structural Idealization:*** the structure is idealization that is assumed, states that all stringers are replaced by booms and that the adjacent skin area is lumped with the area of the booms. This assumption is often taken in preliminary design, as it greatly simplifies the modelling of the structure, while still being a sufficiently accurate representation of reality.

- ***Shear and Normal stresses:*** following from the structural idealization is the assumption that the stringers, modelled as booms, carry only normal stresses. Furthermore, the skin is only effective in carrying shear. As the stringers area is relatively small compared to the the total area of which the cross-sections, this is deemed a valid assumption.

- ***Stiffened panel geometry:*** by applying an idealization the cross section is split up into p number of sections (where p is equal to the number of stringers). Since these sections are small compared to the total cross-section, it is assumed that the area between two booms can be modelled as a stiffened panel geometry.

- ***Max load case:*** for the analysis a maximum load case is considered. For the maximum load case a 2.5g maneuver is assumed.
- ***Main contributing moment:*** to simply the computations of shear and normal stresses, it is assumed that the the moment around the x axis is much larger than the moment around the y axis ($M_x >> M_y$). By using this assumption the M_y, term can be neglected in stress calculations.

Wing

- ***Prandtl wing assumption:*** The Prandtl wing is assumed to be two separate wings, for each wing the structural analysis is performed. It is assumed that the tip deflection of both wings must be equal, resulting in the situation where the vertical attachments of the front and aft wing is unloaded. This assumptions is deemed valid after consulting multiple experts in the field of Prandtl planes and structural experts[1].
- ***Skin between spars:*** As the distance between the spars is relatively small, it is deemed valid to assume that this can be modelled as straight instead of a curved skin.
- ***Product moment of inertia:*** As the wing is more or less symmetrical, the product moment of inertia is small. Therefore the product moment of inertia is neglected in further computations of the wing.
- ***The wing only deflects upward*** The primary load acting on the wing is the lift, this force is considered to be much larger than the drag. Furthermore the wing has a much higher moment of inertia so any deflection of the wings backwards would be small and thus can be neglected.

Fuselage

- ***Double bubble assumption:*** Regarding the pressure stresses in the fuselage, these are modelled with the double bubble assumption. Meaning that the fuselage is represented by to circular sections split by a floor. This greatly simplifies the computations of the hoop and transverse pressure stresses.
- ***Fuselage length:*** The structural analysis is not done for the entire fuselage length. The entire 'straight' section of the fuselage is modelled. Neglecting the nose and tail cone of the fuselage. This is deemed valid because the analysis is still preliminary and the main contributor the fuselage weight is the 'straight' part of the fuselage.

8.2.2. Geometry

Wing

The structural analysis of the wing was done by analyzing the wing box, as this is the main unit carrying the loads. The wing box geometry was computed based on sweep, root chord, taper ratio, airfoil and wing span. Each of these parameters are mainly based on the aerodynamic analysis performed in chapter 7. The analysis was done with the reference frame depicted in Figure 8.1a. The wing was discretized into sections distributed along the span, generating y_n sections. The idealized cross section of the wing box configuration can be seen in Figure 8.1b, this was generated using Python code. Additional booms were placed at the top of each of the spars to model their bending stiffness contribution.

Fuselage

For the structural analysis of the fuselage, the fuselage is modeled as elliptical cylinder with a floor just below the horizontal symmetry line. Furthermore, the nose-cone and tail-cone are not considered in the structural analysis, solely the pressurized section ranging from the front pressure bulk head to the aft pressure bulk head is considered. The reference frame used in the structural analysis is shown in Figure 8.3a. The fuselage is discretized in the longitudinal direction generating z_n sections. Stringers are placed along the circumference of the fuselage whereas frames are spaced in the lateral direction of the fuselage. An example is shown in Figure 8.2[2]. The implementation of the idealization results in a cross section as displayed in Figure 8.3b, this was generated using Python code.

[1] Personal consultation with Prof. Frediani and Dr. ir. Van Campen
[2] URL `http://www.aerospacengineering.net/?p=4279` [cited 20 June 2018]

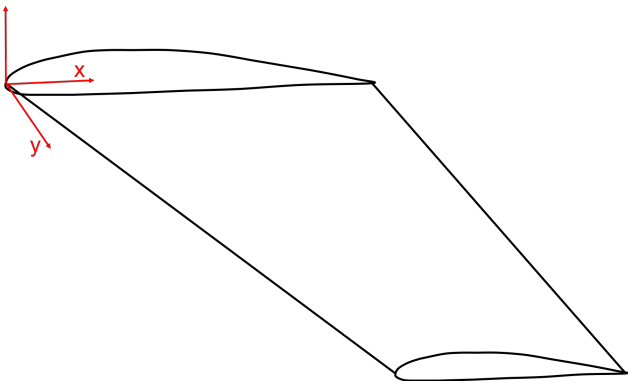

(a) Reference frame used for the structural analysis of the wing

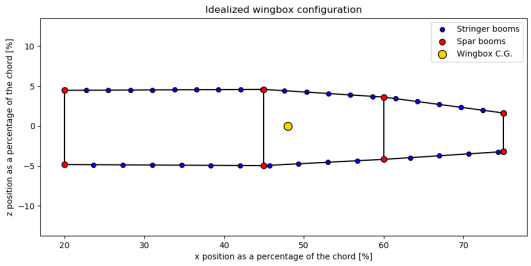

(b) Configuration of the idealized wing box cross section

Figure 8.1: Structural configuration

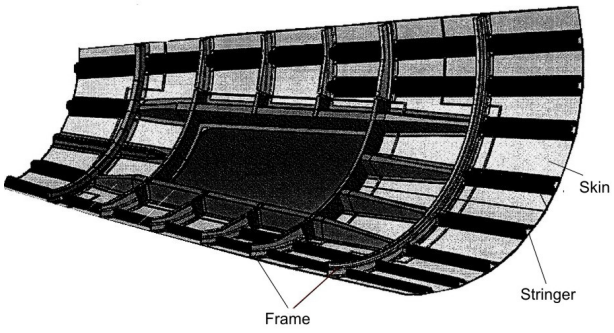

Figure 8.2: Artistic Illustration of a Fuselage Section, Representing the Different Parts (Skin, Stringer, Frame)

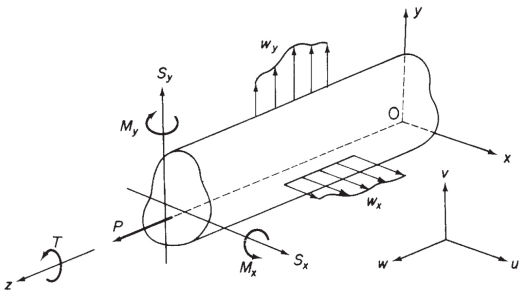

(a) Reference frame Used for the Structural Analysis of the Fuselage

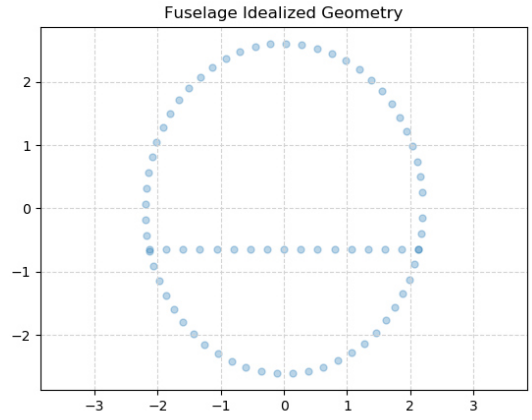

(b) Configuration of the Idealized Fuselage Cross Section

Figure 8.3: Fuselage Geometry

8.2.3. General Section Properties

Along with the geometry are some computations that are necessary for the further analysis. The computations are similar for the wing box and fuselage, and therefore, will only be presented once. By using the idealization the stringers are represented as simple booms, where the adjacent skin area is lumped into the area of the stringer boom. Equation 8.1 shown the computation where the first term in the sum is the area of the adjacent skin and $B_{stringer}$ is the area of the stringer.[39]

$$B = \frac{t \cdot b}{6}\left(2 + \frac{\sigma_{N_2}}{\sigma_{N_1}}\right) + B_{stringer} = \frac{t \cdot b}{6}\left(2 + \frac{z_2}{z_1}\right) + B_{stringer} \tag{8.1}$$

A major benefit of the idealization is that the computations of the centroid and moment of inertia become significantly less complex. As there are single point areas the centroid computations are simplified as depicted in Equation 8.2 and Equation 8.3 for the x location and y location of the centroid respectively. It should be noted, since the fuselage is symmetrical about the y axis, that $\bar{x}$ is zero for the fuselage.

$$\bar{x} = \frac{\sum \tilde{x}_i B_i}{\sum B_i} \tag{8.2}$$

$$\bar{y} = \frac{\sum \tilde{y}_i B_i}{\sum B_i} \tag{8.3}$$

Analogous to the computations of the centroid, the moment of inertia can be computed. The boom areas can be used to compute the area moments of inertia of the wing box. These moments of inertia I_{xx} and I_{zz} can be computed as the sum of Steiner terms for each boom. This method is shown in Equations 8.4 and 8.5 [39] where n is the number of booms.

$$I_{xx} = \sum_{i=1}^{n} B_i z_i^2 \tag{8.4}$$

$$I_{zz} = \sum_{i=1}^{n} B_i x_i^2 \tag{8.5}$$

8.2.4. Stiffened Panel Geometry

The area between each boom of the idealized cross section is modeled as a stiffened panel. For the fuselage the panel is closed in frames and stringers of the fuselage. For the wing box the panel is closed in by the ribs and the stringers of the wing box. An example of this enclosing for the fuselage is displayed in Figure 8.4a[40], a is the frame spacing and b is the stringer/rib spacing.

'Hat' stringer will be used in all locations as these offer good compression performance and are reasonably simple to manufacture[40]. An important difference between the fuselage and wing analysis arises in the optimization (elaborated more extensively in subsection 8.2.9). In the fuselage optimization the only variables that are optimized are the skin thickness and the web/flange/cap thickness of the stringer, meaning that the number of stringers and the stringer pitch is kept fixed. However, in the wing box optimization the optimized variables are the skin thickness and the number of stringers. The geometry of the 'hat' stringers is shown in Figure 8.4b, where the corresponding values are displayed in Table 8.1.

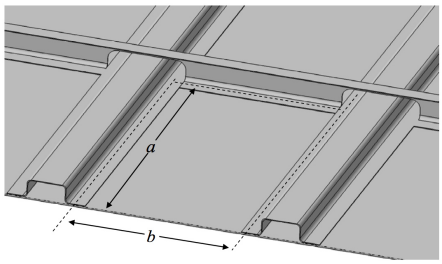

(a) Representation of the Stiffened Panel Geometry

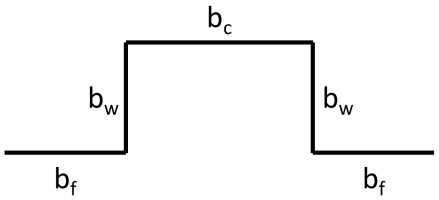

(b) Hat Stringer Geometry

Figure 8.4: Stiffened Panels

8.2.5. Loads

The load cases applied on the structure are extremely important when computing the stresses inside the structure. It is decided to size the structure for the extreme load case: a 2.5g maneuver load case. This is both done for the wing and fuselage.

Wings

The load case experienced by the wings is comparable to that of a conventional aircraft, each wing is treated as such is treated as a simple cantilever beam. The aerodynamic load is distributed across the wing. These loads were

Table 8.1: Geometry Sizing of Stringer and Panel

Parameter	Fuselage	Wing Box
a [m]	0.25	Optimized
b [m]	0.5	$0.6a$
b_f [m]	0.00762	0.020
b_w [m]	0.00889	0.035
b_c [m]	0.0178	0.020

generated by the aerodynamic analysis of the wing planform. In addition to the aerodynamic loads the weight of the wing was taken as a distributed load acting in the opposite direction to the aerodynamic loads. The weight of the engine was introduced as a point load and torsional moment about the y axis on the wing rear wing. The thrust of the engine was also introduced as a a shear force in the x direction and moment about the y axis. The contribution to the torsional moment due to sweep was computed by assuming the resultant aerodynamic force acts at the quarter chord point and integrating the wing load multiplied by the distance to the shear centre between the tip and root. The loads are presented in the free body diagram shown in Figure 8.5.

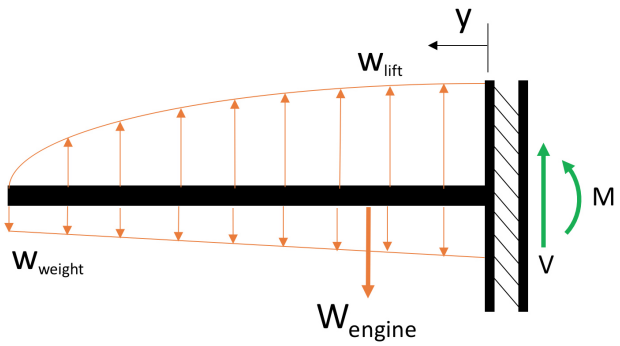

Figure 8.5: Free Body Diagram of the Wing Structure, Modelled as Cantilever Beams

From these loads the wing the shear force, bending moment distribution and torsion could be computed. These distributions are presented.

Fuselage

Unlike conventional aircraft, it is known that the maximum moment on the fuselage does not occur at the root of the wing. In fact, the bending moment near the root chord of the wing is almost zero [41]. To properly model the loads of the aircraft, one must undergo some smart steps. The reason for this is the fact that the load problem itself is statically indeterminate. This is solved by splitting the beam in half in the center of the fuselage, this is convenient as it makes the problem solvable. Moreover, another advantage of modeling the fuselage as two cantilever beams, is that it also models the peculiarity of almost zero bending moments near the root wing.

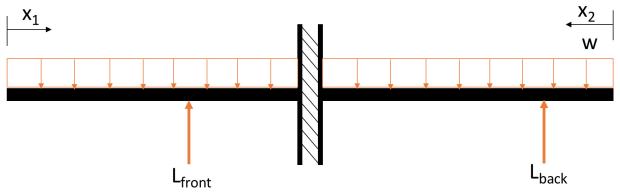

Figure 8.6: Free Body Diagram of the Fuselage Structure, Modelled as Two Cantilever Beams (Load Case: 2.5g Maneuver

In Figure 8.6 it can be seen how the fuselage is split into two cantilever beam and how the forces are modeled on the structure. The weight is modelled as a simple distributed load and the shear forces as point forces. The problem is approached from the two free ends of the beams. Using this method the shear and moments diagram for the fuselage can be derived.

8.2.6. Stress Analysis

The computation of the stresses rely on the same principle for both the wing and the fuselage. In this section this principle and methods applied will be elaborated. The main difference between the stress analysis of the wing and the fuselage is that: (1) for the fuselage the stresses induced by pressurization are taken into account, while for the wing these do not have an influence. (2) The stress analysis of the wing relies on the computing the wing-tip deflection of the front and rear wing, as these should be equal. The use of deflection computations are not used during the stress analysis of the fuselage.

To summarize, the stresses that will be computed are:

- Normal stress
- Shear stress
- Pressure stress (fuselage only)
- Principal and Vonmises stress

Normal Stress

An aircraft structure is subjected to large bending loads. These bending loads cause normal stresses in the structure. The normal stress in a boom can be calculated using Equation 8.6 [39].

$$\sigma_z = \frac{M_y I_{xx} - M_x I_{xy}}{I_{xx} I_{yy} - I_{xy}^2} x + \frac{M_x I_{yy} - M_y I_{xy}}{I_{xx} I_{yy} - I_{xy}^2} y \tag{8.6}$$

As the analyzed fuselage and wing is symmetrical, the product moment of inertia I_{xy} can be neglected. For the wing structure it is assumed that each segment has a constant cross section, allowing to also neglect the product moment of inertia I_{xy}. Also, it is assumed that the main bending load acting on the fuselage is around the x-axis. This means that Equation 8.6 can be simplified and written as Equation 8.7, where y is the y-distance of an element of the structure with respect to the y-location of the structure's centroid.

$$\sigma_{z_i} = \frac{M_i x_i}{I_{xx}} y_i \tag{8.7}$$

With Equation 8.7, the normal stress in each each specific discretized section of the cross section can be computed. These stresses are later used to analyze the failure criteria of the wing and fuselage.

Shear Stress

Shear forces are slightly more complicated to compute, as both the wing and fuselage are multicell closed section shear problems. For the fuselage shear is introduced into the structure by the lift of the wing and the weight of the aircraft itself. These shear forces in turn generate shear stresses in the fuselage structure. For the wing shear is introduced by the main force of an aircraft: the lifting force.

In an idealized structure, the skin of the structure is assumed to take all the shear loads. As an idealized structure consists of booms with a zero thickness skin in between, shear flow (shear stress multiplied with skin thickness) is used to analyze the shear stress in the fuselage structure.

Before distinguishing between the wing and fuselage structure, the similarities between the two methods are detailed. Following the approach for any closed section shear problem: one must first go about computing the shear flow, as with this shear flow the shear force can be computed by taking the product of the shear flow and local skin thickness. It is first necessary to compute the open section shear flow (which can be computed by the use of Equation 8.8 [39]), where after the redundant shear flows for each cell of the multicell problem are computed. This redundant shear flow is then added to the respective cell, yielding the final shear flow through each cell. By connecting the cells again, the total cross-section shear flow is obtained.

$$q_{s_i} = -\frac{S_x I_{xx} - S_y I_{xy}}{I_{xx} I_{yy} - I_{xy}^2} \left(B_{r_i} x_i\right) - \frac{S_y I_{yy} - S_x I_{xy}}{I_{xx} I_{yy} - I_{xy}^2} \left(B_{r_i} y_i\right) + q_{s_{i-1}} \tag{8.8}$$

The fuselage structure can be seen as a two-cell multicell structure. Figure 8.7a illustrates a schematic drawing of the cell division and the cut location. The fuselage structure is divided in two at the location of the floor. Taking a closer look at Equation 8.8 reveals that it consists of the product moment of inertia I_{xy}. Just like in the case of the normal stress equation, due to symmetry, this product moment of inertia can be neglected. Furthermore neglecting the shear force in x direction (this force is much smaller than the force in y direction) greatly simplifies

the equation, yielding Equation 8.9. With the said equation the open section shear is calculated for both sections. This is done by first making a small cut at a convenient place in the cell. For both cells, the cut is made at the intersection of the floor and the fuselage skin at the right hand side of the fuselage cross-section. The open section shear can then be calculated using Equation 8.8, basically 'walking' through each cell in clockwise direction.

$$q_{s_i} = -\frac{S_y}{I_{xx}}\left(B_{r_i}\, y\right) + q_{s_{i-1}} \tag{8.9}$$

The wing structure can be seen as a four-cell multicell structure. Figure 8.7b illustrates a schematic drawing of the cell division and the cut locations. For each of the four sections the open section shear is computed by again 'walking' through each cell in clockwise sense. Similar to the fuselage case, the product moment of inertia can be neglected. This allows Equation 8.9 to be applied.

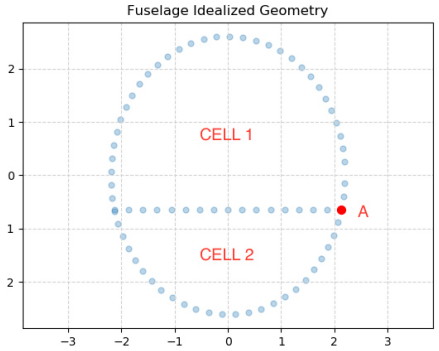

(a) Representation of Cell I and II (Cut is made at point A

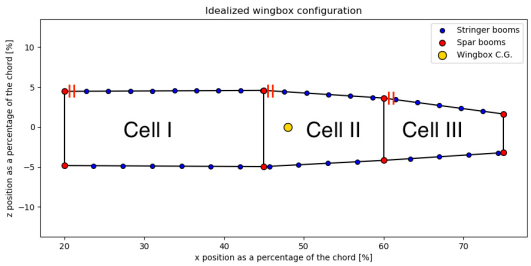

(b) Representation of Cell I, II and III (Cut locations are marked with red lines)

Figure 8.7: Shearflow And Cross-Section

After the open section shear flows are obtained, the closed section shear is calculated for the cells. To get the closed section shear flows, the redundant shear flows corresponding to its respective cell needs to be calculated and added to the open section shear flow. For the fuselage this means that 2 redundant shear flows must be computed: q_{s01} and q_{s02} for cell I and cell II respectively. For the wing this means that four redundant shear flows must be computed: q_{s01}, q_{s02}, q_{s03} and q_{s04} for cell I, cell II, cell III and cell IV respectively. The first step to take when calculating the closed section shear flow is to calculate the moment caused by the open section shear flows around a convenient point in the cross section. This moment must be equal to the torques generated by the redundant shear flows, as depicted in Equation 8.10 [39]. Where A_i and q_{s0i} are the cell area and redundant shear flow of cell i respectively.

$$0 = \sum(M_i) + \sum 2A_i q_{s0i} \tag{8.10}$$

In the fuselage analysis, the moment was taken around the centre of the fuselage floor. This simplifies the moment equation, as now the open section shear in the floor does not generate a moment. For the wing structure, the moments are taken around the centroid of the cross-section.

Currently with Equation 8.9 and Equation 8.10 one is not able to solve for the redundant shear flows, as the problem contains more unknowns than available equations. To solve this issue, the principle of twist is used: it is known that each adjacent cell must twist equally. Using the constraint that adjacent cells twist equally and computing the twist of each section will yield enough equations to solve for the redundant shear flows (q_{s0i}). The twist of a cell due to shear can be calculated using Equation 8.11 [39].

$$\frac{d\theta}{dz} = \frac{1}{2A_r}\oint \frac{qds}{Gt} \tag{8.11}$$

In an idealized cross-section qds will be the shear flow in between booms multiplied with the length in between booms, which means that in this case Equation 8.11 can be written as Equation 8.12, where qi and b_i are the shear flow and length of a particular location of skin.

$$\frac{d\theta}{dz} = \frac{1}{2A_r}\sum \frac{q_i bi}{t} \tag{8.12}$$

With the equations for the twist of the cells and the equation for the total moment in the cross-section (Equation 8.10) the system can be solved and the total shear flow in the section is obtained. The shear stress in the skin of the non-idealized cross-section can then be calculated by multiplying the shear flow with the skin thickness in a section.

Pressure Stress (fuselage only)

As the MoM-liner will operate at a high altitude, the aircraft's fuselage needs to be pressurized to keep a comfortable atmosphere inside the cabin for the passengers. This difference in pressure leads to stresses in the aircraft skin, which need to be taken into account in the fuselage design.
The pressure difference in the fuselage leads to a stress in two directions: the circular and horizontal direction, which can be calculated for a circular pressure vessel using Equation 8.13 and Equation 8.14 respectively [39].

$$\sigma_{circ} = \frac{\Delta pR}{t} \tag{8.13}$$

$$\sigma_{long} = \frac{\Delta pR}{2t} \tag{8.14}$$

As the longitudinal stress acts in the same plane and direction as the normal stress induced by bending, these two stresses must be superimposed.

The equations for pressure stress stated above are only valid for circular pressure vessels. As the MoM-liner has an elliptical fuselage, additional measures need to be taken to analyze the fuselage pressure stress. In an elliptical pressure vessel, the pressure differential wants to push back the elliptical fuselage shape back to a circular shape. This causes stress concentrations at the edges of the semi-major axis of the ellipse. After talking to a structures expert[3], it was advised that a preliminary value for this extra stress can be obtained by modelling the two-cell fuselage structure as a double-bubble configuration. This way, the floor is assumed to take all of the extra pressure loads caused by the elliptical shape. Figure 8.8a shows the double bubble configuration which will be used for this pressure analysis. R1 and R2 are chosen such that they fit the elliptical shape of the fuselage. α_1 and α_2 are calculated using Equation 8.15 and Equation 8.15 respectively.

$$cos(\alpha_1) = \frac{w}{R1} \tag{8.15}$$

$$cos(\alpha_2) = \frac{w}{R2} \tag{8.16}$$

Figure 8.8b shows the force equilibrium at the floor intersection. The shear flow carried by the floor member can then be calculated using Equation 8.17 [42].

$$T = pR_1 sin(\alpha_1) + pR_2 sin(\alpha_2) \tag{8.17}$$

Wing-Tip Deflection (wing only)

For the structural analysis of the wing it is necessary to set a boundary constraint for the wing-tip deflection of the front and rear wing. This constraint is induced by the fact that the structure of the front and back wing are analyzed separately, where in reality, this is one structure. After consultation with an expert in the field of Prandtl planes it was stated that the vertical attachment of the front and back wing is not loaded during cruise[4]. This can only be the case if the deflection of the front and back wing is exactly equal, otherwise compression or tension will occur.

The wing bending deflection can be computed using a combination of the moment at the tip of each section and the aerodynamic and weight forces applied as point loads at center of each section. Additionally the deflection due to the angular deflection, θ, of the previous section is added. The overall and angular deflection equations are presented in Equation 8.18 and Equation 8.19 where l is the length of a section and F is the force due to the wing weight and aerodynamic loads. The deflection equations that were superimposed to create the final equation are taken from Megson [39].

$$\Delta z_i = \frac{F_i \cdot \left(\frac{l}{2}\right)^2}{6 \cdot E \cdot I_{xx_i}} \cdot \frac{5}{2} l + \frac{M_i \cdot l^2}{2 \cdot E \cdot I_{xx_i}} + l \cdot sin(\theta_{i-1}) + \Delta z_{i-1} \tag{8.18}$$

[3]Private communication with TU Delft teacher R.C. Alderliesen, `https://www.tudelft.nl/en/staff/r.c.alderliesten`
[4]Private consultation with Prof. Frediani

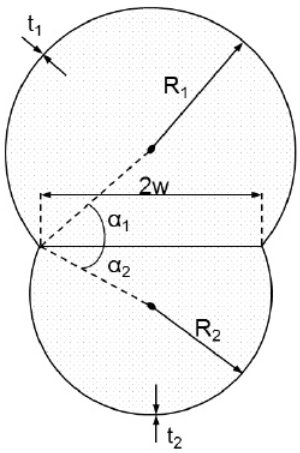

(a) Angles for Double Bubble Pressure Analysis [42]

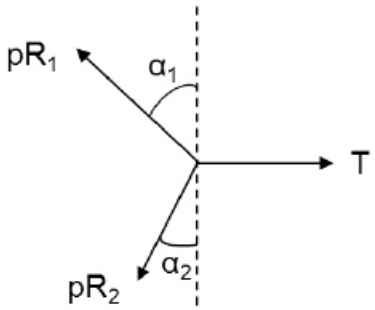

(b) Force Equilibrium Floor Pressure [42]

Figure 8.8: Fuselage Cross-Section Pressure Analysis

$$\theta_i = \frac{F_i \cdot \left(\frac{l}{2}\right)^2}{2 \cdot E \cdot I_{xx_i}} + \frac{M_i \cdot l^2}{\cdot E \cdot I_{xx_i}} + \theta_{i-1} \tag{8.19}$$

Principal and von Mises Stress

The shear and normal stresses are combined to generate the principal and von Mises stresses. These give a clear insight in the stress propagation throughout the structure. The maximum (σ_1) and minimum (σ_2) principal stress are computed using Equation 8.20 and the von Mises stress is computed using Equation 8.21.

$$\sigma_{1,2} = \frac{(\sigma_x + \sigma_y)}{2} \pm \sqrt{\left(\frac{\sigma_x + \sigma_y}{2}\right)^2 + 4\tau_{xy}^2} \tag{8.20}$$

$$\sigma_{VM} = \sqrt{\sigma_z^2 + 3\tau_{xy}^2} \tag{8.21}$$

8.2.7. Material Usage

The material choice of the design is something that has been considered in the preliminary phase and trade-off. The choice of material was decided to be aluminum. Nonetheless, it was decided to re-investigate the uses of composites as it might be beneficial for the fuselage skin. However, after a small investigation of composites the following conclusions were drawn:

- The use of composites will not yield a beneficial weight saving to the structure to the aircraft. The reason for this is that composites need a certain thickness to resist damage. In the case of narrow body aircraft, this minimum thickness will add up to a considerable thickness, therefore, the weight savings induced by the use of composites mainly comes into play when designing large wide body aircraft. Since the MoM-liner will be a narrow body aircraft, the weight savings would not be considered significant[5].

- The use of composites in the wings was investigated however due to computational limitations it was only possible to investigate isotropic composites. The advantage of this type of composite was found to be minimal (the main advantage of composites in wing structures is that their properties can be tailored). The slight if any decrease in structural weight did not outweigh the substantial cost increase and additional maintenance complexity. This is particularly pertinent for the MoM-liner due to the very stringent unit and operational cost requirements.

[5]As stated by Maarten van Mourik, director of programs at GKN Aerospace's Fokker business. URL `https://www.compositesworld.com/articles/fiber-metal-laminates-in-the-spotlight` [cited 20 June 2018]

- The cost of using composites is significantly higher than that of aluminum. The cost range of aluminum for the use of primary structures, is about half the cost of using composites. With a driving cost requirement, the preferable material choice is aluminum[6].

The aluminum used in the preliminary analysis is Al 7074 T6. This aluminum is selected as it has excellent all-round properties and has good fatigue behavior [40]. This is deemed sufficient for a preliminary analysis. The mechanical properties are presented in Table 8.2.

Table 8.2: Mechanical Properties of Al 7074 T6

Parameter	Value
Poisson ratio [-]	0.33
Yield strength [MPa]	503
Young's modulus [GPa]	71.9
Shear modulus [MPa]	27

8.2.8. Failure Modes

In the structural analysis four main failure modes are analyzed: compression buckling, shear buckling, tensile yield failure, crippling of the stringers and spars. For each of these modes the critical failure stress was determined and compared to the maximum stress observed at any point in the structure. If this critical stress was exceeded the structure was deemed to have failed and the configuration modified such that it was able to function properly. More on this is elaborated in subsection 8.2.9.

Aluminum

Compression Buckling

Both the wing and fuselage are subjected to a bending moment. This means that its bottom half is loaded in compression. As panels under compression tend to buckle, compression buckling analysis is critical in the design of an aircraft fuselage/wing.

The aircraft skin is reinforced by stringers. The buckling strength of a reinforced panel is calculated as follows: First, the critical buckling stress of the unreinforced skin is calculated, then the crippling stress of the stiffeners and their effect on the skin is determined and finally, the total strength of the panel can be calculated.

The critical buckling stress of an unreinforced skin panel can be calculated using Equation 8.22. In this equation, C is a parameter based on the boundary conditions of the plate, E is the Young's modulus of the material, v is the Poisson ratio of the material and b is the stringer pitch of the reinforced plate.

$$\sigma_{cr} = C\frac{\pi^2 E}{12\left(1-\nu^2\right)}\left(\frac{t}{b}\right)^2 \tag{8.22}$$

In order to calculate the crippling stress of a stringer, first the crippling stress of each flange of the stringer is calculated using Equation 8.23. If the ratio $\frac{\sigma_{cc}}{\sigma y}$ is smaller than one, this means that the flange will cripple before yielding and the crippling stress of the flange is equal to $\frac{\sigma_{cc}}{\sigma y}$ times the yield stress of the material. If the ratio $\frac{\sigma_{cc}}{\sigma y}$ is larger than one, the flange will fail in yielding.

$$\frac{\sigma_{cc}}{\sigma y} = \alpha\left[\frac{C}{\sigma_y}\frac{\pi^2 E}{12\left(1-\nu^2\right)}\left(\frac{t}{b}\right)^2\right]^{1-n} \tag{8.23}$$

The total crippling stress of a stiffener is calculated using Equation 8.24. This equation shows that the total crippling stress of a stringer is equal to the sum of the crippling stress of each flange multiplied with its area divided by the total area of the stringer.

$$\frac{\sum\left(\sigma_{cc_i} A_i\right)}{A_i} \tag{8.24}$$

[6]URL `https://www.compositesworld.com/articles/fiber-metal-laminates-in-the-spotlight` [cited 21 June 2018]

Shear Buckling

Just as in compression, thin plates can fail in buckling. Equation 8.25 shows the equation for shear buckling. In this equation, C_s is a parameter based on the boundary conditions of the plate. Other parameters affecting the shear buckling stability of a plate are the Young's modulus E_c, the Poisson ratio of the material, thickness of the plate and the stringer pitch.

$$\tau_{cr} = C_s \frac{\pi^2 E_c}{12\left(1-\nu^2\right)} \left(\frac{t}{b}\right)^2 \tag{8.25}$$

Tensile Yield

The final failure mode being considered is tensile yield. This failure mode is critical in sections with high normal stress, either due to bending or due to the pressure differential.

8.2.9. Optimization

With the stresses in the structure known and the critical stresses known, it is possible to optimize the structure such that these criteria are met and the weight of the structure is minimized. In this section this procedure will be detailed upon.

The optimization is set up in such a way that it is generic. Meaning that if a situations occurs that parameters are changed (e.g. by a concurrent working group - the aerodynamics group), it is extremely simple to rerun the optimization to obtain the optimized values.

To distinguish between the optimization of the fuselage and the optimization of the wing:

- ***Wing:*** During the optimization of the wing the optimized variables are the (1) *skin thickness* (t_{sk}) and (2) the *number of stringers*.
- ***Fuselage:*** During the optimization of the fuselage the optimized variables are the (1) *skin thickness* (t_{sk}) and (2) the *stringer flange, web and cap thickness* (t_{str}).

For both the wing and the fuselage all the other parameters such as user defined geometry and material properties are kept fixed. These are selected based on literature research and expert consultation. For the sake of page space economy, the process of optimization will be elaborated by using the fuselage as an example. Mainly because this is almost identical to the process of the wing.

The optimization is started by imputing the user defined fixed variables. These are the geometry parameters, stringer/frame/rib spacing, material properties and loads acting on the structure. The code then uses all these parameters to generate the geometry of the structure, i.e. the fuselage or wing box geometry with stringers, frames and ribs. The structure is discretized along the depth of the structure, generating n number of cross sections.

Minimum Gauge

For both metal and composites a minimum gauge exist, i.e. a minimum thickness an aluminum or CFRP sheet can attain. To allow for this to be implemented into the optimization the range of viable skin thicknesses is selected for the program to run through. These are the so called lower and upper bounds in the optimization. Using these bound the optimization will never return a skin or stringer thickness that is too small to be manufactured.

Safety Margins

Next to the upper and lower bounds that are set for the skin thickness, certain constraints must be defined such that the program is aware of the modes it is sizing for [40]. These constraints are generated by using the failure modes of the structure. An example for compression buckling of metal plates in shown in Equation 8.26. This equations depicts a safety margin for the compression buckling of a reinforced metal plate. As long as this safety margin is smaller than zero, the compression buckling criteria is met and the program is allowed to continue its optimization. As can be seen in Equation 8.26 a safety factor is included in the constraint. This safety margin can be adjusted as preferred. Safety margins are set up for all failure modes. During the optimization all safety margins must be met, meaning that they must all be smaller than zero.

$$SM_{buckling\_c} = \frac{\sigma_{normal}}{SF \cdot \sigma_{cr}} - 1 \tag{8.26}$$

Objective Function

The process of optimizing is done with the goal to minimize the objective function. This is the function that should be minimized within the constraints to achieve an optimal design.

Wings

The objective function for the wing computes the total weight of the wing this is achieved by summing the volume of each of the structural elements for each section and then multiplying by the density. The number of stringers and the skin thickness within a certain allowable range to generate configurations. Each configuration is then the tested to see if they do not fail and meets the tip deflection criteria. The configuration for which the objective function is minimized is ultimately selected.

Fuselage

The objective function for the fuselage computes the total area of the fuselage cross section by using the skin thickness and web/flange/cap thickness of the stringer. The objective function is depicted in Equation 8.27. During the optimization a viable range of skin thicknesses and stringer cap/web/flange thicknesses. This range is bounded by the upper and lower bound selected. Once again the goal is to find the skin thickness and the stringer cap/web/flange thickness such that the objective function is *minimized*.

$$A_{cross-section} = \sum \left(2b_{f_i} t_{str_i} + 2b_{w_i} t_{str_i} + 2b_{w_i} t_{str_i} + b_{c_i} t_{str_i} + t_{sk_i} b_{sct_i}\right) \tag{8.27}$$

Fuselage Example

The complete optimization procedure is presented in the flowchart depicted in Figure 8.9. After the discretization the following procedure is maintained (The following steps described below are all run for a viable range of skin thicknesses and stringer cap/web/flange thicknesses. This range is bounded by the upper and lower bound selected)..:

1. Each discretized cross section consists of an equal number of stringers, as the fuselage optimization is performed with an equal number of stringers. The geometric properties of the discretized cross sections are computed, i.e. the centroid location, moment of inertia, and boom areas.

2. The program computes the stress in the entire geometry using the user defined input parameters and geometric properties.

3. The program runs through each different boom, starting at the boom at the most right location. For each boom is selects the highest normal, shear, vonmises and principal stress.

4. Using the maximum stress selected the safety margins are tested. If the safety margin tested is larger than zero it indicates that the structure would fail for the selected thickness combination

5. The program continues running for each boom until it has selected a combination of skin thicknesses and stringer cap/web/flange thickness such that the objective function is minimum for that boom.

6. After it has finished a boom it moves to the next boom and starts the process again. The process is then done all over again to minimize the objective function for the specific section. Minimizing the area for each boom separately will inevitably minimize the total area of the fuselage. In the end this minimizes the total weight of the aircraft.

8.2.10. Cut-Out Analysis

In order to accommodate for access doors and windows, cut-outs need to be made in the fuselage-structure. These cutouts cause discontinuities in the aircraft structure. All the loads that would otherwise flow through the cut-out hole now need to be redistributed to the surrounding panel sections. These sections will need to be reinforced to take these additional loads, which results in a weight increase of the structure. In this section, a simplified window cut-out is analyzed. The analysis will be done for the most critically loaded fuselage section. The weight penalty calculated for this window will then be used for all windows in the fuselage structure.
Figure 8.10a shows how the window cutout will be analyzed. In this figure, the horizontal lines represent frames, whereas the horizontal lines represent stiffeners. It is assumed that the window cutout is an entire panel cut-out: This means that the entire center panel is removed. q_c, q_h and q_s represent the stress increase in the panels surrounding the cut-out.

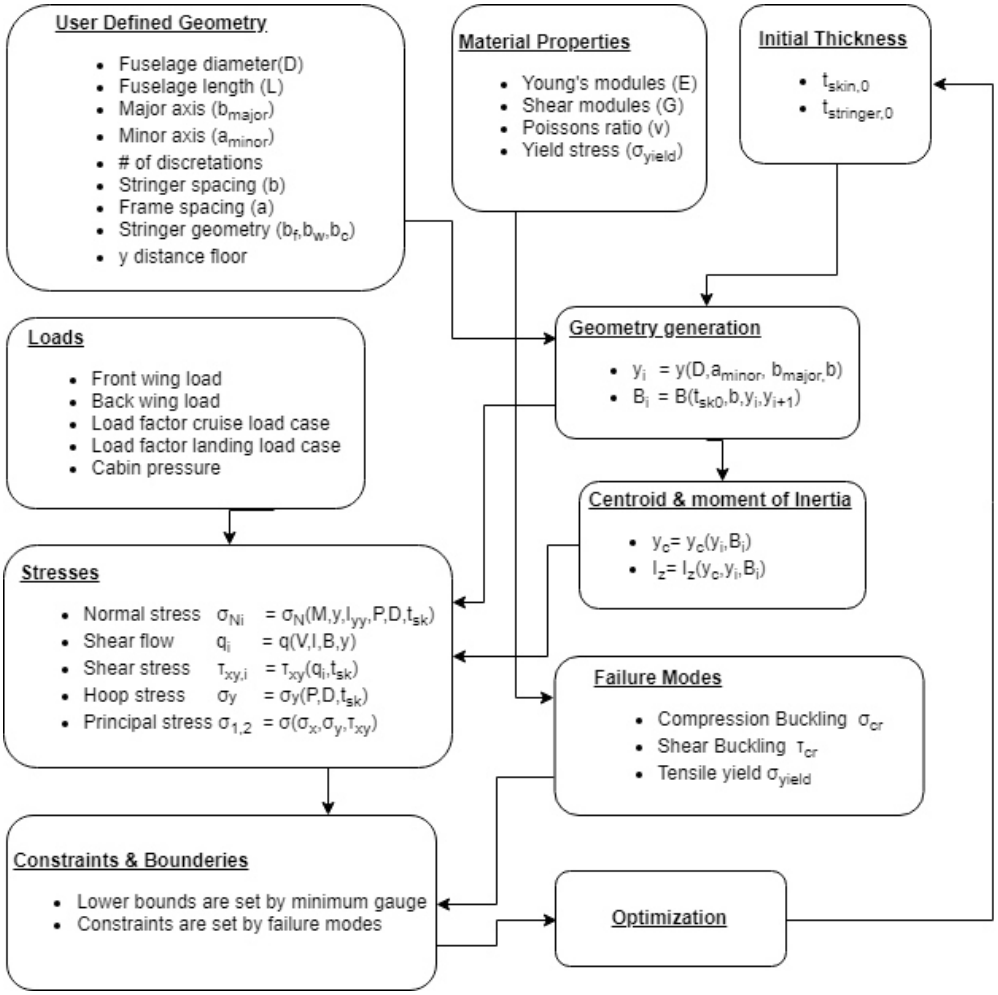

Figure 8.9: Flow Chart for the Structural Analysis (Fuselage Example)

In order to calculate the stress increase in sections q_c, q_h and q_s three cuts are made: Two horizontal cuts above and below the removed panel and one vertical cut to the left of the removed panel. Figure 8.10b shows an example of the vertical cut. The value for q_h can be found by setting up the equilibrium equation, as shown in Equation 8.28 and Equation 8.29. In a similar fashion q_c and q_s can be calculated. The final values for q_c and q_s are shown in Equation 8.31 and Equation 8.30 respectively.

$$q_h H_1 + q_h H_3 = q H_2 \tag{8.28}$$

$$q_h = q \frac{H_2}{H_1 H_3} \tag{8.29}$$

$$q_s = q \frac{L_2}{L_1 + L_3} \tag{8.30}$$

$$q_c = -q_h \frac{L_2}{L_1 + L_3} \tag{8.31}$$

After the stresses q_c, q_h and q_s are calculated, they are added to the original shear flows in these sections. With the new shear flows obtained, the optimization procedure is started again for this section. This yields a new skin thickness.

8.3. Verification of Structures Code

This section describes the verification of the code written for the structural analysis code. The implementation of the method of structural idealization, as well as the calculation of stresses in the structural models and failure modes of the models.

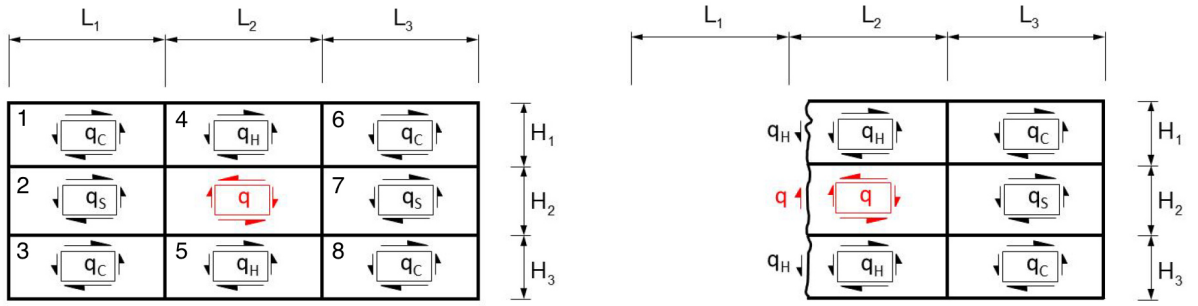

(a) Fuselage Panel with Window Cut-Out [43]

(b) Vertical Cut Equilibrium [43]

Figure 8.10: Fuselage Panel Window Cut-Out

The structural idealization method is verified using a structural idealization example from Megson [39]. The example covers a structural idealization of a single cell fuselage structure using 16 stringer booms. Subsequently, the boom areas, moment of inertia, normal stresses and shear stresses are calculated. The structural analysis code is considered verified when the calculated values lie within 5% of the results given in the Megson example. The percentage difference is calculated using Equation 8.32. As the output of same verification parameters is a list of values, only the value showing the largest percentage difference is showed.

$$\%_{difference} = \frac{x_{calculated} - x_{example}}{x_{example}} \cdot 100\% \tag{8.32}$$

The method for calculating the buckling strength of a reinforced panel is verified using notes from the structural analysis course [44]. As can be seen in Table 8.3, the largest difference between the calculated values and theoretical result is only 0.15%. This means that the structural idealization code is verified.

Table 8.3: Unit Test Results for Structural Analysis

Unit Test ID	Description	Parameter	Unit	UT result	Theor. res.	Difference (%)
UT-Struct-01	Verif. of boom area	B	m^2	216.6	216.6	0
UT-Struct-02	Verif. of MOI	Ixx	mm^4	$2.52 \cdot 10^8$	$2.52 \cdot 10^8$	0
UT-Struct-03	Verif. of open sect shear flow	qb	N/m	66.1	66.0	0.15
UT-Struct-04	Verif. of closed sect shear flow	qs,0	N/m	32.8	32.8	0
UT-Struct-05	Verif. of unreinforced panel buckling strength	$\sigma_{cc_{sk}}$	Mpa	26.1	26.1	0
UT-Struct-06	Verif. of stringer crippling stress	$\sigma_{cc_{str}}$	Mpa	445.6	445.6	0
UT-Struct-06	Verif. of reinforced panel buckling strength	$\sigma_{cc_{panel}}$	Mpa	275	275	0

8.3.1. Validation of Structural Models

Next to determining whether the code of the structural models works properly, it is also necessary to check if the developed models actually represent their real-life counterparts. This is done by validation of the models.

Models can be verified by the following methods [45]:

- **Experience** with application of similar models in similar circumstances.
- **Analysis** showing that the elements of the model are of necessity correct and are correctly integrated.
- **Comparison** with test cases in the form of independent models of proven validity or actual test data.

In case of the validation of the wing and fuselage structural model, comparison seems to be the best method to use. Validating by experience of the model developers was deemed inappropriate, as none of the model developers have sufficient industry experience. Comparison is preferred over analysis, as the limited experience of the developers involved might compromise the accuracy of the analysis. The accuracy of using comparison as a validation method is not an issue, as this involves the use of comparable models of proven validity.

Both models will thus be validated using comparison. Comparing the models to a proven Finite Element Analysis model seems like the best way of validating the models. As no such model is available to this team, the model validation remains for further analysis.

9
Stability & Control

For a commercial aircraft safety is of the utmost importance. The aircraft needs to be sized such that its natural behaviour promotes stability. The aircraft and control surfaces need to be sized such that control of the plane is as easy as possible for the pilot. In this chapter the methodology for stability and control analysis is outlined with regard to a Prandtl plane, furthermore control surface sizing is discussed as well as landing gear placement.

9.1. Summary Methodology

The static stability is analyzed by checking what happens to the aircraft when a disturbance in angle of attack occurs. Then the controllability is analyzed by seeing how controllable the aircraft still is at the most critical speed; the lowest speed, which is the landing speed. After it has been determined the aircraft is stable and controllable, it needs high-lift devices and control surfaces for special maneuvers, like landing, take-off, pitching, rolling, and yawing.

9.2. Methodology

In this section the methodology for stability & control is outlined. First, static stability & control is explained. Then, a loading diagram is given. Lastly, high-lift devices and control surfaces are explained.

9.2.1. Static Stability & Control

Static stability describes the reaction of an aircraft in steady flight to a disturbance in the air affecting its angle of attack. The aircraft is said to be statically stable if the resulting pitching moment counteracts this disturbance, and the aircraft returns to its undisturbed condition without any control input. Static controllability refers to the ability of the tail and elevator to counteract the aerodynamic pitching moment and change the angle of attack on the aircraft as desired by the pilot. For a successful aircraft design, it is of utmost importance that the aircraft is both statically stable and controllable. This is not only necessary for good handling characteristics, but is a certification requirement as set forth in CS-25.171 [20]. Modern fly-by-wire systems are easily able to cope with statically unstable aircraft (e.g. air superiority fighters), however, in case of failure of the system, the aircraft can become difficult to impossible to control. Thus, static stability & control is an absolutely integral part of every aircraft design.

Standard aircraft designs have a main wing with an upward lifting force and a smaller tail with a small positive or even negative force. This distribution easily allows for moment equilibrium and thus allows for stability. The specialty of this box-wing design is that its main wing is split up in two surfaces with strong upward lifting forces. This inherent configuration characteristic imposes additional challenges on this topic. According to Prandtl [46] and Frediani [47], the optimum lift distribution to result in minimum induced drag, and thus best efficiency, is an equal split of the total lifting force over the two wings. However, following an extensive stability analysis, Schiktanz [48] concluded that static stability is impossible to achieve for an equal distribution. He concluded that for stability the main wing needs to generate more lift than the aft wing. A careful manipulation of this ratio is necessary to create a sufficient static margin while not increasing induced drag more than necessary. Another special consideration should be given to the positioning of the wings. Due to their large lateral distance, the drag forces could potentially create a non-negligible moment around the center of gravity of the aircraft. However, studies by Schiktanz [48] and Jemitola [49] have found that for a preliminary design, it is justified to neglect all thrust and drag forces. Thus, for this analysis, only longitudinal distances are of relevance and the wings can be assumed to be on the same level. This assumption reduces the model complexity significantly and allows the use of established formulae and procedures for normal tail sizing for this configuration. For this analysis, the method proposed by Torenbeek [26] will be used and the individual steps will be elaborated upon in the following. Equation (9.1) is used for the static stability analysis and Equation 9.2 for controllability. Based on these two equations, the allowable most forward and most

aft c.g. locations can be determined, which in turn influence the wing positioning in order to assure that the c.g. can be kept within these boundaries throughout all phases of flight.

The controllability equation limits the most forward position, the stability equation the most aft c.g. position. These c.g. limits then need to be compared with the c.g. excursion in loading diagrams and, if necessary, restrictions must be placed on the allowable loading conditions. Lastly, using the most aft c.g. location, the landing gear can be positioned along the aircraft.

$$\bar{x}_{cg} = \bar{x}_{ac} + \frac{C_{L\alpha_h}}{C_{L\alpha_{A-h}}}\left(1 - \frac{d\epsilon}{d\alpha}\right)\frac{S_h l_h}{S\bar{c}}\left(\frac{V_h}{V}\right)^2 - SM \tag{9.1}$$

$$\bar{x}_{cg} = \bar{x}_{ac} - \frac{C_{m_{ac}}}{C_{L_{A-h}}} + \frac{C_{L_h}}{C_{L_{A-h}}}\frac{S_h l_h}{S\bar{c}}\left(\frac{V_h}{V}\right)^2 \tag{9.2}$$

Static Stability

For an aircraft to be statically stable, the c.g. must lie in front of the neutral point, that is, the point at which both the net moment and the change in moment due to a change in angle of attack is zero. The location of this point is dependent on the speed of the aircraft. At higher speeds, the neutral point moves forward due to compressibility effects of the air and the formation of shock waves on the wing. As the c.g. must always lie in front of the neutral point, the most critical flight condition to evaluate the static margin is high-speed cruise. Thus, all coefficients used to generate Equation 9.1 are evaluated at cruising speed and with the aircraft in clean configuration. Most of these coefficients can be obtained directly from the general layout, e.g. wing areas and arms, and the aerodynamics department, e.g. lift curve slopes.

However, aerodynamics only analyses the performance of the wing, which is not sufficient for a reliable stability analysis. Thus, several correction factors were implemented, mostly regarding the influence of the fuselage (Equation 9.3). This equation implements two correction factors and strongly depends on the shape and size of the fuselage and wing position. The first term describes a forward a.c. shift. This destabilizing contribution is mostly due to the lift generation by the nose section of the aircraft. The second term is stabilizing; it shifts the a.c. aft due to a loss of lift at the wing fuselage intersection. The coefficient $C_{L_{\alpha_{A-h}}}$ is the corrected lift curve slope for the front wing. The correction is shown in Equation 9.4 and describes how the lift curve changes due to the loss in lifting wing area (S_{net}/S) and the influence of the fuselage. The second correction factor, Equation 9.5, corrects for the position of the engines. For back mounted engines, the factor k_n should be set equal to 2.5. Next to the position, the influence of the engines also strongly depends on the size of the nacelles and the amount of engines.

$$\left(\frac{x_{ac}}{\bar{c}}\right)_{wf} = \left(\frac{x_{ac}}{\bar{c}}\right)_{w} - \frac{1.8}{C_{L_{\alpha_{A-h}}}}\frac{b_f h_f l_{fn}}{S\bar{c}} + \frac{0.273}{1+\lambda}\frac{b_f c_g (b-b_f)}{\bar{c}^2(b+2.15b_f)}tan\Lambda_{1/4} \tag{9.3}$$

$$C_{L_{\alpha_{A-h}}} = C_{L_{\alpha_w}}\left(1 + 2.15\frac{b_f}{b}\right)\frac{S_{net}}{S} + \frac{\pi b_f^2}{2S} \tag{9.4}$$

$$\Delta\left(\frac{x_{ac}}{\bar{c}}\right) = \sum k_n \frac{b_n^2 l_n}{S\bar{c}C_{L_{\alpha_{A-h}}}} \tag{9.5}$$

The second important factor that needs to be determined is the downwash gradient of the first wing on the second ($\frac{d\epsilon}{d\alpha}$). Equation (9.6) shows the formula to determine the gradient; Equation 9.7 and Equation 9.8 give the two coefficients that account for wing sweep in this formula. The strength of the down wash strongly depends on the lateral and longitudinal distance from the front to the back wing. The coefficient r is equal to $2l_h/b$, $m_{tv} = 2h/b$. Due to the large vertical separation (h) of the two wings is the effective free stream velocity at the back wing not influenced by the front wing, thus $V_h = V$. Lastly, a stability margin (SM) is employed. This is done to gain a safety margin against instability. Furthermore, this static analysis is done assuming a 'stick-fixed' neutral point. If the elevator is free to move ('stick-free'), the neutral point will slightly move forward. Also, other aerodynamic effects can have a small influence on the exact position. By assuming a stability margin of $0.05\bar{c}$, not only the safety margin, but also changes due to aerodynamics and 'stick-free' effects can be accounted for, thus simplifying the design process significantly as only one stability limit needs to be evaluated.

$$\frac{d\epsilon}{d\alpha} = \frac{K_{\epsilon_\Lambda}}{K_{\epsilon_{\Lambda=0}}}\left(\frac{r}{r^2+m_{tv}^2}\frac{0.4876}{\sqrt{r^2+0.6319+m_{tv}^2}} + \left[1+\left(\frac{r^2}{r^2+0.7915+5.0734m_{tv}^2}\right)^{0.3113}\right]\left\{1-\sqrt{\frac{m_{tv}^2}{1+m_{tv}^2}}\right\}\right)\frac{C_{L_{\alpha_w}}}{\pi A} \tag{9.6}$$

$$K_{\epsilon_\Lambda} = \frac{0.1124 + 0.1265\Lambda + 0.1766\Lambda^2}{r^2} + \frac{0.1024}{r} + 2 \tag{9.7}$$

$$K_{\epsilon_{\Lambda=0}} = \frac{0.1124}{r^2} + \frac{0.1024}{r} + 2 \tag{9.8}$$

Controllability

The most important aspect for any aircraft design is that it is controllable in all phases of the flight. The most critical phase for controllability is the lowest flight speed in landing configuration, just before touchdown. At the lowest speeds, the wings' lift coefficient are highest, thus also the resulting aerodynamic moments. Additionally, the extension of flaps in landing configuration has a significant impact on the total pitching moment. For these reasons it is imperative to have a wing/stabilizer configuration that is able to counteract these moments and can trim the aircraft for stable flight. Equation (9.2) gives the basic equation that must be satisfied for controllability. While the lift coefficients can be obtained from the performance and aerodynamics departments, they can only provide the wing pitching moments. Thus, these values need to be corrected for the actual aircraft configuration. The final moment is comprised of several parts: wing, flaps, fuselage and engines (Equation 9.9). Equation (9.10) gives the correction of the 2D airfoil pitching moment to the actual 3D wing, Equation 9.11 the influence of the fuselage. For the engine position at the back of the fuselage, a general correction factor of 0.2 is added. Lastly, Equation 9.12 gives the change in pitching moment due to the flaps. This factor strongly relies on the high-lift device design department to provide the necessary characteristics and size of the used flap system. Once the flaps are sized, their parameters can be used to determine the coefficients μ_1, μ_2 and μ_3, based on Figure 9.1, Figure 9.2a and Figure 9.2b.

$$C_{m_{ac}} = C_{m_{ac_w}} + \Delta_f C_{m_{ac}} + \Delta_{fus} C_{m_{ac}} + \Delta_{nac} C_{m_{ac}} \tag{9.9}$$

$$C_{m_{ac}} = C_{m_{0_{airfoil}}} \left(\frac{A cos^2 \Lambda}{A + 2cos\Lambda} \right) \tag{9.10}$$

$$\Delta_{fus} C_{m_{ac}} = -1.8 \left(1 - \frac{2.5 b_f}{l_f} \right) \frac{\pi b_f h_f l_f}{4 S \bar{c}} \frac{C_{L_0}}{C_{L_{\alpha_{A-h}}}} \tag{9.11}$$

$$\Delta C_{m_{ac}} = \mu_2 \left\{ -\mu_1 \Delta C_{l_{max}} \frac{c'}{c} - \left[C_L + \Delta C_{l_{max}} \left(1 - \frac{S_{wf}}{S} \right) \right] \frac{1}{8} \frac{c'}{c} \left(\frac{c'}{c} - 1 \right) \right\} + 0.7 \frac{A}{1 + \frac{2}{A}} \mu_3 \Delta C_{l_{max}} tan\Lambda_{1/4} \tag{9.12}$$

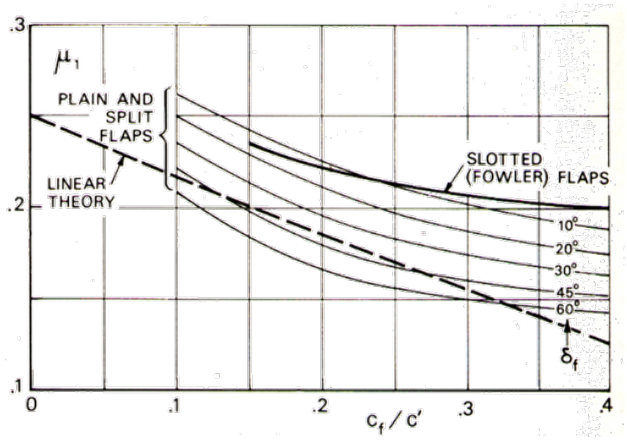

Figure 9.1: μ_1 for Equation 9.12

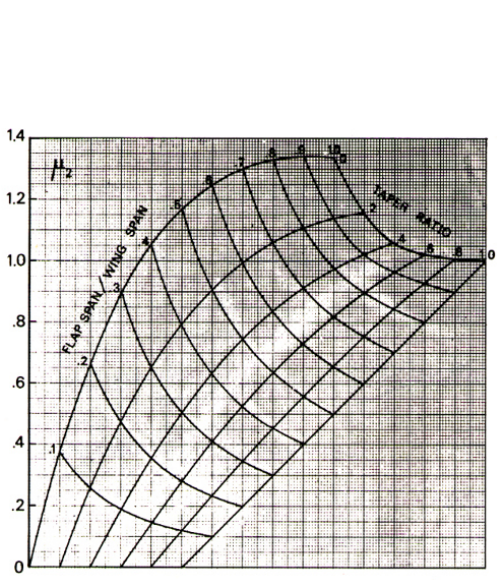

(a) μ_2

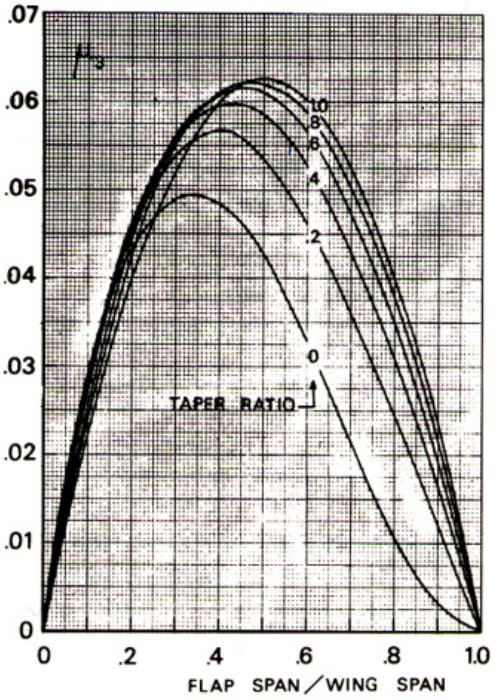

(b) μ_3

Figure 9.2: Coefficients for Equation 9.12

Loading Diagram

The loading diagram of an aircraft shows the position of its center of gravity, based on the way the aircraft is loaded. The fuel, cargo and passengers are added consecutively. The passenger loading was done in the following order: window, aisle, center. And both from front to back and back to front. The loading diagram is important as it shows all the possible c.g. locations, these locations should fall inside of the static margin. Equation 9.13 shows how the center of gravity changes when a new 'item' is added.

$$x_{cg} = \frac{\Sigma(x_{cg_i} * W_i)}{\Sigma W_i} \tag{9.13}$$

After performing these calculations a loading diagram can be constructed, this diagram is shown in chapter 12.

High-Lift Devices

High-lift devices of an aircraft are needed to overcome the deficit in maximum lift coefficient in clean configuration versus in (take-off and) landing configuration. The high-lift devices (HLDs) of the MoM-liner have been designed by first evaluating the $\Delta C_{L_{max}}$ needed. Then an appropriate type and combination of HLDs must be selected. Then, using Equation 9.14, the necessary wing flapped area can be calculated [26][50]. This equation was split up for the leading and trailing edge of the wing, since different types of HLDs are used on both edges. Appropriate $\Delta C_{l_{max}}$ values for various types of HLDs can be found and calculated using Torenbeek's methods [26][50].

$$S_{wf} = \frac{\Delta C_{L_{max}} * S}{0.9 * \Delta C_{l_{max}} * cos(\lambda_{hinge})} \tag{9.14}$$

Input values needed for this equation are the needed extra lift coefficient, spar locations, and various wing parameters; area, span, taper ratio and sweep angle.

Wing Control Surfaces

Aircraft need to be controlled over three axes, which calls for control surfaces. Aircraft need lateral control, longitudinal control, and directional control. These three and the design of the corresponding control surfaces are discussed in this subsection. The MoM-liner, a Prandtl plane, is not a conventional aircraft, of course, and thus control surfaces cannot be fully designed using conventional methods. However, when analyzed in more detail, it

could be concluded that a conventional method could be applied and then altered for the Prandtl plane. As the Prandtl plane is bluntly said a conventional aircraft with another wing instead of a horizontal tail, so two wings instead of one. Therefore, the MoM-liner will have two sets of ailerons and elevators instead of one, one set on each wing. Hence, it is chosen to design the control surfaces according to conventional methods, this gives the area of the control surfaces. This area is the total control surface area needed, so as the MoM-liner has two sets of each, the area could be halved for each wing.

Aileron Design

First, there is the aileron design, this gives lateral controllability. The motion around this axis is called roll. The MoM-liner is a medium-weight transport aircraft and thus falls into class II aircraft [50]. This calls for a 45 degree roll in 1.4 s, which is the requirement the ailerons on the MoM-liner need to be designed for. To design for this, the roll rate of the aircraft must be known, this can be calculated using Equation 9.15 [50].

$$P = -\frac{C_{l_{\delta a}}}{C_{l_P}} \delta a_{max} \left(\frac{2V}{b} \right) \tag{9.15}$$

The input variables for this equation are the maximum deflection angle of the aileron - this is a design choice, the speed and span, the aileron control derivative ($C_{l_{\delta a}}$) and the roll damping coefficient (C_{l_P}). The latter two can be calculated using Equation 9.16 and Equation 9.17. Which, in turn, have their respective input variables, too. These are mainly wing and airfoil characteristics, $c(y)$ is the chord length at point y along the wing span, which is a linear function.

$$C_{l_{\delta a}} = \frac{2c_{l_\alpha}\tau}{S_{ref} b} \int_{b1}^{b2} c(y) y dy \tag{9.16}$$

$$C_{l_P} = -\frac{4(c_{l_\alpha} + c_{d_0})}{S_{ref} b^2} \int_0^{b/2} c(y) y^2 dy \tag{9.17}$$

Elevator Design

Next, the elevators ensure longitudinal controllability. The design of the elevators is a bit more distinct from a conventional design, since the MoM-liner will have one set of elevators in front of the c.g. besides the normal set of elevators aft of the c.g. Therefore, the elevator is sized using the sum of moments around the main landing gear. An artistic visualization of all the forces acting on the MoM-liner can be seen in Figure 9.3. It should be noted L_h will be upwards for the MoM-liner. With the help of Equation 9.18 the elevator can be sized, as it gives the increase in C_L with increasing elevator angle. It can thus be calculated what moment the elevator creates and in this manner it can be sized. The conventional method also uses moments to size the elevators, that is why it is chosen to do it this way. The moment around the main landing should be larger than zero to be able to rotate and take off, where the clockwise moment in Figure 9.3 is defined positive. In Equation 9.18, the dynamic pressure ratio (η) and area ratio both reduce to one, since the front and aft tail have the same geometry and the spacing is large enough to assume no influence for this part of the design.

$$C_{L_{\Delta E}} = C_{L_{a_h}} \eta_h \frac{S_h}{S} \frac{b_E}{b_h} \tau_E \tag{9.18}$$

Spoiler Design

One of the main means to brake at landing is the use of spoilers. Spoilers are essentially flat plates placed on top of the wing which can be deflected upwards. Deflecting these plates results in a controlled stall over the section of the wing behind the spoiler. Next to braking at landing, spoilers also help descend an aircraft without increasing its speed and can be used as a device to control roll. Spoilers contribute to better landing characteristics in two different ways. The spoilers increase drag due to the separation that takes place behind the spoiler and the spoilers decrease the lift of an aircraft. A decrease in lift results in a higher normal force of the aircraft and hence the braking power of the landing gear can be used with a smaller risk of skidding [51].

To design the spoilers, several coefficients and parameters have to be calculated. These can be seen in Equation 9.19 to Equation 9.24. First, the spoiler deflection angle and span ratio (span of the spoilers divided by span of the wing) are assumed. Then the seven equations are used to ultimately find an area and chord length of the spoilers. This process is iterated until "normal" and acceptable values of the area and chord length are found.

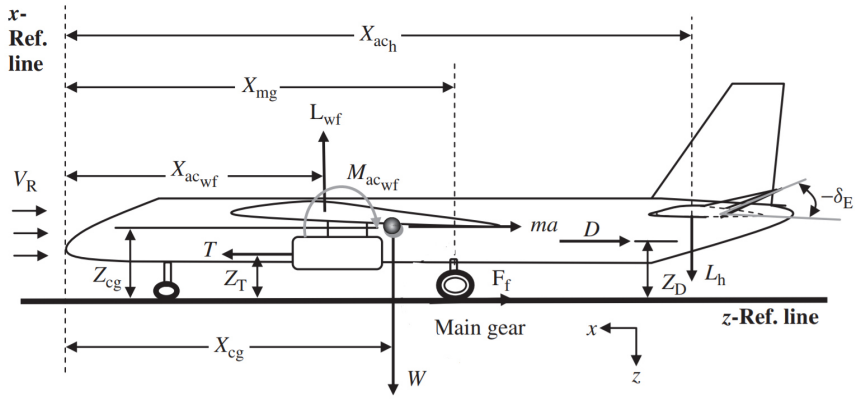

Figure 9.3: Schematic Impression of All Moments [51]

$$\Delta C_{L_S} = -C_L \frac{b_s}{b} \tag{9.19}$$

$$C_{L_L} = C_{L_{ref}} = C_{L_C} + \Delta C_{L_{flap_L}} + \Delta C_{L_s} \tag{9.20}$$

$$S_G = \frac{m}{\rho S(C_{D_L} - \mu_G C_{L_L})} * ln\left[1 + \frac{\rho S(C_{D_L} - \mu_G C_{L_L})}{2(\mu_G + k_1\mu_B)mg}\right] \tag{9.21}$$

$$C_{D_L} = C_{D_{0L}} + KC^2_{L_{wf}} + C_{D_S} \tag{9.22}$$

$$C_{D_{O_L}} = C_{D_0} + C_{D_{0_{LG}}} + C_{D_{0HLD_L}} \tag{9.23}$$

$$C_{D_S} = 1.9sin(\delta_S)\frac{b_S C_S}{S} \tag{9.24}$$

Vertical Tail Design

The main purpose of the vertical tail is to provide lateral and directional stability. For the tail to achieve this, the most important parameters are the area of the tail and the tail arm to the wing. In preliminary tail design, the most important parameter is the vertical tail volume coefficient $\bar{V}_v$. It is defined in Equation 9.25. For an initial estimate, this value is based on statistical data. Based on values provided by Sadraey [52], an average tail volume of 0.078 was computed and used for this tail sizing. Based on the lay-out of the aircraft, the total vertical surface can now be determined. Based on this, the geometry is found. Typical values for the relevant parameters are shown in Table 9.1.

$$\bar{V}_v = \frac{l_v S_v}{bS} \tag{9.25}$$

Table 9.1: Typical Ranges for Vertical Tail Parameters

Parameter	Range
$\bar{V}_v$	0.02 - 0.12
$\Lambda_{v,LE}$	Λ_w - 50°
A	1 - 2
λ	0.3 - 0.7
K_{f1}	0.65 - 0.85

To determine if the tail is sufficiently large, the stability derivative C_{n_β} can be used (Equation 9.26). This value describes the reaction of the aircraft around the vertical axis due to a sideslip angle. For the aircraft to be stable,

this value needs to be positive. If the tail does not meet the requirement, then the tail volume should be increased. Regarding airfoils, a symmetrical airfoil must be selected in order not to create any moment in normal flight. Additionally, the tail must be clear of compressibility effects in order not to reduce the tail effectiveness. Thus, the Mach number at the tail must be less than at the wing. For this, the maximum thickness of the vertical tail should be less than that of the main wings.

$$C_{n_\beta} \approx C_{n_{\beta_v}} = K_{f1} C_{L_{\alpha_v}} \left(1 - \frac{d\sigma}{d\beta}\right) \eta_v \frac{l_{vt} S_v}{bS} \tag{9.26}$$

Rudder Design

The design of the rudder is tightly connected to vertical tail design. While the tail provides for directional stability, the rudder assures controllability. Important design parameters for the rudder are: area, chord, span and maximum deflection. This design step can be done in a similar fashion to the tail design; based on statistical values and checked against imposed constraints. Again, the rudder sizing is done following the method described by Sadraey [52]. An important parameter for the rudder is $C_{n\delta r}$, a measure for the yawing moment due to rudder deflection (Equation 9.27). The parameter τ_r is called the rudder angle of attack effectiveness parameter and directly dependent on the selected rudder chord-to-vertical tail chord ration $\frac{b_r}{b_v}$. This relationship is shown in Equation 9.27.

$$C_{n_{\delta r}} = -C_{L_{\alpha_v}} \bar{V}_v \eta_v \tau_r \frac{b_r}{b_v} \tag{9.27}$$

For every multiengine aircraft, losing an engine is a realistic consideration. Thus, the rudder needs to be able to create a large enough moment to counteract the moment induced by the remaining engine. The most critical condition for this occurrence is at low speeds, as less air flows around the rudder surface, thus decreasing its effectiveness. Thus, CS-25 [20] require every multiengine airplane to be controllable at a critical speed of no more than 1.13 stall speed and under full power. This speed is referred to as V_{mc}, the minimum control speed. To include a safety margin and account for any potential unfavorable conditions present in flight, Sadraey recommends that the tail is sized for a V_{mc} of 80% of the stall speed. This recommendation is followed for this design. Equation (9.28) describes the rudder deflection necessary to counteract the engine moment. The critical speed is indirectly incorporated through the dynamic pressure $\bar{q}$. Based on statistics a maximum value for δ_r was chosen to be 30°. In order to satisfy the engine failure constraint, the maximum value for Equation 9.28 needs to be smaller than the maximum deflection angle.

$$\delta_r = \frac{T}{y}_T - \bar{q} S b C_{n_{\delta_7 r}} \tag{9.28}$$

The second major constraint that the rudder design must be tested against are crosswind landings. For these, the rudder must be able to counteract the moment created by the wind force pushing from the side of the plane. CS-25 requirements dictate that a transport category aircraft must be able to fly safely in a minimum crosswind of 25 kts. However, in flying practice, it often happens that wind exceeds these values. Thus, most aircraft are designed and certified to higher crosswind speeds. Here, having a larger tail and rudder is very beneficial, as it extends the effective flight envelope of the aircraft by allowing it to land in stronger crosswind conditions. This fact will be taken into account for the tail design, and the aircraft will be designed to safely fly in crosswinds up to 40 kts, a value most current transport aircraft are certified for. To determine if the requirement is satisfied, they system of Equation 9.29 and Equation 9.30 has to be solved. This set gives two unknowns, the rudder deflection δ_r and the crab angle σ. The remaining derivatives are given in Equation 9.26, Equation 9.27, Equation 9.31 and Equation 9.32. eq. (9.33) shows the determination of the side force acting on the aircraft, the value C_{D_y} is typically in the range of 0.5-0.8. K_{f2} is the contribution of the fuselage to C_{y_β} and typically between 1.3 and 1.4.

$$0.5 \rho V_T^2 S b \left(C_{n_\beta}(\beta - \sigma) + C_{n_{d_r}} \delta_r\right) + F_w d_c cos\sigma = 0 \tag{9.29}$$

$$0.5 \rho V_w^2 S_S C_{D_y} - 0.5 \rho V_T^2 S b \left(C_{y_\beta}(\beta - \sigma) + C_{y_{d_r}} \delta_r\right) = 0 \tag{9.30}$$

$$C_{y_\beta} \approx C_{y_{\beta_v}} = -K_{f2} C_{L_{\alpha_v}} \left(1 - \frac{d\sigma}{d\beta}\right) \eta_v \frac{S_v}{S} \tag{9.31}$$

$$C_{y_{dr}} = C_{L_{\alpha_v}} \eta_v \tau_r \frac{b_r}{b_v} \frac{S_v}{S} \tag{9.32}$$

$$F_w = \frac{1}{2}\rho V_w^2 S_S C_{D_y}; \qquad V_T = \sqrt{V^2 + V_w^2} \tag{9.33}$$

Control Allocation Method

Now that all the control surfaces have been designed, it must first be explained why they are configured like this and how they are controlled. First, since the MoM-liner has two wings, and thus essentially twice the place to install control surfaces, it must be explained why the choice is made to put control surfaces on both wings. Firstly, it was chosen to separate roll and pitch control, so separate ailerons and elevators, instead of elevons. Then, it was chosen to put both control surfaces on both wings. Both of these choices are made based on a trade-off performed by Van Ginneken et al. [53]. Separating the two controls substantially increases effectiveness and lowers complexity. Combining the two controls leaves more room for HLDs, however as there was enough room for HLDs anyway (see Equation 9.2.1), this is not important for the MoM-liner, so the two controls are separated [53]. Then, both controls are put on both wings mainly for better maneuverability, as it can create a pure torque and a double moment arm. Furthermore, the symmetry is beneficial for the Best Wing System [53].

Moreover, in this system there is double the amount of control surfaces as strictly necessary, so there is some kind of redundancy here. I.e. elevators can be used as inboard ailerons in high speed flight and ailerons can assist in pitch control and vice versa. This is favorable, as in this configuration, there is no need for an outboard and an inboard aileron, as is common for conventional aircraft. In conventional aircraft the elevator is placed on the horizontal stabilizer, and thus an inboard aileron is needed on the wing in high speed flight, as the wing will twist and aileron reversal will occur if the outboard ailerons are used [26]. This need for an extra inboard aileron is omitted, since in this configuration the elevator can be used for this purpose in high speed flight. This redundancy calls for various benefits and these have to be researched and optimized. For future research it has to be analyzed whether different control allocation schemes are more beneficial for this layout. Some of the widely used control allocation techniques are the Daisy chain, direct allocation, weighted pseudo-inverse, and cascaded generalized inverse. Therefore, for future work it should be analyzed what works best. It should also be taken into account that direct lift control will be possible with this configuration of control surfaces. Direct lift control is the phenomenon where the aircraft can ascend and descend steeper with a relative lower angle of attack. For conventional aircraft this is hard, since it has one set of control surfaces. However, since the MoM-liner will have two sets of them, it can use direct lift control. All in all, the two sets of control surfaces and spoilers call for extra benefits, which are hard to analyze and quantify at this stage in the design, but should definitely be researched in more detail in further research.

9.3. Landing Gear Design

Another important aspect of a complete stability analysis is the behavior on the ground. The main gear needs to have a sufficient trackwidth to prevent tip-over, the front wheel needs to have sufficient load for steerability and the elevator needs to be able to rotate the aircraft around the landing gear for take-off. Thus, proper landing gear design is an important aspect for a stable and well controllable aircraft. Landing gear design can be split in two parts: Wheel sizing and positioning.

Wheel Sizing

The first step in the sizing process is to determine the total amount of wheels necessary. Equation (9.34) allows to determine the amount of wheels necessary for nose and main gear. If the main gear has less than 12 tires, they should be grouped in two struts; for more wheels, three or four struts should be considered. The computed amount of wheels should be rounded to the nearest multiple of four, to allow even distribution amongst the struts.

$$N_{nw} = 2; \qquad N_{mw} = \frac{W_{TO}}{210,000} \tag{9.34}$$

$$p_{max} = 430 ln(LCN) - 680 \tag{9.35}$$

The second step is to determine the maximum allowable tire pressure. For this, the Load Classification Number (LCN) was defined. Every runway has its own limit LCN that the aircraft may not exceed. Otherwise the pressure on the surface is too large and the runway might be damaged. Based on the market analysis for potential destinations, the most critical LCN should be selected. The maximum allowable tire pressure can then be computed with Equation 9.35. Next to the pressure, also the static load, that is the total load at MTOM divided by the amount of

wheels, needs to be found. Usual load distributions are that the nose wheel takes 8-15% of the total load to have sufficient force for steerability; the rest is taken by the main gear. Having determined these two values, they can now be combined in tables (e.g. Torenbeek [26]) to select suitable tire sizes.

Landing Gear Positioning

The positioning along the fuselage is mostly done based on geometric constraints and easiest done on a sketch of the final aircraft layout. Figure 9.4a and Figure 9.4b show the relevant geometric constraints and angles.
For longitudinal positioning of the main landing gear, the tipover angle β should be at least 15°; the scrape angle θ should be less, and is usually taken as 10-13°. The nose gear position can then be found by setting up an equation for moment equilibrium around the most aft c.g. and assuming the load in the nose wheel to be in the range of 0.08-0.15W_{TO}. The higher the load on the front wheel, the better the controllability on the ground, however the bigger the required elevator for take-off rotation.
In lateral positioning, the most important aspect is to have a sufficient trackwidth that assures that the aircraft does not tip over during turns in taxi operations. Additionally, a sufficient clearance between the wingtip and ground should be kept to prevent the wingtips touching the ground in crosswind landings. Thus, the lateral positioning must satisfy both equations in Equation 9.36. The angle ϕ should be less than 55°for stability. The required parameters are shown in Figure 9.4b. Although the required fuselage height is implicitly incorporated in both parts of the placement, it is necessary to have a final check that the landing gear height allows sufficient clearance.

$$Y_{LG} > \frac{b}{2} - \frac{Z_t}{tan(\phi)} \qquad Y_{LG} > tan\left(arcsin\left(\frac{Z_{cg}}{tan(\phi)b_N}\right)\right) \tag{9.36}$$

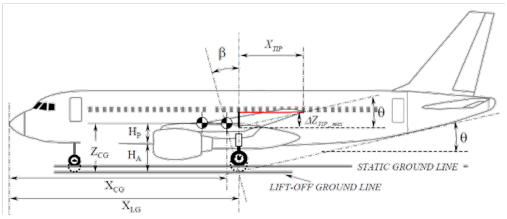

(a) Longitudinal Positioning of the Landing Gear

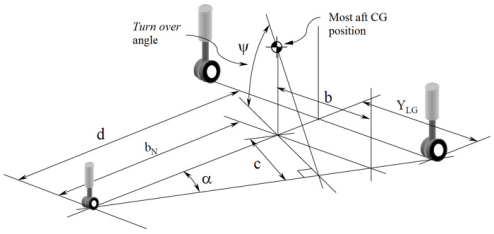

(b) Lateral Positioning of the Landing Gear

Dynamic Stability

For a successful aircraft, of course not only static but also inherent dynamic stability is required. This will be tested by performing a preliminary eigenmotion analysis based on a linearised model for the longitudinal and lateral equations of motion. In preliminary design, estimating dynamic coefficients is difficult. Most stability derivatives are difficult to estimate and can only be determined after thorough wind tunnel and flight test campaigns. Nevertheless, it can be important to see how the proposed design is expected to perform, especially to answer the question if the aircraft design would be stable. This analysis is based on a set of simplified equations of motion as described in [54]. These simplifications allow for an easy determination of the eigenvalues while retaining a good accuracy in their respective values. This section will only describe the individual equation that needs to be solved for every eigenmotion. For a more detailed description and justification for the simplifications, please refer to [54].
Most of the eigenmotions are oscillatory, that is they result in an equation of the form $Ax^2 + Bx + C = 0$. This quadratic equation can be solved using Equation 9.37 and will have two complex roots. For brevity's sake, only the coefficients A, B, C will be given for the individual motions. For stability, it is required that their real part has a negative sign, thus dampens out over time. Next to stability, several other characteristics are used to analyze the behavior of the aircraft such as the period of the motion (P), the damping ratio (ζ) and time to half amplitude ($T_{1/2}$). Their respective formulas are presented in Equation 9.38. This equation gives the parameters for the symmetric case. For the asymmetric case, replace the $\bar{c}$ with the wingspan b. Based on these values, conclusions can be drawn towards handling qualities of the aircraft. Such values are, for example, specified in [55].

$$\lambda_{1,2} = \xi \pm j\eta = \frac{-B \pm j\sqrt{4AC - B^2}}{2A} \tag{9.37}$$

$$P_c = \frac{2\pi}{\eta}\frac{\bar{c}}{V}; \quad \zeta = \frac{-\xi}{\sqrt{\xi^2 + \eta^2}}; \quad T_{1/2} = \frac{-0.693}{\xi_c}\frac{\bar{c}}{V} \tag{9.38}$$

Symmetric Eigenmotions

There are two longitudinal eigenmotions: the short period and the phugoid. Both are oscillatory, thus will have two imaginary eigenvalues respectively. The required stability coefficients are given through Equation 9.39, Equation 9.40 and Equation 9.41, the parameters A, B and C are defined in Equation 9.42 and Equation 9.43 respectively for each motion.

Stability Derivatives

$$C_{X_u} = -2C_D; \quad C_{X_\alpha} = C_L\left(1 - \frac{2C_{L_\alpha}}{\pi Ae}\right) \tag{9.39}$$

$$\begin{gathered} C_{Z_0} = \frac{-Wcos(\gamma_0)}{0.5\rho V^2 S}; \quad C_{Z_u} = -2C_L; \quad C_{Z_\alpha} = -C_{N_{w_\alpha}} - C_{N_{h_\alpha}}\left(1 - \frac{d\epsilon}{d\alpha}\right)\frac{S_h}{S}; \\ C_{Z_{\dot\alpha}} = -C_{N_{h_\alpha}}\frac{S_h l_h}{S\bar{c}}\frac{d\epsilon}{d\alpha}; \quad C_{Z_q} = -2C_{N_{h_\alpha}}\frac{S_h l_h}{S\bar{c}} \end{gathered} \tag{9.40}$$

$$\begin{gathered} C_{m_u} = -2C_D(-l_e); \quad C_{m_\alpha} = C_{N_{w_\alpha}}(x_{cg} - x_w) - C_{N_{h_\alpha}}\left(1 - \frac{d\epsilon}{d\alpha}\right)\frac{S_h l_h}{S\bar{c}}; \\ C_{m_{\dot\alpha}} = -C_{N_{h_\alpha}}\frac{S_h l_h^2}{S\bar{c}^2}\frac{d\epsilon}{d\alpha}; \quad C_{m_q} = -1.1C_{N_{h_\alpha}}\frac{S_h l_h^2}{S\bar{c}^2} \end{gathered} \tag{9.41}$$

Short Period

$$A = 2\mu_c K_{yy}(2\mu_c - C_{Z_{\dot\alpha}}); \quad B = -2\mu_c(K_{yy}C_{Z_\alpha} + C_{m_{\dot\alpha}}C_{m_q}; \quad C = C_{Z_\alpha}C_{m_q} - (2\mu_c + C_{Z_q})C_{m_\alpha} \tag{9.42}$$

Phugoid

$$A = -4\mu_c^2; \quad B = 2\mu_c C_{X_u}; \quad C = -C_{Z_u}C_{Z_0} \tag{9.43}$$

Asymmetric Eigenmotions

The asymmetric eigenmotions are analyzed in an analogous way. Now, however, there are three eigenmotions, two not oscillatory, one oscillatory: aperiodic roll, spiral, Dutch roll. Again, the required stability coefficients are given through Equation 9.44, Equation 9.45 and Equation 9.46. The parameters A, B and C are defined in Equation 9.48 for the Dutch roll. As the other two eigenmotions have real eigenvalues, they can be computed directly. All wing contributions required for the derivatives were directly obtained from the aerodynamics department and then adjusted for the influences of fuselage and tail.

Stability Derivatives

$$C_{Y_\beta} = -K_{f2}C_{L_{\alpha_v}}\left(1 - \frac{d\sigma}{d\beta}\right)\eta_v\frac{S_v}{S}; \quad C_{Y_r} = 2C_{L_{\alpha_v}}\eta_v\bar{V}_v \tag{9.44}$$

$$C_{l_\beta} = C_{l_{\beta_{wing}}} + C_{Y_\beta}\left(\frac{(z_v - z_{cg})}{bcos(\alpha_0)} - \frac{(x_v - x_{cg})}{bsin(\alpha_0)}\right); \quad C_{l_p} = C_{l_{p_{wing}}}; \quad C_{l_r} = C_{l_{r_{wing}}} + C_{Y_r}\left(\frac{(z_v - z_{cg})}{bcos(\alpha_0)} - \frac{(x_v - x_{cg})}{bsin(\alpha_0)}\right) \tag{9.45}$$

$$C_{n_\beta} = K_{f1}C_{L_{\alpha_v}}\left(1 - \frac{d\sigma}{d\beta}\right)\eta_v\bar{V}_v; \quad C_{n_p} = C_{n_{p_{wing}}}; \quad C_{n_r} = -C_{Y_r}\frac{l_v}{b} \tag{9.46}$$

Aperiodic Roll

$$\lambda_{AR} = \frac{C_{l_p}}{4\mu_b K_{xx}} \tag{9.47}$$

Dutch Roll

$$A = 8\mu_b^2 K_{zz}; \quad B = -2\mu_b(C_{n_r} + 2K_{zz}C_{Y_\beta}); \quad C = 4\mu_b C_{n_\beta} + C_{Y_\beta}C_{n_r} \tag{9.48}$$

Spiral

$$\lambda_{SP} = \frac{2C_L(C_{l_\beta}C_{n_r} - C_{n_\beta}C_{l_r})}{C_{l_p}(C_{Y_\beta}C_{n_r} + 4mu_b C_{n_\beta}) - C_{n_p}(C_{Y_\beta}C_{l_r} + 4\mu_b C_{l_\beta})} \tag{9.49}$$

10
Engine Sizing

This chapter will cover the engine selection, and possible improvements in engine efficiency that can be expected in the upcoming years. First the thrust requirements of the MoM-liner will be analyzed, and some engine parameters will be determined. Afterwards market research on currently available turbofan engines will be performed, promising engines that will become available in the future will be added to this list as well. The final engine selection will take place, and the implications for required fuel volume will be discussed. Additionally the effect of the engine placement on the structure and aerodynamics of the aircraft will be discussed.

10.1. Summary Methodology

The engine sizing method consists of a couple of steps. It is important to note that designing an entire engine from scratch is outside the scope of this project, as this would cost too much time. The method that will be used is based on rubberizing, or scaling, which will be explained in more detail in subsection 10.2.1. To scale an existing engine, a lot of information has to be known about these types of engines. The first step in the engine sizing process is to collect data on all current, and future, engines that could meet the efficiency needs of the MoM-liner. The thrust needs do not necessarily need to be met by these engines, since the engine will be scaled to produce the correct amount of thrust. The database will be used find correlations between some key parameters. The relation between the bypass ratio and the specific fuel consumption in cruise will allow the improvements of a higher bypass ratio engines to be estimated more accurately. Additionally, the takeoff thrust weight correlation and the cruise thrust fan diameter correlation will be used in the sizing of the engine itself. New technologies, and their effect on the efficiency of the engines, will also be taken into account. After the trend lines and corresponding equations have been determined, the method needs to be verified. This will be done using a selection of slightly older generation turbofans. The final step is to obtain the thrust requirements of the MoM-liner, scale an existing engine to meet those requirements and apply new technologies, e.g. a higher bypass ratio, to improve the efficiency.

10.2. Methodology

The MoM-liner has a number of performance requirements that affect the propulsion system, for example the short takeoff distance results in a high takeoff thrust requirement. Combining this with the low thrust requirements at cruise, due to the inherent lower drag of the Prandtl plane, is a challenge. This section will go through the steps used to perform the engine sizing.

10.2.1. Rubberizing-Scaling

As mentioned before, designing a completely new engine does not fit within the scope of this project, this would simply take too much time. A common practice used in the conceptual design phase is the scaling of existing engines, this process is called rubberizing as learned from a conversation with Ir. J. Melkert[1]. On top of the scaling, emerging technologies will be incorporated into the 'new' engine design. Some of the emerging technologies that will be considered are: Geared turbofan, Ultra-high bypass & Electrically boosted turbofans.

[1] Private communication with TU Delft teacher J. Melkert, URL: `https://www.tudelft.nl/en/staff/j.a.melkert`

10.2.2. Important Engine Sizing Parameters

Some of the important parameters that affect the engine sizing are described in this section.

Take-Off

The take-off thrust is a parameter that is obtained from the design space. For the MoM-liner the take-off thrust will be relatively high due to the short runway length requirement.

Cruise

The cruise drag of the box wing is significantly lower than comparable aircraft, this is due to the aerodynamic benefits of a box wing described in chapter 7. A lower cruise drag is great for cruise performance, lower drag allows for a lower required thrust which in turn results in a lower fuel burn. However, the ratio between takeoff thrust and cruise thrust is also increased which poses a problem when selecting an engine. The average ratio between takeoff thrust and cruise thrust is around 5.4, lowering the cruise drag will increase this ratio [5]. Furthermore, the MoM-liner is designed for long range cruise flight which implies that the engines should be sized (and optimized) for the cruise phase of the flight. A high bypass ratio is beneficial for cruise performance, and this will be considered in the engine selection [26]. Reducing the cost and emissions during cruise is part of the sustainability plan for this project. This does not just improve economic sustainability, by reducing fuel cost but also improves the societal and environmental sustainability through noise and emissions reduction.

Engine Placement

The engine placement is an important considerations, especially for a box wing configuration as there are some limitations but also some unique possibilities for engine attachment. The front wing is so low to the ground making mounting engines underneath it more or less impossible. This leaves two options: attaching the engines to the fuselage or attaching them somewhere on the rear wing. Considering the engine will have a very high bypass ratio and produce significant thrust, the engine will be quite heavy. A heavier engine means it cannot be placed everywhere, if the engines become too heavy mounting them on the fuselage will become complicated. According to airline pilot Doug Hancard the mounts would have to be very complicated and heavy to support the engines if they are mounted to the fuselage[2]. This leaves the MoM-liner with one suitable option, mounting the engines underneath the rear wing. There are some obvious pros and cons for this configuration, first of all the engines will be mounted quite high off the ground which means maintainability will be more cumbersome. However, mounting the engines higher above ground allows for higher bypass ratios (which increases the fan diameter) without running into ground clearance restrictions. Installing the engines underneath the wing requires less complex mounting systems which will reduce structural complexity as well as reducing the cost of this part.

Thrust Settings

Some engine parameters are necessary to determine the takeoff and cruise power requirements. Aircraft engines do not run at 100% power all of the time, there are actually different throttle settings for different phases of flight.
Of these There are two thrust ratings that are certified for: maximum takeoff (TMTO) and maximum continuous thrust (TMCT) [56]. The difference between the TMTO and TMCT is taken as 10.5% [3]. The TMTO thrust setting is limited to 5 minutes, after which the engine performance will degrade. This means that this throttle setting should only be used when absolutely necessary, for example for takeoff at a so called 'hot and high' airports or for takeoff on a short runway at MTOW. After takeoff the throttle setting should be reduced to not reduce unnecessary wear on the engine.
The throttle setting at cruise depends on the the weight of the aircraft, the altitude at which cruises and the air temperature. The cruise thrust setting can vary anywhere between 69-97%, however for the MoM-liner mission an average value of 75% will be assumed [57]. To summarize:

Maximum take-off thrust = 110.5% of maximum continuous thrust
Cruise thrust = 75% of maximum cruise thrust (69-97% range)

[2] URL https://www.quora.com/Is-there-a-performance-difference-between-having-jet-engines-mounted-on-the-rear-of-a-plane-versus-o [cited 21 June 2018]
[3] URL http://www.airliners.net/forum/viewtopic.php?t=735549 [cited 22 June 2018]

10.2.3. Engine Database

In order to scale an engine to fit the MoM-liner's performance needs a market analysis of the current generation and next-gen engines should be performed. The results of which are shown in this section. The engine types shown in Table 10.1 are the engines that were analyzed to see if they meet the thrust requirements of the MoM-liner. The data collected for the power plants shown in Table 10.1 consists of a wide range of parameters. The SFC and thrust at cruise and takeoff settings are analyzed, taking into account that the thrust reduces at altitude. The weight of every engine was also collected. To estimate the parameters of the newer engines, the manufacturer specification were used.

Altitude impacts engine performance in two ways, first of all the temperature decrease increases the density of the air which in turn increases the thrust. However, the increase in altitude also causes a decrease in pressure, which in turn decreases density and thus decreases thrust. The decrease thrust due to the lower pressure outweighs the thrust increase due to the temperature change [56][58]. Furthermore, the increase in airspeed decreases the net thrust of the engine. While other factors impact the thrust that an engine can produce at altitude there impact is small and therefore will be neglected. The correction for altitude is therefore assumed to be $(\frac{\rho_0}{\rho})^{0.75}$.

Table 10.1: Engines Used in Comparison Process [5][59][60][61][62][63][64][65]

Current Generation				**Next Generation**	
EA GP7270	GE CF6 80A2	PW PW2037	RR RB-211-524	PW PW1100G	P&W PW1400G
IAE V2500	GE CF6 80C2-B1F	P&W PW4052	RR RB-211-535	PW V2533-A5	PW PW1431G
IAE V2522	GE CF6 80C2-B2	P&W PW4056	RR SPEY 511-8	RR TRENT XWB-84	RR TRENT XWB-97
IAE V2533	GE CF6 80E1-A2	P&W PW4152	RR TRENT 772	CFM LEAP-1A	CFM LEAP-1B
IAE V2525	GE 90-85B	P&W PW4168	RR TRENT 892	CFM LEAP-1C	RR TRENT 7000
GE 90-76B	GE 90-85B	RR TRENT 890-17	RR TRENT 900	RR TRENT 1000-B	RR TRENT 1000-C
GE 90-94B	PW PW4084	CFM 56-5B3	CFM 56-7B	RR TRENT 1000-TEN	RR TRENT 1700
				GE GenX-1A72	GE GenX-1b70

10.2.4. Future Technologies

The engine database that was created does not only consist of old aircraft engines, but also newer and near future engines. As the MoM-liner is planned to enter service around 2030, next generation turbofans should be considered as well. The new turbofans that were analyzed, as shown in Table 10.1, have some new technologies that can significantly improve efficiency. Some of the technological developments are described below.

Geared Turbofans: In a conventional turbofan everything is connected to one single shaft, and thus rotates at the same angular velocity. Due to the large radius of the fan blades, the tips of these blades are actually the limiting factor in determining the rotational speed of the shaft. These tips will experience sonic flow first, and thus determine the maximum angular velocity of the entire engine. This angular velocity will likely be sub optimal for the other turbine and compressor stages. A geared turbofan allows lets the fan rotate at a slower speed while still allowing the rest of the engine to rotate at a higher speed. This means the engine actually operates more efficiently, as all components can rotate much closer to their optimal speed. The geared system, which slows down the fan's speed means the fan tips will not reach sonic flow as soon. This can potentially allow for larger fan diameters and therefore higher bypass ratios [59][66]. This technology has already been implemented in the PW1000G series used on the Bombardier CS300 and the A320neo.

High Bypass Ratio: The trend towards increasing bypass can be seen quite clearly by what engine manufacturers are developing right now[4]. Engines like the CFM International LEAP and PW1100G have bypass ratios as high as 12.5, which is a significant improvement over the bypass ratio of 5.4 of the CFM56 [5][59][60]. Using the geared turbofan technology mentioned above, bypass ratios as high as 15 can be obtained [66].

Boosted Turbofans: A boosted turbofan is an electrically assisted turbofan, an electrical motor is attached to the main shaft and helps supply power during takeoff. Most engines are oversized for cruise, as the engine has to produce so much power at takeoff, this is also the case for the MoM-liner. A boosted turbofan would allow the engine to be optimized for cruise, and the power that is lacking at takeoff due to this optimization can be covered by the electrical boost system. A downside to this system is the added complexity and the increase in weight due to batteries.

[4] URL `http://www.propfan.net/turboanalysis.html` [cited 22 June 2018]

10.2.5. Trend Lines

Using all of the data collected on the engines shown in Table 10.1 a couple of correlations have been made. These correlations can help to estimate missing engine parameters, as well as estimate what the performance of a totally new engine would be. These correlations can be assumed to be pretty accurate, considering that a lot of reference engines were used. A strong correlation was observed with coefficient of determination (R^2) values of of 0.9189 and 0.8935. A correlation between the bypass ratio and the specific fuel consumption in cruise was also found as shown

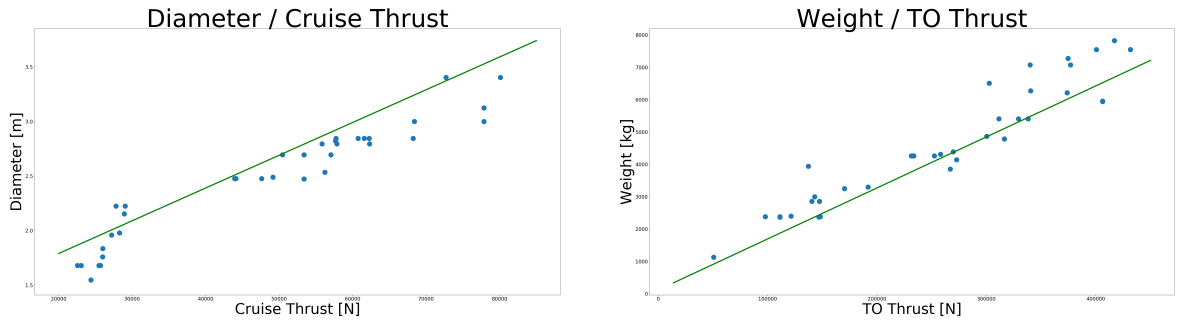

(a) Diameter / Cruise Thrust

(b) Engine Weight / Take-Off Thrust

Figure 10.1: Trendlines For Engine Sizing

in Figure 10.2, with an R^2 value of 0.8455. While lower than the before mentioned R^2 value, it is still an indicator that statistical methods can be used for engine sizing in the conceptual design phase. The relationship helps to estimate the future specific fuel consumption of a new engine with an increased bypass ratio.

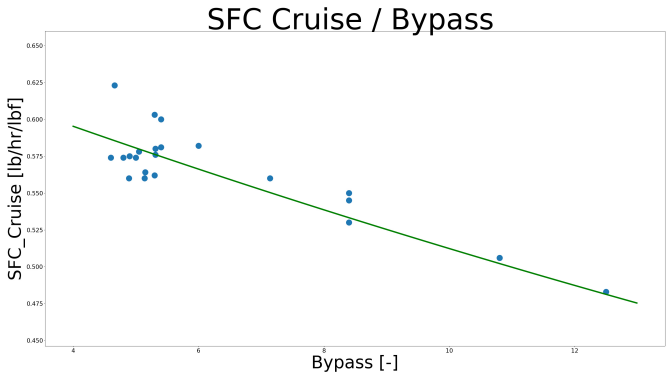

Figure 10.2: SFC Cruise / Bypass Ratio

Finally it is important to realize that correlation does not imply causation. Therefore the links that the trend lines try to prove need to be checked, to see if they even make sense.

Diameter/Cruise Thrust: Fan diameter and cruise thrust are linked, especially for newer turbofans, as newer turbofans have a higher bypass ratio that leads to a higher fan diameter.

Weight/TO Thrust: The relation between takeoff thrust and weight is quite straightforward, a higher takeoff thrust requires a more powerful engine which is inherently heavier.

SFC-Cruise/Bypass: The relation between the SFC-Cruise and the bypass ratio stems from the idea that higher bypass ratio turbofans have a lower SFC. Newer long-range aircraft have higher bypass ratio engines, and their SFC is lower. This can be seen by the trend line shown in Figure 10.2.

The relation between the bypass ratio and SFC-cruise is the most important one, and the relation is given in Equation 10.1. This equation has the same coefficient of determination as the trend line: 0.85.

$$SFC_{Cruise} = 0.6578 \cdot e^{-0.025 \cdot (\text{Bypass Ratio})} \tag{10.1}$$

10.2.6. Fuel Requirement

The fuel requirement will be calculated using a combination of the fuel fractions method, and the SFC obtained in subsection 10.2.5. The fuel fractions method estimates the required fuel as a fraction of the MTOW [26][67]. The list below shows the fuel fraction used for the MoM-liner [67].

Engine Start, Warm-Up: 0.990
Taxi: 0.990
Takeoff: 0.995
Climb and Acceleration: 0.980
Descent: 0.990
Landing, Taxi, Shutdown: 0.992

By multiplying the fuel fractions, and using Equation 10.2 the fuel of the non-horizontal flight phases can be calculated.

$$W_{F-used} = (1 - M_{ff}) \cdot W_{TO} \tag{10.2}$$

For the cruise phase, the SFC-cruise will be used. Using the aerodynamic analysis performed in chapter 7 the drag coefficient during cruise can be obtained. Using this drag coefficient, the thrust required per engine can be calculated. Using the thrust setting from subsection 10.2.2, the cruise power setting is assumed to be 75% of the available power in cruise. Multiplying the SFC-cruise with the total drag results in a fuel flow per hour, multiplying this with the flight time results in total fuel burn for the cruise phase.

10.3. Verification and Validation

To verify that the trend lines shown in subsection 10.2.5 are correct, they need to be tested. Since every engine in Table 10.1 was used to generate the trend lines, they cannot be used to verify the trend lines. That is why some older engines, that were not included in the database, will be used here. Table 10.2 shows the 7 engines used for verification.

Table 10.2: Engines Used for Verification

CFM 56 (3 versions)	IAE V5200	IAE V2522	IAE V2533	IAE V2525

The weight, fan diameter and SFC-Cruise were calculated for all of the engines above. Afterwards the average delta (w.r.t. the actual value provided by the manufacturer) was calculated. The values can be seen in Table 10.3.

Table 10.3: Verification Values

Category	**Delta** [%]
SFC_{cruise}	-1.55
Diameter	4.51
Weight	-53.69

From the results in Table 10.3 it can be seen that for the SFC-Cruise the trend line slightly underestimates the SFC-Cruise, however a value of 1.55% on average is deemed acceptable. For the diameter, the value is slightly overestimated by a value of 4.51%, still totally acceptable. For the weight the value is significantly higher, the trend line underestimates the actual value significantly. The actual engine is twice as heavy as the trend line would suggest, but there is an explanation for this weird occurrence. The engines used for the verification are old, and actually supersede some of the earliest turbofans. These 1st generation turbofans stem from a time where bypass ratios and turbofans were still relatively new. Over the decades the weight of engines has significantly dropped, due to improvements in materials and a giant leap in the amount of power can be extracted from a turbofan. Also, looking at the coefficient of determination of the trend line shown in Figure 10.1b, the correlation is clearly visible for modern engines. For that reason, considering the turbofans on the MoM-liner will also be a modern turbofan, the correlation is still accepted. During the entire calculation process, the results were compared to similar aircraft to check if the values were in the correct range [5].

To validate this data a prototype engine would have to be built, and after extensive testing the obtained engine parameters could be compared to the calculated ones.

10.4. Sustainability

The selection of the engines has a big effect on almost every item on the sustainability checklist. Of course looking at the economics, a more efficient engine with a lower fuel burn is great for the operational cost. Furthermore, modern fuel efficient engines produce less emissions which is better for the environment and thus improves the sustainability. It is important to note that the engines are the most expensive components of an aircraft, and with the above mentioned they will most likely become more expensive. But, the increased cost for the modern engines is well worth it considering the immense fuel savings they lead to. Since fuel cost is the largest contributor to the operational cost, and considering that fuel costs will increase a more fuel efficient engine is definitely worth the cost. Sustainability will be discussed further in chapter 16.

Noise

Noise is a very important criterion, considering the engines selection has a huge effect on the amount of noise an aircraft produces, noise should therefore be taken into account when selecting the engines. In the last decade giant leaps have been made in reducing the noise of turbofans. Higher bypass ratios reduce the noise, by reducing the fraction of the total thrust generated by the core of the engine. Chevrons reduce the noise even further, and new technologies like 'trailing edge blowing' could reduce the noise even further. Pratt & Whitney and Boeing have been researching ways to further reduce turbofan noise. Scarf inlets, Active-Passive liners, Advanced case treatment and treated primary nozzles can reduce the noise by an estimated 10 EPNdB (Effective perceived noise in Decibels), this is with respect to the Boeing 747-200 which is an old and noisy aircraft. A 10 EPNdB reduction would be massive, as decibels work on a logarithmic scale, this reduction equates to a 50% reduction in noise energy[5] [68].

10.5. Limitations

It is important to realize this method has limitations, especially considering trend lines are used. First of all extrapolation of data cannot be assumed to be 100% accurate, the trend line does not resemble the data perfectly. Also a trend line does not take technical limitations into account, so a bypass ratio of for example 50 are possible according to the trend line but in practice are not achievable. Furthermore, it is assumed that the technological improvements implemented in the MoM-liner engines will be ready before the aircraft enters service. However, there is no data to support this and if a development problem occurs the newer engines might not be ready on time. Finally, engine scaling is a valid assumption but does come with some scaling effects [26]. Also a cruise power setting of 75% is on the lower end of the range (69-97%), more research needs to be done into the effects of a lower throttle setting in cruise.

[5] URL: `http://quiet-rack.com/percentages-explained.php` [cited 26 june 2018]

11
Performance Analysis

Once the final design parameters are determined, a second performance analysis is performed. This is done in a more refined and detailed manner than for the design space diagram and is aimed to verify that the initial requirements and sizing constraints are still accounted for; i.e. that the design still performs as expected. Figure 11.1 shows a typical performance diagram for a jet airplane. As thrust is constant, the power available is a straight line with the slope of maximum thrust. In this chapter, all significant points on the curve for required power will be analyzed. All methods described in this chapter are based on Ruijgrok [69].
Section 11.1 presents simple calculations to determine minimum (point 1) and maximum speed (point 6) of the aircraft for a given configuration. Section 11.2 then analyzes different important characteristics of climbing and descending flight, such as maximum angle (point 4) and rate of climb (point 5) as well as minimum angle (point 4) and rate of descend (point 3) in gliding flight. Lastly, section 11.3 shows methods to estimate take-off and landing performance of the aircraft at design.

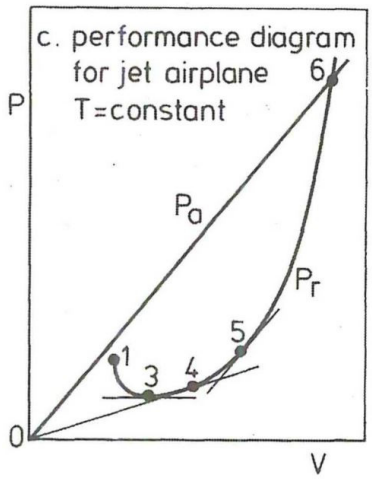

Figure 11.1: Generic Performance Diagram for a Jet Aircraft [69]

11.1. Speeds

Minimum Speed

The minimum speed in any configuration is commonly referred to as the stall speed and directly follows from the mass of the aircraft and the maximum lift coefficient in the aircraft's respective configuration (Equation 11.1).

Maximum Speed

The maximum possible speed of the aircraft is mostly constraint by the maximum engine thrust and the drag coefficient. Equation (11.2) also clearly shows the benefits of flying at higher altitudes; having the air density in the denominator increases the maximum possible flight speed as altitude increases.

$$V_{s1} = \sqrt{\frac{2W}{\rho S C_{L_{max}}}} \tag{11.1}$$

$$V_{max} = \sqrt{\frac{T}{\rho C_{D_0} S}\left[1 + \sqrt{4\frac{C_{D_0}}{\pi A e}\left(\frac{W}{T}\right)^2}\right]} \tag{11.2}$$

11.2. Climb Performance

Maximum Angle of Climb

For jet aircraft, that is aircraft that deliver a constant thrust, the maximum climb angle is achieved at the speed for minimum drag, so the speed for best lift-to-drag ratio. In practice, this is mostly relevant fro a steep climb to avoid obstacles in the flight path of the aircraft. Equation (11.3) allows to compute the maximum angle of climb for a given configuration. $C_{L_{opt}}$ is the lift coefficient corresponding to a maximum L/D value. The speed for the best angle of climb, V_x can be found by using this lift coefficient in the lift equation and solve for the airspeed.

$$\gamma_{max} = arcsin\left(\frac{T}{W} - \frac{1}{(C_L/C_D)_{max}}\right); \quad C_{L_{opt}} = \sqrt{C_{D_0}\pi Ae} \tag{11.3}$$

Minimum Glide Angle

In case of total engine failure, it is important for the pilot to be well aware of the glide performance of his aircraft in order to make informed decisions on choosing an airport within the gliding distance of the aircraft for the emergency landing. The minimum glide angle is a direct derivative of the maximum climb angle and corresponds to the best glide performance. Thus, also the formula bears strong resemblance, with the only difference being the missing term involving thrust (Equation 11.4).

$$\gamma_{max} = arcsin\left(-\frac{1}{(C_L/C_D)_{max}}\right); \quad C_{L_{opt}} = \sqrt{C_{D_0}\pi Ae} \tag{11.4}$$

Maximum Rate of Climb

This parameter is often more important than the maximum climb angle, as the speed for maximum rate of climb, V_y, denotes the condition for best climb performance per distance. While V_x is often used right after take-off, to clear obstacles, V_y is then used for the rest of the en-route climb segment for optimum performance. This condition is given by the point where excess power is maximum. The optimum lift coefficient for this condition is given in Equation 11.5 which should then be used in Equation 11.6. Again, the corresponding airspeed, V_y can be found by using C_{L_c} in the lift equation.
The maximum rate of climb is also used to determine the ceiling of the aircraft. The *service ceiling* is defined as the altitude at which a steady climb rate of 0.5 m/s can still be achieved, the absolute ceiling the altitude at which no further climb is possible.

$$C_{L_c} = \frac{\pi Ae}{2}\frac{T}{W}\left[-1 + \sqrt{1 + 12\frac{C_{D_0}}{\pi Ae}\left(\frac{W}{T}\right)^2}\right] \tag{11.5}$$

$$ROC_{max} = V_y sin(\gamma) = \sqrt{\frac{2W}{\rho S C_{L_c}}}\left[\frac{T}{W} - \frac{C_D}{C_L}\right] \tag{11.6}$$

Minimum Rate of Descent

The minimum rate of descent is relevant for the pilot in case he needs to remain in the air as long as possible following an engine failure. The aircraft will not be able to cover as much distance in gliding flight as for the minimum glide angle, however, due to its lower speed will also not sink as fast. This flight condition corresponds to a condition of minimum drag and thus minimum power required. The optimum lift coefficient for this point is found by minimizing the ratio C_L^3/C_D^2. The resulting equation for the lift coefficient and the minimum rate of descent are given in Equation 11.7.

$$ROD_{min} = \frac{-\rho V_{ROD_{min}}^3 S\left(C_{D_0} + \frac{C_{L_{RODmin}}^2}{\pi Ae}\right)}{2W}; \quad C_{L_{RODmin}} = \sqrt{4C_{D_0}\pi Ae} \tag{11.7}$$

11.3. Airfield Performance

Take-Off Performance

The total take-off run can be decomposed in three phases, ground roll, transition and climb-out, as can be seen in Figure 11.3a and Equation 11.8. Regulations additionally mandate the runway to be at least 115% of the required runway distance as a safety factor [20].

$$x_{tot_{TO}} = x_{ground} + x_{transition} + x_{climbout} \tag{11.8}$$

The ground run distance and its relevant parameters are given in Equation 11.9. The lift-off speed V_{LOF} is usually equal to $1.2V_{s_{TO}}$. Special consideration should be given to the mean acceleration $\bar{a}$. This value is evaluated at the so called characteristic velocity $\bar{V} = V_{LOF}/2$. The last term is also referred to as D_g and describes the ground friction of the aircraft. As the aircraft is still level on the runway, the corresponding lift coefficient for the ground segment must be found for an angle of attack of 0°. It must also be noted that the use of flaps and the landing gear will have an impact on the Oswald efficiency factor and the zero-lift drag coefficient and must be accounted for in this equation.

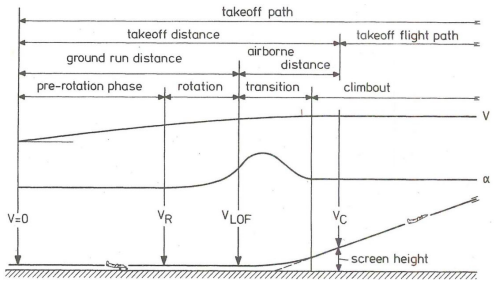

(a) The Take-off Maneuver

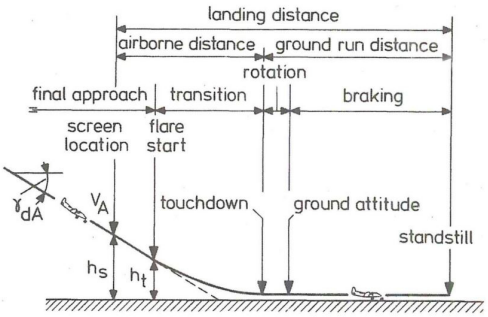

(b) The Landing Maneuver

Figure 11.2: Airfield Performance [69]

$$x_{ground} = \frac{V_{LOF}^2}{2\bar{a}}; \quad \bar{a} = \frac{g}{W}(\bar{T} - \bar{D} - \mu(\bar{L} - W)) \tag{11.9}$$

The transition phase has a very short duration during which the aircraft accelerates to the safe climb speed V_2 and pitches towards its climb angle (Equation 11.10). V_2 is usually about 1.2 to 1.3 V_s.

$$x_{trans} = \frac{V_{LOF}^2}{0.15g} sin(\gamma_{climb}); \quad \gamma_{climb} = \left(\frac{T-D}{W}\right)_{climb} = \left(\frac{T - 0.5\rho V_2^2 \left(C_{D_0} + \frac{2W}{\rho S V_2^2 (\pi A e)}\right)}{W}\right) \tag{11.10}$$

Lastly, the climb out distance is given by Equation 11.11. The minimum screen height, h_{scr}, is defined by regulations to be 50 ft or 15.2 m. In case that the engines are potent enough to reach screen height before finishing the transition to the climb angle, Equation 11.12 should be used for the total airborne phase and replace x_{trans} and x_{climb}. This equation only computes the part of the transition phase until the aircraft reaches the screen height.

$$x_{climb} = \frac{h_{scr} - (1 - cos(\gamma_{climb}) \frac{V_{LOF}^2}{0.15g}}{tan(\gamma_{climb})} \tag{11.11}$$

$$x_{air} = \sqrt{2Rh_{scr}}; \quad R = \frac{V_{LOF}^2}{0.15g} \tag{11.12}$$

Regulations require the minimum runway length to be the largest of either 115% of the normal take-off distance with all engines operative and the balanced field length. The balanced field length is defined as the distance at which, if an engine failure would occur, the remaining runway required for stopping the aircraft is equal to the distance required to climb to screen height on the remaining engine (Figure 11.5a).
The required ground roll distance is computed in the same manner as for the take-off. However, now the take-off run is interrupted by the engine failure. Thus, the total ground run has to be split up in an AEO and an OEI phase. Equation (11.13) describes the accelerate-go curve. The first integral computes the total distance traveled until the engine failure, the second integral computes the remaining distance until lift-off and the last two terms the airborne phase until screen height. Equation (11.14) describes the accelerate-stop distance. The first term is again the distance traveled until engine failure, the second term the required stopping distance with full brakes and engines idle. The resulting distances for all possible engine failure speeds are computed and graphed. From the intersection of the two lines, the balanced field length and the decision speed V_1 can now be determined (Figure 11.5b)

$$x_{accelerate-go} = \int_0^{V_{EF}} \frac{VdV}{g\left[\frac{T}{W} - 2\mu - \mu\frac{C_{Lg}\rho V^2 S}{W}\right]} + \int_{V_{EF}}^{V_{LOF}} \frac{VdV}{g\left[\frac{0.5T}{W} - 2\mu - \mu\frac{C_{Lg}\rho V^2 S}{W}\right]} + x_{trans} + x_{climb} \tag{11.13}$$

$$x_{accelerate-stop} = \int_0^{V_{EF}} \frac{VdV}{g\left[\frac{T}{W} - 2\mu - \mu\frac{C_{Lg}\rho V^2 S}{W}\right]} + \int_{V_{EF}}^{V_{LOF}} \frac{VdV}{g\left[-2\mu - \mu\frac{C_{Lg}\rho V^2 S}{W}\right]} \tag{11.14}$$

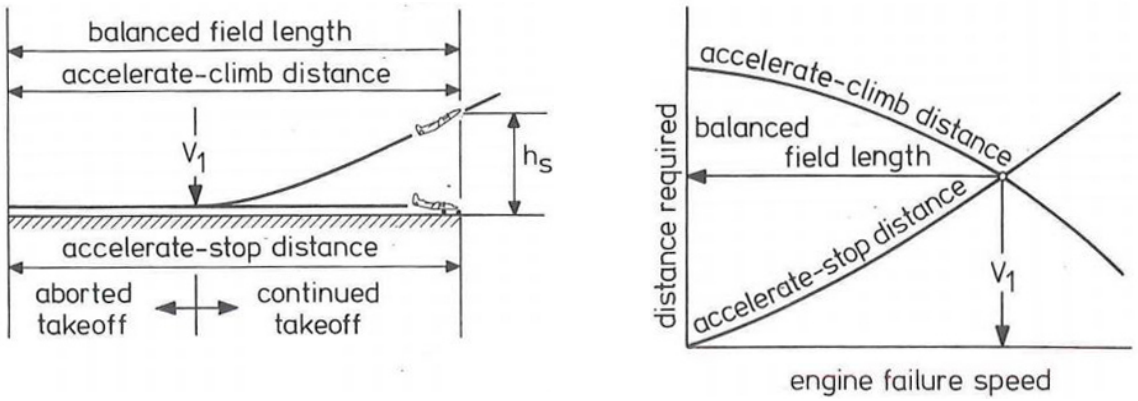

(a) Graphical Representation

(b) Determination of BFL and Decision Speed V_1

Figure 11.4: Balanced Field Length (BFL) [69]

Landing Performance

The landing phase is treated in a similar manner to the take-off phase. Again, the whole maneuver is split into three parts, approach, transition and braking distance (Figure 11.3b). Regulations demand the minimum field length for landing to be 10/6 of the computed distance [20].

The approach phase begins in a steady descent with the respective glide slope angle (commonly 3°) at screen height over the runway (Equation 11.15). The round-out is included through the parameter R. Shortly before touchdown, the aircraft is flaring above the runway to bleed off some more speed and attain the right attitude. This is accounted for in the transition phase, Equation 11.16. The transition is still flown with the approach speed of 1.3 $V_{s,landing}$ and statistically lasts about 2 seconds.

$$x_{air} = Rsin(\gamma_a) + \frac{h_{scr} - (1 - cos(\gamma_a)R)}{tan(\gamma_a)}; \quad R = 1.3^2 \frac{\frac{2W}{\rho S C_{L_{max,landing}}}}{0.10g} \tag{11.15}$$

$$x_{tr} = 2V_{ap} = 2.6V_{min,landing} \tag{11.16}$$

Finally, after touchdown, brakes, spoilers and thrust reversers are deployed to slow down the aircraft. The analysis of the braking distance is done in an analogous manner to the ground run for take-off as again the average deceleration at the characteristic velocity is used. However, now this value is based on the approach speed instead of lift-off speed and the value for μ is significantly higher as now brakes are used to increase friction. Regarding the drag coefficient, it must again be noted that significant differences in zero-lift drag coefficient and Oswald factor arise when landing flaps, spoilers, and the landing gear are extended and must be accounted for in this formula.

$$x_{brake} = \frac{1.3^2 W^2}{g\rho S C_{L_{max,landing}}} \frac{1}{\bar{T}_{rev} + \bar{D} + \mu(W - \bar{L})} \tag{11.17}$$

12
Results & Optimization

This chapter presents the final results of the optimization and design process. section 12.1 presents a general overview of the optimization structure of the optimization. Section 12.2 details the preliminary sizing, section 12.3 shows the results of the aerodynamic analysis, section 12.4 gives the fuselage structural analysis, section 12.5 shows the wing structural analysis. Next, the engine sizing is shown in section 12.6, the static stability and controlability are explored in section 12.7 and the performance characteristics in section 12.8. The external, internal layuot and ground handling and operations are shown in sections 12.9, 12.10 and 12.11 respectively.

12.1. General Discipline Interaction

This section describes the general data-flow of the optimization process, it indicates the interaction between aerodynamics, structures, performance and stability and control. A color code has been provided to indicate processes, databases and decisions. The an indication of the finalized optimization process is shown in Figure 12.1. It can be observed that the feedback loops will be used for the optimization:

1. Check for wing structural failure and that the tip deflection criteria is met for the given load case generated by the aerodynamic analysis.

2. A check will be built in concerning the fuel capacity. Can the fuel be stored completely in the wing, or potentially there is leftover space in the fuselage. If it is impossible the base geometry will have to be updated and the process starts from scratch.

3. A final check is built in to check if the stability & control and the performance requirements are met. Based on this check the software will decide to either store the data or update the main design parameters.

The results obtained from this optimization are presented in their respective sections in this chapter.

12.2. Preliminary Sizing

The preliminary sizing consists, as described in chapter 5, out of a class-I weight estimation, design space diagram and class-II weight estimation. A breakdown of the mass components resulting from this preliminary sizing, including the vertical tail, nacelles, main landing gear, nose gear, power plant, fixed equipment, wing, APU and the fuselage is included in Figure 12.2.
The summing up the components in the pie chart yields an empty weight of 77,449 kg and an operational empty weight, including crew and their luggage, of 78,262 kg. From the design space diagram provided in Figure 12.3 a $\frac{T}{W}$ of 0.31 was found. This resulted in a thrust of 223,951 N per engine (a total take-off thrust of 447,902 N). The maximum takeoff weight was ultimately found to be 149,831 kg.

12.3. Aerodynamic Characteristics

Before the simulations can be run, the separation between the wings needs to be considered. In the validation it was shown that the separation between the wings influences the optimal taper ratio the optimizer converges to. A large separation between the wings poses additional problems with regard to mounting of the wings to the fuselage and tail, and the stability of the aircraft. The engines are mounted on the aft wing; during take-off the thrust would produce a very large pitch down moment if they are mounted far above the fuselage. A separation of 7.5 meters is chosen with a 70 degrees connector strut angle between the wings.

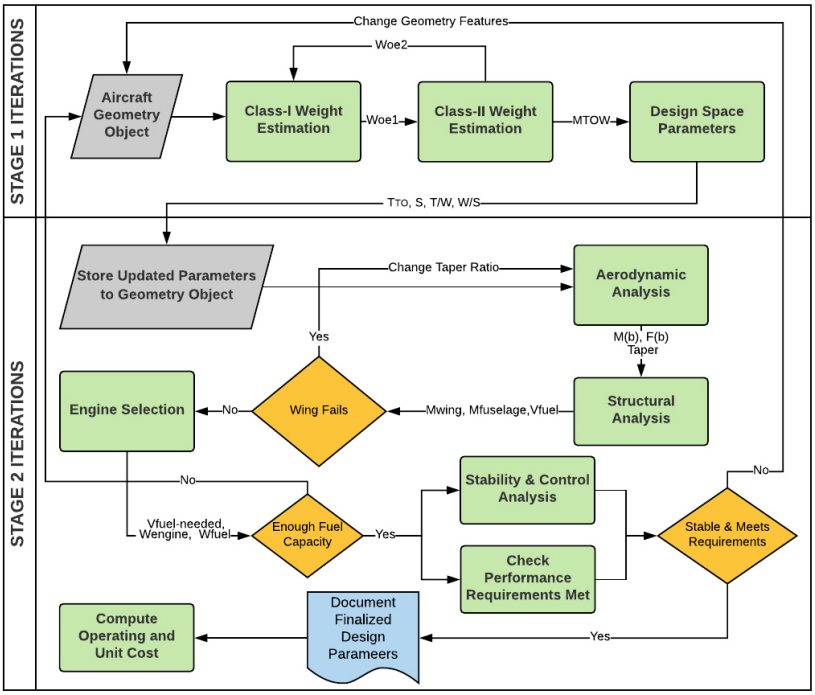

Figure 12.1: General Optimization Flow

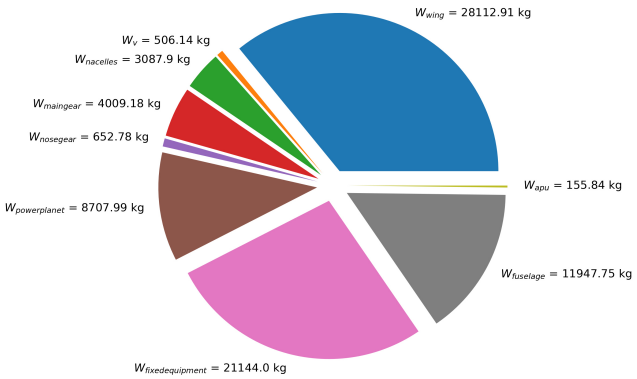

Figure 12.2: Breakdown of the OEW From Class II

After several iterations the optimizer settled at a taper ratio of about 0.6. As described in chapter 7, this is due to the different sweep angles of both wings in conjunction with the constraint that both wing should have the same aspect ratio. However, the structural module returns that at that taper ratio it is unable to generate a configuration for the wing box that is able to sustain the loads. Higher taper ratios make the root of the wing more slender and put more load on the tip, increasing the bending moment at the root while also making it more difficult to carry that load. Therefore a limit on the maximum taper was set to 0.44. Running the optimizer with this limit did yield a working design. The convergence of the L/D with respect to the taper is shown in Figure 12.4.
Figure 12.5a shows the number of panels on the wing planform. For the first couple of iterations the number of panels is reduced, when a solution is found the number of panels is increased significantly. This ensures that the final results will be as accurate as possible. The pressure distribution over the aircraft is given in Figure 12.5b.
The optimizer finds a value way above the maximum taper ratio, therefore the taper 0.433 was selected. For this taper ratio the general planform design is given in Table 12.1.

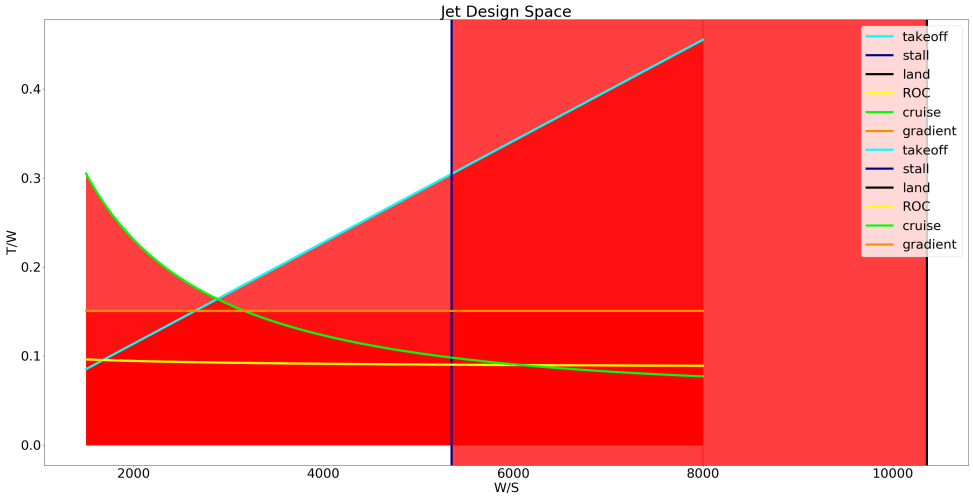

Figure 12.3: Final Design Space Used for Detailed Design

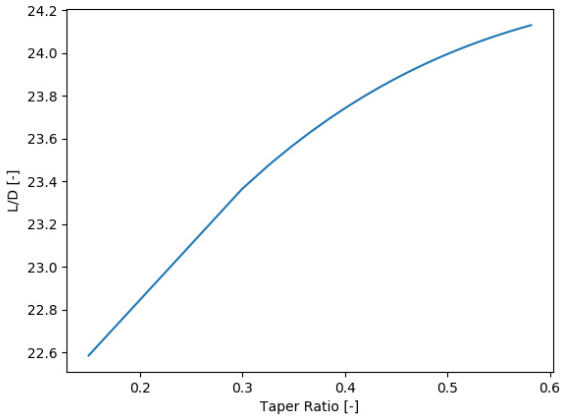

Figure 12.4: L/D of the Optimizer

Table 12.1: Final Box Wing Planform

		Front Wing	Aft Wing	Connecting Strut
Area	$[m^2]$	132.95	132.95	N/A
Span	[m]	40	40	6.103
Sweep	[degree]	33	-33	70
Dihedral	[degree]	2	-2	N/A
Root Chord	[m]	4.55	4.76	2.02
Tip Chord	[m]	2.02	2.11	2.11
Taper Ratio	[-]	0.433	0.433	1.045
Incidence Angle	[degree]	-1.4	-2.4	N/A
Local C_L	[-]	0.292	0.181	N/A

For stability the incidence angle of the rear wing is set to be one degree lower than the front wing. As the rear wing generates a large component of the total lift it induces a negative pitching moment; to compensate the the front wing has to generate more lift to remain stable. The front wing now carries 61 % more lift than the rear wing. The front wing will also stall before the aft wing due to the higher angle of attack, meaning the aircraft will be stable at

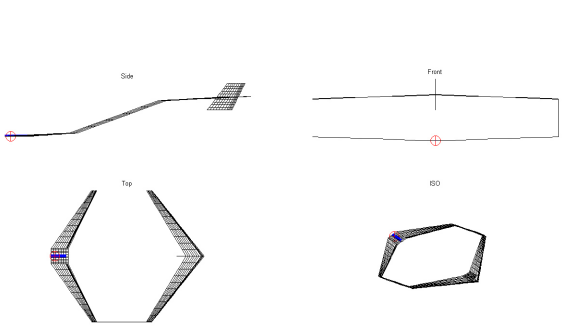

(a) Panels on the Wing Planform

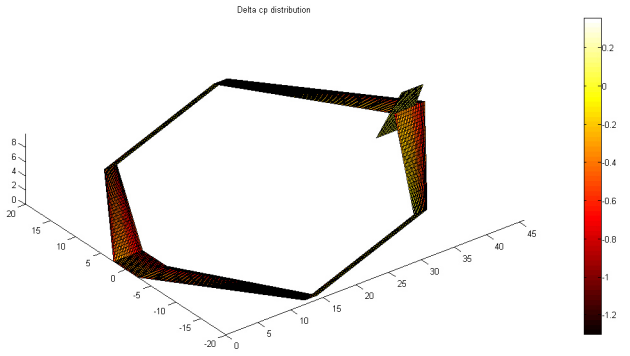

(b) Pressure Distribution over the Planform, with Panels

Figure 12.5: Aerodynamic characteristics

stall. The considerations for stability are discussed in more detail in chapter 9.

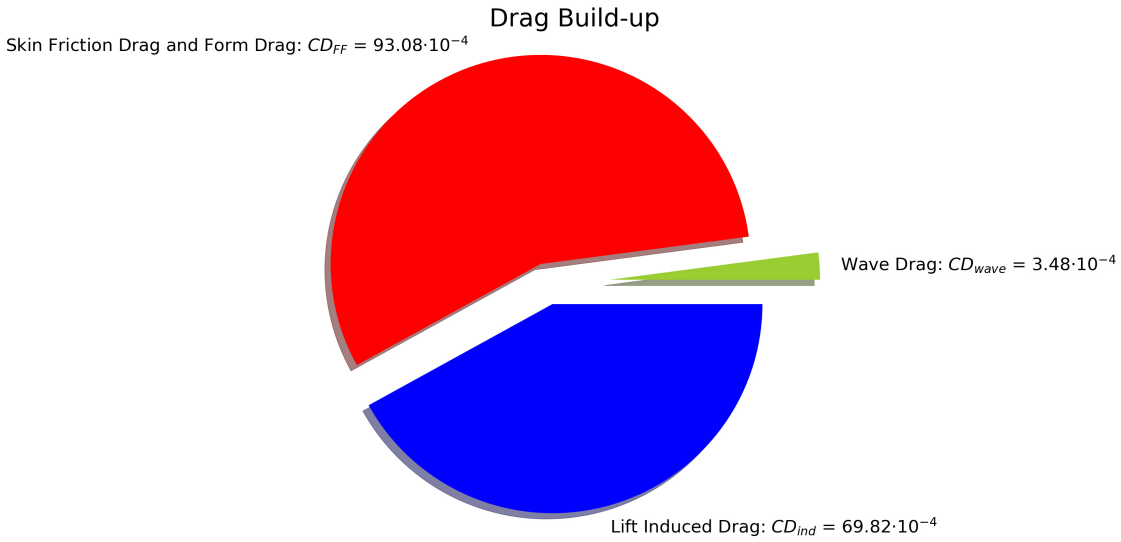

Figure 12.6: Breakdown of the Different Drag Components

During the cruise phase the drag contributions can be broken down into the components as shown in Figure 12.6. As can be seen from this figure the lift induced drag component is equal to 0.00698. A conventional wing with the same reference area and taper ratio, flying in the same conditions is simulated as well. This resulted in lift induced drag of 0.012; meaning a 42.5 percent reduction for this drag component. This drag reduction is in line with the predictions from literature [48]. If both wings of the box wing were ideally loaded this would result in $\frac{C_{D_i,box}}{C_{D_i,ref}} = 0.5$. The box wing does however have a high form and friction drag component due to the struts on the side of the wings, thus damping the total gain in drag reduction.
The resulting aerodynamic results are given in Table 12.2. The obtained Lift over drag is a lot higher than the lift over drag values seen in current generation aircraft [28], but the results obtained are in line with other estimates for the lift over drag from other box wing concepts [70].
The lowest induced drag is obtained when the lift distribution over the wings is elliptical. The lift distribution of the front and aft wing are displayed in Figure 12.7a and Figure 12.7b respectively. The distribution of the front wing follows a nice elliptical shape, the rear wing shape is more triangular. The negative sweep of the aft wing migrates the lift more towards the center of the wing, this is coupled with the taper which has the same effect. This all leads

Table 12.2: Aerodynamic Analysis results

Parameter	Value
$C_{L_{cruise}}$	0.474
$C_{D_{cruise}}$	0.0200
L/D	23.61
V_{cruise} [m/s]	236
h_{cruise} [km]	11

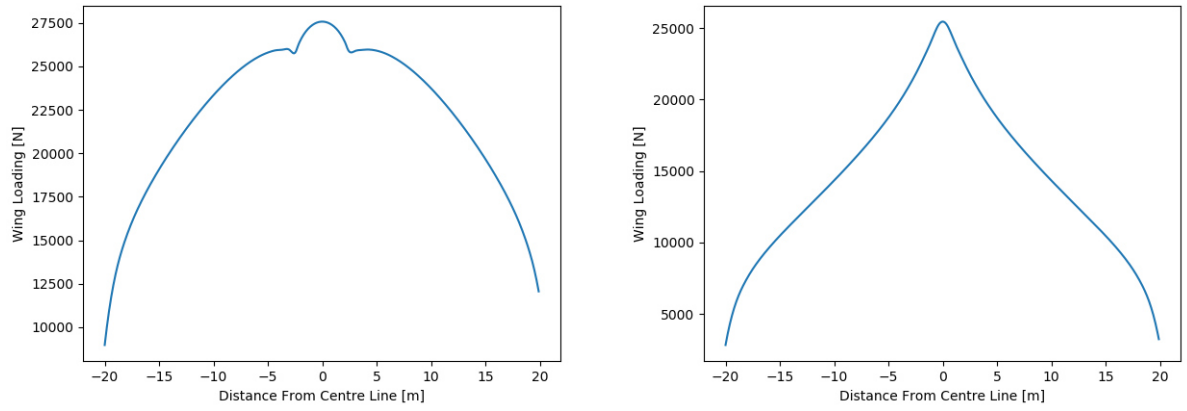

(a) Front Wing **(b)** Aft Wing

Figure 12.7: Lift Distribution Over the Wings

to a less ideal lift distribution. The front wing has a higher loading than the rear wing leading the optimizer to favor a more optimal lift distribution than on the rear wing.

The lift curve and drag polar are also computed for the aircraft using tornado. As can be seen from Figure 12.8a the amount of lift the wing is generating is still very high at negative angles of attack. The SC-21010 airfoil that is used on the wings has a very high camber, this moves the zero lift angle of attack to more negative values. Due to this characteristic the wings will be mounted on the aircraft at a negative angle of attack. Using the drag obtained from the simulation a C_L/C_D curve is made, shown in Figure 12.8b.

12.4. Structural Characteristics: Fuselage Analysis

This section will discuss the results obtained from the stress analysis, optimization and cut-out analysis for both the fuselage and wing design.

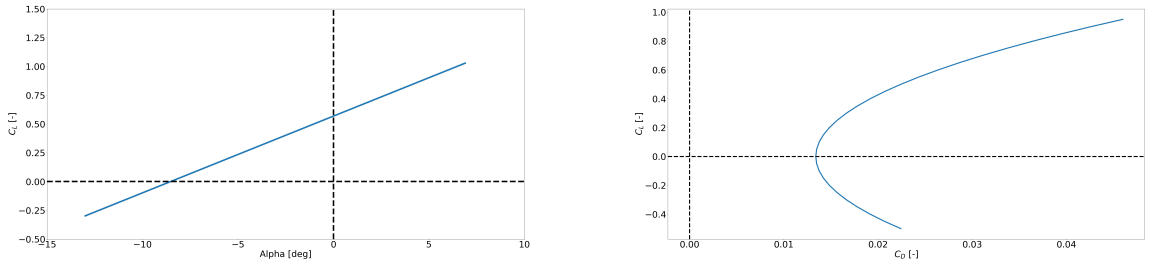

(a) C_{L_α} Curve **(b)** Drag Polar Plot

Figure 12.8: Aerodynamic Coefficient Plots

12.4.1. Results of Fuselage Load Case Analysis

The load case analysis as presented in subsection 8.2.5 yield the shear and moment diagrams for both the wing and fuselage at the most critical load case of 2.5g loading.

In Figure 12.9 the shear and moment diagram of the fuselage loads are displayed respectively. It can be seen that the shear forces are induced by the wing. Furthermore, the maximum bending moment occurs somewhere around the middle of the forward and aft wing.

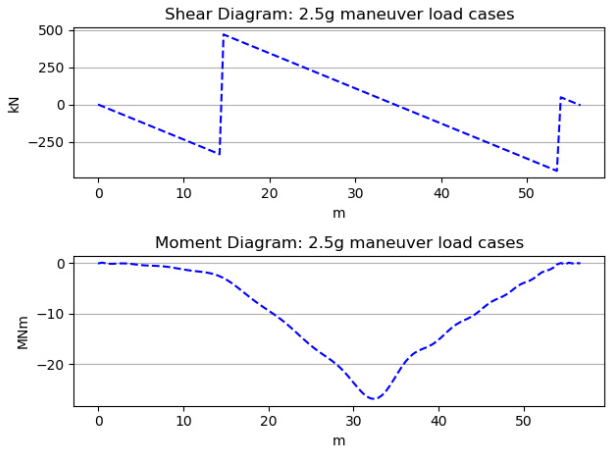

Figure 12.9: Shear and Moment Diagram of the Fuselage (Load Case: 2.5g Maneuver)

12.4.2. Results of Fuselage Stress Analysis

Figure 12.10a and Figure 12.10b show the normal and shear stress distribution of the fuselage structure in a 3D stress plot. These stress plots are useful to get a general insight into how the stresses flow through the structure of the aircraft. Also, these plots can be used to see if the results obtained from the optimization make sense.

When comparing the shear force and moment diagrams of the fuselage to the 3D stress plots, similarities can be noted between the plots. Looking at the moment diagram, it can be noted that the maximum moment lies near the rear of the plane. When looking at the normal stress plot, Figure 12.10a, a peak in stress can be observed in this location. Another observation that can be made for the normal stress plot is the fact that the top of the fuselage is loaded in compression while the bottom of the fuselage is loaded in tension. This is common for a Prandtl plane configuration, as for this type of configuration the fuselage structure is suspended by two lifting wings.

Figure 12.10b shows the shear stress distribution of the fuselage. It can be seen that the shear stress peaks at the sides of the fuselage, which is expected for a fuselage only loaded by shear forces in the y-direction. In the front of the fuselage, a change in sign can be observed. This is the location at which the front wing exerts its shear force onto the fuselage structure. The change in sign occurs because the lifting force acts in the opposite direction of the distributed load of the aircraft weight. The lifting force of the aft wing cannot be observed in this figure, as this force acts behind the analyzed fuselage structure.

Figure 12.11 shows the Von Mises stress in the fuselage. This is a combination of the normal and shear stress.

12.4.3. Results of Fuselage Optimization

The optimization is run to find the skin thickness along the circumference of fuselage and the stringer web/-cap/flange thickness. In general, when running the optimization, the safety margin that was limiting was mostly that of shear. This safety margin ended up being the limiting factor for sizing the skin thickness. The evolution of the skin thickness throughout the circumference of the fuselage is depicted in Figure 12.12a. In this plot it can be seen that the most critical points in shear, that is the most left and right section of the fuselage (0,180 and 360 degrees) has the largest skin thickness.

Regarding the optimization of the stringer web/flange/cap thickness, this thickness is kept constant throughout the entire fuselage cross-section. This means that the stringers used in the fuselage will be identical, which is beneficial for manufacturing. The sized stringer web/flange/cap thickness is depicted in Figure 12.12b.

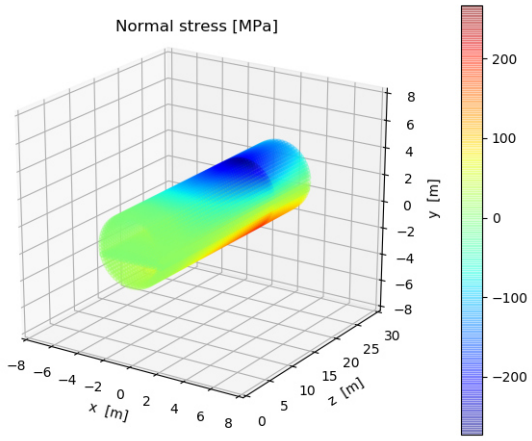

(a) Normal Stresses in the Fuselage, Compression can be Seen on the Crown and Tension on the Belly

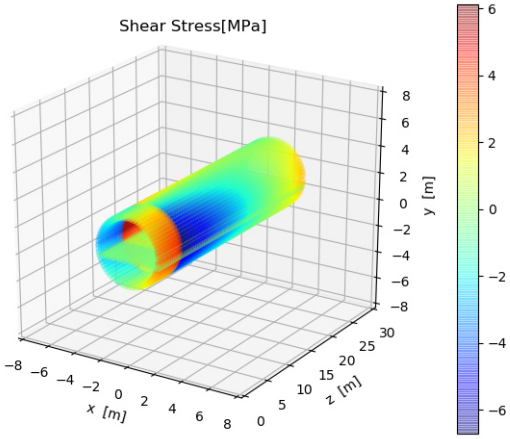

(b) Shear Stress in the Fuselage

Figure 12.10: Fuselage Stress Distributions

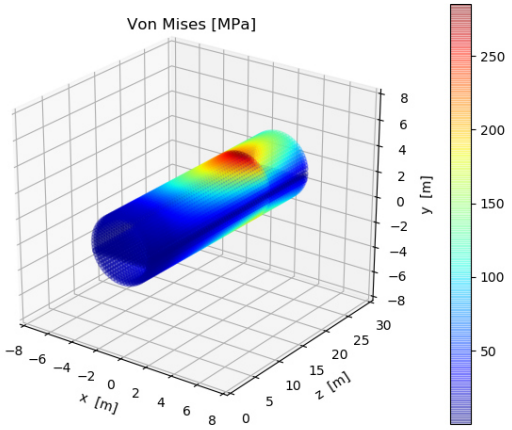

Figure 12.11: Von Mises Stress in the Fuselage

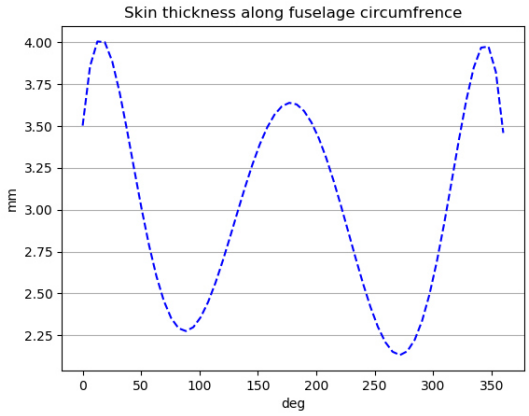

(a) Skin Thickness Around the Fuselage Circumference

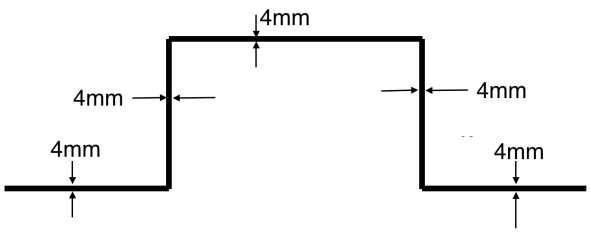

(b) Final Stringer Web/Flange/Cap Thickness

Figure 12.12: Skin And Stringer Sizing

12.4.4. Results of Fuselage Cut-Out Analysis

As stated in subsection 8.2.10, the weight penalty of a window cut-out was calculated for the most critically loaded fuselage section. A window of 12.5 by 9 inches, which is similar to the Boeing 767 window size, was analyzed. The panel layout can be found in Figure 8.10a. It is assumed that the window cut-out is a square hole with the same dimensions as the oval shaped window. For L_1 and L_3, the frame spacing was chosen. The length L_2 is set equal to 10 inches. Similarly, H_1 and H_3 are set equal to the stiffener spacing, while H_2 is set to 12.5 inches. The panel numbering is as follows: Panel one is the panel located at the top left. The numbering continues downwards and moves from top to bottom each row. The numbering convention of the cutout panels is shown in Figure 8.10a. Table 12.3 shows the results of the cut-out analysis. As expected, the panels directly surrounding the window cut-out (panel 2, 4, 5 and 7) are also most heavily influenced by the cut-out.

The weight increase of the panel can now be calculated using Equation 12.1. The final weight penalty per window is calculated to be 2.42 kg. Equation 12.2 shows a statistical relation to calculate the weight penalty for an aircraft window cut-out based on the amount of passengers and pressure differential of the fuselage. Using this relation, a weight penalty of 2.75 kg per window indicating that the calculated value is approximately correct. As the MoM-liner will have 40 windows on each side, the total weight penalty for adding windows equals 193.6 kg.

$$\Delta_{weight} = \sum \left(A_{panel_i} \Delta t \right) + W_{window} - A_{cut-out}\, t_{cut-out} \tag{12.1}$$

$$\Delta_{weight_{stat}} = 109 \left(n_{pax} \frac{1 + \Delta p}{100} \right)^{0.505} \tag{12.2}$$

Table 12.3: Change in Skin Thickness near Window Cut-Out

Panel	Old Skin Thickness [mm]	New Skin Thickness [mm]	Delta [mm]
1	4.3	4.9	0.6
2	4.3	5.8	1.5
3	4.3	4.9	0.6
4	4.3	6.1	1.8
5	4.3	6.1	1.8
6	4.3	4.9	0.6
7	4.3	5.8	1.5
8	4.3	4.9	0.6

12.5. Structural Characteristics: Wing Analysis

12.5.1. Results of Wing Load Case Analysis

The loads that were ultimately used to find the stresses and to come up with the final wing box geometry and configuration were generated. These loads are presented below. All loads were calculated assuming at load factor of 2.5 (The maximum maneuvering load factor that the aircraft is required to sustain during flight).

The shear force distribution on each wing was computed due to the aerodynamic loads are presented for the front and rear wing in Figure 12.13a and Figure 12.13b respectively. The maximum shear force of 1008 kN is experienced at the root of the front wing this is because the front wing not only generates the most lift for static stability reasons but also does not have the bending relief generated by the engine.

The bending moments distribution are similarly presented in Figure 12.14a and Figure 12.14b. The maximum bending moment is also located at the root of the front wing and was found to be 8,996 kNm.

The final parameter that was considered was the torque acting on the wing (primarily as a result of the wing sweep). It can be seen in Figure 12.15a and Figure 12.15b that the forward sweep of the rear wing generates a negative torque whereas the regular, forward sweep of the front wing produces a positive torque. The largest magnitude torque 8048 kNm.

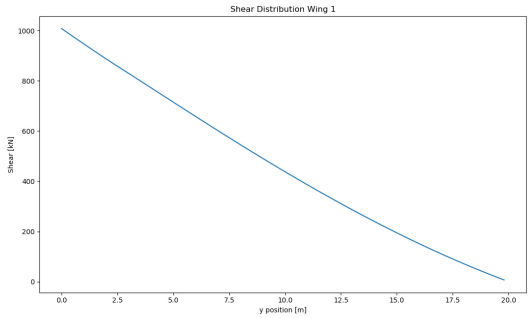

(a) Shear Force Distribution on the Front Wing

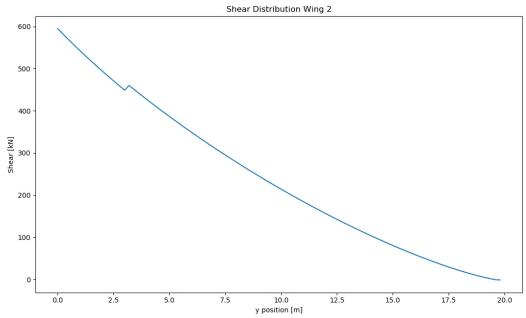

(b) Shear Force Distribution on the Rear Wing

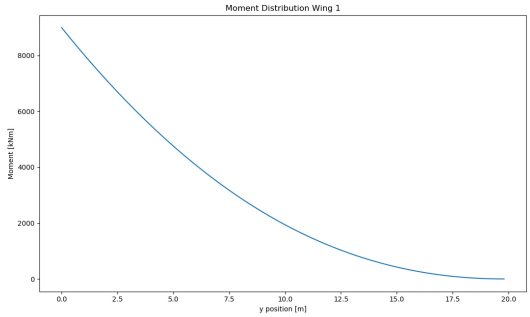

(a) Moment Distribution on the Front Wing

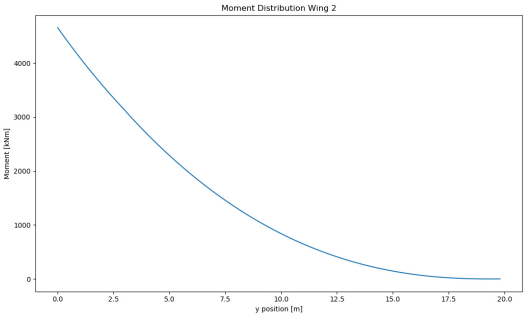

(b) Moment Distribution on the Rear Wing

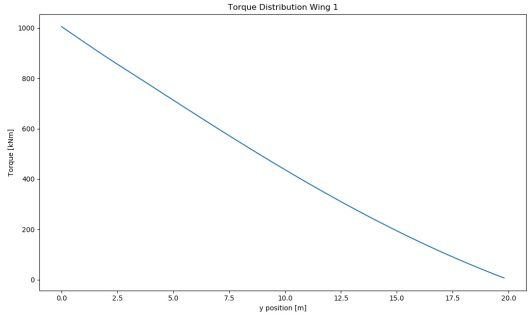

(a) Torque Distribution on the Front Wing

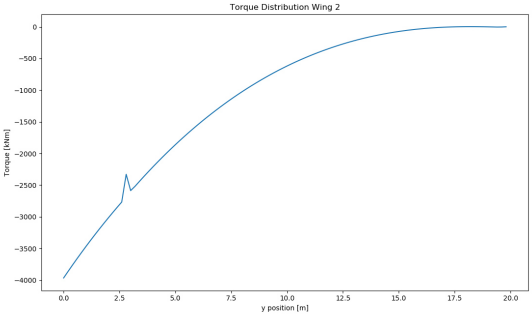

(b) Torque Distribution on the Rear Wing

12.5.2. Results of Wing Stress Analysis

Normal Stress

A 3D plot of the normal stress distribution over the wing is presented in Figure 12.16a and Figure 12.16b. In addition to this the plot indicates the deflection of the wing. to ensure that the bending of the wing tip was limited to 10% of the wing semi-span. This was done to ensure that the stresses introduced to the connecting strut remain small. Moreover the deflection of each wing was constrained to be within 1% of each other. The final deflection at the load factor of 2.5 was 1.8 m. The maximum normal stress is dependent on the moment and therefor the maximum normal stress is found at the root of the wings. The maximum normal stress was 1,035.8 MPa in the front wing and 1,192.8 MPa for the rear wing. These values are very similar because although the forces acting on the rear wing are much lower it also has fewer stringers to allow it to have the same tip deflection as the front wing.

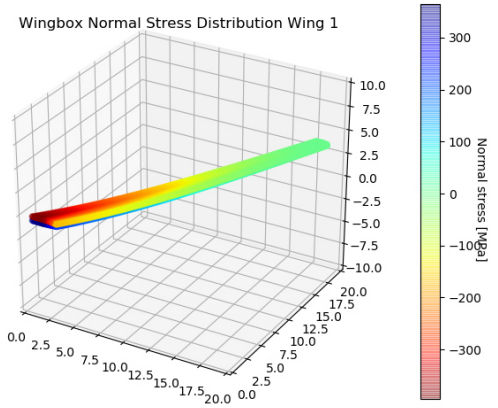

(a) Normal Stress Distribution on the Front Wing

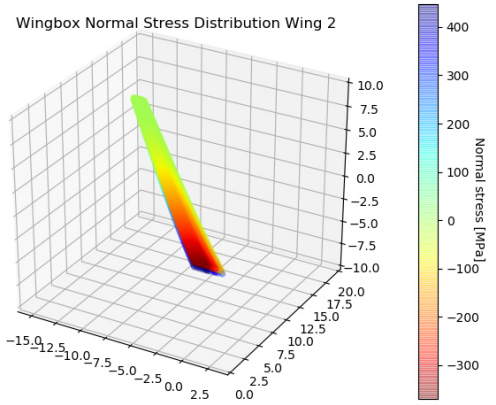

(b) Normal Stress Distribution on the Rear Wing

Shear Stress

A 3D plot of the shear stress distribution as a result of the torques and shear force presented in subsection 12.5.1 is shown in Figure 12.17a and Figure 12.17b. It can be seen quite clearly the presence of the engine on the rear wing significantly reduces the shear stress experienced at the root of the wing. The maximum stress on the front and rear wings was 176.9 MPa and 176.5 MPa respectively. As the shear stress is dependent on the moment of inertia, which is adjusted so both wings experience similar tip deflection by changing the number of stringers and skin thickness, the maximum stress values do not differ significantly. Constraining the problem in this way leads to very similar stresses in each wing.

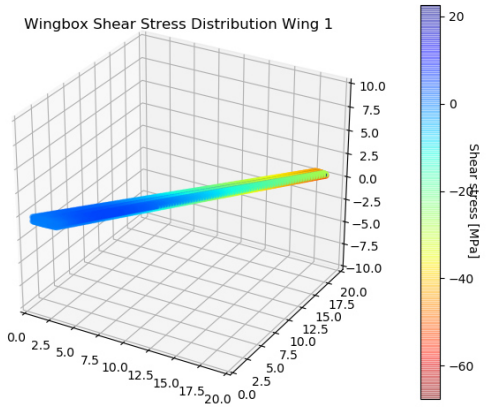

(a) Shear Stress Distribution on the Front Wing

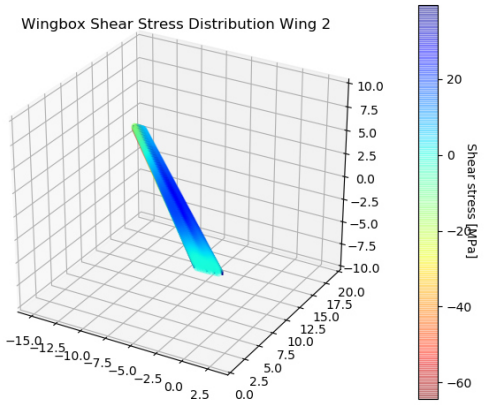

(b) Shear Stress Distribution on the Rear Wing

12.5.3. Results Final Optimized Wing Configuration

The final configuration resulting from the optimization is presented below in Table 12.4. It can be seen that the the front wing is considerably more reinforced than the rear wing.

Table 12.4: Final Wing Box Configurations

Parameter	Front Wing	Rear Wing
Number of Stringers Upper Skin [-]	59	18
Number of Stringers Lower Skin [-]	56	10
Skin Thickness [mm]	3.6	2.0
Number of Spars [-]	4	4
Spar Thickness [mm]	10.0	10.0
Spar Locations [%c]	0.20, 0.45, 0.6, 0.75	0.20, 0.45, 0.6, 0.75

12.6. Engine Sizing

Using the methods described in chapter 10, and the thrust requirements from the final design optimization, the final engine sizing and selection can take place.
Now as described in subsection 10.2.3, a wide range of engine parameters were collected on all the engines shown in Table 10.1. The newer engines, that had some missing information, were completed using the trend lines shown in subsection 10.2.5. This means that for every engine the required information is present.
The preliminary engine selection will take place based on the ratio between the takeoff thrust and the cruise thrust. However, if an engine does not quite meet the required ratio this can still be resolved by using boosted turbofans, as explained in chapter 10. Table 12.5 shows the required engine thrust per engine, and the corresponding ratio of the two values. The maximum thrust the engine can produce at takeoff is 110.5%N1 and The ratio of 5.46, shown in Table 12.5, eliminates a lot of engines but leaves a few promising ones.

Table 12.5: MoM-liner Thrust Requirements (Per Engine)

Parameter	Value
Take-off Thrust (100% N1)	202.7 [kN]
Cruise Thrust (100% N1 @ 35,000ft)	37.1 [kN]
Ratio TO/ CR	5.46 [-]

The method that was described in chapter 10 states that 'rubberizing', or scaling as it is more commonly known, can be used in this stage of the design. What this means is that an existing engine can be scaled to fit the thrust requirements of the MoM-liner. However, the trend between SFC-cruise and Bypass ratio, as shown in Figure 10.2, will also be used here. This way a scaled engine can be 'upgraded' with a higher bypass ratio, and an estimate of the performance can be obtained.

Table 12.6: Final Engine Selection Options [5][59][60][62][63][64][65][66]

Engine Type	TO/CR Ratio	Bypass	Scaling Factor	Boosted?
PW 1100G	5.07	12.5	+27%	Yes
RR Trent XWB-84	5.48	9.6	-45%	No
CFM LEAP-1C	5.04	11.0	+36%	Yes
RR Trent 7000	5.40	10	-37%	No
RR Trent 1000-C	5.42	10.80	-39%	No

Table 12.6 shows the engines that meet the requirements, not just in terms of TO/CR ratio but also in terms of efficiency. The PW 1100G is a geared turbofan, which bring some major benefits as described in subsection 10.2.4. If the thrust ratio is not close enough, boosting the performance could be an option. This is would need some further research to see if is a viable option for the MoM-liners mission.
A bypass ratio of 15 was chosen, as the technology will be ready in 2030 and the clearance of the engines on the MoM-liner will be sufficient to accommodate these large engines. Using Equation 10.1 the SFC-cruise becomes 0.452. The specific fuel consumption of the other engines can be seen in Table 12.7.

Table 12.7: Final Engine Selection Options [5][59][60][62][63][64][65][66]

Engine Type	SFC_{cruise}
PW 1100G	0.483
RR Trent XWB-84	0.517
CFM LEAP-1C	0.510
RR Trent 7000	0.512
RR Trent 1000-C	0.502
MoM-liner Custom	**0.452**

Table 12.8: Fuel Requirements MoM-liner

Parameter	Value
Fuel Weight [kg]	49,894
Fuel Volume for Design Range [m^3]	62.37
Max Fuel Volume [m^3]	77.37

12.6.1. Fuel Consumption

Now that the final engine selection has taken place, the engine parameters found above can be used to calculate the required fuel volume. The fuel fraction method uses standard fuel fractions for every non-horizontal flight phase. For cruise the SFC from Table 12.7 can be used to calculate the required fuel. A typical mission does not just consist of fuel for the climb, cruise and descent. A flight has to be able to deal with bad weather (headwind), a diversion or a go-around. These required values are taken from ICAO Annex 6 Part I [67][71].

- Contingency: 5% of trip fuel added as extra
- Alternate: 30 minutes of flight time
- Reserve: 30 minutes of holding

Using the methods described above, the results shown in Table 12.8 were obtained. These fuel values are for a flight of 5,000 NM with max payload. This is however not the size of the fuel tank, as this is usually larger to accommodate more fuel for flights with a lower payload.

The wings on their own are too small to hold all of the fuel, so fuel will need to be stored in the tail cone as well. The split of fuel between the two wings and the tail cone can be found in subsection 12.7.1. For the design range the tail cone will not be 100% filled, otherwise MTOW will be exceeded. The maximum amount of fuel that can be stored in the tail cone is set at: $15 m^3$.

12.6.2. MoM-liner Custom Engine

The final engine selection of the MoM-liner does not have one winner, but a couple of options. A scaled Rolls Royce XWB-84 with a higher bypass ratio would fit the MoM-liners needs almost exactly. The thrust ratio fits almost exactly, and it is already an efficient engine so increasing the bypass will lead to even better efficiency. The engine with the lowest SFC-cruise in the comparison is the P&W 1100G, the geared turbofan technology in this engine is also state of the art. The thrust ratio of this engine does not fit the required value, but installing an electrical boosted system could solve this. Using the trend line shown in Figure 10.1b, and the thrust from Table 12.5 the weight of the engine will be around 4,050 kg.
So there are two option for the MoM-liner, on more advance than the other.

RR XWB-84: A 45% smaller version of the existing engine, with an increased bypass ratio (9.6 -> 15).

PW 1100G: A 27% larger version, with an increased bypass ratio (12.5->15). To boost the thrust ratio, an electrically boosted turbofan will be necessary.

In the end, the custom MoM-liner can be either of the two engines shown above. Either the regular high-bypass RR, or the the newer geared PW engine with again the high-bypass. Considering the PW has to be scaled less than the RR, and it already incorporates the geared turbofan system this engine would seem like the best choice to scale. Future technologies like boosted turbofans could lead to even further improved efficiency, as the engine would be sized for cruise making it optimal for this flight phase.

12.6.3. Payload - Range diagram

The payload-range diagram in Figure 12.18a shows the range the aircraft can fly, based on the amount of payload it can bring. If payload is exchanged for fuel the aircraft can fly further, until the maximum fuel capacity is reached. If the aircraft is loaded with the maximum amount of fuel it can travel 6200nM, a 1200 nautical mile increase. However, as payload is swapped for fuel, the aircraft can then only carry around 105 passengers. Flying from Amsterdam, this would open direct routes to Singapore, with for example a full business class interior. Also flights from Los Angeles to Hong Kong, and Moscow to Rio de Janeiro become feasible. These are huge business routes, and a legacy carrier might be able to operate full business class flights on these routes.

12.7. Static Stability & Control Characteristics

The analysis described in chapter 9 was performed using the final values of the wing and fuselage design. The outputs are summarized in Table 12.9 It was concluded that the aircraft is can be stable and controllable. However, this is achieved at the cost of higher induced drag, due to the unequal lift split between the two wings. Furthermore, compared to a normal aircraft, the allowable c.g. range is rather far in the back. This is completely reasonable, and mostly due to the wing placement. As the box wing has large lifting surfaces at the front and back of the aircraft, the allowable c.g. range must lie in between the two, closer to the aft wing. This is as the front wing has to counteract the lifting moment from the back wing as well as both pitching moments, hence it needs a larger moment arm.

Table 12.9: Static Stability and Control Results

Parameter	Value	Value
Most Forward c.g. Location	287 % MAC	33.6 m from nose
Most Aft c.g. Location	328 % MAC	36.4 m from nose
Static Margin	41 % MAC	2.82 m

12.7.1. Loading Diagram

The loading diagram takes into account how the C.G. of the aircraft shifts under different loading options of the aircraft. The fuel weight, calculated in Table 12.8, was used and the location of the fuel tanks are distributed as follows.

- Front Wing: 20.8 m^3
- Rear Wing: 22.8 m^3
- Tail Cone: 18.8 m^3

The loading diagram, shown in Figure 12.18b, is the loading diagram for the MoM-liner. As expected for a long range aircraft, the fuel weight is a substantial part of the total weight. Also, for a conventional aircraft the c.g. location is usually somewhere over the main wing. But, as this is a two wing aircraft the stability margin is located in between the first and second wing. It is quite obvious that the fuel weight, and more specifically its location, has a huge impact on the center of gravity. This is not necessarily an issue, as fuel can actively be pumped around, and for the MoM-liner should be kept as far aft as possible during flight.

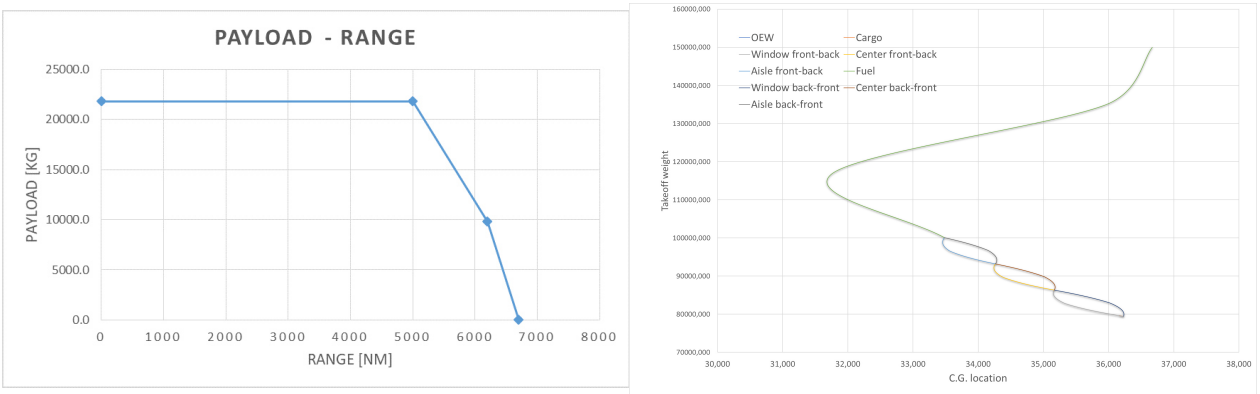

(a) Payload-Range Diagram

(b) Loading Diagram

Figure 12.18: Performance Results MoM-liner

12.7.2. High-Lift Devices

Since a high $\Delta C_{L_{max}}$ was needed for such small wings, it called for more complex high-lift devices. For the leading edge slats are used, for the trailing edge double slotted Fowler flaps. Furthermore, they are hinged from the front and aft spar in the wing. This leads to slats running along the entire usable leading edge. Where a meter is left free on the inboard side for stalling reasons. The slats will be deflected around 20 degrees. The slats thus run from 3.2 m to 19.1 m spanwise and from the leading edge to 0.1c. (Where 0 m is the middle of the wing in the middle of the fuselage, this holds for this entire chapter.) This is possible, because no other devices are needed on the leading edge. On the trailing edge, however, ailerons and elevators are also needed, leaving less space for HLDs. This is also a reason why double slotted Fowler flaps are more suitable than single slotted Fowler flaps. The double slotted Fowler flaps run from 4.75 m to 17.45 m, from 0.75c to the trailing edge. The flaps are placed in the middle in between the elevator and aileron with 0.55 m spacing on either side. Furthermore, the flaps will be deflected 50 degrees at landing and 20 degrees at take-off. flaps The result is tabulated in Table 12.10 and an overview can be seen in Figure 12.21.

12.7.3. Wing Control Surfaces

The results for the control surfaces are also tabulated in Table 12.10 and visualized in Figure 12.21. The aileron and elevators are slightly oversized, to compensate for the loss of efficiency, since they are split up in half and put on both wings. Both are 1.0 m long, where the ailerons are put as far outboard as possible, and the elevators put inboard. Furthermore, both have a maximum deflection angle of 20 degrees, this will not cause too much twist in the wing compared to higher deflection angles. Since, the area can be split over two wings, it is chosen to opt for lower deflection angles because of this twist reduction. This results in an elevators running from 3.2 m to 4.2 m, from 0.75c to the trailing edge and ailerons on the same chordwise position, from 18.0 m to 19.0 m spanwise. The last surfaces on the wing are the spoilers. These run from 4.75 m to 11.75 m, from 0.52c to 0.75c, and will have a deflection angle of 60 degrees. This angle may seem rather high, however it is not unconventional for spoilers. The spoilers will be hinged at 0.75c, so there will be enough material to handle the twist created by the spoilers, therefore the deflection angle of 60 degrees is acceptable and gives best performance with least twist.

Table 12.10: HLD & Wing Control Surfaces

Surface	**Spanwise Position** [m]	**Chordwise Position** [m]	**Deflection Angle** [deg]
Slats	3.2 - 19.1	0.0c - 0.1c	20
Double Slotted Fowler Flaps	4.75 - 17.45	0.75c - 1.0c	50 & 20
Elevator	3.2 - 4.2	0.75c - 1.0c	20
Aileron	18.0 - 19.0	0.75c - 1.0c	20
Spoiler	4.75 - 11.75	0.52c - 0.75c	60

12.7.4. Vertical Tail & Rudder Sizing

The design of the vertical tail and the rudder are closely related, thus they will be discussed together. In order to determine the shape of the vertical tail, a number of geometric parameters have been selected, these are shown in Table 12.13. The results are summarized in Table 12.13. The first table shows the inputs to the design process. As the second wing is attached to the surface, the rudder cannot run through the whole fin height. Thus, it will be split in two at the wing intersection. To account for the wing running though the tail, the total rudder span is taken as 0.9 of the total tail span. In accordance with the considerations discussed in Equation 9.2.1, a NACA0009 airfoil was chosen for the tail. This choice is necessary, as the wing only has a t/c of 0.1, thus this airfoil with a t/c of 0.09 is the maximum allowable to avoid significant impediments due to compressibility effects.
Investigating the rudder deflection angles, it is seen that the required deflections are much lower than the maximum. This gives confidence that the aircraft will have excellent directional stability and will be able to cope with engine failures in all critical conditions as well as have safe handling characteristics in strong crosswinds. Lastly, the stability derivatives all have the expected sign, meaning that the aircraft will be stable. Additionally, the magnitude of each value is within the expected range, thus the aircraft will not be overly stable. Having a too large tail and thus too much stability could also be detrimental for flying characteristics, as the aircraft would lose controllability. Having all values in a stable region, yet no derivative of too large magnitude is ideal for a good tail design.

Table 12.11: Planform Layout Inputs

Parameter	**Value**
$\Lambda_{LE,v}$	35°
A_v	1.5
λ_v	0.7
Cr/Cv	0.3
τ	0.52
br/bv	0.9
Airfoil	NACA0009

Table 12.12: Vertical Tail Sizing Results

Parameter	**Value**
Vertical Tail Volume	0.078
Vertical Tail Area	31.5 m^2
Vertical Tail Height	6.87 m
Vertical Tail Root Chord	5.39 m
Vertical Tail Tip Chord	3.77 m
$\delta_{r,max}$	30°
$\delta_{r,OEI}$	19.3°
$\delta_{r,XWIND}$	14.0°

Table 12.13: Stability Derivatives

Stability Derivative	**Value**
C_{n_β}	0.375
$C_{n_{dr}}$	-0.234
C_{y_β}	-0.990
$C_{y_{dr}}$	0.343

12.7.5. Landing Gear Design

Based on the final planform and the stability margin/c.g. excursion, the landing gear was sized and positioned. Regarding the Load Classification Number (LCN), it was assumed that the MoM-liner will fly to similar airports as the B757-200 and thus the same LCN of 50 was used [26]. For the tire selection, both british and american tires were considered, with the final decision to use british sizes as they allow a slightly smaller tire. The results are summarized in Table 12.14. The geometric positioning including dimensions can be seen in Figure 12.20. An aerodynamic fairing was added as the trackwidth of the main gear exceeded the fuelage width. This fairing is shaped to minimize the additional weight and drag.

Table 12.14: Landing Gear Design Results

Parameter	Value
N_{mw}	8
N_{nw}	2
LCN	50
p_{max}	1,002.2 Pa
Tire Dimensions (nose)	762 mm x 229 mm [d x w]
Tire Dimensions (main)	1270 mm x 400 mm [d x w]

12.7.6. Dynamic Stability

For the dynamic analysis, values from all other disciplines were necessary. As it is nearly impossible to compute accurate mass moments of inertia of the aircraft at this stage of the design, a statistical regression was done based on similar aircraft from [54]. The results show that except spiral, all eigenmotions are stable in cruise. The spiral is often an unstable motion and regulations accommodate for that. Thus, in the current state, this aircraft is not only statically but also dynamically stable. However, many coefficients are not accurately predictable through analytical methods. Thus, these very good results give confidence in the design, yet a final conclusion about dynamic stability can only be done though actual flight test.
Considering the handling requirements as given by MIL-F-8785C [55], this analysis would be a type II/III aircraft in a category B flight phase. Checking with the appropriate requirement, it is easily visible that this aircraft would handle very well and on a competitive level. The only possible area of improvement is the spiral mode. For level 1 handling, the time to double amplitude should be at least 20s.

Table 12.15: Dynamic Stability Results and Handling Characterstics

	Short Period	Phugoid	Aperiodic Roll	Dutch Roll	Spiral
Eigenvalue	-0.0454 ± 0.0734j	-0.000417 ± 0.00303j	-56.6	-0.0978 ± 0.809j	0.00947
Period	2.56 s	61.9 s	-	1.32 s	-
Damping Ratio	0.527	0.0725	-	0.120	-
$T_{1/2}$	0.455 s	72.0 s	0.00207 s	1.20 s	-12.4 s
Handling [55]	Level 1	Level 1	Level 1	Level 1	Level 2

12.8. Performance

As a final analysis once every other department has finished their work, the final design parameters were used to conduct a final performance analysis of the aircraft. Using the equations presented in chapter 11, a multitude of characteristic values were computed and are summarized in Table 12.16. As the aircraft not only has to perform close to the ground, but also at cruise altitude, all parameters are given for sea level and cruise conditions. For certification, mostly the max. climb gradients, the max. climb angles, with all engines operating and in case of engine failure are relevant. The top part shows theoretical results and thus the theoretical maximum from a purely mechanics point of view. In reality, compressibility effects would severely lower especially the values at highest speeds. However, climb gradients and climb rates are most important just after take-off, when the aircraft may have to clear terrain. Thus, climb rate and climb gradient were computed for the minimum safe climb speed (V_2) both for all engines operative and in case of engine failure. Comparing these values with the CS-25 [20] minimum requirements yields that the current design easily meets and exceeds all regulatory minima.

Table 12.16: Results from Performance Analysis of Final Design

Parameter	Value at S.L.	Speed at S.L.	Value at 35,000 ft	Speed at 35,000 ft
Min. Speed (Take-off)	-	62.99 m/s	-	113.15 m/s
Min. Speed (Landing)	-	56.86 m/s	-	102.1 m/s
Max. Speed	-	304.0 m/s	-	376.0 m/s
Max. Angle of Climb (AEO)	0.27 rad	96.4 m/s	0.09 rad	173.1 m/s
Max. Angle of Climb (OEI)	0.12 rad	96.4 m/s	0.03 rad	173.1 m/s
Min. Angle of Descent	-0.03 rad	96.4 m/s	-0.03	173.1 m/s
Max. Rate of Climb	47.2 m/s	263.5 m/s	21.16	279.5 m/s
Min. Rate of Descent	-2.88 m	68.14 m/s	-5.21 m/s	122.4 m/s
Max. Angle of Climb @ V_2 (AEO)	0.247 rad	75.6 m/s	0.0665 rad	135.8 m/s
Max. Angle of Climb @ V_2 (OEI)	0.0924 rad	75.6 m/s	0.00314 rad	135.8 m/s
Max. Rate of Climb @ V_2 (AEO)	18.49 m/s	75.6 m/s	9.02 m/s	135.8 m/s
Max. Rate of Climb @ V_2 (OEI)	6.973 m/s	75.6 m/s	0.427 m/s	135.8 m/s

Secondly, take-off and landing distances were analyzed at MTOM and sea level conditions. The break-down in the different flight segments is presented in Table 12.17 and Table 12.18. For take-off, the screen height was reached before the transition phase is finished, thus the second formula is used to account for this. For the minimum required field length for take-off, both regulatory requirements were investigated (115 % of required take-off distance with AEO and balanced field length). It was found that the take-off distance with AEO is the limiting factor, with a margin of about 50 m over the balanced field length (Figure 12.19). However, the required take-off distance is still well below even the initial requirement. This indicates that the final aerodynamic parameters were significantly better than the initial estimates used for the design space. As a next step, another iteration should be done to reduce the thrust to a lower level, and thus save mass and increase efficiency of the design even further. Regarding the landing distance, it has to be considered that currently no thrust reversers are included. As the aircraft is able to meet all requirements, they are not necessary at the current state, however, including them might be beneficial to increase the effective performance envelope of the aircraft.

Table 12.17: Take-off Maneuver Analysis Results

Parameter	Value
x_{ground}	990.7 m
x_{air}	315.4 m
$x_{total,take-off}$	1,306.1 m
$x_{take-off,CS-25}$	1,502.0 m
$BalancedFieldLength$	1,453.9 m

Table 12.18: Landing Maneuver Analysis Results

Parameter	Value
x_{air}	436.7 m
x_{trans}	147.8 m
x_{brake}	796.2 m
$x_{total,landing}$	1,353.7 m
$x_{landing,CS-25}$	2,256.1 m

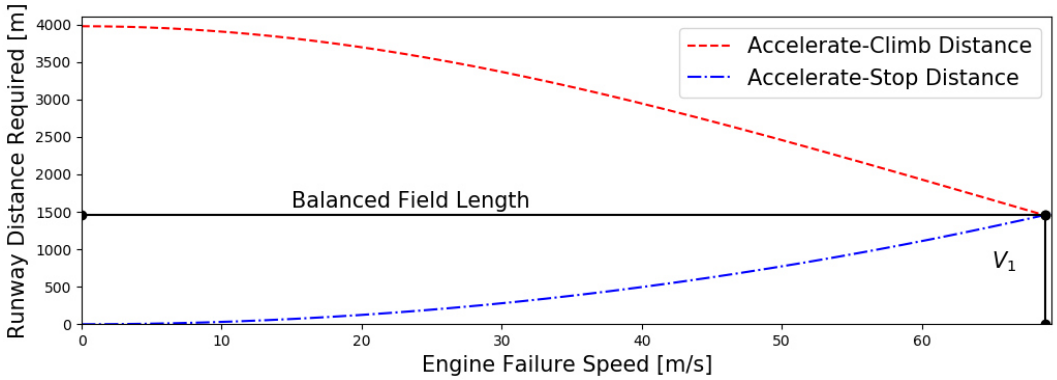

Figure 12.19: Balanced Field Length for the MoM-Liner at MTOM

12.9. External Layout

The external layout and dimensions have been presented in Figure 12.20. These dimensions have been obtained from the respective disciplines after completion of the optimization process.

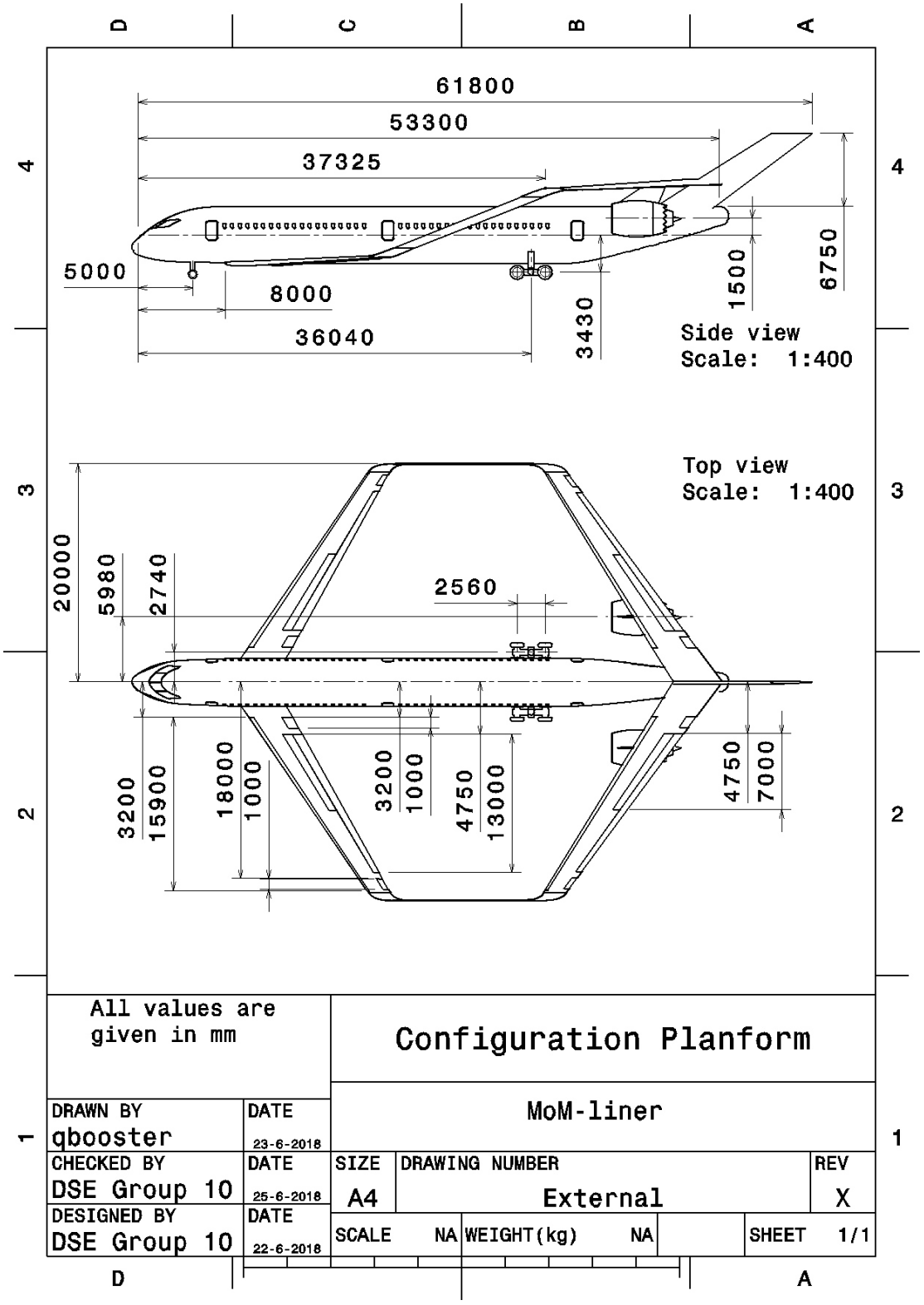

Figure 12.20: Exterior Layout with Dimensions

12.10. Internal Layout

In this section the interior design of the fuselage is considered. The main items covered in this section are the cross-section layout of the fuselage, the layout of doors, emergency exits and windows, selection and sizing of galleys and lavatories, sizing of cargo and baggage holds and fuselage systems such as the environmental control unit [72].

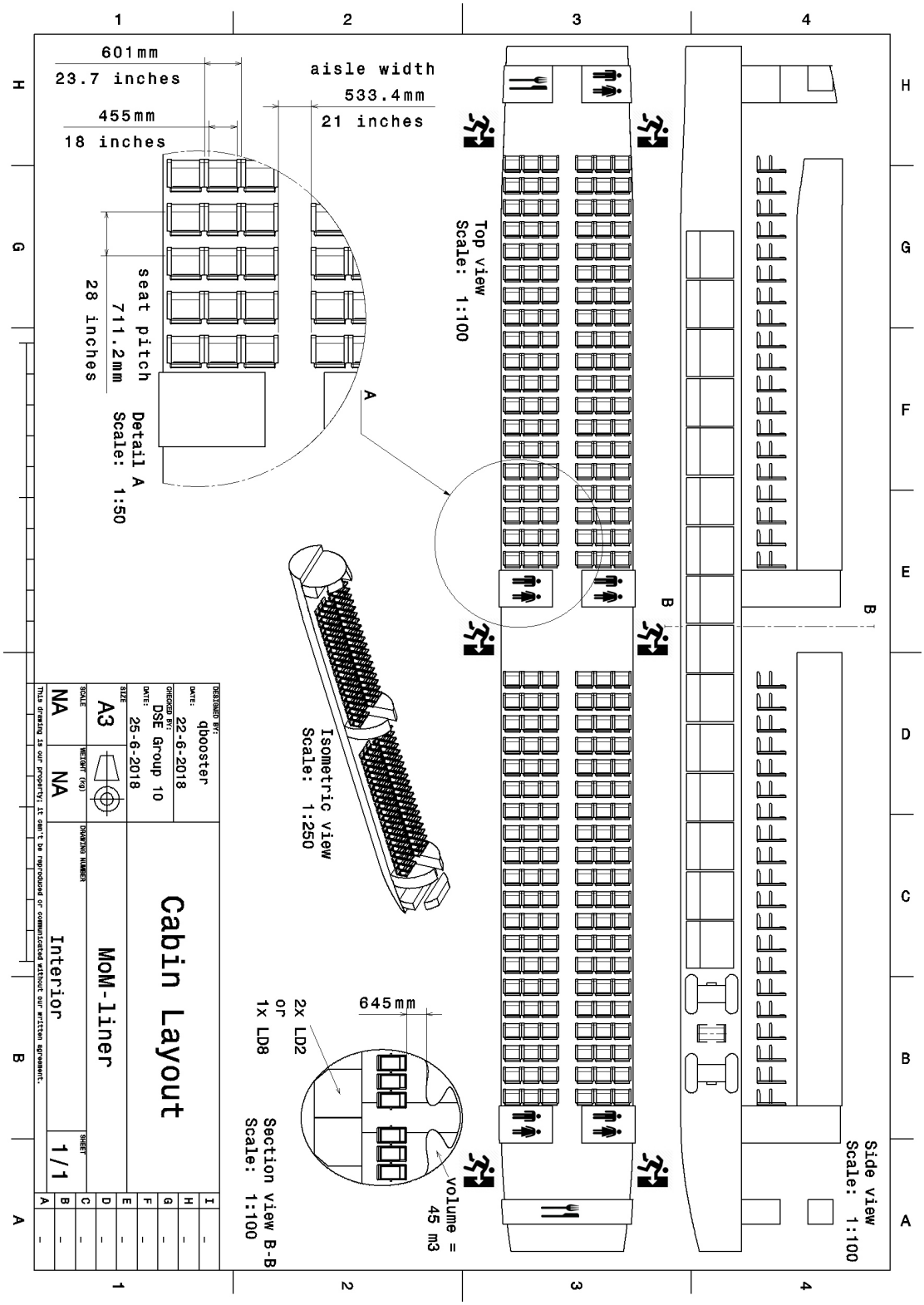

Figure 12.21: Cabin Layout

12.10.1. Cross-Sectional Layout of Fuselage

The MoM-liner will carry 234 passengers in a single-class configuration. In the selection of the final design of the MoM-liner it was decided that the MoM-liner would have a single aisle fuselage configuration. Even though the twin aisle configuration offers superior comfort levels when compared to the single aisle configuration, the single aisle configuration was still deemed superior as the twin aisle configuration would generate as much as 56% more fuselage profile drag due to its larger fuselage diameter [4].

In the cross-sectional design of the fuselage, several aspects need to be taken into account. The amount of seats per row, the width of each seat and the aisle width will mainly determine how wide the aircraft fuselage needs to be. Also the cargo hold is an important factor in the design of the aircraft cross-section.

The MoM-liner will incorporate a single aisle configuration with six seats abreast per row. As the MoM-liner shall have a passenger comfort level comparable to the Airbus 350 and Boeing 787, these aircraft will be used as a reference for seat width. The MoM-liner will use seats with a width of 17.9 inches plus an additional 2.95 inches of armrest width. The minimum allowable width of aisles between seats is dictated by emergency evacuation considerations. CS 25.815 states that the passenger aisle width for a passenger aircraft having a seating capacity of more than twenty people shall be at least 20 inches at any point in between seats. The MoM-liner will have an aisle width of 21 inches. The overhead compartment of the MoM-liner is sized in such a way that there is enough space for each passenger to store a carry-on bag. Also, the headroom of the passenger and aisle height are designed keeping passenger comfort in mind.

The cargo hold of the MoM-liner is designed in such a way that it can contain a variety of standard cargo containers. It can hold an LD-8 type B container, two LD-2 containers side by side, or a single LD-1 container. Figure 12.20 shows the general layout and sizing of the MoM-liner fuselage cross-section.

12.10.2. Design of Fuselage in Top View

This section will discuss the design of the fuselage in top view. It considers the cabin section, and will give a location of the seats, doors, emergency exits, windows, galleys, lavatories and service access holes.

As mentioned previously, the MoM-liner will transport 234 passengers. These seats will be placed in rows of six in a single aisle configuration. The rows will be spaced at a seat pitch of 28 inches, which is in accordance with the seat pitch in high density configuration in long range flights. As stated by aviation regulations, a minimum of one flight attendant per 50 passengers should be included. This means that an extra 5 seats should be included in the fuselage layout to accommodate for these flight attendants.

Layout of Doors, Emergency Exits and Windows

Transport aircraft generally have three types of doors or exits: Passenger access doors, service access doors and emergency exits. The passenger access doors are usually located at the port side (left hand side) of the aircraft, whereas the service access doors are usually located at the starboard side of the aircraft. In total three passengers access doors are provided on the MoM-liner: One in the front of the aircraft and two in between the front and the rear wing. This will allow for a much faster passenger disembarkation time, and thus turnaround time, of the aircraft.

The number and size of emergency exits are defined in CS-25 807-813. It defines five types of emergency exits [20]:

1. **Type I:** This type is a floor level exit with a rectangular opening of not less than 61 cm (24 inches) wide by 1.22 m (48 inches) high, with corner radii not greater than one-third the width of the exit.

2. **Type II:** This type is a rectangular opening of not less than 51 cm (20 inches) wide by 1.12 m (44 inches) high, with corner radii not greater than one-third the width of the exit. Type II exits must be floor level exits unless located over the wing, in which case they may not have a step-up inside the airplane of more than 25 cm (10 inches) nor a step-down outside the airplane of more than 43 cm (17inches).

3. **Type III:** This type is a rectangular opening of not less than 51 cm (20 inches) wide by 91 cm (36 inches) high, with corner radii not greater than one-third the width of the exit, and with a step-up inside the airplane of not more than 51 cm (20 inches). If the exit is located over the wing, the step-down outside the airplane may not exceed 69 cm (27 inches).

4. **Type IV:** This type is a rectangular opening of not less than 48 cm (19 inches) wide by 66 cm (26 inches) high, with corner radii not greater than one-third the width of the exit, located over the wing, with a step-up inside the airplane of not more than 74 cm (29 inches) and a step-down outside the airplane of not more than 91 cm (36 inches).

5. **Type A:** This type is a floor level exit with a rectangular opening of not less than 1.07 m (42 inches) wide by 1·83 m (72 inches) high with corner radii not greater than one-sixth of the width of the exit.

CS-25 states that an aircraft with a passenger seating configuration of 140 to 179 passengers (not including cabin crew seats) needs at least two type I and two type III emergency exits at each side of the fuselage. Additional emergency exits are required if the passenger seating configuration is greater than 179 seats. Since the Prandtl plane configuration of the MoM-liner allows for a third passenger access door, which also acts as an emergency exit, the extra two type III emergency exit are deemed redundant in the emergency evacuation of passengers from the aircraft. This means that the MoM-liner will have in total three large emergency exits on each side of the aircraft. If these exits prove to be insufficient in the emergency evacuation of passengers, extra Type III over wing emergency exits can be added to the fuselage.

The window spacing of aircraft is determined by the frame spacing of the fuselage structure. The MoM-liner fuselage has a frame spacing of 0.5m. Using this frame spacing and the length of the cabin, a total of 40 windows are fitted at each side of the fuselage.

Galley and Lavatory Layout

Galley and lavatory layouts are determined by looking at reference aircraft [72]. Galleys come in different shapes and sizes. In the MoM-liner, two large galleys will be installed, of which one will be placed in the front of the aircraft and one near the aft doors. This will allow for an efficient distribution of food and drinks. Considering lavatories, on average the reference aircraft had one lavatory per 50 passengers. Using this as a reference, the MoM-liner will have a total of five lavatories.

Layout of Cargo and Baggage Holds

The MoM-liner will have two large cargo holds in the belly of the aircraft, separated by the landing gear stowage area in the middle section of the fuselage. The cargo access doors of both cargo holds are located away from the center of gravity of the aircraft, as this will allow the cargo to be loaded close to the aircraft center of gravity. This will prevent the airplane from tipping over during loading. The cargo access doors are sized such that they allow for quick loading and unloading of LD-1, LD-2 and LD-8 standard air cargo containers.

Inspection, Maintenance and Servicing Considerations

In order to make the inspection and maintenance, as well as the servicing time of the MoM-liner as quick as possible. It is essential that these access holes are easily accessible for ground crew. Also the location of the service doors is an important aspect to consider, as servicing vehicles must not interfere with objects protruding from the fuselage [72].

Passenger Comfort

One of the requirements for the MoM-liner is that it shall have passenger comfort levels comparable to the Airbus 350 and Boeing 787. The passenger comfort level of an aircraft can be measured in matters like seat pitch/width, cabin pressure, cabin humidity, lavatory access, overhead bin space and internal noise. The Boeing 787 and Airbus 350 are more comfortable than other aircraft in their class for a couple of reasons: First of all, the cabin altitude in these aircraft is significantly lower than their rivals, which reduces passenger fatigue. Also, the aircraft environmental control system is not bleed air fed. Instead, it takes its air from ram air ducts. The air is then subsequently compressed by electrical compressors. This way, the air retains more moisture, which keeps passengers from getting dry mouths or eyes[1]. Finally, both aircraft have significantly larger windows, which creates a lighter cabin environment.

The high pressure differential in the Boeing 787 and Airbus 350 is achieved by using a composite fuselage structure. This is because the composite fuselage structure is not susceptible to fatigue[2]. As there is a minimum skin thickness requirement when using composites as a fuselage structure, composites were deemed to be not viable in the design of the MoM-liner subsection 8.2.7. This means that the MoM-liner will not have a comparable cabin pressure as in the Boeing 787 and Airbus 350. The same is true for the larger windows on these aircraft: They are also only used in composite fuselage aircraft. However, the MoM-liner will have a similar environmental control system as the Boeing 787 and Airbus 350, adding to the passenger comfort. Also, the current seating configuration shown for the MoM-liner is in high density configuration. Individual MoM-liner operators can choose to increase their passenger

[1] URL `https://www.boeing.com/commercial/aeromagazine/articles/qtr_4_07/article_02_1.html` [cited 22 June 2018]
[2] URL `http://www.boeing.com/commercial/787/by-design//advanced-composite-use` [cited 22 June 2018]

comfort by choosing a more spacious seating configuration. Finally, the MoM-liner fuselage allows for a high aisle height, plenty of headroom and large overhead compartments. A total of five lavatories can be found in the high density configuration, distributed over the whole fuselage to make it easily reachable for all passengers on board. A large galley can be found at the back of the fuselage. An additional smaller galley can be found forward in the fuselage increasing overall comfort level of the passengers on long flights as more food can be stored.

The high density configuration uses a seat pitch of 28 inches. However, airlines can use the cabin to their own liking. In Table 12.19 multiple larger seat pitches can be found together with their respective passenger limit as constrained by the cabin dimensions. The Boeing 787 is commonly used with a seat pitch of 31 inches in high density configuration, and the Airbus A350 has a 32 inch seat pitch for full economy configurations. As can be seen this would lead to a passenger level of 216 and 198 respectively. Whether the cabin is to be used as such, is up to the costumer to decide. The 32 inch configuration leaves room for an additional row when the layout it tweaked, leading up to 204 passengers, as all seat location patterns are calculated from the same starting location.

Table 12.19: Seat pitch comparison

Seat Pitch [inch]	Passengers
28	234
29	222
30	216
31	210
32	198/204

12.11. Ground Handling and Operations

Wing span forms a critical parameter of the external dimensions of an aircraft when looking at ground operations. Aiming to replace the B757 the MoM-liner must be able to reach a sufficient amount of airports. The B757 is able to land on category D airports[3]. A maximum wingspan of 52 meters enables the MoM-liner to accesses and operate on similar airports.

The ground operations that are performed once the airport is reached include (but are not limited to) (de)boarding, cleaning, fuelling, cargo (un)loading, maintenance. This must all be done properly, but to decrease the turn-around time and with that increasing the turn-over of a single aircraft in a given time limit the time usage must be as low as possible. Important factors for this are the placement of both cargo and passenger doors, reach-ability of components such as engines for inspection, and location(s) of fuel storage. This low turn-around time improves the usability for low-cost carriers, which is one of the target markets of the MoM-liner.

Fuel being stored in the wings and fuselage is very common for conventional aircraft and thus no additional equipment will need to be adopted, this thus leads to no inconvenience with regards to the turn-around time. Refueling can be done as long as the refueling valves are not placed on the top end of the wings, this holds especially for the back wing as this is relatively more elevated from the ground, thus keeping the valve easy to reach for refueling services.

Besides this passenger (de)boarding and cargo (un)loading need to be taken into account. A total of six passenger doors are placed along the fuselage, which should be adequate for fast de-/boarding. Usually only the front door is used during boarding, but due to easy accessible doors on the MoM-liner multiple boarding stair could be used to speed up boarding. The driving requirements for doors are safety regulations, and in particular the exit limit. The locations of these doors are such that they are distributed throughout the whole aircraft so that all passengers can safely leave. Also it has been taken into account that during ground operations trash needs to leave the aircraft and food needs to be stored into the galleys. To keep turnaround time to a minimum the galleys in the high density configuration are located near the forward and aft passenger doors. To store and unload cargo two cargo bulk doors are implemented. This MoM-liner does not have a wing in the center of the fuselage, that splits up the cargo hold. This is beneficial for loading time, as the cargo hold can be loaded from both the front and the back.

[3] URL `https://www.skybrary.aero/index.php/ICAO_Aerodrome_Reference_Code` [cited 22 May 2018]

13
Sensitivity Analysis

This chapter presents several sensitivity analysis to look at which parameters affect the design the most. In section 13.1 a sensitivity analysis is performed on the take-off weight on the basis of a set of parameters. Then in section 13.2 a sensitivity analysis is performed on the parameters within the aerodynamics section, mainly the wing placement is addressed here. Furthermore a sensitivity analysis has been performed on both the fuselage - and the wing structure in section 13.3 and section 13.4 respectively. Also a sensitivity analysis on the engine sizing has been included in section 13.5.

13.1. MTOW Sensitivity Analysis

A thorough analysis of the design parameters has to be performed, this can create more awareness about the driving design parameters. Furthermore, the effect of pessimistic or optimistic parameter selection can be pinpointed and addressed. Also this will allow an understanding of the effect of certain requirements on a more quantitative level. The take-off weight and its interaction with certain parameters will be observed and tabulated for every configuration. The parameters that will be observed are:

- $\frac{\partial W_{TO}}{\partial W_{PL}}$ which looks at the effect of a changes in payload on the take-off weight, such as a change in passengers taken on board or other payload services.
- $\frac{\partial W_{TO}}{\partial W_E}$ which looks at the empty weight and its relation to the take-off weight. What does a change in material, or a potentially lighter structure do to the take-off weight. This could indicate that a potential higher resource allocation has to be given to research into material usage in the aircraft.
- $\frac{\partial W_{TO}}{\partial W_R}$ which looks at the effect of the 5,000 NM range requirement. What happens when the required range is reduced, potentially a range reduction creates much more potential without limiting the aircraft purpose too much.
- $\frac{\partial W_{TO}}{\partial W_{c_j}}$ which looks at the specific fuel consumption and therefore the engine efficiency. This can provide information on if the requirements can be met by using older engines, or that the newest generation engines are required, or provide a lot more product potential in later detailed design.
- $\frac{\partial W_{TO}}{\partial W_{\frac{L}{D}}}$ which looks at the aerodynamic characteristics of the design. This parameter is also closely related to the range, since over long ranges you would like this to be as high as possible.

The sensitivity analysis is meaningful to perform, to find and re-evaluate bottlenecks before performing a detailed design. This way one can mitigate before something becomes a serious bottleneck in the design. Therefore, a sensitivity analysis on the above mentioned parameters has been performed. This is done by simply adding 30% to a certain parameter (such as W_{PL}), then calculating the percentage difference in take-off weight. In Table 13.1 the growth factors for the above mentioned parameters are provided.

Table 13.1: Growth Factor for 30% Mutation of Specified Parameters

Growth Factor Type	30% Mutation
Payload	11%
OEW	9%
Range	12%
SFC	14%
$(\frac{L}{D})_{cruise}$	-9%

The sensitivity analysis shows clearly that the MTOW is most sensitive to the range and the SFC. This was already established in the midterm report [4] and therefore the range was already decreased to 5,000 NM. For the final design, since the SFC has such a high impact, should be as low as possible, to obtain an optimal reduction in MTOW, which is done by shaping the engines based on historical trends in chapter 10. Finally, the $(\frac{L}{D})_{cruise}$ still has a significant effect on the MTOW. The box wing is well known to reduce drag and therefore optimize the $\frac{L}{D}$, therefore this sensitivity parameter is also taken into account during the design.

13.2. Aerodynamic Sensitivity Analysis

In order to be able to make well informed engineering decisions it is required to know how the design choices made propagate into the performance of the system.

In the aerodynamic analysis it is interesting to look at what effect the wing placement has on the convergence of the module. To test this the aft wing was placed at approximately 50 meters from the front wing at an angle of 10 degrees behind it. This yielded the convergence plot as shown in Figure 13.1.

The plot is on a steep incline to a taper ratio of 0.15, but stops at 0.15 due to a constraint put on the taper for structural reasons. Without the constraint, the optimizer would continue to a taper of 0. It can clearly be seen that in that instance the lift induced drag is a lot smaller than the drag caused by the size of the strut; the optimizer therefore tries to get rid of the strut. However this does not yield any information about the effect of the wing placement. By disabling the part of the code that adds the strut drag this effect will be removed. The module is run again and now yields a completely different convergence as show in Figure 13.2a.

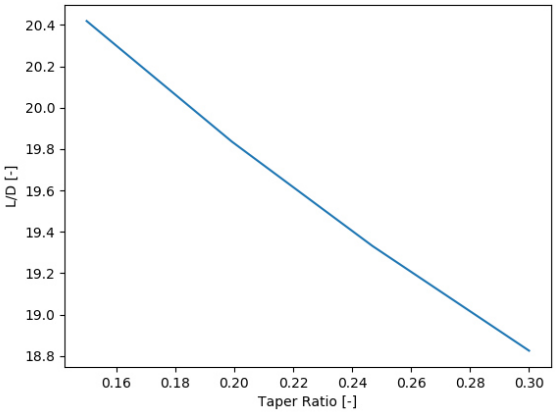

Figure 13.1: Convergence with Strut Drag, and Separation of 50 Meters

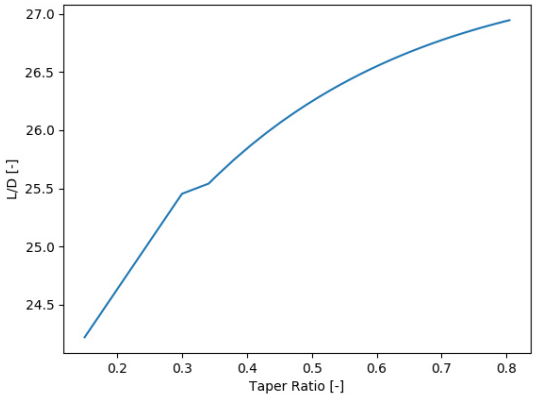

(a) Convergence without Strut Drag, and Separation of 50 Meters

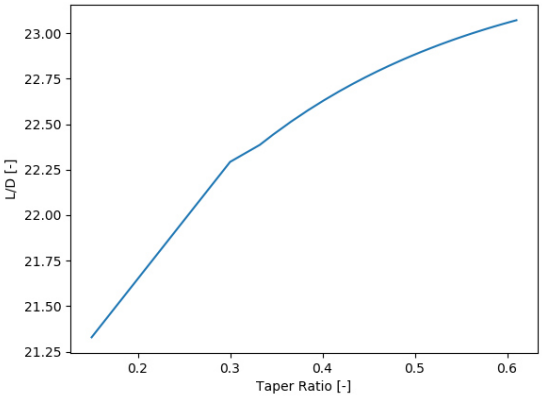

(b) Convergence without Strut Drag, and Separation of 4 Meters

Here the optimizer finds an optimum at a taper of 0.8.

This might seem high as usually the optimal taper for unswept wings lies at 0.4 [73]. However, for simplicity reasons it was assumed that the taper ratio of both wings would be the same. Torenbeek formulated Equation 13.1 to predict the optimal taper based on sweep [26]. For the aft wing a taper of 1.476 is predicted and for the forward swept wing a taper of 0.137 is predicted. The optimizer tries to find an optimum in the middle of these two values.

$$\lambda_{opt} = 0.45 \cdot e^{-0.036\lambda_{c1/4}} \tag{13.1}$$

In Figure 13.2b the wings are placed really close to each other at a distance of 4 meter with a 60 degree angle between the two. The optimizer clearly settles on a lower taper ratio at this point. The interference between the

wings does indeed have an effect on the effectiveness of the wings. When the wings are placed at a sufficiently large distance they practically become independent, and thus the attainable L/D is a lot higher; in reality these structures would never be feasible. Furthermore, the vlm is probably not able to simulate the the wake interference with the highest accuracy, introducing some error in the L/D values it obtains and therefore also the taper ratio it obtains. According to literature the reduction in lift induced drag can be modeled with a relation between the separation of the wings. Prandtl predicts a ratio of induced drag over the reference drag with Equation 13.2 [74]. Whereas a more recent study by Rizzo found Equation 13.3 by the use of CFD [75]. With a span of 40 and a separation of 50 meters between the wings Equation 13.2 yields $\frac{D_{i,box}}{D_{i,ref}} = 0.343$ and Equation 13.3 yields $\frac{D_{i,box}}{D_{i,ref}} = 0.510$. When comparing the results obtained for the par placed wings to a reference wing this yields a value of 0.405 which is almost directly in the middle of the values predicted by Prandtl and Rizzo. The predictions are for ideally loaded wings, and in the current configuration the wings are not ideally loaded. It is however clear that a lathe separation is advantageous and that the results obtained form the vlm method do follow the predictions from literature.

$$\frac{D_{i,box}}{D_{i,ref}} = \frac{1 + 0.45\frac{h}{b}}{1.04 + 2.81\frac{h}{b}} \tag{13.2}$$

$$\frac{D_{i,box}}{D_{i,ref}} = \frac{.44 + 0.9594\frac{h}{b}}{0.44 + 2.219\frac{h}{b}} \tag{13.3}$$

13.3. Sensitivity Analysis of the Fuselage Structure

To test what the effect of slight changes in input parameters would be, a sensitivity analysis is performed. This analysis is set up with the use Figure 8.9. It can be seen that the main input parameters in the optimization of the fuselage are (1) user defined geometry, (2) material properties and (3) the loads acting on the aircraft. It is therefore chosen to alter these inputs and see what the effect on the fuselage weight would be. The result of this analysis is presented in Table 13.2. In this table it can be seen what the effect on the structural fuselage weight would be when a certain parameter is increased/decreased by 25%.

Table 13.2: Sensitivity analysis on the fuselage structure. Showing the percentage change in structural weight when implementing a ±25% change in input parameter.

		+25%	**-25%**
User Defined Geometry	Stringer Spacing	+11.27%	-6.3%
	Frame Spacing	+4.0%	-3.2%
	Stringer Geometry	+1.6%	-0.9%
	y Distance Floor	-2.5%	+1.1%
Loads	Lift Front Wing	+22.3%	-21.7%
	Lift Back Wing	+4.3%	-1.1%
	Pressure Difference	+4.2%	-1.2%
	Load Factor	+16.9%	-14.8%
Material Properties	Young's Modulus	-4.4%	+3.5%
	Poisson Ratio	-1.4%	+0.06%
	Yield Stress	-18.8%	+14.7

Using the results in Table 13.2 a approach for further analysis can be set up. From the sensitivity analysis it can be concluded which parameters have the largest influence on the design, and which parameters are driving. It can be concluded that the following parameters are driving: stringer spacing, lift force of front wing and yield stress. The load factor is a factor that can actually be disregarded as this is directly correlated with the lift force of the front wing. Including this parameters would yield multicollinearity. For the three other parameters the following can be noted:

- **Stringer spacing**: as the stringer spacing is increased, yielding less stringers throughout the cross section, the total weight increases significantly. This is because each stringers will yield a larger area. However decreasing the stringer spacing will slightly decrease the weight. For future research the stringer spacing is a parameter which should be considered to find an optimum.
- **Lift force of front wing:** the reason that this factor is of large influence is mainly because of the fact that a change in lift force generates a large change in moment diagram. It is very important that resources are put on the exact computations of these moment and shear diagrams because of their sensitivity.

- **Yield stress:** the yield stress is the material property that is highly sensitive: an increase in maximum yield stress of 25% decreases the structural weight with almost 19%. Efforts should be put into material research to test whether a material with larger yield stress would be possible.

13.4. Wing Box Sensitivity Analysis

The impact of modifying user inputs to the wing structure optimization was assessed to compute the sensitivity of the system. The user inputs were increased by 25% and the percentage increase in wing structural weight of each wing computed. The parameters that were investigated are presented in Table 13.3.

Table 13.3: Table Indicating the Change in Wing Weight as a Result of a 25% Increase in Input Factors

Factor Changed	Front Wing Weight Change [%]	Rear Wing Weight Change [%]	Total Wing Weight Change [%]
Aerodynamic Loads	+23.6	+16.6	+21.3
Stringer Dimensions	+4.7	+10.1	+6.4
Stringer Thickness	-0.0	+0.5	+0.2
Spar Thickness	+6.54	+7.3	+6.8
E-modulus	-10.7	-7.5	-9.6

The sensitivity analysis gives a good idea of what factors are most influential as far as wing weight is concerned helping to guide future research and optimization. From Table 13.3 some conclusions can be drawn.

It can be seen that the aerodynamic loads have the most significant impact on the wing weight. This is logical as the loads directly influence the shear and bending moment distribution on the wings and therefore the stresses. The simplest way to reduce the wing loads is to reduce the aircraft weight reducing the required lift. This is a clear illustration of the snowball effect and reinforces the importance of weight saving.

The stringer dimensions have an important impact on weight of the wing. Although not as significant as the loads it does seem important. There is likely an optimum value for the size of a stringer as such it is recommended that further research be focused on optimizing this geometry.

The impact of changing the thickness of the stringers is minimal. This indicates that it is not worth dedicating further resources to optimizing this parameter.

The spar thickness also has a significant impact on the overall weight of the wings and as such, much like the stinger dimensions, it is recommended that the spar geometry be optimized in further research.

The E-modulus of the material has a significant impact on the overall mass of the material it is therefore of critical importance that resources be placed into the investigation of other materials (other than aluminum) to further improve the wing box design. While some investigation into CFRP was done only isotropic composites were considered. Further research into an isotropic composites is therefore recommended.

13.5. Engine Sizing Sensitivity Analysis

To estimate the engine size various input parameters were used, but the most important one is the SFC-cruise as it effects the total amount of fuel required for a flight. This in turn effects how strong the structure needs to be, which leads to a heavier aircraft. The SFC-cruise was calculated using the bypass ratio, as described in subsection 10.2.5. The assumption was made that a bypass ratio of 15 is obtainable, but what happens if a bypass ratio of 14 is maximum? This sensitivity analysis will show the effect of not reaching the required bypass ratio. The analysis will be performed by analyzing the difference in required fuel weight when the before mentioned bypass ratio change will be applied.
Table 13.4 shows the effect of not being able to obtain a bypass ratio of 15, but instead having a ratio of 14. A 6.67% reduction in bypass ratio results in a 1.6%. Furthermore the SFC-cruise increases by 2.4%, but this is still considered a small change. This small increases in fuel weight will be partially countered by the decreased engine weight. This shows that even if the very high bypass ratio is not reached, the aircraft will still be able to obtain a high efficiency.

Table 13.4: Engine Sizing Sensitivity Analysis

Bypass	**15**	**14**	**-6.7%**
Fuel [liters]	49,894	50,690	+1.6%
Fuel Volume	62.37	63.36	+1.6%
SFC-cruise	0.452	0.463	+2.4%

14
Aircraft Systems Analysis

14.1. Aircraft System Characteristics

This section analyzes four important systems on board of aircraft, namely the fuel system, hydraulic system, electrical system, and environmental control system.

14.1.1. Fuel System

The fuel system consists of fuel tanks, fuel pumps, fuel venting system, fuel quantity indicating system, fuel management system, fuel dumping system, and a refueling method. Furthermore, there should also be a fire extinguishing system (connected to the fuel system). The function of the fuel system is rather straightforward, providing the propulsion system with fuel to burn. When sizing the fuel system, a few design parameters have to be taken into account. These are the total volume required, the size, location and number of fuel tanks required, the number, location and required capacity of the fuel pumps and lines [76]. There are a lot of guidelines and regulations on the fuel system, since the fuel is highly combustible and thus dangerous if not placed or installed correctly. For example, fuel tanks may not be damaged in case of landing gear failure. Another example is that at the lowest point of the fuel tanks there must be a drainage system. All in all, the fuel system consists of various components, guidelines and regulations, all of which influence the systems weight [76]. A diagram indicating the configuration of the fuel system is shown in Figure 14.1a.

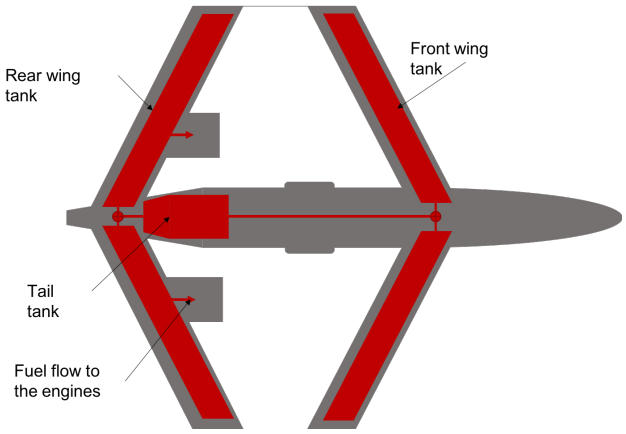

(a) Diagram Indicating the Fuel Tank Layout of the MoM-liner

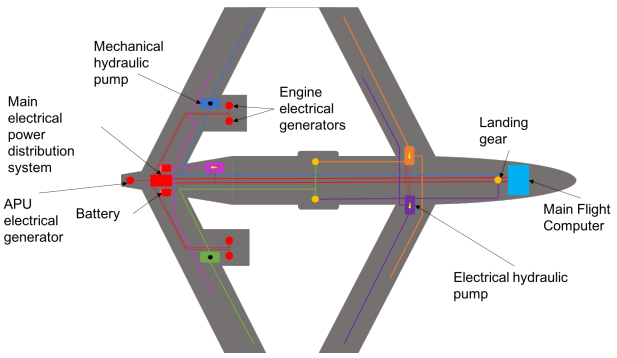

(b) Diagram Indicating the Hydraulic an Electrical System Layout of the MoM-liner

Figure 14.1: System Description

The MoM-liner will use a rather conventional fuel system where possible, i.e. five fuel tanks, one tank in each of the four wings and one in the tail cone of the fuselage. The required fuel capacity was calculated to be 62.37 m^3. This is divided across the 5 tanks as follows; 20.80 m^3 are stored in the front wing tanks, 22.80 m^3 are stored in the back wing tanks and the remaining 18.77 m^3 is stored in the tail tank as is indicated in Figure 14.1a. The fuel pumps need to be able to deliver 1.5 times the maximum fuel flow. The engines selected in section 12.6 require 9,525 kg/h (21,000 lbs/hr) of fuel per engine at maximum thrust. Based on this the design throughput of the pumps should therefore be 28,576 kg/hr. The density of aviation fuel is approximately 840 kg/m^3[1] therefore the fuel pump system must be able to deliver 34 m^3/hr. The fuel pumps themselves will not be designed at this stage.

[1] URL `https://exxonmobil.co/2MqS9Is` [cited 25 June 2018]

In addition to the fuel pumps required to deliver fuel to the engines fuel pumps will also be needed to transfer fuel between tanks to maintain stability. Only the rear wing tank is able to provide fuel to the engines directly in case of a pump failure, due to gravity. The fuel tanks should be connected so fuel can be pumped around.

14.1.2. Hydraulic System

Next, there is the hydraulic system. This system provides hydraulic power to actuators of flight controls, landing gear, and braking systems. The hydraulic system consists of a hydraulic fluid reservoir, hydraulic pumps, accumulators, lines, valves, and cockpit controls to operate it. The hydraulic system of the MoM-liner is more complex than for a conventional aircraft. The presence of two wings with engines located only on the rear wing makes a conventional hydraulic system very difficult as long hydraulic hoses would be needed in order to actuate the front wing system. Moreover, it was decided that the engines used on the MoM-liner will not accommodate bleed air meaning that an alternative system will have to be used to drive back up systems. Two mechanical hydraulic pumps will be mounted to each engine providing hydraulic power to each of the rear wings and landing gear. An additional electrical pump will be positioned at the rear of the aircraft to act as back up for the rear wing. This redundant system is similar to the system used on the Boeing 787[2]. The front wings will be serviced entirely by electric pumps only with each pump acting as back up for the other, not only powering the systems of its wing but also the key systems of the adjacent wing. The aircraft is able to function with just the control surfaces on the rear wing therefore this system has a mechanical and back up electrical system and is fully redundant whereas the font wing is reliant on electrical power to achieve hydraulic pressure. A schematic of the hydraulic loops is indicated in Figure 14.1b.

14.1.3. Electrical System

An aircraft needs electricity for almost all subsystems and in the case of the MoM-liner is reliant on electricity to run many of the control surfaces. Electrical power generation is divided into two parts: primary power generation consists of two electrical generators mounted on each engine. When the aircraft is parked and the engines are not running or in the event that the engine generators fail and auxiliary power unit (APU) will power the electrical systems. A ram-air turbine (RAT) will be installed to provide electrical power in the event that all other systems fail [76]. Batteries are installed in the aft of the fuselage to deal with surges in demand for electrical power (for instance during landing when all the hydraulic pumps will be active to deploy flaps and landing gear).The batteries also provide additional redundancy, in the event that all generators fail the aircraft will be able to function at least temporarily. A schematic of the electrical system is also presented in Figure 14.1b.

14.1.4. Environmental Control System

The environmental control system encompasses the pressurization system, pneumatic system, air-conditioning system, and oxygen system. The environmental control system is highly important as it creates a livable environment inside the aircraft without pressurization passengers will begin to develop altitude sickness above 10,000 ft (3,000 m). In addition the pressurization the environmental system must also control the humidity and scrub the air to ensure the air is clean and the oxygen content remains within tolerable levels. The environmental system is also responsible for providing high pressure air to the pneumatic systems.

The MoM-liner engines do not have bleed air systems so the aircraft will have to draw air from the free stream using ducts mounted to the fuselage. This non-bleed air system offers superior fuel efficiency, weight, and maintainability[3] [77]. The non-bleed air system may also go some way to allaying the health concerns of some passengers regarding the quality of cabin air produced by bleed air systems [78]. In the event of a loss of cabin pressure the MoM-liner is required to have emergency chemical oxygen generator to allow the aircraft to descend to a safe altitude. These systems will be installed above the seats.

[2]URL https://www.boeing.com/commercial/aeromagazine/articles/qtr_4_07/article_02_3.html [cited 20 June 2018]
[3]URL https://www.upinthesky.nl/2017/11/15/bleed-air-versus-boeing-787-dreamliner-hoe-werkt-het/ [cited 18 May 2018]

14.2. Communication Flow Diagram

A communication flow diagram was created to visualize the flow of information between systems. This diagram, presented in Figure 14.2, indicates the flow of both information and commands between the various sensors, actuators and individuals within the aircraft system and its environment beyond the cockpit (OOC). Figure 14.2 shows that the majority of information flows directly to the pilot (or autopilot when active) as the central unit. The pilot then processes the information and translates these into commands for the rest of the system.

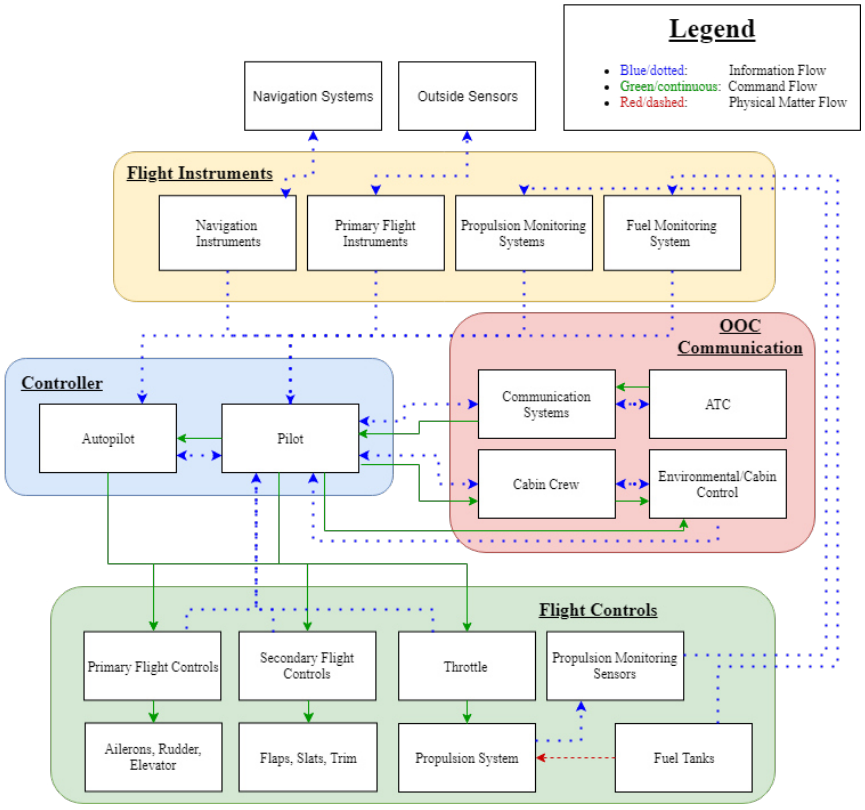

Figure 14.2: Communication Flow Diagram

Figure 14.2 shows the communication flow between different aircraft components, below a few of these flows are described in more detail.

Autopilot: The autopilot receives information from the flight instruments, it then processes this information and decides how to control the aircraft, this leads to an input for the flight controls. The autopilot can be manipulated by the pilot as well, leading to an input from the pilot for the autopilot. Information that can be communicated here is for example: heading, altitude and speed as well as approach, RNAV and VNAV autopilot modes.

Flight Instruments: The flight instruments receive their information from outside sensors and the navigation systems. These consist of a barometer, pitot tube, compass a GPS system and more. The propulsion monitoring system and fuel tanks also provide inputs for the flight instruments, for example the power setting or amount of fuel left. This information is then processed and the resulting outputs are used by the pilot and autopilot system as inputs. The information processed by this system consists of the heading, altitude, attitude, speed, vertical speed, longitude/latitude and more.

Communication Systems: The communication system is used to convey messages between the pilot and ATC. The pilot receives an input, in the form of an instruction from ATC, and generates in output stating the pilot will comply and execute the instruction. Information that can be communicated are for example: altitude change, speed change and heading change. Also if the aircraft experiences an emergency, the communication system becomes a very important system used to describe the emergency, and might even be used to help solve the issue.

14.3. Hardware & Software Block Diagram

The aircraft system contains a large amount of hardware and software. It is important to identify and understand the building blocks of the system and their interactions. This can assist understanding the system better and identifying possible mistakes moving towards product roll-out. For the hardware and software analysis eight sub-divisions have been made for: the cockpit system, the wing system, the aircraft exterior, the landing gear, the electrical power system, the cabin system and the engine system. Guidelines for component functioning and what is consists off has been obtained from Roskamp [76]. The hardware & software block diagram can be found in Figure 14.3.

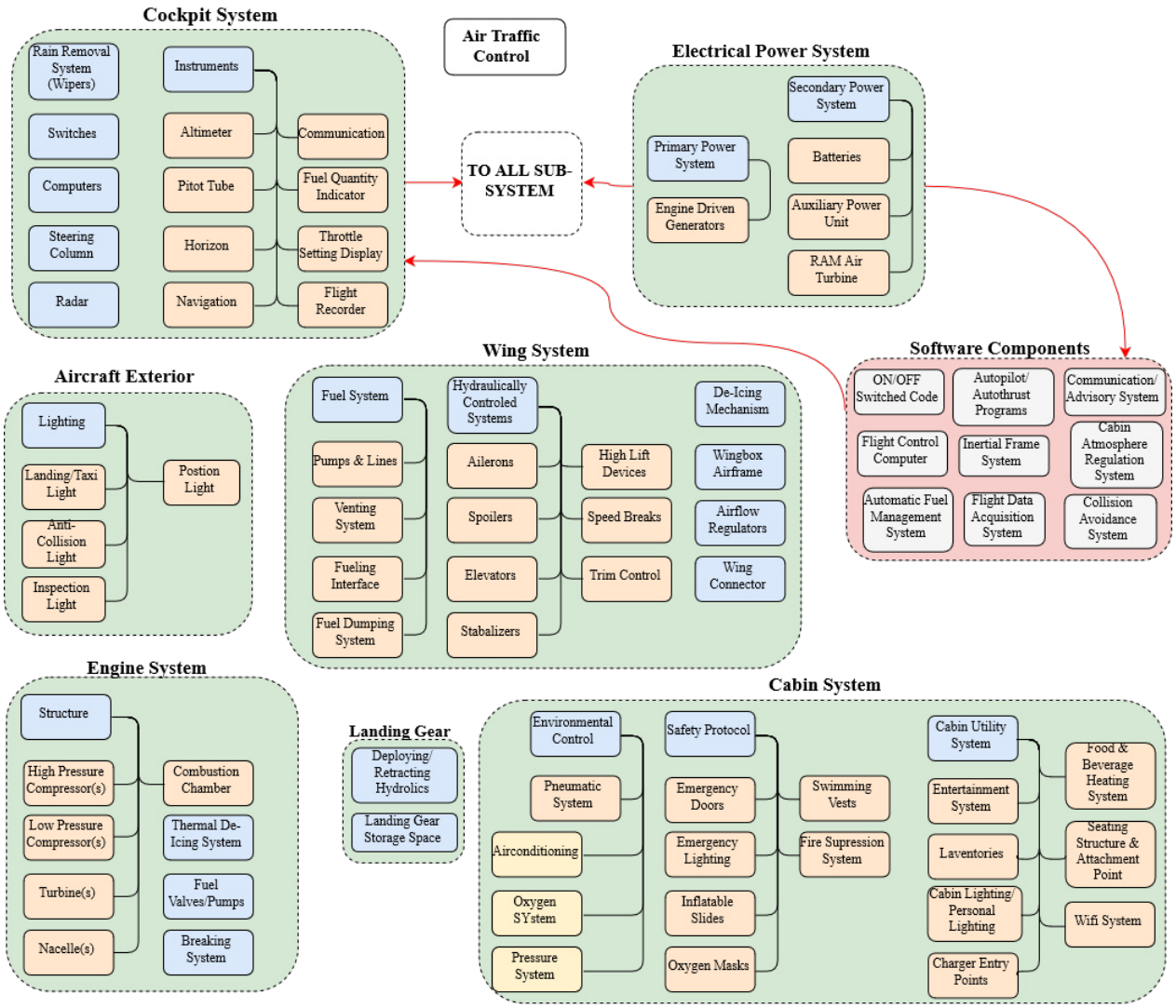

Figure 14.3: Hardware & Software Identification and Correlations

14.4. Electric Block Diagram

The section presents the electrical components within the aircraft system in the format of an electric block diagram. A precise circuit cannot be determined yet, therefore this will be a more global model of the circuit. The primary circuit components have been included such as: the conversion devices, the protection devices, the generator dependent processes represented in the avionics- and primary bus, the non-generator dependent services and the initiation sequence. These components have been presented in Figure 14.4.

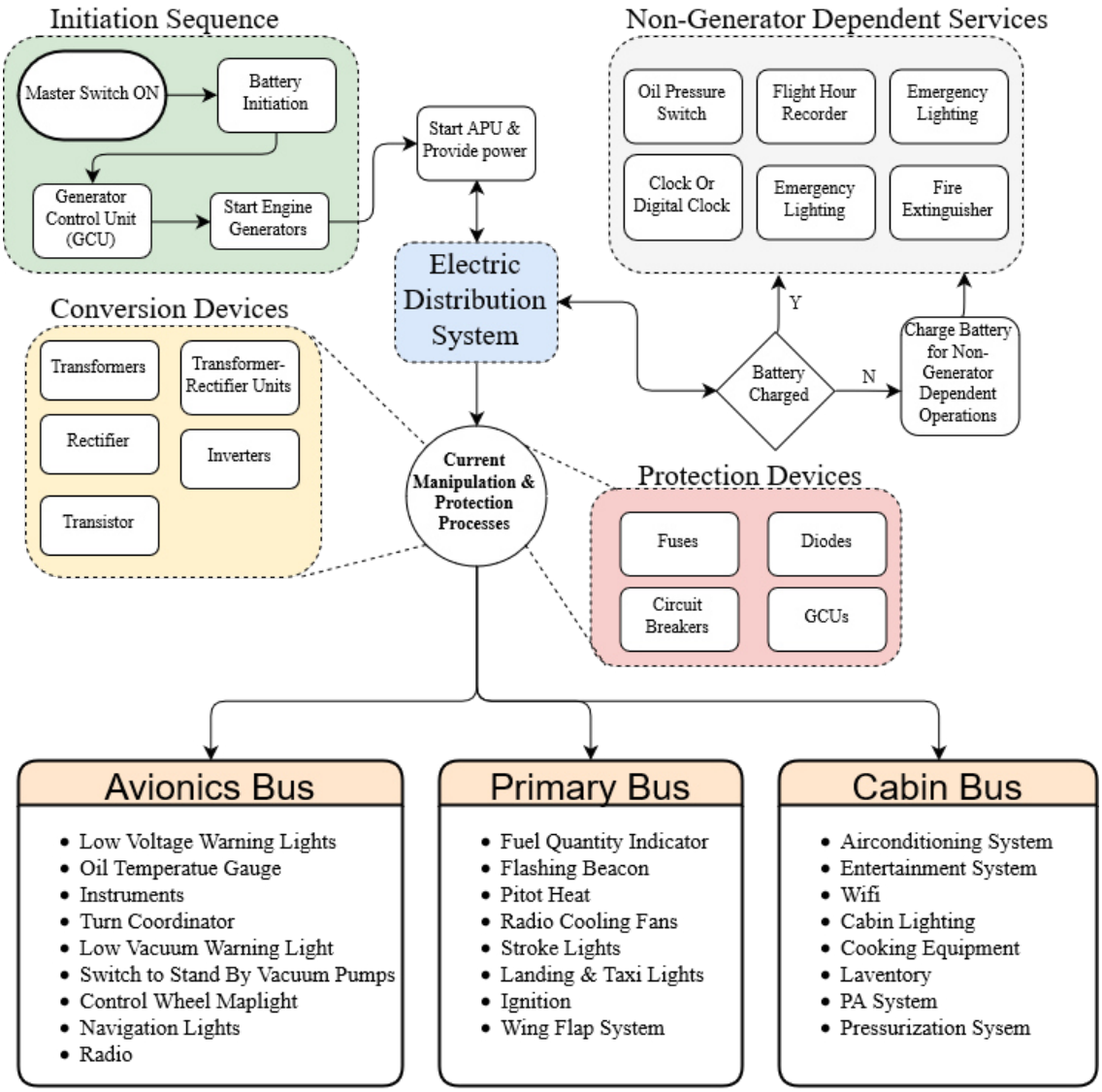

Figure 14.4: Electric Block Diagram

14.5. Data Handling Diagram

This section presents all the components that allow for on board data processing within the aircraft system. The main components of the data handling system are the buses, which can be sub-divided into three types: address buses, data buses and control buses. Address buses specify the location in the memory a specific piece of data gets assigned. The data bus is the main data source which transfers data and thus stores major part of the data handling software needed to convert equipment readings into meaningful data. Which is done by using the processing power of the CPU. Finally the control buses provide timing and control signals running through the system, therefore these also play a major role in the aircraft system, since these buses allow for operator inputs to be processed. The global overview of the data handling has been presented in a block diagram in Figure 14.5.

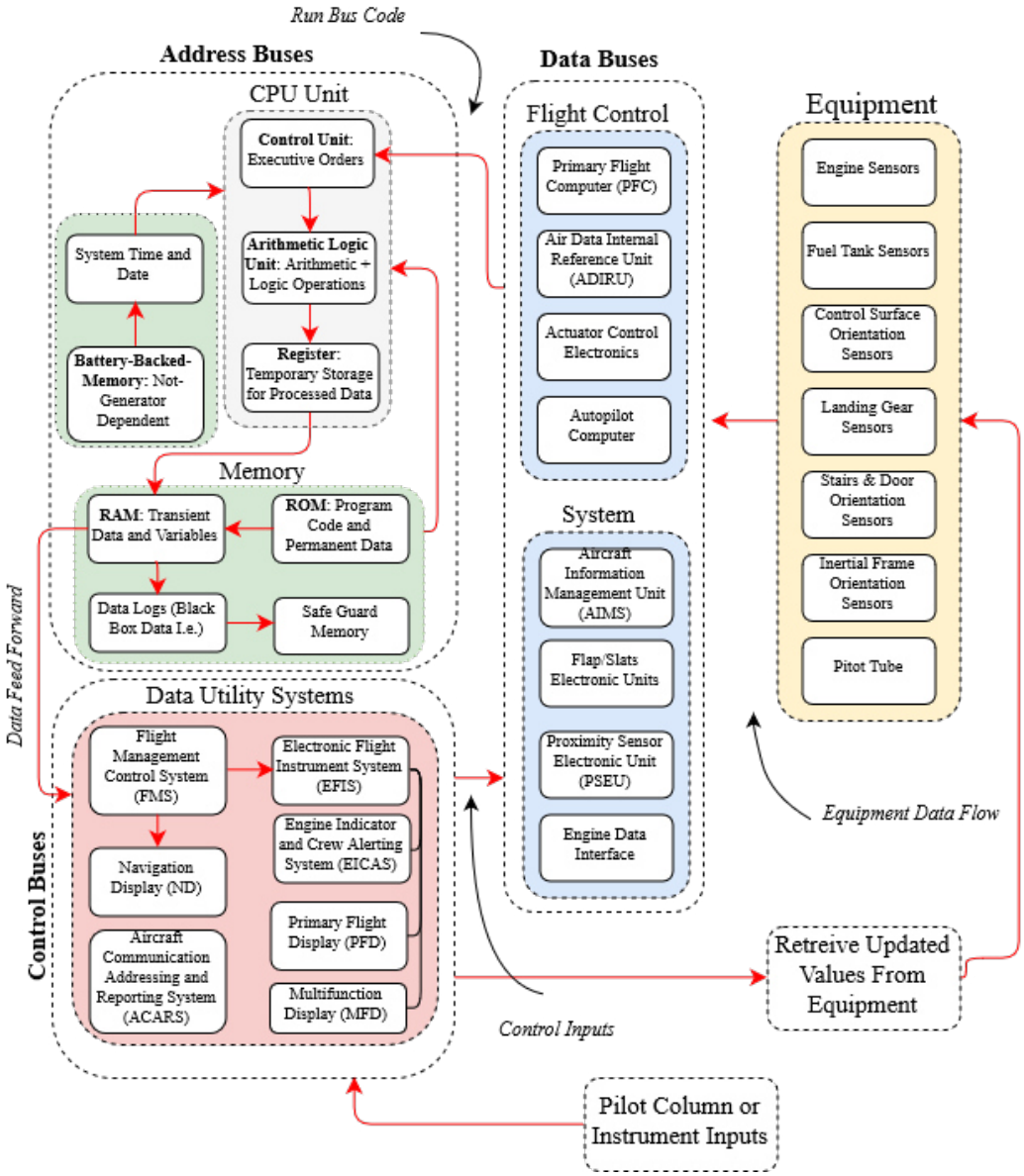

Figure 14.5: Data Handling Block Diagram

Data Buses Description

Primary Flight Computer (PFC): contains the information system to allow the aircraft to perform fly-by-wire operations. It allows for controlling elevators, rudder, ailerons, flaperon, spoiler and horizontal stabilizers [79].

Air Data Reference Unit (ADIRU): is used to measure the pitot airspeed and barometric altitude in fixed wing aircraft. The information obtained from the air data reference unit can be used for the navigation systems, and will be providing information to pilot instruments[4].

Actuator Control Electronics: provides the ability to control the actuators from the control buses. When the pilot provides inputs from the data utility buses, this will pass through the address buses and physically update the aircraft control surfaces orientation.

Autopilot Computer: bulks data such as airspeed, orientation, navigation such that the pilot can initiate fly-by-wire for hands free flight.

Aircraft Information Management Unit (AIMS): integrates several functions, such as managing data displayed in the cockpit, providing a thrust management system, monitors the aircraft condition and manages datalink for communication[5].

Flaps/Slats Electron Units: automatic measuring system which provides flaps and slats control for variable flight conditions. For example flaps will be automatically retracted when velocity for flap extension level is exceeded[6].

Proximity Sensor Electronic Unit (PSEU): the PSEU receives a bulk of signals from e.g. flaps settings, orientation of the gears and orientation of the doors. These received signals, by use of the PSEU, get transformed into warning signals for: landing and take-off configurations, stairs and door and landing gear position[7].

Engine Data Interface: Provides all data with regards to the engines, such as quantity, heat, fuel flow, etc.

Control Buses

Aircraft Communication Addressing and Reporting System (ACARS): is a digital link system which allows transmissions between the aircraft and the ground, such as route clearance and landing clearance, which is communicated with ATC. Also Aeronautical Operational Control (AOC) and Airline Administrative Control (AAC) is possible, which entails for example weather updates, aircraft ETA, technical performance data and load and trim sheets[8].

Electronic Flight Instrument System (EFIS): is an instrument that can be found on the flight deck and generally contains a primary flight display (PFD), a Multifunction Display (MFD) and an Engine Indicator and Crew Alerting System (EICAS). The EFIS is simply an information platform for the pilots, however also allows for inserting control, often in larger aircraft the EFIS contains data processors[9].

Flight Management Control System: The FMS uses sensors such as GPS, to determine the position of the aircraft. Using gathered data, the aircraft follows the plotted course and then sends information the EFIS and Navigation Display (ND)[10].

[4] URL https://www.advancednavigation.com.au/sites/advancednavigation.com.au/files/Air20Data20Unit20Reference20Manual.pdf [cited 19 June 2018]

[5] URL https://aerospace.honeywell.com/en/products/cockpit-systems/airplane-information-management-system [cited 19 June 2018]

[6] URL http://www.b737.org.uk/flightcontrols.htm [cited 19 June 2018]

[7] URL hhttp://www.industrial-electronics.com/aircraft_9.html [cited 19 June 2018]

[8] URL https://www.skybrary.aero/index.php/Aircraft_Communications,_Addressing_and_Reporting_System [cited 19 June 2018]

[9] URL https://www.skybrary.aero/index.php/Electronic_Flight_Instrument_System [cited 19 June 2018]

[10] URL http://www.davi.ws/avionics/TheAvionicsHandbook_Cap_15.pdf [cited 19 June 2018]

15
Risk Assessment

Technical risk assessment is the activity of identifying and ranking technical risks that may occur in the development of the system or product, with the consequence that technical performance, schedule or cost requirements are not met. Elements, characteristics, technologies or conditions are identified that may form a risk, the probability that they occur is estimated and the consequence for the success of the mission of the system, if the risk occurs, is assessed. The risks are plotted in a risk map, which shows on one axis the probability of occurrence and on the other the consequence. For the highest ranked risks (high probability and consequence combination) measures, in terms of alternative design or additional development activities, are identified to decrease the risk (risk mitigation)[1].
Identifying and ranking technical risks is an important step in mitigating potential risks and assuring that the system meets all requirements. Previously, research of the technical risks regarding the MoM-liner project was done in the Baseline report [3] and this was then changed accordingly in the Midterm report [4]. In this chapter, a log can be found with all changes regarding this technical risk assessment and an updated mitigated risk map is provided.

15.1. Main Risks

The Prandtl plane has a couple of components that are inherently more risky than they would be on a conventional aircraft. Some of the main risks of the Prandtl plane will be discussed. This section covers the main risks associated with the Prandtl plane [3][4].

Electrical Failure
The Prandtl plane relies on a lot of electrical systems, as described in chapter 14. Considering these electrical systems will be complicated, and require a complex system to power, the chance of an electrical failure or electrical fire is higher than for a conventional aircraft. This can be mitigated by using two completely separate systems, thus making it fail safe. As well as making the entire system fire-retardant, furthermore encasing the batteries should contain an overheating battery.

Anti-/De-Icing Failure
The risk of an anti-icing system failure has been increased for the Prandtl plane as this design has two wings and thus two anti-icing systems. If the anti-icing system does not perform, ice from the first wing could eventually break off and get sucked into the turbofans. The consequence of an anti-icing failure has not changed compared to the Midterm report, and is therefore still set at marginal. The mitigation technique has not changed either, a fail safe system or regular maintenance will need to be applied to reduce risk of failure [4].

Manufacturing
There are currently no flying commercial versions of the box wing configuration, this together with the complexity of the Prandtl plane, are the reasons that manufacturing these new components will require new production facilities. It might be discovered that some components pose an unreasonable cost for production, which would have catastrophic consequences for the design as it cannot be built. Furthermore, as discussed in section 16.2, the assembly factory will be a renewable energy source powered Gigafactory. Building this factory comes with a lot of financial risk, and might therefore not be feasible.

Manufacturing Error
Manufacturing the Prandtl plane's wings come with an increased risk. This is due to the non-existing facilities for this type of wing, increasing the risk of errors in the production due to the lack of experience. The large dimensions of the wing subsystems results in splitting of the production in smaller sub-assemblies. The higher amount of

[1] URL `https://www.investopedia.com/articles/professionals/021915/risk-management-framework-rmf-overview.asp` [cited 20 June 2018]

different parts that need to be produced increases the risk of manufacturing errors. Mitigating manufacturing errors is done with quality checks throughout the whole production. Extra care needs to be taken for these quality checks to ensure the required level of precision.

Structural Failure
There are no flying Prandtl planes at this time, so there is not a lot known about potential structural failures that could occur. A way to mitigate this risk is to perform extensive flight testing, and analyze what flight hours do to the structural rigidity of the aircraft. Analyzing the material for crack propagation is a great way to examine how fast structural failure could occur.

To conclude, compared to a conventional aircraft there are some regions where the Prandtl plane has a higher risk. As there are no commercial Prandtl planes flying around currently, there is no data on which components are more prone to failure. Compared to a conventional aircraft the main increase in risk is structural failure, but this can be mitigated with an extensive flight testing program. Another risk where box wing aircraft have a disadvantage is the electrical failure and electrical fire, as the chances of these occurring are increased. However, these risks can be mitigated properly.

Additional Risk

There are some risks that do not qualify as technical risk, but they still pose a risk to the project and should therefore be discussed. These risks are much harder to mitigate, as they are intrinsic risks of doing business. Nonetheless, there are some things the MoM-liner company could do to 'semi-mitigate' these risks.

Business Risk
Business risk is the risk that less MoM-liners are sold than expected, leading to a lower profit or maybe even a loss. This is a risk that cannot be mitigated, every company doing business in a free market experiences this risk. The easiest way to reduce the consequences of business risk is to choose a capital structure with a lower debt ratio. This means the MoM-liner company can fulfill its financial obligations at all time, which is a challenge for a lot of start-up companies[2]. Business risk has a low risk, but the consequences can be severe.

Financial Risk
Building the MoM-liner Gigafactory and performing the R&D (Research and Development) required to develop the aircraft costs a lot of money, this money will need to be paid by investors. If the investors would lose faith in the company and pull money, this would be disastrous for the development of the aircraft. This is a difficult risk to mitigate, as investor sentiment cannot be influenced. The best way to ensure investors do not lose faith is to fulfill the promises made, and deliver an aircraft that meets the requirements. Financial risk is a low risk, but just like the business risk the consequences can be severe.

15.2. Risk Map

The mitigated risk map is shown in Table 15.1, it incorporates the risk mentioned in section 15.1 and risks that were already assessed in the Midterm report [4]. The non-technical risks described in section 15.1 are not shown in Table 15.1 as they are not technical, the risk and consequence of these risks has already been discussed in the corresponding section.

Table 15.1: Mitigated Technical Risk Map Final Design

	Negligible	Marginal	Critical	Catastrophic
Low		• Instrument failure • Engine failure • Pressure failure • Sensor failure • Unit conversion failure • Windshield fracture	• Electric failure • Actuator failure • Cabin fire • Landing gear failure	• Unable to manufacture • Cargo fire • Hydraulic failure • Electrical fire
Medium		• Manufacturing errors • De-icing failure		• Structural failure
High	• Overflow errors			

[2]URL `https://www.investopedia.com/terms/b/businessrisk.asp` [cited 18 June 2018]

15.3. Contingency Management

Due to uncertainties in the design process, contingency margins should be used to ensure that the final design meets the requirements. These contingency margins can be reduced as the design becomes more mature. Table 15.2 presents the contingency factors for some major design budgets at five different stages of the design process.

Table 15.2: Contingency Margins

	Mass	**Maximum Loads**	**Fuel Consumption**	**Size**
Conceptual Design	30%	30%	15%	10%
Preliminary Design	20%	20%	10%	5%
Specification	5%	5%	8%	1%
Measurements Acceptance Hardware	1%	1%	1%	0%
Measurements Flight Hardware	0%	0%	0%	0%

15.3.1. Mass Budget

Usually the conceptual design is based on statistical data of similar aircraft. In the category of medium sized aircraft there are a number of examples available which may be used for initial estimates. However, this aircraft might require more unconventional designs, which means the statistical data will be less accurate than for a conventional configuration. In the preliminary phase the component design happens. Some deviations might still happen after this phase due to a number of iterations caused by the increasingly accurate mass estimates of the components. In the specification stage the design is fixed and the weight of each component will be calculated. Some changes might need to be made after this, due to the iterative nature of the design process, a margin of 5% is an acceptable estimate. The acceptance hardware will most probably equal the flight hardware. If something does not perform adequately a minor adjustment can be made to the component, but that change should not be more that 1%. The flight hardware will equal the mass of the final assembly, no changes in the mass are expected at this stage.

15.3.2. Maximum Loads

The design loads are largely defined by regulations. The EASA CS-25 regulations stipulate load factors the aircraft should be able to withstand to operate safely. A fairly large amount can, therefore, be said about the load factors at a relatively early stage. The load factors must be multiplied with the mass of the aircraft to obtain the loads on the aircraft. The load estimate will thus become more accurate as more is known about the weight. The load contingencies hence are the same as those that were specified for weight.

15.3.3. Fuel Consumption

The engine characteristics for the Mom-liner can be scaled based on current day trends. Since the actual service roll out is not until 2035, it is a reasonable assumption efficiency will increase, for this the trends over the last decades for increased specific fuel consumption will be looked into. Since this is an expectation, after specification a 8% contingency was thus taken. This estimate becomes more and more accurate as the concept gets closer to the production version. Minimal variation is expected between the prototype and production versions in terms of fuel consumption. A margin of 1% was hence selected. Prior to engine extrapolation (in the conceptual and preliminary design phases) the fuel consumption is based on statistics from similar aircraft. The majority of modern aircraft use similar high-bypass turbofan engines, therefore the variation is still likely to be small. The values of 15% and 10% were selected for the conceptual and preliminary margin respectively. These initial contingency margins should be re-evaluated for concepts that rely on experimental engines, for instance open rotor technology.

15.3.4. Size

The size is mainly determined by the aerodynamic requirements and the capacity requirements. The sizing is predominantly done in the conceptual design phase. The size of the aircraft is thus not expected to change by a margin larger than 10% after this phase. In the preliminary phase the size is determined on a per component basis, which, even for unconventional configurations, make the sizing relatively accurate. Therefore, no major changes are expected after this phase, and a margin of 5% is thus a safe estimate. In the specification phase the sizes are mostly fixed, changing the sizes after this will severely alter your design and is thus not expected. After the acceptance hardware the sizes will not change.

15.4. Resource Allocation/ Budget Breakdown

15.4.1. Cost Breakdown

The cost of an aircraft from beginning of life to the end of life can be split into several subdivisions. The life cycle of an aircraft sees four phases which influence the cost: the design-, manufacturing-, operational- and disposal phase. Each phase has its characteristic costs. As an example, the operating cost can be sub-divided into several domains: airplane related operating costs (AROC), passenger related operating cost (PROC), cargo related operating cost (CROC) and system related operating cost (SROC). AROC can be described as the capital costs and the cash airplane related operating cost (CAROC). The capital costs can be seen as the financing, the insurance and the depreciation of the airplane, which make up about 40% of the AROC. The CAROC comprises the processes involving crew, fuel, maintenance, landing, ground handling, Gross Profit Estimation (GPE) depreciation, GPE maintenance and control & communication which makes up about 60% of the AROC [80].

Within the cost scheme one can have recurring and non-recurring cost. Non-recurring cost includes engineering processes such as systems engineering, tooling processes, such as fabrication of tools, but also flight testing and development support. Recurring cost comprises of cost involved with the making of multiple units, such as labor cost, material and manufacturing costs and production support. However, over the production of multiple units there is a learning curve, which means that due to experience in the building of a unit, less man hours are needed to produce the next unit. An overview of the cost breakdown in given in Figure 15.1.

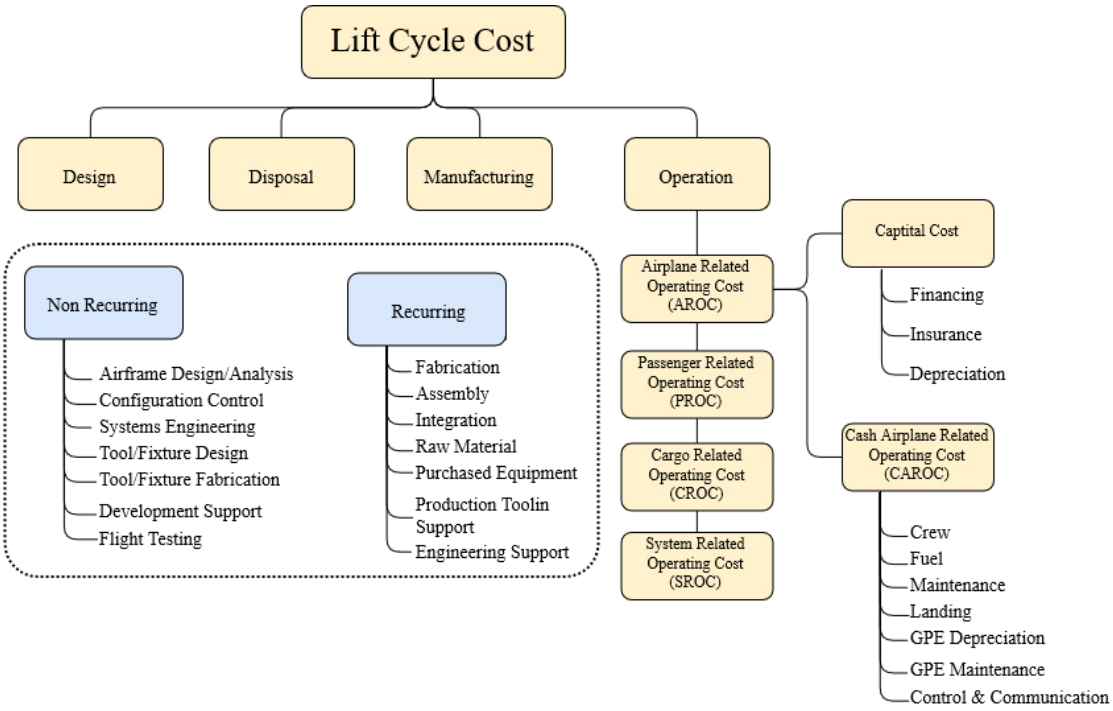

Figure 15.1: Cost Breakdown Structure

For the initial estimates established in the Baseline report [3], aircraft with similar mission profiles were selected. They were selected based on seats and range, their unit costs have been normalized for both range and seats. The least variance was observed in the cost per range for all aircraft. The initial cost estimated based on the 5,000 NM requirement yielded 202.6 MUSD. However, in communication with the client it has been decided to lower the requirement to 5,000 NM as stated in chapter 4. This 1,000 NM reduction causes the unit cost estimation to drop to about 160 MUSD. The cost analysis of the unit price and range is shown in Table 15.3 The variance in cost per seat was high. Thus, it was concluded that this is not an appropriate metric for conceptual estimations.

15.4.2. Mass Breakdown

In the initial design phase of an aircraft it is useful to generate an initial mass budget. In the preliminary design stage, the mass of an aircraft is estimated by a Class-I weight estimation. Using the results from this Class-I weight estimation, the operating empty weight (OEW) and the maximum take-off weight (MTOW) can be updated using

Table 15.3: Conceptual Unit Cost Estimate Based on Current Airliner Unit Cost [81]

Aircraft	**Cost** [MUSD]	**Range** [NM]	**Cost/NM** [MUSD]
B787-8	229.5	7,343	0.0313
B737 MAX 10	124.7	3,128	0.0398
A321neo	127.0	4,041	0.0314
B767-300ER	201.5	5,952	0.0339
A330-200	233.8	7,213	0.0324
MoM-liner	**202.6**	-	-

a Class-II weight estimation. Alternatively, even before starting the Class-I weight estimation, the OEW and MTOW can be estimated by analyzing statistical data. In the following sections, the Class-I and Class-II weight estimations will briefly be explained. Subsequently, an initial weight estimation based on statistical data will be given.

Class-I Weight Estimation

The Class-I weight estimation can be performed when some initial parameters are known, such as the mission profile of the aircraft and statistical data from comparable aircraft. First, the OEW is estimated based on statistical data. Then the drag polar is estimated. This is done by looking at the average skin friction drag coefficient for the considered aircraft type, the aspect ratio of the wing, the Oswald factor and the $\frac{S_{wet}}{S}$ of the aircraft. Using the drag polar and the mission profile of the aircraft, the fuel weight can be estimated. The estimated MTOW is then obtained by adding the calculated fuel weight to the OEW and the estimated payload weight.

Class-II Weight Estimation

For the Class-II estimation, next to the results of the Class-I method, also the main geometrical parameters of the aircraft, such as the wing surface area, taper and sweep, are required as inputs. The Class-II weight estimation then estimates the weight of individual components, such as the wing structure, based on the aircraft geometric parameters. The output of the Class-II weight estimation will again be the OEW, as well as the weight of individual components. More accurate values can subsequently be found by performing both Class-I and Class-II again using the updated values; and continuing this iterative process until the outputs of both methods converge to a sufficient degree.

Initial Weight Estimation

In order to generate a conceptual weight estimation some data was collected on similar aircraft. This data is presented in Table 15.4.

Table 15.4: Maximum Take-Off Weight and Operational Empty Weight of Comparable Aircraft

Aircraft	**MTOW** [kg]	**OEW** [kg]
Boeing 757-200 [5]	115,900	58,040
Boeing 767-200ER [5]	175,540	83,788
Airbus A310 [5]	150,000	79,666
Boeing 787-8 [11]	227,930	119,950
A321neo [10]	96,978	50,800

This data was then standardized by various parameters, such as number of passengers and range. Data on range and passenger numbers for each reference aircraft can be found in Table 3.1 and Table 3.2. This is done to check which parameter had the most significant impact on mass. It was concluded that the mass was most dependent on the passenger capacity. An average was computed and then multiplied by the MoM-liner design seat number of 234 to find a very preliminary weight estimate for the MoM-liner. The initial estimate for MTOW is 126,104 kg and 64,320 kg for OEW. A contingency margin is applied to this value as is outlined in chapter 15. With contingency margin the MTOW is 163,936 kg and an OEW of 83,616 kg. These values was then updated in the Midterm report [4] to MTOW of 169,000 kg without contingency, adding the conceptual design contingency, a MTOW of 210,000 kg is obtained.

15.5. Project Resource Monitoring

Arriving at the more detailed design phase, it is useful to check if all resources are still within predefined bounds. If they are not, mitigation strategies will have to be implemented to make sure those bounds are adhered to. In this section the mass budget, SFC budget and the cost budget monitoring and mitigation strategies will be presented.

15.5.1. Mass Budget Monitoring

The estimated mass of the eventual product is based on similar aircraft, in this case the B767-200ER, which has a maximum payload range of 3,000 NM and has about the same passenger capacity[3]. Given the lower range, yet the similar middle of the market flight profile and passenger capacity, a similar (slightly higher to account for higher range) MTOW has been used as guideline for monitoring, to make sure the mass increase is limited. The data for the actual mass with and without contingency, and the estimated mass budget is presented in Table 15.5. The graphical presentation can be found in Figure 15.2. The estimated mass has been reproduced by using the contingency margins provided in section 15.3 in reverse, to reproduce the trend of the B767-200ER design.

Table 15.5: Graph Data Mass Budget Monitoring

Project Phase	**Actual Mass Without Contingency** [kg]	**Estimated Mass** [kg]	**Actual Mass With Contingency** [kg]
Conceptual Design	163,936	146,000	213,117
Preliminary Design	169,000	158,000	202,800
DSE Conclusion	146,000	165,000	174,000
End of Project	-	190,000	-

It can be seen in Figure 15.2 that the actual mass, both with and without contingency are above the initial value for the 'produced' B767-200ER curve. This is because during the conceptual design phase the estimates were rough and not nearly accurate enough, since statistical data was used for estimation, where the box wing is not accurately presented by this regression. When going into the actual class-I and class-II estimation, the mass increased slightly. At this point the mass increase needed to be mitigated and a more accurate modelling of the box wing mass should be obtained. After contact with experts, a more accurate class-II weight estimation was established, causing the mass to converge during the DSE conclusion phase. Material choice and airframe optimization are required in the later phases to stay on goal.

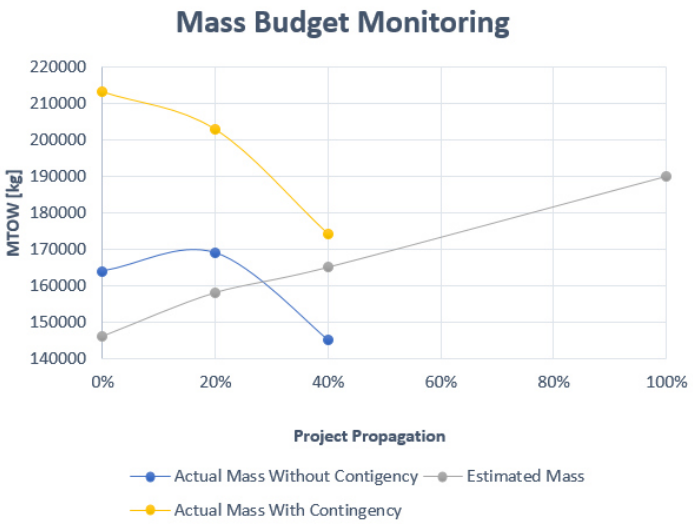

Figure 15.2: Graphical Representation of Actual Mass Figures

15.5.2. Specific Fuel Consumption Budget Monitoring

For the SFC the Trent-1000A has been used, which has a value of 0.506 lb/hr/lbf. Similar to the mass budget, the SFC has been reverse engineered with the contingency margins from section 15.3. The data is provided in Table 15.6 and the graphical representation in Figure 15.3.

[3]URL `http://www.cargojet.com/fleet/spec767-200.htm` [cited 21 June 2018]

Table 15.6: Graph Data SFC Monitoring

Project Phase	**Actual SFC Without Contingency** [lb/hr/lbf]	**Estimated SFC** [lb/hr/lbf]	**Actual SFC With Contingency** [lb/hr/lbf]
Conceptual Design	0.55	0.582	0.6325
Preliminary Design	0.56	0.557	0.616
DSE Conclusion	0.488	0.546	0.52704
End of Project	-	0.506	-

Over the conceptual and preliminary design phase this value was establish through statistics. Since efficiency is key to meeting the requirements stated in section 4.3, and the final release of the product is still far away, it was decided to size the engines based on engine trends of the last decades. By doing this, it was found that it is potentially possible to attain a SFC of 0.452 lb/hr/lbf, which would be slightly better than the Trent-1000A. Furthermore, the update of the minimum runway requirement allows for smaller engines, which will be more efficient when used in cruise. As a mitigation in the earlier phases, a client discussion was triggered to find a new runway take-off length solution, to avoid a design with disproportionate and inefficient engines in cruise.

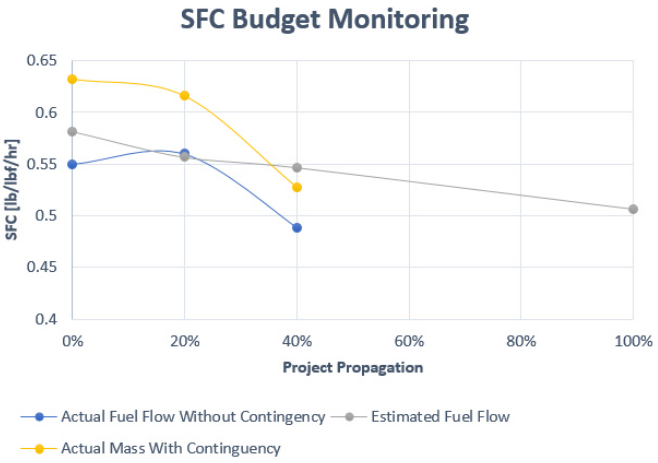

Figure 15.3: Graphical Representation of Actual SFC

15.5.3. Cost Budget Monitoring

The cost requirement is a very stringent constrain in the design process and should be monitored closely. The initial cost requirement of 100 MUSD was simply not attainable. This was discovered after going through simple statistical data. This extreme constraint was mitigated by updating the user requirement after client communication. A statistical regression showed that a unit cost of around 160 MUSD should be attainable. Table 15.7 shows the data related to Figure 15.4.

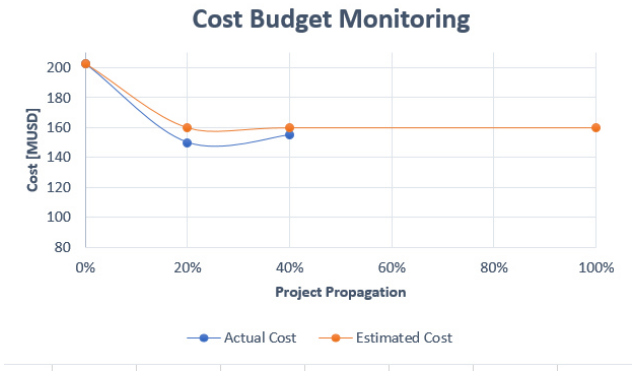

Figure 15.4: Actual Cost vs. the Estimated Cost

The overall cost is right on the goal, but proper mitigation towards the final design will have to make sure the unit cost does not shift above (at least significantly) the 160 MUSD. However, when the unit price will be higher allowing for lower operation cost, allowing for lower life cycle cost, having a higher unit price could be considered in a trade-off.

Table 15.7: Graph Data Cost Monitoring

	Actual Cost	**Estimated Cost**
Conceptual Design	202.6	202.6
Preliminary Design	150	160
DSE Conclusion	159	160
End of Project	-	160

16
Sustainable Development Strategy

Determining a single definition for sustainable manufacturing is difficult, the US Department of Commerce states the following: "The creation of manufactured products that use processes that minimize negative environmental impacts, conserve energy and natural resources, are safe for employees, communities, and consumers and are economically sound" [82]. This statement shows that sustainability combines environmental, societal and economical aspects to improve the manufacturing process on all fronts. In a world of dwindling resources, sustainability can no longer be neglected and should be seen as a mandatory part of every production process. Sustainable manufacturing is not just a catchy buzzword, it actually generates value for your company. Research has shown that companies can cut their energy bill with about 20%, with just a small investment. This equates to a 5% increase in overall profits, this should by itself be enough motivation to consider these investments [83]. Furthermore, workers value sustainability and demand a green work space [84]. Therefore, it is obvious that there are multiple benefits to having a sustainable manufacturing process, as well as having a sustainable product. It takes some effort to accomplish this, but options will be discussed in the following sections.
Figure 16.1a shows the three aspects of the manufacturing process that should be taken into account. For the MoM-liner 'Inputs' consist of material choice, 'Operations' consists of the the entire manufacturing process from raw material to finished product and 'Products' consist of the finished product and how it is sustainable as well as how the product can be recycled at end of life.

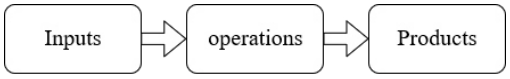

(a) Flow of Sustainability [85]

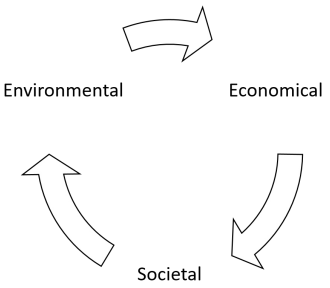

(b) Three Aspects of Sustainability [85]

16.1. Inputs

As discussed before, the input category consists of the material selection but it also consists of the part suppliers and the products they provide. First of all, material selection is very important in making the aircraft sustainable, not only economically but also environmentally. As described in chapter 8, the material that will be used is aluminum, this is a great choice in terms of sustainability. Foremost, aluminum is one of the best materials in terms of recyclability. It is one of the few suitable materials for the MoM-liner that can be classified as a true closed loop material, meaning that it can be recycled into itself and used as a raw material again. Aluminum is economical to recycle, and the infrastructure is already in place[1]. Contrary to the recycling of composites, which is still in a very early stage and probably will not be feasible in the near future. The combination of being a very recyclable material, and the infrastructure already being in place means the requirement of being 75% recyclable will be attainable, which is great as in the early design stages this seemed like a difficult requirement to meet. Current metal aircraft

[1] URL `http://www.aluminum.org/industries/production/recycling` [cited 22 June 2018]

can already be recycled up to 85% which greatly outperforms the requirement of 75% recyclable[2]. The aircraft is not completely made out of aluminum, so the other materials should be made as sustainable as possible as well. For example, a lot of aircraft seats are made of leather, and while this is a good option in terms of wear and tear resistance, leather has a huge environmental impact[3]. Tesla has now managed to make a material just as durable as leather, but with a significantly lower environmental footprint[4]. Using this material, which has no apparent downsides, is a great way to reduce the impact of the materials used for the MoM-liner. There are a lot of components that will need to be made of plastic, due to specific shapes or weight restraints. However, recent development in recycling of plastic, has drastically improved how well it can be recycled[5]. There is even an option to use biodegradable plastic, which would make all the plastic in the aircraft not necessarily recyclable but compostable[6]. Further research will have to be done to determine if biodegradable plastic meets the stringent safety requirements set for materials used in aircraft.
As for the part suppliers, they deliver a significant part of the components of the MoM-liner. As employers of these part suppliers, the demand can be made for sustainable manufacturing practices. The employer can demand the same level of sustainability from its part suppliers as it uses itself. Companies will alter their production techniques in order to compete for these contracts.

16.2. Operations

Operations covers the entire process of going from the raw material to a finished product. There are a lot of ways to incorporate sustainability into the operations process. In section 17.3 the lean manufacturing process is described as well as ways to improve the efficiency of the manufacturing process. As described in section 17.3 the manufacturing facility consists of one main assembly plant, and a number of smaller part suppliers. This main assembly factory is huge, the Boeing assembly line in Seattle is the largest building in the world[7], so making this factory as efficient as possible would be beneficial to the operational cost of the factory. Tesla decided to build a Gigafactory, which runs completely on local renewable resources. This does not just cancel out the energy bill of the factory, it also makes the final unit price of the MoM-liner lower. A Gigafactory requires a massive investment, but is a great investment over the long run. A Gigafactory is beneficial for all three of the categories shown in Figure 16.1b. A Gigafactory is also good for societal sustainability, as this factory does not influence the environment around the factory. This means the factory does not negatively influence the surrounding area, and looking at the plans for Apple's new campus might even have a positive effect on the surrounding area[8]. The Gigafactory does not just reduce energy consumption, and reduce pollution, it should also reduce the following [85]:

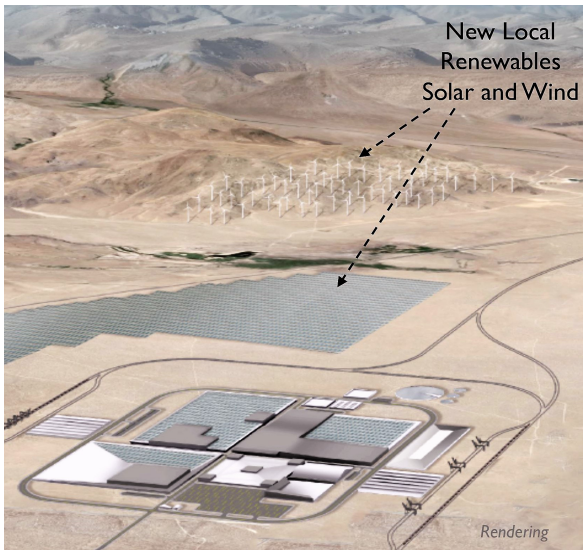

Figure 16.2: MoM-liner Gigafactory Artist Impression [86]

- Water intensity
- Energy intensity
- Greenhouse gas intensity
- Residuals intensity
- Air releases intensity
- Water releases intensity

[2] URL http://airlines.iata.org/analysis/aircraft-recycling-the-life-and-times-of-an-aircraft [cited 25 June 2018]
[3] URL https://www.greenlivingtips.com/articles/leather-and-the-environment.html [cited 20 June 2018]
[4] URL https://nyti.ms/2KtZd6I [cited 20 June 2018]
[5] URL http://www.norcalcompactors.net/processes-stages-benefits-plastic-recycling/ [cited 20 June 2018]
[6] URL http://www.pepctplastics.com/resources/connecticut-plastics-learning-center/biodegradable-plastics/ [cited 20 June 2018]
[7] URL http://www.boeing.com/company/about-bca/everett-production-facility.page [cited 20 June 2018]
[8] URL https://www.wired.com/2017/05/apple-park-new-silicon-valley-campus/ [cited 20 June 2018]

Reducing the aspects mentioned above would minimize the impact the MoM-liner production has on the environment.
The engines are the most expensive component of an aircraft, and are delivered by a part supplier. The engine selection has a huge impact on the operational cost of an aircraft, as the fuel cost is a major part of it. In the Midterm report the cost calculation showed that with the increasing cost of fuel, the fuel cost could grow to 70% of the operational cost [4]. The engine selection has a major impact on the fuel consumption, therefore choosing the most efficient engines (even if the unit cost is higher) is worth it. The engine contributes not only to economical sustainability by reducing fuel cost, but choosing the correct engine can also lower societal sustainability by being less noisy. The methods of reducing noise were described in section 10.4, and those noise reductions are going to be beneficial for people living around the airport.
Other ways to improve the sustainability of the production process would be to effectively use raw materials, and to not waist any material. This can be accomplished by planning cut-outs ahead of doing them, and making sure the least amount of material is wasted. Reducing the amount of unique parts is also a great way to reduce the cost of production, as described in section 17.3 the amount of unique stringers is kept to a minimum and the wing box is made using the same skin thickness everywhere. These are just a few examples of the measures used to minimize operational cost, which is great for economical sustainability.

16.3. Products

The products category consists of the final product and how it can be used as sustainable as possible. For the MoM-liner this means how to operate the aircraft in an efficient way, and how the end-of-life (EOL) process would work. There are actually quite some not immediately obvious reuse options that could be used to re-purpose the aircraft.
First, the operations side of the MoM-liner, it is important to note that the aircraft manufacturer has no control over how an airline uses their aircraft. But recommendations can be given on how to operate it most efficiently. The efficiency of an aircraft depends on: fuel efficiency of the aircraft, seating configuration, passenger load factor and air cargo [87][88]. The efficiency is measured in 'PAX-km/L', so amount of passenger kilometers per liter of fuel. One of the best ways to increase the PAX-km is to increase the load factor, the average load factor right now is about 80% [87][88]. Figure 16.3 shows the PAX-km/L fuel of the major airlines flying Atlantic routes, as you can see the airlines offering first class are quite low on this chart. This is due to the fact that for one first class seat, you could have multiple economy seats. As you can see, this means flying with a super dense cabin configuration would be great for the PAX-km/l (this is the Ryanair and LCC business model). It is up to the airlines to decide if they want to go for comfort, or a fully maxed out 234 seats to maximize PAX-km/L. This is a great driver for not just environmental but also economical sustainability.

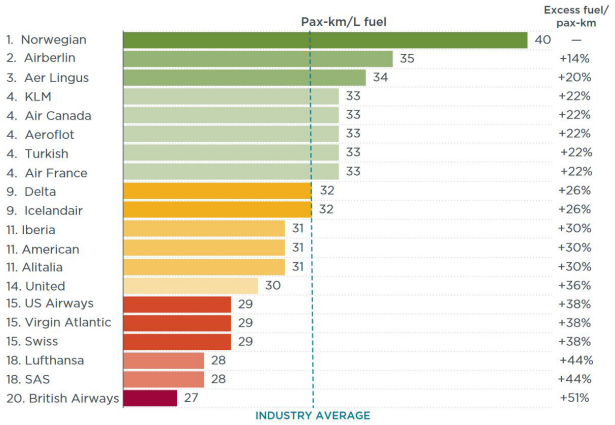

Figure 16.3: Fuel Efficiency of the Top 20 Airlines on Trans-Atlantic Routes, 2014 [87]

If time constraint is not an issue, the choice can be made to fly at a lower velocity. This reduces the drag the aircraft experiences, and thus decreases the fuel burn[9]. However, for airlines time is a major aspect and there is thus a constraint on it. Furthermore, optimizing the vertical flight profile can lead to significant savings. The aircraft should be flying at its optimum altitude during the entire flight, this optimum altitude will change and therefore step climbs will have to be performed. A great way to earn back the unit cost of the aircraft quicker is to reduce the

[9]URL `http://aviationweek.com/business-aviation/getting-most-miles-your-jet` [cited 21 June 2018]

turnaround time, thus increasing the amount of block hours per day. Reducing turnaround time cane be done by having infrastructure in place that can diagnose maintenance issues before the aircraft even arrives, thus the airport can have mechanics on standby for when the aircraft arrives, which again reduces the time the aircraft spends on the ground. This can be summarized under the motto: "Make the unpredictable predictable" [89]. Another easy way to reduce fuel burn is to get rid of excess weight, this can be done by removing unused and non-essential items [89]. Besides, using only one engine during taxiing and shutting down the engines during ground delays are great ways to reduce fuel consumption and noise pollution on the ground. This can be taken on step further by using ground tugs for aircraft movement on the ground, and using electrical ground power instead of the APU [89]. Especially the last solution would greatly reduce the noise generated by a parked aircraft.

16.4. End-of-Life (EOL)

Once the aircraft is no longer economically viable to operate, it will be retired. The MoM-liner has an estimated lifetime of about 30 years. After 30 years the aircraft will be shipped to one of the recycle facilities located around the world, and the re-use/recycle process will begin. First, the aircraft will be stripped of all recyclable materials, including the metals the structure will be made of, as well as the aforementioned bio-degradable plastic. Aluminum has very good recycle properties, it takes only 5% of the energy used to make the original part from bauxite[10] [90]. This means, as the MoM-liner is mostly made of aluminum, the aircraft will be highly recyclable. The remaining, non-recyclable, parts will be re-used in other ways. For example, aircraft chairs are often bought by aviation enthusiasts or student societies. Considering the MoM-liner will be a revolutionary aircraft, it is expected almost all of these residual parts will be sold or at least re-used. This is great on all three fronts of the sustainability aspects mentioned in Figure 16.1b. First of all, recycling and re-using takes less of a toll on the environment than producing something from scratch[11], which is good for the environmental aspect of sustainability. Then, instead of throwing away the aircraft, or parking it in a desert at the EOL, recycling means the aircraft is actually still worth money. This means at EOL the aircraft still has a resale value, which is great for economical sustainability. Then, finally, aviation enthusiasts can own a piece of MoM-liner memorabilia which is great for societal sustainability. Furthermore, the manufacturer has a much better public image if it takes the time to design an almost fully recyclable aircraft.

[10] URL https://www.economist.com/leaders/2007/06/07/the-price-of-virtue [cited 21 June 2018]

[11] URL https://www.downtoearth.org/environment/reuse-reduce-recycle/recycling-more-just-good-idea [cited 21 June 2018]

17
Post DSE Consideration

This chapter deals with the processes to happen after the conclusion of the DSE. The first section will talk about the concept of autonomous flight in section 17.1. Then the project design & development logic will be discussed in section 17.2, which outlines the phases which will be encountered post DSE. Then a global outline will be provided on the manufacturing, assembly and integration plan in section 17.3. Furthermore the reliability, availability, maintainability and safety will be discussed in section 17.4. Finally, a very global Gantt chart is provided in section 17.5, following from the phases described in section 17.2.

17.1. Autonomous Flight

Currently during a flight most operations are already conducted by the on-board computers of the aircraft. Around 50 years ago a gradual change appeared in the aviation industry removing the additional flight engineer, handling propulsion, fuel usage, electronic-, pressurization- and hydraulic-systems, leaving the nowadays commonly seen two pilots to operate the flight [1]. This change was possible due to the effectiveness of so called auto-pilots, artificially intelligent computer full filling the role of flight engineer. This has come so far that currently almost all of the flight phases are done by auto-pilot, and pilots only handle extreme situations such as heavy turbulence[2]. Asian carriers commonly even require pilots to leave the landing of the aircraft to the on board computers[3].

More than 50% of air-crashes occurring are due to errors made by humans [91], this shows the advantage in safety that can be gained with automation. Besides this the total aviation industry can save up to $ 35 billion per year as there will be no pilots to be paid and additional fuel savings can be gained by more efficient flight patterns, compared to human commandeered flights [91]. This can also lead to cheaper flights for commercial airliners. However, research has shown that only 17% of the passengers would like to fly on a fully automated flight, even if it would be cheaper than a flight flown by pilots [4].

Boeing believes that the principle of pilot-less flights will need to find its way into the aviation industry through cargo flights before being put into use in commercial passenger flights [5]. While Embraer is currently developing a single pilot aircraft and believes to have the technology implemented by 2025, in concurrency with the launch of Europe's and the US' new ATC systems SEASAR and NextGen[6]. Although more than 50% of the aviation accidents happen due to human errors, it cannot be proven that a fully automated system guarantees 100% safety. Humans also provide a flexible capability during unforeseen events and emergency situations that cannot be found in the current technologies available. A solution that might satisfy both parties pro and against automation is a single human flight overseer in the cockpit that manages difficult and non-frequently occurring situations. This pilot may also be supported by a co-pilot on the ground managing many different flights at the same time. Additionally, some argue that with this concept the crew cost would simply be moved from the sky to the ground. However, by giving these pilots multiple flights they manage their flexibility would be increased, leading to not just a reduction in labour costs but reducing accommodation and training cost as well.

[1] URL https://read.bi/2lEeO8Q [cited 18 June 2018]
[2] URL https://qz.com/1047825/your-airplane-could-fly-itself-by-2025-if-youre-cool-with-that/ [cited 18 June 2018]
[3] URL https://www.wired.com/story/boeing-autonomous-plane-autopilot/[cited: 18 June 2018]
[4] URL https://qz.com/1047825/your-airplane-could-fly-itself-by-2025-if-youre-cool-with-that/ [cited 18 June 2018]
[5] URL https://www.boeing.com/features/2018/01/cargo-air-vehicle-01-18.page [cited 18 June 2018]
[6] URL https://www.flightglobal.com/news/articles/embraer-reveals-vision-for-single-pilot-airliners-343348/ [cited 24 June 2018]

Whether this is in line with the current advancements of the aviation industry can only be shown with more advanced research and would be for a more detailed design, as cockpit lay-outs might change this is not a design choice that has a lot of impact on the usage of the aircraft. Therefore, it has been decided that the final design choice is out of the scope of this project, but for further detailed designs it is something that can bring advantages into the concept.

17.2. Project Design & Development Logic

The Project Design & Development logic represents the actions that need to be taken after the finalization of the DSE project. It is hard to pinpoint every exact task, however a global representation can be provided. Several phases have been identified, such as the final design phase, which can be broken down into: technical design and the organizational operation phase. After which the production and construction, including building of the parts and the system, the certification and the costumer delivery. Then the service period of about 25 years (as outlined in the midterm report [4]), during which the system is used and life-cycle support has to be provided. Finally the decommission and recycling of the aircraft happens during the system retirement.

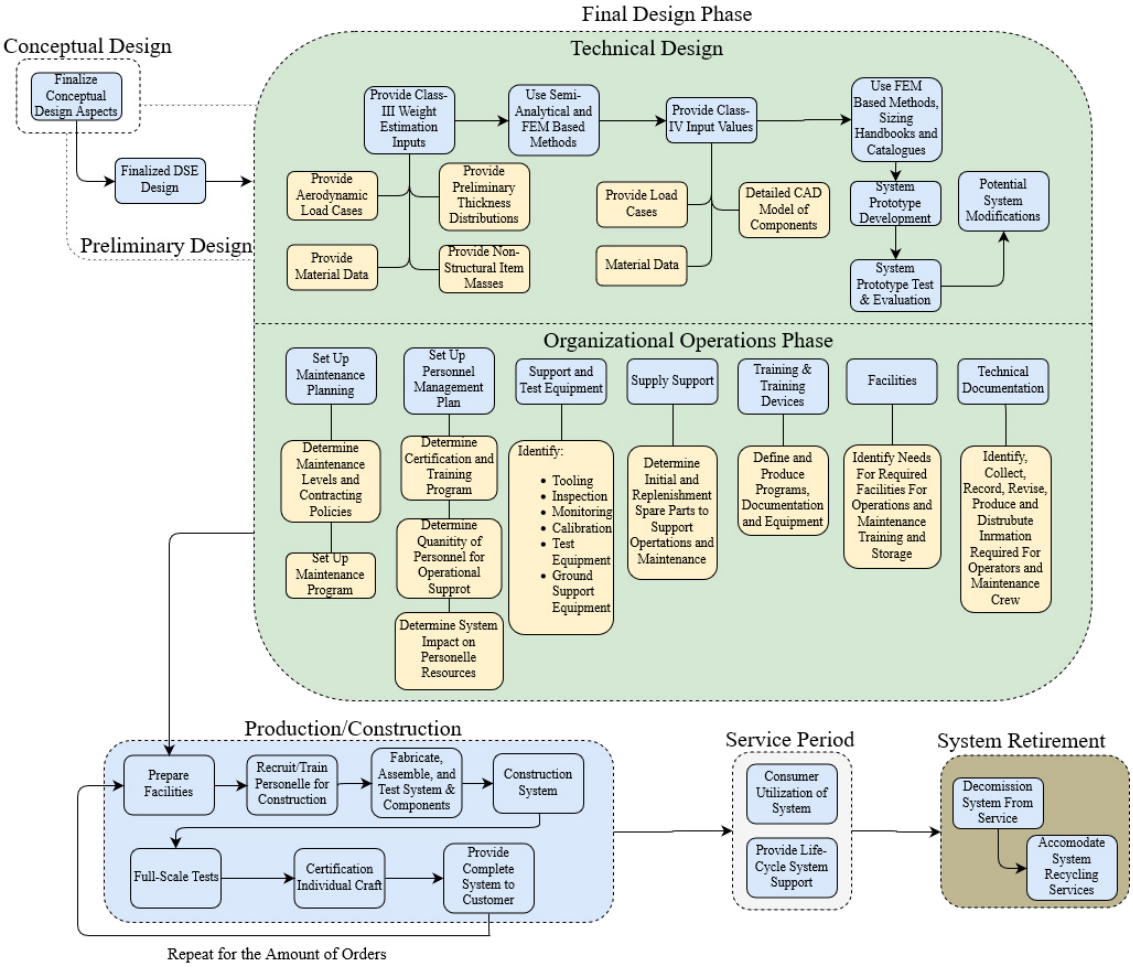

Figure 17.1: Design & Development Logic and Representation

17.3. Manufacturing, Assembly and Integration Plan

The process of manufacturing, assembly and integration, if not done correctly, can be a time consuming expensive process. In order to make manufacturing of components easy and as cheap as possible the complexity and commonality of parts should be taken into account. For the assembly process, inspiration will be taken from the Boeing and Airbus assembly lines. If there is room for improvement or automation, these options will be considered. A production plan will be proposed as well, which gives a general overview of how the aircraft will be produced.
In order to make the manufacturing process as smooth and cheap as possible, the manufacturability of a part should be envisaged in the design process. The complexity of the parts should be reduced and where possible standardized components should be used instead of custom solutions in order to reduce costs and decrease the manufacturing time for each unit.
The manufacturing process consists of non-recurring and recurring processes, both of which require a different form of planning. Non-recurring processes consists of design selection, selection and preparation of the material, process planning and facility planning. Recurring processes consist of the manufacturing of parts, component assembly and final assembly. Both of these processes consists of much more of course, and should be taken into account in the manufacturing preparation process [92]. Throughout the pre-manufacturing and manufacturing phase the five aspects mentioned in Table 17.1 should be considered, all of them are important.

Table 17.1: Five Aspects of Manufacturing [92]

Quality	Product quality according to specification
Time	Delivery reliability
Money	Within cost limits
Volume	Flexibility
Law	Obedience to law and regulations

To touch on a couple of aspects mentioned in Table 17.1, quality management is paramount. If part suppliers cannot deliver quality parts, the assembly process will not work (this is elaborated further on in subsection 17.3.3). For the MoM-liner keeping an eye on the cost of the process is very important, since the requirements requires a low cost aircraft. Money effects every decision in the production process, some compromises will have to be made and smart manufacturing techniques should be used to cut costs. For example, minimizing part transport by keeping part suppliers close to the assembly plant will cut cost [92]. The last item that will be explained further is law, the aircraft should meet the JAR and FAR regulations, but for production the local ecological laws as well as health and safety laws need to be considered. Improving the manufacturing process can be done in a couple of ways, a few of which are mentioned in the list below. These items were taken from the Systems Engineering & Technical Management course taught by the TU Delft [92].

- Aim for fitness for use, not for top quality
- Control the quality of the production process at every step
- Minimize long lead time items
- Apply target costing
- Minimize the number of parts
- Aim for commonality
- Apply the Same, Symmetrical, Unique sequence
- Allow for maximum tolerances in assembly
- Apply low cost materials
- Limit the use of material
- Install costly parts as late as possible
- Use conventional transport means, and minimize the transport distance
- Design for 'first time right'
- Test upstream

17.3.1. Lean Manufacturing

When discussing efficient and cost saving manufacturing techniques, lean manufacturing should also be discussed. Lean manufacturing is a process that minimizes waist, but not just material waist this includes every form of waist. From an employee waiting for a machine, thus wasting time, or having poor plant layout which waists resources to move parts around. The system of lean manufacturing, if applied correctly, can greatly reduce waste and will therefore lead to improvements in almost every category mentioned in Table 17.1 [92][93][94].

- Overproduction
- Waiting time
- Work in Progress
- Processing Waste
- Transportation
- Rework
- Underutilizing people

17.3.2. Manufacturing

Now using the methods described in section 17.3 and subsection 17.3.1 the planning of how components will be manufactured can begin. There are a couple of main components that take up most of the manufacturing time, for example the wing box and fuselage section are intricate and time intensive parts to produce. Using lean manufacturing methods becomes essential here, and should therefore be taken into consideration in the planning process. The engine is also a very complex component to build, but this is done by the engine manufacturer.

Fuselage

The fuselage consists of a number of stringers and skin sections, as described in chapter 8. To reduce manufacturing complexity, a couple of considerations were taken into account in the design of the fuselage. First of all using constant stiffener spacing reduces the intricacy of the fuselage design[7]. Using constant stiffener spacing and constant stiffener geometry means something else needs to be varied to be able to deal with the loading at certain critical regions of the fuselage. The choice was made to vary the skin thickness, instead of the stiffener geometry and spacing. Varying the stiffener thickness can still be very time consuming, considering stringers are usually extruded. This means a number of different dies is needed. A way to make this entire process less complex, is to assume that only 5 different stiffener sizes are allowed. This would decrease the time and cost of manufacturing, but would mean that some stiffeners are oversized and thus make the fuselage slightly heavier. This method of setting a fixed number of stringers adheres to the method described in the first section of section 17.3, as it minimizes the amount of unique parts (and thus strives towards commonality). This reduces production cost, and thus unit cost. The skin of a fuselage is made up of a number of skin panels, which cover multiple stiffeners. To withstand the shear loading on the aircraft. The method used is to vary the skin thickness between the stiffeners. Varying the skin thickness between every stiffener would be very challenging to manufacturer. However after closely studying fuselage components in the aircraft hall of the TU Delft, skin thickness variation over one panel is actually possible and is actually used. While difficult to manufacture, this is an elegant solution as it minimizes excess weight. Again, this technique adheres to the methods described in the first section of section 17.3 as it minimizes material use.

Wing Box

The wing box is is made to sustain the loading on the wings, as the MoM-liner has smaller wings the wing box will be smaller as well. This actually makes it more difficult to produce as reaching the inside of the wing box to fasten rivets and attach cabling is much more difficult.

The wing box consists of three main components: Spars, stringers and skin. To ensure ease of manufacturing some key considerations were taken into account. The same stringer geometry and thickness will be used in both wings to ensure that it is not necessary to produce multiple stringer profiles. The Wing skin thickness will also be kept constant at all locations to ensure ease of construction. This is a simplification, but is deemed acceptable for the conceptual design stage. Differences in strength will be accomplished by increasing or decreasing the number of stringers used to stiffen the panel. The spars and upper skin should be bonded in such a way that they form an airtight bond so that the fuel can be stored in the aircraft wing box directly without requiring additional tank components. The fuel storage in the wings called a wet wing, which means the inside of the wing box is in direct contact with the fuel [95]. This also means the inside of the wing box needs to be treated so that it does not corrode or deteriorate due to contact with the fuel.

The construction of the wing adheres to multiple aspects of the methods described in the first section of section 17.3. Using the same stringer size and skin thickness minimizes the amount of unique parts. This reduces the production cost of the aircraft, but does mean the wing is slightly over designed.

[7] Private communication with TU Delft teacher R.C. Alderliesen, `https://www.tudelft.nl/en/staff/r.c.alderliesten`

17.3.3. Assembly

The assembly process of an aircraft is an elaborate process, and requires a lot of facilities to complete. Boeing and Airbus have huge facilities, scattered all over the world. The way this process works is that different parts of the aircraft get built at different locations, and then get transported to a main assembly facility. A great example of this process is the Boeing 787, the Boeing 787 has part suppliers all over the world. A benefit of this system is that outsourcing reduces the cost of parts, since these part suppliers have to compete with each other for the Boeing contract. This free market, that encourages technological development, means companies have to keep improving to retain their Boeing contracts. There are some downsides, Boeing ran into some issues when parts built across the world did not fit together when they were assembled in Boeing's factory in Everett[8]. This issue was solved by increasing the quality control, and worked out in the end. This problem could have been avoided if some of the facets mentioned in the beginning of section 17.3 would have been considered. For example, upstream testing would have avoided the nasty surprise of parts not fitting in the assembly plant.

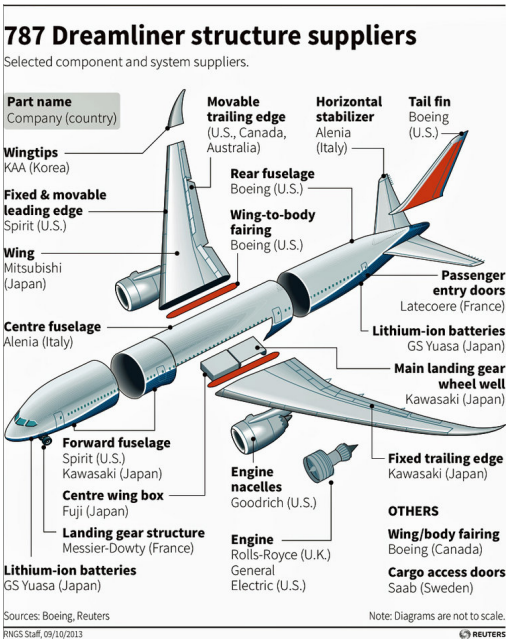

Figure 17.2: Boeing 787 Part Suppliers [96]

Developing an entire manufacturing facility, and the corresponding buildings falls outside of the scope of this project. But realizing that making smart decisions in the planning of the manufacturing process, and layout of the facilities can greatly reduce cost and increase efficiency [97]. But if this aircraft would go to the market, and require a manufacturing facility, the lean method described in subsection 17.3.1 should be incorporated into the design of the facility. Using this method would greatly reduce manufacturing cost, and would make an impact on the final unit cost of the aircraft.

17.4. Reliability, Availability, Maintainability & Safety Characteristics

Reliability, Availability, Maintainability, and Safety (RAMS) are all linked together and must be considered in order to ensure that the design functions optimally. They are critical for the effective running of the system and to ensure that the aircraft operating cost is minimized. The links between these key aspects is presented in Figure 17.3. The linked nature of these aspects means that the impact of each aspect on every other aspect must be determined. for instance positioning a part in such a way that it is easier to maintain may impact safety as it may make it easier in order to achieve better access protective shielding may have to be removed.

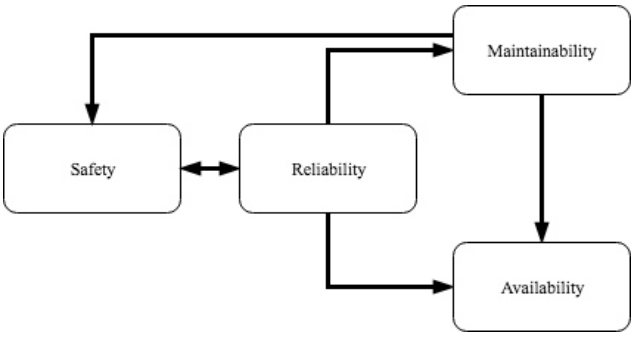

Figure 17.3: Relation Between Reliability, Maintainability, Availability and Safety

At this early conceptual it is difficult quantify reliability as the majority of the aircraft sub components have not been defined yet however the approach to RAMS has been defined and some general techniques to improve the aircraft performance in this regard are defined.

[8]URL `https://www.seattletimes.com/business/boeing-787rsquos-problems-blamed-on-outsourcing-lack-of-oversight/` [cited 19 June 2018]

17.4.1. Reliability

The reliability is a critical consideration to ensure the profitability of the aircraft. Reliability flow diagrams should be generated to help visualize which subsystem are needed in order to achieve the required functionality. These diagrams will then give a clear picture of the required subsystem reliability that is needed in order to achieve the overall system reliability. The overall system reliability is determined by safety regulations and market pressures.

From a reliability perspective the MoM-liner should not differ substantially from a conventional aircraft. Although the wing configuration is unconventional the engines and other key subsystems like control surfaces and high lift devices are similar to those used in most modern transport aircraft. The use of two sets of high lift devices flaps and control surfaces does ultimately increase the risk of a subsystem failure, as you have double the amount of subsystems. However it also reduces the impact of this by adding additional redundancy reducing the required reliability to ensure the system requirement for controllability is met.

17.4.2. Maintainability

The maintainability is is also something to consider when evaluating the operational cost of an aircraft. For the most part from am maintenance perspective the MoM-liner is similar to a conventional aircraft the positioning of the engines on the rear, upper wing has both advantages and disadvantages. The high engines allow for shorter landing gear making access to many subsystems easier however the access to the engines is reduced significantly due to their distance above the ground making engine repairs at the gate difficult without additional equipment. The majority of the systems on the MoM-liner will be updated versions of existing systems. The maintenance infrastructure is already in place for these types of system so ensuring that airlines and airports will not have to invest in new technology in order to operate the MoM-liner.

Maintenance should be taken into account at every step of the design process. In the detailed design phase ease of access should be considered, the accessibility of subsystems and the inclusion of cutouts to allow for inspection should be implemented when computing the structural elements.

The MoM-liner does not require any new specific maintenance regime however the aircraft should receive regular A,B,C and D checks in accordance with CS-25.1529 [20]. As this is an entirely new type of aircraft configuration additional checks may be required by regulators. This is something that should be considered during the certification process. It may be possible to reduce the maintenance time through the inclusion of advanced self diagnostic systems making use of neural networks allowing problems to be detected early and rectified quickly before the problem becomes more severe. Furthermore, diagnostic systems allow maintenance crews to be notified of a faulty component quicker. The use of these neural networks can improve both the accuracy of diagnosis by over 5% and reduce the probability of incorrect fault detection substantially [98]. Drones can also be used to perform visual inspections reducing the need for telescopic handlers or other equipment to inspect the aircraft to improve safety and reduce the time taken fro routine visual inspections[9].

17.4.3. Availability

Availability is intrinsically linked to both reliability and maintainability. In order to achieve high availability the reliability should be maximized and the time required to carry both scheduled and non-scheduled maintenance should be minimized. The availability is ultimately the metric that is of most interest to airlines and so should be considered during all design decisions in the detailed phase.

17.4.4. Safety

All the potential hazards associated with operating the MoM-liner should be identified and mitigated to ensure that the aircraft is safe for passengers, crew, and ground staff but also does not damage itself or other hardware. The safety of the system will be achieved primarily in two ways: redundancy and procedures. The aircraft will have redundant systems to ensure that the consequence of a failure is not catastrophic. Critical subsystems should not have any single points of failure, key subsystems will have duplicate systems. The procedures presented in the various operating manuals should ensure that damage is or injury is avoided. This information shall include but not be limited to the: operating envelope of the aircraft, the positioning of ground systems to prevent injury of damage, maintenance and inspection procedures etc. More details on the risks and how they will be mitigated is presented in chapter 15.

[9] URL `https://www.wetalkuav.com/airbus-demonstrates-aircraft-inspection-drone-farnborough/` [cited 20 June 2018]

17.5. Project Gannt Chart

This section outlines the continuation of the project, after the DSE is finished. The outline is based on the Figure 17.1 as presented in section 17.2. The planning is provided in a very global manner, from detailed design and organization, to aircraft recycling process in 2063 as shown in Figure 17.4. The color coding has been made such that it matches the one of Figure 17.1

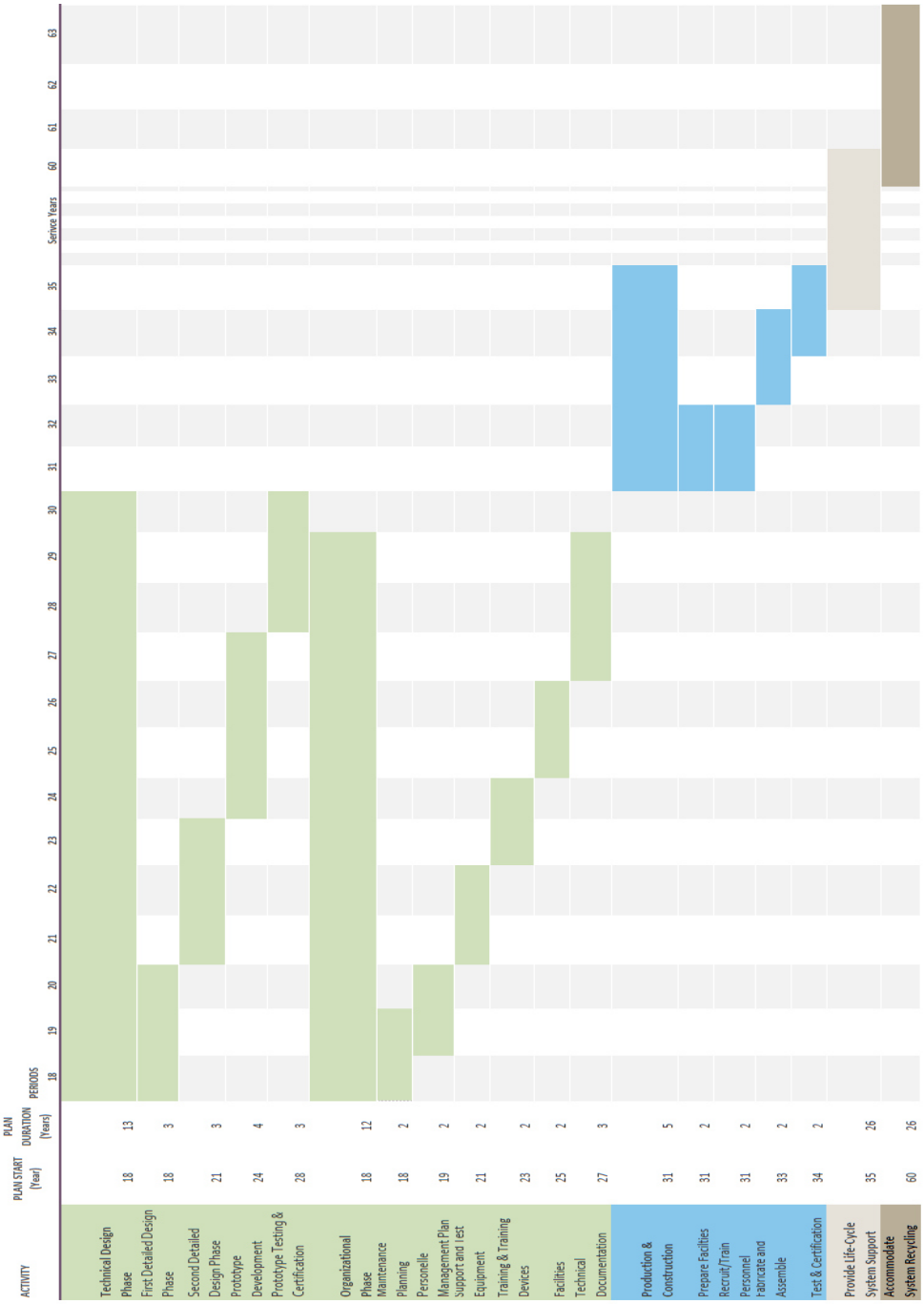

Figure 17.4: Project Gantt-Chart in Years, Starting from the DSE Finalization

18
Cost Analysis

During the preliminary design phase of an aircraft, it is highly important to take cost considerations into account. During this design phase decisions are made which might end up driving the cost to an unacceptable extent. Therefore, it is necessary to clearly break down the cost and investigate what the contribution of the different segments (e.g. direct and indirect operating cost) are. The return on investment (ROI) is seen as main financial indicator on which the aircraft design should be judged. However, in aircraft design, the ROI is a complex parameter due to the variability in aircraft operations and the large initial investments that accompany aircraft design [99]. Difficulties in accessing the ROI lie in the long term nature of aircraft design. Financial indicators that influence the ROI are usually considered over a shorter timescale than the aircraft developments. This has led to the adoption of a life-cylce cost analysis of an aircraft: taking the total costs of operating, purchasing and supporting an aircraft into account.

In this chapter the cost breakdown is given, displaying the division of indirect and direct operating cost. Furthermore an analysis of the different cost segments is presented. These are then used to compute a preliminary life-cycle cost analysis and a brief return on investment.

18.1. Cost Breakdown

From a top level cost can be broken down into two main contributions, i.e. the indirect operating cost and the direct operating cost. The indirect operating cost consist of components that are not directly connected to a particular aircraft type or flying cost of a particular flight [99]. Examples of indirect operating cost are: public relation cost expenses, facility maintenance costs, administrative costs, facility leasing costs. In a preliminary design it is difficult to consider and quantify indirect operating cost, as the designer does not have control over such costs. Namely, these costs are mainly driven my managing and operative decisions of the airliner. It is common to ignore the effect of indirect until a later stage of design [99]. For this reason, the focus of the cost analysis will lie on direct operating cost.

Direct operating cost (DOC) are expenses that are directly related with flying and maintenance of an aircraft.

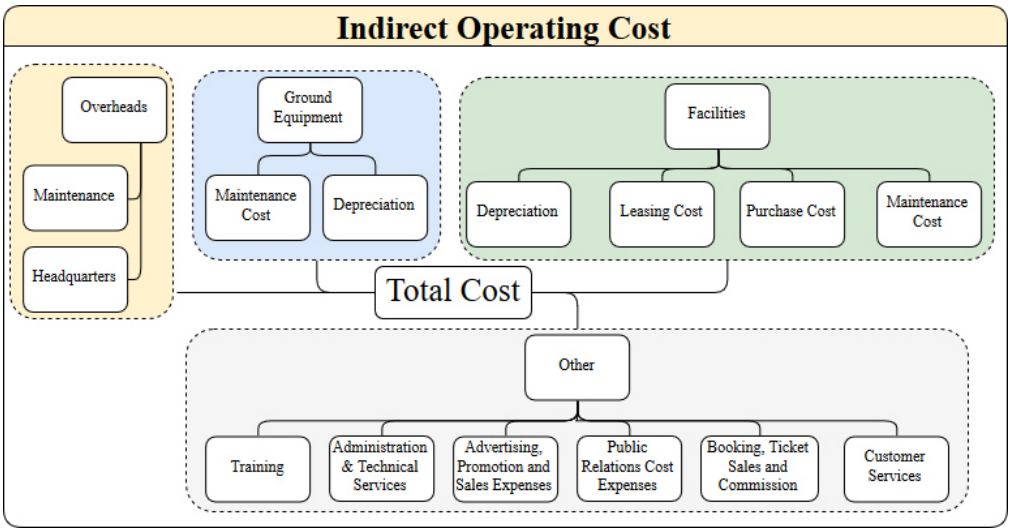

Figure 18.1: Indirect Operating Cost Representation

Figure 18.2 graphically illustrates what a typical cost breakdown would look like. Components such as maintenance and flight operating cost are large contributors to the DOC. As the lifetime of an aircraft is much larger than usual financial contracts, economical shifts must be taken into account. That is, taking inflation and depreciation into consideration when analyzing the cost of the aircraft.

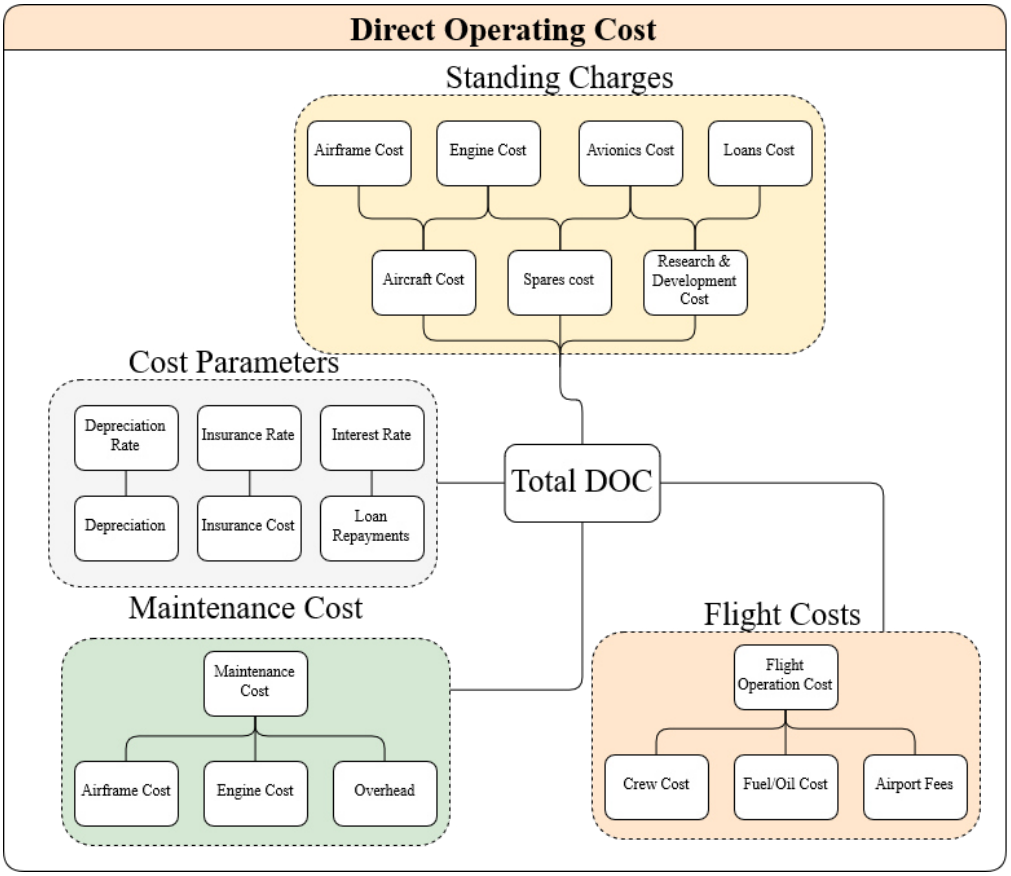

Figure 18.2: Direct Operating Cost Representation

18.2. Direct Operating Cost

18.2.1. Development & Production Cost

Learning Curve in Manufacturing

The learning curve described or rather estimates the effect of learning on the time needed to finish a certain task. Therefore, especially when estimating the unit cost price, it is important to be aware of the learning curve effect, to make sure the production costs are not overestimated. The basic learning curve equation can be described by Equation 18.1.

$$Y = KX^{-N} \tag{18.1}$$

Where 'Y' represent the cumulative average cost of 'X' units, 'K' represents the cost of the first unit, 'X' represent the number of the produced unit and 'N' the learning exponent. During startup of the production, the labor hours reduces rapidly thus the unit cost reduces rapidly with it. However, this is highly dependent on the willingness, ability or investment that is put into increasing the efficiency. The factors such as management styles, organization structure, technology, capital investment and engineering are directly related to the slope of the learning curve [100]. One can describe several sources which can cause improvements on cost such as:

- **Product Design** can be improved upon, this means that some aspects of the design might be revised, to make production easier and less expensive. Also designers can become more familiar with the production and manufacturing, this causes improved coordination and communication.

- **Direct Labor Efficiency** is related to the improvements related to the workforce. Improvement can be attained in for example equipment used, work space arrangement, working times and employee motivation as a product of becoming familiar with the design process
- **Indirect Labor Efficiency** is related to the material handling, scheduling, maintenance and support activities of such sort. These activities are often even more time consuming than the production. Over time, this can be improved by experience in the process.
- **Economies of Scale** can have a considerable effect on the production and manufacturing cost. When for example several units have to be made, large rubber presses can be used to make many parts, operated by an x amount of people. However, for the smaller scale rubber press about the same amount of people could be needed, producing less parts. However, also an opposite effect can be seen (dis-economies of scale), where large factories are often less efficient than smaller ones.
- **Plant Layout** is a simple but very pressing factor in the cost. An efficient layout can speed up the process by having a smooth workflow, providing the opportunity to produce faster and thus reduce inventory. An efficient layout can be obtained by use of cellular manufacturing, which is a method of lean manufacturing.

An overall proper learning percentage for the aerospace industry lies at 80%[1], this translates to a learning exponent 0.32. This can be used to provide an adjustment to the man hour labor performed in subsection 18.4.1.

18.2.2. Maintenance Cost

Main contributors to the direct maintenance costs are the following factors [5]:

- Labor cost
- Material cost
- Servicing and overhaul costs
- Non-revenue with not flying

Predicting the cost accumulated by maintenance is difficult, especially in the preliminary design phase. This is justified by the fact that predicting failure of systems which are not completely designed yet is complex. In later design stages accurate forecast models for the failure of certain subsystems must be derived.

For a preliminary analysis, however, relationships exist that are able to capture an indication of the maintenance cost during the lifetime of an aircraft. In order to estimate the maintenance cost component per block hour Equation 18.2 can be used [101].

$$DOC_{maint} = C_{lab/af} + C_{lab/eng} + C_{mat/af} + C_{mat/eng} + C_{amb} \tag{18.2}$$

Roskam divides the maintenance cost into five different components: the labor airframe and systems cost $C_{lab/ap}$, the labor cost of the engine maintenance $C_{lab/eng}$, the materials cost for the airframe and systems $C_{mat/ap}$, the materials cost for maintaining the engines $C_{mat/eng}$ and the applied maintenance burden C_{amb}, which is the cost derived from labor and material overheads that contribute to the maintenance. Each of these contributions can be estimated for the MoM-liner.

$$C_{lab/af} = 1.03(MHR_{maf/bl})\frac{R_{l_{af}}}{V_{bl}} \tag{18.3}$$

Equation 18.3 estimates the labor contribution for the airframe and systems. The factor of 1.03 is a non-revenue factor, which accounts for the extra maintenance costs incurred due to flight delays [101]. $MHR_{map/bl}$ is the man hours needed per block hour, $R_{l_{af}}$ the labor rate for the airframe in \$/hr and V_{bl} is the block speed. Equation 18.4 gives an estimate based on the airframe weight W_a for $MHR_{map/bl}$.

$$MHR_{maf/bl} = 3 + \frac{0.067W_a}{1{,}000} \tag{18.4}$$

$$C_{lab/eng} = 1.03 * 1.3 * N_e * MHR_{meng_{bl}}\frac{R_{leng}}{V_{bl}} \tag{18.5}$$

The labor cost can be estimated as a function of the number of engines N_e, the number of man hours per engine per block hour $MHR_{meng_{bl}}$, the labor rate per man hour in dollar per hour R_{leng} and the block speed V_{bl}.

[1] URL `http://strategosinc.com/downloads/learning-curves-dl1.pdf` [cited 26 June 2018]

The $MHR_{meng_{bl}}$ can be estimated using Equation 18.6, in which H_em is the time between engine overhaul in hours. Note that the T_{TO} is given in pounds force.

$$MHR_{meng_{bl}} = (0.718 + 0.0317\frac{T_{TO}/N_e}{1,000})\frac{1,100}{H_{em}} + 0.10 \tag{18.6}$$

$$C_{mat/af} = 1.03\frac{C_{mat/afblhr}}{V_{bl}} \tag{18.7}$$

Equation 18.7 yields the material cost related to the airframe and systems. The cost per block hour can be estimated using Equation 18.8.

$$C_{mat/afblhr} = 30 + 0.79 \cdot 10^{-5} P_{af} \tag{18.8}$$

$$C_{mat/eng} = 1.03 \cdot 1.3 N_e \frac{C_{mat/engblhr}}{V_{bl}} \tag{18.9}$$

The material cost per block hour required for Equation 18.9 can be estimated using Equation 18.10. The EP is the engine price, ESPPF is the engine spare part price factor. Roskam recommends a value of 1.5. The K_{H_em} can be estimated with Equation 18.11.

$$C_{mat/engblhr} = (5.43 \cdot 10^{-5} EP \cdot ESPPF - 0.47)\frac{1}{K_{H_em}} \tag{18.10}$$

$$K_{H_em} = 0.021\frac{H_{em}}{100} + 0.769 \tag{18.11}$$

Lastly the applied maintenance burden can be calculated with Equation 18.12. Here the variables $f_{amb/lab}$ and $f_{amb/mat}$ are overhead distribution factors that cover costs such as lighting and heating.

$$C_{amb} = 1.03(f_{amb/lab} \cdot MHR_{maf_{bl}} \cdot R_{l_{af}} + N_e \cdot MHR_{eng_{bl}} \cdot R_{l_{eng}} + f_{amb/mat} \cdot C_{mat/afblhr} + N_e \cdot C_{mat/engblhr})/V_{bl} \tag{18.12}$$

Roskam suggest taking a value between 1.0 and 1.4 for the $f_{amb/lab}$ and $f_{amb/mat}$ of between 0.4 and 0.7.
As current engine prices usually range between 12 to 35 million dollars, the values in the tables in Roskam only go up to about 3 million. The maintenance cost obtained from the engine data is thus a factor 10 too high. This can be accounted for by removing a factor of 10 from the engine cost. The results obtained now yield a reasonable result. Furthermore the cost resulting from the maintenance burden is a lot higher than what can be be observed that is actually spent by airlines. The maintenance cost usually lies between 26-29 percent of the total operational cost per block hour [22]. Equation 18.12 yields a value of 46.3 %. This also pushes the maintenance cost beyond what is expected for an aircraft in this class.

Table 18.1: Input Parameters

Parameter	**Value**	
W airframe	[lbs]	95,126.29
T_{TO}	[lbf]	45,607.5
Airframe Price	[k$]	48.23
Price per Engine	[m$]	22.5
labor Rate	[$/hr]	40 [102]

Using the data in Table 18.1 the cost per block hour of the MoM-liner is estimated. These inputs take into account the higher airframe cost due to the unconventionality of the design and therefore will also propagate into the maintenance as well, the computation of that value is described in Equation 18.3.1. This results in the following estimate for the maintenance cost, seen in Table 18.2.

Table 18.2: Computed Maintenace Cost per Block Hour

Parameter	**Value**	
Airframe cost	[$/hr]	413.16
Engine Cost	[$/hr]	417.48
Burden	[$/hr]	304.11
Total Cost	[$/hr]	1,134.75

In recent years there have been a lot of investments into self-diagnostic systems have reduced the costs of aircraft maintenance. Newer aircraft like the 787 require less inspections partially due to these new techniques [103]. For example, by combining piezoelectric sensors in the structure with models to monitor health the man hours required for maintenance can be reduced [104]. It is expected that this reduction in maintenance man hours is a function of the aircraft produced. Using several structural health monitoring techniques might even reduce the total maintenance cost up to 40% [105] The models will get more accurate the more data is fed into them. This effect is estimated using a learning percentage of 95% this effect is modeled. This yields the breakdown as observed in Table 18.3. This learning curve leads to a 32.5% decrease in the total maintenance cost.

Table 18.3: Maintenance Cost Incorporating SHM per Block Hour, Compared to Other Aircraft

		MoM-liner	**B757-200**	**B767-300ER**
Airframe Cost	[$/hr]	353.77	371.68	500.15
Engine Cost	[$/hr]	206.90	272.43	259.72
Burden	[$/hr]	205.27	260.16	311.16
Total Cost	[$/hr]	765.94	904.27	1,071.03
Improvement	[%]	-	15.3	28.5

18.3. Unit Cost & Profit Margins

For computing the return on investment in subsection 18.4.1, a further investigation has to be done into the unit cost estimation. For determining the return on investment one has to compute the cost related to the research, development, test and evaluation (RDTE), however also the actual unit manufacturing cost and profit margins. A clear outline to compute these entities was provided in Roskam Vol. 8[101] on cost estimation. The unit cost or the acquisition cost can be described by Equation 18.13. The difference between the acquisition and manufacturing cost is the profit.

$$C_{ACQ} = C_{MAN} + C_{PRO} \tag{18.13}$$

Where the C_{ACQ} is the acquisition cost, C_{MAN} the manufacturing cost and C_{PRO} the profit. The acquisition cost is highly dependent on several aspect, such as: the number of aircraft build by the manufacturer ($N_{program}$), the acquired aircraft by some airliner (big sales packages may be sold at lower profit) and the cost of the RDTE program. Given this knowledge, one can express the price per aircraft as:

$$AEP = \frac{(C_{MAN} + C_{PRO} + C_{RDTE})}{N_{program}} \tag{18.14}$$

Where C_{RDTE} is the cost related to RDTE and the AEP is the unit price per airplane. Since the actual worked out method for computing the RDTE and the manufacturing cost would be rather long, only key equations and variables will be discussed. The first step is computing the cost related to the RDTE.

18.3.1. Research, Development, Test and Evaluation Cost Calculation

For computing the RDTE related cost, the RDTE cost have been broken down into several components. Such as the airframe engineering and design cost (C_{aed_r}), development support and testing cost (C_{dst_r}), flight test airplanes cost (C_{fta_r}), flight test operating cost (C_{fto_r}), test and simulation facilities cost (C_{tsf_r}), RDTE profit (C_{pro_r}) and cost to finance the RDTE phases (C_{fin_r}).

$$C_{RDTE} = C_{aed_r} + C_{dst_r} + C_{fta_r} + C_{fto_r} + C_{tsf_r} + C_{pro_r} + C_{fin_r} \tag{18.15}$$

Airframe Engineering and Design Cost

the airframe engineering and design cost are associated with the man hour cost (MHR_{aed_r}) and the engineering man hour rate (R_{e_r}), which can also be found in Roskam and scaled towards the current date by using the CEF factor, also known as the escalation factor [101]. Such that this cost components can be computed by the following set of equations:

$$MHR_{aed_r} = 0.0396(W_{ampr})^{0.791}(V_{max})^{1.526}N_{rdte}0.183F_{diff}F_{cad} \tag{18.16}$$

$$C_{aed_r} = MHR_{aed_r}R_{e_r} \tag{18.17}$$

For the computation of the man hours work needed, quite a lot of new variables, however these are used throughout many following man hour computations. In Equation 18.16 W_{ampr} is the so called aeronautical manufacturers planning report, which can be estimated by adding the wing-, fuselage- and nacelle weight, as can be found in Figure 12.2. Furthermore, V_{max} is the maximum speed in knots equivalent airspeed, the N_{RDTE} is the number of airplanes produced for the RDTE phase, which for commercial programs lies between 2-8 units (the average of this range is used), finally the F_{diff} accounts for the difficulty of the design (which ranges from 1 for conventional to 1.5 for not usual and 2 for radically different) and the F_{cad} described computer aided effects on the design process. Since this description is Roskam is rather old in this respect, a lower than prescribed factor of 0.8 can be used, since use of CAD is quite normal.

Development Support and Testing Cost

The development support and testing cost can be determined with a relatively simple relation, described by Equation 18.18. The cost related to this components is mainly wind tunnel testing, system testing, structural testing, propulsion testing and simulation and development support testing.

$$C_{dst_r} = 0.008325(W_{ampr})^{0.873}(V_{max})^{1.890}(N_{rdte})^{0.346}CEFF_{diff} \tag{18.18}$$

All quantities have been defined before.

Flight Test Airplane Cost

This segment can be broken down into several components, such as the cost of the engine and avionics ($C_{(e+a)_r}$), manufacturing labor cost (C_{man_r}), manufacturing material cost (C_{mat_r}), tooling cost (C_{tool_r}) and the quality control of the cost (C_{qc_r}). The engine and avionics cost has been set at 22.5 MUSD as obtained from a scaling comparison with for example the Trent XWB by Rolls-Royce[2].The avionics cost can be estimated at about 10% of the listing price, a estimate of around 16 MUSD is taken. The manufacturing labor costs can be estimation by use of Equation 18.19 and Equation 18.20.

$$MHR_{man_r} = 28.984(W_{ampr})^{0.740}(V_{max})^{0.543}N_{rdte}0.524F_{diff}F_{cad} \tag{18.19}$$

$$C_{man_r} = MHR_{mar_r}R_{m_r} \tag{18.20}$$

Where R_{m_r} is the manufacturing labor rate in dollars per hour. Furthermore the manufacturing material cost can be estimated by use of Equation 18.21.

$$C_{mat_r} = 37.632F_{mat}(W_{ampr})^{0.689}(V_{max})^{0.624}(N_{rdte})^{0.792}CEF \tag{18.21}$$

Where the only new variable is the F_{mat} which is related to the type of material used. Where one can distinguish between aluminum alloys, stainless steel and composites. This value is chosen to be 1, since aluminum alloys were used in the end. Then the tooling cost can also be estimated on a basis of man hours tooling needed and the payment rate trend, following Equation 18.22 and Equation 18.23.

$$MHR_{tool_r} = 4.0127(W_{ampr})^{0.764}(V_{max})^{0.899}N_{rdte}0.178F_{diff}(N_{r_r})^{0.066} \tag{18.22}$$

$$C_{tool_r} = MHR_{tool_r}R_{t_r} \tag{18.23}$$

Where N_{r_r} units produced per year, for which a general value can be taken at 0.33.Finally the quality control costs can be easily estimated by use of Equation 18.24.

$$C_{qc_r} = 0.13C_{man_r} \tag{18.24}$$

This all adding up to the computation of the flight test aircraft cost:

$$C_{fta_r} = C_{(e+a)_r} + C_{man_r} + C_{mat_r} + C_{tool_r} + C_{qc_r} \tag{18.25}$$

[2]URL https://www.rolls-royce.com/products-and-services/civil-aerospace/airlines/trent-xwb.aspx#/ [cited 26 June 2018]

Flight Test Operating Cost

This components can be easily computed by the use of Equation 18.26. These cost generally are derived from simulation activities associated with the actual flight testing. Also a large amount of time has to be dedicated to determination of radar cross section, infrared, acoustic and optical signature.

$$C_{fto_r} = 0.001244(W_{ampr})^{1.160}(V_{max})^{1.371}(N_{rdte} - N_{st})^{1.281}CEFF_{diff} \tag{18.26}$$

Test/Simulation, RDTE Profit and Finance Cost

The test and simulation facilities, RDTE profit and financial cost for the RDTE phases can be determined by relatively simple relations. The RDTE profit are the costs related to the profit privately held enterpirses will want to make, when involved for the production process. The finance related cost have to do with the loans the manufacturer has to establish to finance the process. These respective components are described in Equation 18.27, Equation 18.28 and Equation 18.29 respectively.

$$C_{tsf_r} = 0.2C_{RDTE} \tag{18.27}$$

$$C_{pro_r} = F_{profit}C_{RDTE} \tag{18.28}$$

$$C_{fin_r} = 0.2C_{RDTE} \tag{18.29}$$

Where F_{profit} is the profit factor, which depends on the profit margin that the company wants. This can later on be interesting to look at what happens to the break even point when increasing and decreasing this.

18.3.2. Manufacturing and Acquisition Cost Estimation

To determine the actual unit price per aircraft, one has to find the values represented in Equation 18.14. Thus one has to find means to estimate the manufacturing cost, which can be broken down into: the airframe engineering and design cost (C_{aed_m}), the airplane production cost (C_{apc_m}), the production flight test operation cost (C_{fto_m}) and the cost of financing the manufacturing program (C_{fin_m}). This lead to all necessary inputs for Equation 18.30.

$$C_{MAN} = C_{aed_m} + C_{apc_m} + C_{fto_m} + C_{fin_m} \tag{18.30}$$

Airframe Engineering and Design Cost

The airframe engineering and design cost are computed in a similar fashion as done for the RDTE phase. This phase consists of: engineering needed for problems uncovered during RDTE phases, special customer integration requests, sustaining errors and release of drawings regarding maintenance and specifications. The cost can be expressed as Equation 18.31.

$$C_{aed_m} = (MHR_{aed_{program}}R_{e_m}) - C_{aed_r} \tag{18.31}$$

Where the complete engineering labor hours for the program for x units of aircraft can be determined by Equation 18.32.

$$MHR_{aed_{program}} = 0.0396(W_{ampr})^{0.791}(V_{max})^{1.526}(N_{program})^{0.183}F_{diff}F_{cad} \tag{18.32}$$

Airplane Program Production Cost

The airplane program production cost is build up out of several components, such as: the cost of the engine and avionics ($C_{(e+a)_m}$), the cost of the interior (C_{int_m}), the manufacturing labor cost (C_{man_m}), the manufacturing material cost (C_{mat_m}), the tooling cost (C_{tool_m}) and the quality control cost (C_{qc_m}). The engines and avionics did not change in comparison the the RDTE phase. The interior costs must be accounted for, since this can be a substantial cost components, this includes things as: seats, galleys, lavatories, storage bins, etc. Assuming an interior cost factor (F_{int}) of 2000$ per passenger for jet transports, one can express Equation 18.33.

$$C_{int_m} = F_{int}N_{pax}N_mCEF \tag{18.33}$$

Where N_{pax} is the amount of passengers on board. Furthermore the manufacturing labor cost can be determined by Equation 18.34 and Equation 18.35.

$$C_{man_m} = (MHR_{man_{program}}R_{m_m}) - C_{man_r} \tag{18.34}$$

$$MHR_{man_{program}} = 28.984(W_{ampr})^{0.740}(V_{max})^{0.543}(N_{program})^{0.524}F_{diff} \tag{18.35}$$

Then the material cost can be computed by using Equation 18.36 and Equation 18.37.

$$C_{mat_m} = C_{mat_{program}} - C_{mat_r} \tag{18.36}$$

$$C_{mat_{program}} = 37.632 F_{mat} (W_{ampr})^{0.689} (V_{max})^{0.624} (N_{program})^{0.792} CEF \tag{18.37}$$

Finally the tooling and the quality control cost associated with build N_m aircraft can be found by Equation 18.38, Equation 18.39 and Equation 18.40.

$$C_{tool_m} = (MHR_{tool_{program}} R_{t_m}) - C_{tool_m} \tag{18.38}$$

$$C_{tool_{program}} = 4.0127 (W_{ampr})^{0.764} (V_{max})^{0.899} (N_{program})^{0.178} (N_{r_m})^{0.066} F_{diff} \tag{18.39}$$

$$C_{qc_m} = 0.13 C_{man_m} \tag{18.40}$$

When these components are added, the airplane program production cost can be obtained.

Production Flight Test Operations Cost

This value can be easily obtained by applying Equation 18.41. This cost is related with flight testing of finalized products and delivery.

$$C_{fto_m} = N_m C_{ops/hr} t_{pft} F_{ftoh} \tag{18.41}$$

Where $C_{ops/hr}$ is the operational cost per hour, for which 9000$ was found an appropriate estimate. Furthermore t_{pft} is the number of flight hours which are being flown by the manufacturer before delivery occurs, which for jet transport is estimated at 10 hours. Finally, F_{ftoh} has to do with the overhead factor, which should be taken at 4 when a lack of knowledge is the case.

Cost to Finance The Manufacturing and Profit Rates

The finance and profit can be determined by use of a very simple statistical relations respectively:

$$C_{fin_m} = 0.2 C_{man} \tag{18.42}$$

$$C_{PRO} = F_{pro_m} C_{MAN} \tag{18.43}$$

Where F_{pro_m} is the profit rate, which can be varied and for which its effect will be assessed shortly.

18.4. Flight Operation Cost

The flight operation cost can be broken down into 3 different subgroups: crew cost, Fuel/ Oil Cost and Airport fees. Of these 3 subgroups only 2 are design dependent, and will thus be further analyzed. Although it could be argued that due to the design of the MoM-liner the accessibility to smaller airports might make it easier to negotiate lower airport fees with these airports, this is more of a cost related to the airlines specific business model and will not be analyzed in great detail.

Crew Cost

Several methods of crew cost estimation were analyzed in order to obtain the highest order accuracy figure. Zhao et al [106] compiled the equation given in Equation 18.44. When looking at the crew cost per block hour the last terms can be neglected.

$$C_{crew} = (482 + 0.590(\frac{MTOW}{1000}) + \frac{n_{seat}}{30} 78)\, t_{operatingcrew} (1 + r_{inflation})^{y - y_0} \tag{18.44}$$

Using data obtained from the airline monitor a regression is made comparing the number of passengers in max configuration and the MTOW with the average crew cost per block hour. The MTOW based approach leads to the best fit with an R^2 of 0.931; the passenger based regression leads to an R^2 of 0.878. Using these regressions a prediction is made as shown in Table 18.5. Here the MTOW based method strongly deviates from the other two methods, while both the passenger regression and Equation 18.44 yield similar results. The estimate of 1165.31 incorporates

Table 18.4: Average Crew Cost per Block Hour for Different Aircraft [22]

Aircraft	B737-200	B37-800	A320	A321	B757-200	A330-200	B777-200	B787-8
Cost [$/hr]	962.23	987.63	831.31	1,021.16	1,151.26	1,648.57	1,902.03	1,945.15
PAX [-]	130	175	156	230	239	406	440	359
MTOW [kg]	58,100	85,100	78,000	93,500	115,660	242,000	247,200	227,930

Table 18.5: Crew Cost Prediction Using Different Methods

Method	$/hr
Zhao et al.	1,165.31
Passengers	1,160.52
MTOW	1,337.78
Average	1,221.20

both the number of passeners and the weight of the aircraft, and will thus yield the most accurate result for an airacraft that has both a long range and a smaller capacity. Furthermore, according to federal regulations for flights of up more than 8 hours 3 pilots are required to legally fly the aircraft[3]. The MoM-liner has a significantly higher range than any of the other single isle aircraft in the comparison; the MoM-liner's range enables it to fly past the 8 hour threshold, meaning a third pilot would be required for those flights increasing crew cost for those flights.
By automating several systems the crew cost might be reduced. In the past automation has made positions as for example radio operator, flight engineer and navigators redundant [107]. Harris, [108] however, argues that this has led to an increase in the required technical skills and training of pilots. He points out that more complex systems are usually harder to operate and maintain. Furthermore, current automation has decreased the workload in situations where the workload was already low, like cruise, and increased the workload during high workload phases like terminal maneuvering. The only real advantage can be obtained by the removal of a pilot from the flight deck. Considering the aim to release the MoM-liner to market in 2035 and current advancements in machine learning and artificial intelligence it is interesting to have a quick look at the effect that automation will have on the crew cost.
The crew cost for a Boeing 767-300ER without on-cost is €565 per block hour on average, of which the first officer earns €127 on average [109]. Assuming that the first officer is moved to a ground station and able to oversee 5 flights simultaneously this would result in a crew cost of €463.40 per block hour, a reduction of about 18%. Translating this into the total crew cost estimate for the MoM-liner results in 955.76 $/hr. However as stated in section 12.11 the exact implementation and its effect on unit cost and operational cost is beyond the scope of this report. Such a system requires more in depth design of the cockpit and communication systems to ensure safe operations. The results stated are just for illustrative purposes, they may be used in future research in reducing the operational cost of the MoM-liner.

Fuel Cost

In the next decade, demand for fuel and oil based products is expected to increase. Using data from the U.S. Bureau of Transportation Statistics Hendricks et al. make several predictions for the fuel prices in the coming decades [110]. In their medium increase scenario they predict an increase of approximately 5% per year. This prediction assumes that new extraction methods will be implemented, but that the production of these unconventional sources will not be able to keep up with the increasing demand. Furthermore, it assumes that other energy sources will alleviate some of the demand for oil based energy sources. Assuming this trend continues up to 2035 yields a more than doubling in the cost per liter. Taking the current day price of $2.07 per gallon gives a price of $4.744 per gallon. This emphasizes the need for fuel burn reduction on next generation aircraft. The fuel consumption in Liter per km can be obtained from Equation 18.45. The specific fuel consumption is given in lb/hr/lbf, the cruise drag in Newton and the velocity in km/hr.

$$FC = SFC \cdot \frac{D_{cruise}}{V} \cdot 0.126830 \tag{18.45}$$

[3]URL `https://www.ecfr.gov/cgi-bin/text-idx?SID=3106877474ac09000d0514ac960925c7&node=14:3.0.1.1.7.18&rgn=div6` [cited 24 June 2018]

Using data performance data of several aircraft a comparison can be made in fuel consumption displayed in Table 18.6.

Table 18.6: Fuel Consumption of Different Aircraft[5]

Aircraft	**B757-200**	**A330-300**	**B767-300ER**	**MoM-liner**
Fuel Consumption [L/km]	6.60	7.02	7.44	3.88
Compared to MoM-liner [%]	41.0	44.7	47.8	-

For airlines seeking to replace their current middle of the market airliner it is particularly of interest how a new aircraft performs compared to the older one. As the cost of purchasing a new aircraft are high it is interesting to look at the saving the aircraft will be able to offer the airline. The Boeing 757 is of particular interest as a lot of airlines are currently seeking to replace this aircraft.

Table 18.7: Fuel consumption compared to other MoM-liners

Aircraft	**B757-200**	**B767-300ER**	**MoM-liner**
Number of Passengers	221	290	234
Fuel consumption [L/pax/hr]	28.37	23.23	14.10
Fuel consumption [$/pax/hr]	134.603	110.22	66.88

Using the predicted fuel price at introduction of the aircraft in 2035 of 4.744 $ per gallon the total fuel cost can be predicted per block hour. The results of which are shown in Table 18.7. The MoM-liner performs really well compared to the other aircraft. A decrease of 50.3 % in the fuel consumption per seat-km can be observed when comparing to the B757-200. This exceeds requirement MOM-SUST-02 set by the customer, requiring a 40% more fuel efficient aircraft.

18.4.1. Return on Investment

MoM-liner Project Return on Investment

By using Equation 18.14 one can compute the unit price of one aircraft, however this value is highly dependent on the set profit rate, which as discussed earlier can be highly dependent on the quantity of purchase. Therefore, the effect of a changing profit margin, ranging from 0.3 to 0, has been investigated. In this investigation the effect on the unit cost, total profit and average profit per aircraft was looked at in detail. The results have been presented in Table 18.8, there results are with applied learning curve phenomenon as prescribed in subsection 18.2.1.

Table 18.8: Unit price, total profit, profit per aircraft and break even point for different profit margins

Cost RDTE	723.6	MUSD			
Manufacturing Cost	117,871.1	MUSD			
Profit Margin 0.5			Profit Margin 0.4		
AEP	216.7	MUSD	AEP	202.3	MUSD
Total Profit	58,985.9	MUSD	Total Profit	47,188.7	MUSD
Profit per Aircraft	71.9	MUSD	Profit per Aircraft	57.5	MUSD
Break-Even-Point	547.8	Units	Break-Even-Point	587	Units
Profit Margin 0.3			Profit Margin 0.1		
AEP	187.9	MUSD	AEP	159.1	MUSD
Total Profit	35,391.5	MUSD	Total Profit	11,797.2	MUSD
Profit per Aircraft	43.16	MUSD	Profit per Aircraft	14.4	MUSD
Break-Even-Point	632	Units	Break-Even-Point	746	Units
Profit Margin 0.2			Profit Margin 0		
AEP	173.5	MUSD	AEP	144.8	MUSD
Total Profit	23,594.3	MUSD	Total Profit	0	MUSD
Profit per Aircraft	28.77	MUSD	Profit per Aircraft	0	MUSD
Break-Even-Point	684	Units	Break-Even-Point	820	Units

These results show that the eventual profit that can be obtained will be highly dependent on the profit rate selected, which will be determined per sales package per airline. Therefore these profit figures are ballpark figures.
For example when an airline orders 2 units, the decision might be made to select a profit margin of 0.3. However, when an airliner request 10 units, since the profit can be larger, a lower rate might be selected for the bulk purchase. For this a more detailed research has to be performed into potential customers and they interest in single or bulk purchases.

Total Operation Cost

The total operational cost is the sum of the cost contributions calculated in the previous chapter. There are 2 additional financial contributions that have not been estimated up to this point. The depreciation cost and the cost of financing. Roskam states that the financial costs are difficult to estimate, it is stated that the finance cost usually make up about 7% of the total operational cost; However, after examining the latest data a percentage of 4% is observed [22]. The depreciation of aircraft is a function of many different variables. It depends on the demand for the aircraft, as well as how well the technology ages. The depreciation rate of the Boeing 757-200 is 8.5%, that of the A321 is 5.5% over the past 10 years[4]. Because the MoM Liner has a more unconventional design its airframe is expected to be able to be more competitive in the future. Furthermore, the MoM liner is designed to serve markets which the A321 and 757 are currently not able to tap into. Therefore, the depreciation is expected to be at around 5%.

Because investing in new aircraft is very costly it is important to look at how the advantages weigh against the increase in cost. The 757-200 is of particular interest due to the large number of airlines seeking to replace this aircraft. To make a fair comparison it is assumed that both aircraft have a utilization of 11 block hours per day and both aircraft are used for a 30 year period. The MoM-liner will only be introduced in 2035, so the fuel prices at time of launch are used for the comparison. The MoM-liner and the B757 are compared in high density configuration, with the MoM-liner having 234 passengers and the B757-200 having a maximum of 219 [111]. Table 18.9 details the operational cost of the MoM-liner and the 757 in 2035.

Table 18.9: Operational Cost in 2035 Compared to the Boeing 757-200

		MoM-liner	**B757-200**
Fuel	[$/hr]	4,133.58	7,858.57
Maintenance	[$/hr]	765.94	904.27 [22]
Crew	[$/hr]	1,165.31	1,151.26 [22]
Finance	[$/hr]	295.90	341.04
Depreciation	[$/hr]	1,036.71	713.26
CASK	[c$/Pax/km]	3.72	5.32

The cost per available seat-km has been reduced by as much as 30.1%; exactly meeting the requirement as set by our customer. The B757 costs 92.3 MSUD in current day currency which means the MoM liner is almost twice as expensive. However due to the reduction in operational cost this increase in price will be more than compensated for. Over a 30 year period the MoM-liner is expected to save the airline about 442 MUSD, this figure already includes the higher unit price of the MoM-liner. The depreciation rate of the aircraft is slower than the operational cost savings with respect to the 757, meaning the MoM-liner will translate into effective profit immediately.

[4] `https://leehamnews.com/2014/10/29/aircraft-values-of-end-of-life-a320737-families-to-neomax/` [cited 26 June 2018]

19
Compliance Matrix

To investigate whether the requirements that are set are met a compliance matrix is made, as seen in Table 19.1. Some requirements were discarded until later design stages, mainly concerning CS-25 requirements, which at this moment in time were not specific or verifiable with the available information such as: **MOM-CERT-14**: in accordance with CS-25.143(d), for long term application for pitch control, the wheel force shall not exceed 22 N. Requirements for which compliance has not been confirmed, will be discussed in more detail, the actual values will be included in the case a requirement is met or not met.

Identifier	Requirement	Value	Compliance
Airport			
MOM-AIRP-01	The aircraft shall be able to land on tarmac runways	LCN > 50	✓
MOM-AIRP-02	The aircraft shall be able to land on concrete runways	LCN > 50	✓
MOM-AIRP-03	The aircraft shall comply with ICAO Aerodrome Reference code IV-D	Span smaller than 52 m	✓
MOM-AIRP-04	The landing gear shall be positioned such that no tip-over will occur during any phase of operation	Stability Check TRUE	✓
MOM-AIRP-05	The landing gear shall be able to carry the aircraft weight at Maximum Ramp Weight	Gears sized according to load/ YES	✓
MOM-AIRP-06	The aircraft shall be steerable on the ground for all loading conditions	Design for	✓
MOM-AIRP-07	The aircraft shall have at least one fuel interface	YES	✓
MOM-AIRP-08	The aircraft shall be able to communicate with ground staff	YES	✓
MOM-AIRP-09	The aircraft shall be able to configure with jet-bridge interfaces	YES	✓
MOM-AIRP-10	The aircraft shall be able to receive pushback	YES	✓
MOM-AIRP-11	The aircraft shall be able to load passengers	YES	✓
MOM-AIRP-12	The aircraft shall be able to load cargo	YES	✓
MOM-AIRP-13	The aircraft shall be able to communicate with Air Traffic Control	YES	✓
Certification			
MOM-CERT-01	The aircraft shall comply with CS-25 regulations	More detailed analysis needed in later phases	✓
MOM-CERT-02	The aircraft shall meet the climb gradient specified in CS-25.121	2 Engines: 0.25 rad. 1 Engine: 0.09 rad	✓
MOM-CERT-07	In accordance with CS-25.143(a), the aircraft shall be safely controllable and manoeuvrable in climb, level flight, descent and landing	Stability was checked	✓
MOM-CERT-19	In accordance with CS-25.231(a), the aircraft shall have no uncontrollable tendency to nose over in any reasonably expected operating condition or when rebound occurs during landing or take-off	Stability was checked	✓
MOM-CERT-20	In accordance with CS-25.341, the aircraft shall be able to withstand a positive load factor of 2.5	Structural analysis performed	✓
MOM-CERT-21	In accordance with CS-25.783(a), each cabin shall have at least one easily accessible external door	6 Doors	✓
MOM-CERT-28	The aircraft shall have a sufficient amount of emergency exits	6 Doors	✓
Comfort			
MOM-COMF-01	The aircraft shall have a pressure higher than 0.8 bar	0.5 bar	✗
MOM-COMF-02	The aircraft shall have a comparable humidity to the Boeing 787 and Airbus A350	No bleed air systems used, similar to 787-Dreamliner	✓
MOM-COMF-03	The seating area per passenger shall be comparable to the Boeing 787 and Airbus A350 (1030 $inch^2$)	1050 $inch^2$	✓

MOM-COMF-04	The aircraft overhead compartment shall be able to contain at least one standard size carry-on bag per passenger	45 m^3	✓
MOM-COMF-05	The aircraft shall have an in-flight entertainment system	YES	✓
MOM-COMF–07	The aircraft aisle shall be able to contain a service trolley	21 inches	✓
MOM-COMF-08	The aircraft cabin noise shall be comparable to the Boeing 787 and Airbus A350	10 EPNdB reduction	✓
Performance			
MOM-PERF-01	The aircraft shall have an operational range of at least 5,000 NM	5000 NM	✓
MOM-PERF-02	The aircraft shall have an operational long range cruise speed of 0.8 Mach	0.8 M	✓
MOM-PERF-03	Required runway length for take-off shall be less than 2,600 m at MTOW in ISA conditions	1930 m	✓
MOM-PERF-04	The maximum passenger capacity shall be greater than or equal to 230 in a single-class configuration.	234	✓
Sustainability			
MOM-SUST-01	At least 75% of the material used on the aircraft shall be reusable	> 75%	✓
MOM-SUST-02	The aircraft shall burn 40% less fuel than the B757-200 per seat-km	50%	✓
MOM-SUST-03	The aircraft shall comply with airport noise regulations	50% noise reduction w.r.t. 747-200	✓
Economic			
MOM-EC-01	The operational cost shall be 30% lower than the Boeing 757-200 per seat kilometer.	30.1%	✓
MOM-EC-02	The unit cost shall not exceed 160 MUSD, which includes amortization of development costs	159 MUSD possible at profit margin of 0.1 of the manufacturing cost	✓
MOM-EC-03	The aircraft shall enter into service before 2035	YES	✓

MOM-COMF-01

In order to meet the required pressure differential composites would need to be used for the fuselage. A material analysis showed that composites were not a viable material choice for the MoM-liner. Therefore, the required pressure differential requirement could not be met. However, the pressure doesn't define comfort in a one to one scale, therefore not meeting this requirement doesn't mean the comfort requirement is not met. The comfort can for example be compensated by allowing for better air quality, a less dense configuration allowing for more space per passenger, large overhead storage compartment and sufficient access to lavatories.

20
Conclusion

The box-wing, MoM-liner concept is a high efficiency, small, long range aircraft that is designed to fill the gap in the middle of the market. The concept was fleshed out into a preliminary design that can replace the the aging Boeing 757 and Airbus A310s and open up new markets. Sales of approximately 820 units are expected split over three major market sectors: replacement of current middle of the market aircraft, low cost long haul and new point to point services.

A trade-off resulted in a turbofan powered box-wing wing concept. Design studies were performed to evaluate the feasibility of the concept and to ensure that it is able to meet the market requirements. The aerodynamic, structural and performance parameters were optimized using a MDO approach. The optimal maximum takeoff weight after optimization was found to be 149,831 kg and it was found that The MoM-liner will have a cruise CD of 0.02 and an L/D of 23.61. These values offer a substantial improvements over current generation aircraft. The structure was optimized and it was found that the wing structure can indeed sustain the aerodynamic loads. An engine was selected to meet the requirements. Using a higher bypass ratio and a geared fan the MoM-liner is able to achieve much higher specific fuel consumption values than the legacy small long rang aircraft. The aircraft was able to meet the stability constraints and accommodate all the key subsystems needed to allow the aircraft to function (flaps, control surfaces, landing gear etc.). The aircraft is able to operate from any airfield with a runway length greater than 2600m at max payload allowing it to operate from the smaller airports that are essential to fill the point to point market identified at the outset of the project.

The box-wing, MoM-liner design meets all the requirements that were set out for it and will be able to fill the gap in the market that was defined at the beginning of the project. The concept is feasible as has been shown in this report however, more resources and time are needed to obtain an optimal solution. Currently, it was not possible to consider all aspects of the design, therefore recommendations for further research are presented in chapter 21. These recommendations are based on analysis of the sensitivity of the design to key factors that were not considered, and discussion is offered on the accuracy and limitations of some methods used.

21
Recommendations for Future Research

Throughout the process of designing the MOM-liner multiple steps were taken to simplify the complexity of the analysis. This was off course done with the main goal of this report in mind: *a preliminary analysis of the MoM-liner*. Further research on this preliminary analysis can be performed, refining some of the assumed simplifications. This chapter elaborates the recommendations of each expertise and describes what future steps can be taken to increase the accuracy of the analysis.

21.1. Structural Recommendations

Both the recommendations for the wing and fuselage structures are given below.

21.1.1. Fuselage

The structural analysis performed in chapter 8 gives a good preliminary indication of the performance of an aircraft structure. However, there is still room for improvement. This section will describe some recommendations which could be implemented to improve the structural models in the future.

The first thing that can be improved in a later, more detailed, structural analysis is the loading diagram. In the current structural fuselage analysis, the weight of the aircraft was modeled as a uniform force distribution, while this is of course not the case in reality. Also, forces in the y-direction and moments around the y-axis were not considered in the fuselage analysis, while these forces in reality do act on a fuselage structure. Also, adding a variety of different loading cases, such as gust loading and landing, would make the loading analysis of the fuselage structure more complete.

Next to an improvement in the loading diagrams of the fuselage, the way the fuselage structure is modeled can also be improved. For a preliminary analysis, the current method suffices, however, in a later stage more accurate measures must be taken. For example, The stringers could be subjected to a further analysis: different shapes of stringers are used throughout the aerospace industry so choosing a different stringer geometry might lead to a more efficient design. Furthermore, closely related to the loading is the discretizations throughout the length of the fuselage. Currently the stringers are sized throughout the complete length of the fuselage. This causes that at the ends of the fuselage (nose and tail), there are more stringers than needed to sustain compression/tension. To improve this, the fuselage length would have to be split up into multiple sections for which the analysis should then be performed separately, preferably with a different number of stringers in each section. It is recommended to split the fuselage length into three sections: a front section, middle section and rear sections. The middle section will then most likely have more stringers than the front and rear section. Doing this analysis it must be minded that stress concentrations are not generated by the start and end of stringers. This could be overcome by tapering.

Further improvement to the fuselage model can be made regarding the fuselage cut-outs. The cut-out analysis performed in this report is very preliminary and is only performed for the window cut-outs. In an actual fuselage structure, many more types of cut-outs exist, such as passenger and cargo access doors and inspection holes. Also, the analysis of a cut-out can be performed in more detail in order to obtain a more accurate weight penalty of such cut-outs.

21.1.2. Wing

Due to time constraints and limited computing power the structural calculations are more of a proof of concept than a detailed final configuration. It was not possible to optimize all the wing variables as the computations became prohibitively time consuming to run. Currently the number, position and spar thickness were not optimized by the optimization algorithm. To further improve the concept, it is therefore recommended to investigate this further in the future. Moreover, the configuration, as it is currently, assumes that the skin thickness, number of spars and number of stringers is constant throughout the whole wingbox. This means that the wing tips where the loads are much lower are substantially over designed compared to the rest of the wing. In further design iterations splitting the wing up into several sections that can be optimized independently should be considered.

The front wing has to be heavily reinforced, this is the result of its relatively small cross section and high loads it is therefore recommended that the possibility of adding a Yehudi is investigated to locally increase the thickness and chord at the root of the wing. This would reduce the need for stringers and spars and ultimately may lead to substantial weight savings. Additionally while some investigation into composites was done it was found to not yield any substantial weight savings. Currently only isotropic composites have been considered as designing with non-isotropic composites is a complex time consuming process. The major advantage of composites however is that their properties can be tailored in each direction. The potential weight reduction due to the use of composite should therefore be reevaluated.

The wing was currently optimized for the maximum maneuvering loads however the wing experiences considerably more load cases for instance landing and gust loading than just this but it was not possible simulate the wing loading using the aerodynamic software.

The wing connection strut is currently ignored and assumed to be unloaded and the connection between the strut and the wing assumed to be flexible however this may lead to serious flutter issues. Therefore, in further research the implications of the strut connections should be investigated. Currently the wings are optimized separately with only boundary conditions applied based on each other. To achieve a more optimal solutions the entire wing system should be optimized as one unit. This was unfortunately not possible with the current tools as the time required to run an iterative optimization within the overall optimization loop would make designing in the time available difficult.

The tools developed for this report are excellent for gaining a preliminary indication of the feasibility of the wing structural concept however more advanced FEM models must be used in the more detailed phase of the design. The suitability and setup of such tools must be considered in further research, this holds for the entire structural analysis, i.e. both the wing and fuselage.

21.1.3. Further Structural Recommendations

Currently the structural analysis of the MoM-liner is limited to a fuselage and wing analysis. However, there are many more structural aspects which should be considered in an aircraft design. In further research, aspects such as the landing gear design and the design of structural connections need to be addressed.

21.2. Aerodynamic Recommendations

The accuracy of these methods is limited by the accuracy of estimating the drag components. A more detailed method should be used to obtain better drag estimates for this aircraft. Furthermore, it should be considered to remove the constraint on the taper ratio of the wings such that a near-elliptical lift distribution can be obtained on both wings. Additionally, an analysis should be done on the optimal span of the wing. Reducing the span of the wing will reduce the bending moments in the wing possibly making it easier to obtain a wing configuration with an even better aerodynamic performance. A better integration and feedback between the several different modules must be made to get better optimization results. The aerodynamics module receives no information from the structural module. Things like maximum stress locations and structural weight estimation should be fed back to the aerodynamics module in order for it to optimize properly.

21.3. Performance Recommendations

There are quite some areas that would be beneficial to research more in the future. The method described in chapter 11, of sizing an engine for cruise and then using electrical boost to meet the power deficit is a very interesting prospect. More research is required to estimate the amount of power an electrical system could deliver.

The most important recommendation for future performance research would be the engine thrust, due to the fact that the design had to be frozen at a certain point to allow the design of sub-systems. As it stands now the thrust requirements used to size the engine are too high. To obtain a 2600 meter takeoff distance a 45% TO-thrust reduction is required. This means the takeoff thrust of the engine can be greatly reduced, resulting in a lighter engine. To improve the design, a new design iteration would be required. Due time constraints, as described before, a new iteration was not possible. This weight reduction is significant, these lighter smaller engines will also be significantly cheaper. Further research will be necessary to determine the cost savings these smaller engines could generate. However, it should be noted that historically the mass estimations of the aircraft are increasing as the design matures. While the engine thrust could be decreased by 45% to just meet the requirement with the current MTOM, an increase in MTOM of just 35% would necessitate this engine size. Thus, for the next iteration consideration should also be put towards reasonable contingency values for MTOM, as otherwise the risk of this situation happening again in later stages arises, yet then simply inverted.

21.4. Engine Sizing Recommendations

The main recommendation for the engine sizing would be to re-iterate the thrust requirements. At a certain moment the design had to be fixed, to have sufficient time left for the sub-system sizing. This means the current engine sizing is based on thrust requirements that are now outdated. The thrust the engine can produce is too high, and downsizing would result in a reduction in engine weight and an improvement in fuel consumption.

The RR XWB-84 is not a geared turbofan, but with the suggested bypass ratio it will probably need to be one. More research should be done into how this affects the engine performance and weight. Furthermore, the implementation of a geared turbofan should be further researched and the potential efficiency benefits need to be quantified. A bypass ratio of 15 is a big step forward from currently operational turbofans, further research is necessary to determine not just the benefits but especially the downsides of such a high bypass ratio.

One more thing, the effects of scaling need to be analyzed further. Right now the assumption is made that major scaling does not bring with it scaling effects. This is probably not the case, so further research is required to analyze these potential effects.

21.5. Sustainability Recommendations

The sustainability plan is not perfect yet, there is still a lot of room for improvement and development of current technologies. More research will have to be done to understand if bio-degradable plastic meets the strict aviation regulations for materials inside the cabin. Also, new production techniques that are not yet on the market right now could be used to make the production even less impact full. Also, research into new materials should be done. Recycling aluminum is great, but what would be even better is if an entire aircraft could be built out of recycled aluminum or at least partly.

The Gigafactory that was mentioned in chapter 16 is a huge undertaking, and relies heavily on renewable energy sources. The idea of a huge, sustainable, assembly factory that runs on renewable energy sources is relatively new so further research should be done into the long-term viability of this concept and ways to improve the idea even further.

21.6. Landing Gear Recommendations

The unconventional landing gear storage induces changes in structural and aerodynamics values when compared to used reference aircraft. Forces on the landing gear have been taken into account for the structural calculations. The main gear system is broader than the fuselage and thus additional aerodynamic structures must be placed to store the landing gear with the least amount of drag. In this report this has been taken into account for the renders, by using an arbitrary shape commonly seen with similar configurations. Calculations for aerodynamic values and the additional structural weight should be considered for further detailed design including an investigation on mass and the lift and drag characteristics of this fairing. In case the bulge produces a non-negligible lifting force, a thorough analysis on the impact for static stability and control should be conducted. As the stability margin is already small, having another lifting surface behind the aircraft c.g. could reduce the static margin even further.

Bibliography

[1] Daniel P. Raymer. Aircraft Design: A Conceptual Approach, 2004.

[2] V Badal, Q Booster, D Van Der Horst, M Korzelius, N Suard, and N Wahler. Project Plan Group 10.

[3] V Badal, T Van den Berg, J De Bont, Q Booster, G Van Dekken, D Van der Horst, M Korzelius, N Suard, and N Wahler. Baseline Report Group 10. Technical Report Version 1.5, 2018.

[4] V Badal, Q Booster, D Van Der Horst, M Korzelius, N Suard, and N Wahler. Midterm Report Group 10. (1), 2018.

[5] Lloyd R Jenkinson, Paul Simpkin, and Darren Rhodes. *Civil Jet Aircraft Design*. 2003.

[6] Flightglobal Insight. World Airliner Census 2016. *Www.Flightglobal.Com*, page 25, 2016.

[7] Ted Reed. Boeing, Airbus Can't Replace the 757. *TheStreet*, aug 2011.

[8] Dan Thissel. ANALYSIS: 787 stars in annual airliner census. *Flight International*, 2017.

[9] Boeing. Airport Compatibility Brochure 737 MAX. 2017.

[10] Airbus. Family Figures. 2017.

[11] Boeing. 787 Airplane Characteristics for Airport Planning. 2015.

[12] Guy Norris and Jens Flottau. Boeing Sees No Business Case For 757 MAX. *Aviation Week*, 2015.

[13] Boeing. Current Market Outlook 2017-2036. Technical report, 2017.

[14] Mathieu Weber Urs Binggeli. A short life in long haul for low-cost carriers. *Airline Business*, 2013.

[15] Thomas Pallini. Low-Cost Airlines Crossing the Pond: Norwegian Long Haul. *Airline Geeks*, 2018.

[16] Airbus S.A.S. Global Market Forecast: Growing Horizons 2017/2036. *Art & Caractère*, April(4):1–127, 2017.

[17] Shawn Tully. Southwest bets big on business travelers. *Fortune*, 2015.

[18] C. Ball. Rethinking hub versus point-to-point competition: A simple circular airline model. *Journal of Business & Economic Studies*, 13(1):73–87, 2007.

[19] RyanAir. Ryanair Buys Another 10 Boeing 737 MAX 200s, Bringing Firm Orders To 110 (With 100 Options Outstanding), 2017.

[20] Easa. European Aviation Safety Agency.

[21] Boeing. 757 Airport Planning Manual. 1999.

[22] ESG Aviation Services. Block hour operating cost by airplane type for the year 2016. Technical Report August, 2017.

[23] B.H. Little, H.W. Bartel, N.N. REddy, G. Swift, and C.C. Withers. PROPFAN TEST ASSESSMENT (PTA) FLIGHT TEST REPORT. Technical report, Lockheed Aeronautical Systems Company, 1989.

[24] Egbert Torenbeek. *Advanced Aircraft Design*. 2013.

[25] Jan Roskam. Airplane Design Part I: Preliminary Sizing of Airplanes. 1989.

[26] Egbert Torenbeek. *Synthesis of subsonic airplane design*. 1979.

[27] Kristian Schmidt and Roelof Vos. A Semi-Analytical Weight Estimation Method for Oval Fuselages in Conventional and Novel Aircraft. In *52nd Aerospace Sciences Meeting*, 2014.

[28] C. N. Zohlandt. Conceptual design of high subsonic Prandtl planes. page 141, 2016.

[29] R.N.J. Rousseau. Semi-Analytical Closed-Wing Weight Estimation during Conceptual Design. Technical report, TU Delft, 2017.

[30] D Howe. The prediction of aircraft wing mass. 210:135–145, 1996.

[31] P. O. Jemitola, G. Monterzino, and J. Fielding. Wing mass estimation algorithm for medium range box wing aircraft. *The Aeronautical Journal*, 117(1189):329–340, 2013.

[32] R. Vos and B.T.C. Vos, R. Melkert, J.A. Zandbergen. Aerospace Design and Systems Engineering Elements I - A/C Preliminary Sizing.

[33] John D. Anderson. Fundamentals of Aerodynamics, 2001.

[34] Drag Polar. 13 Drag Prediction 13.1. pages 1–16.

[35] Fabrizio Oliviero. Aerospace Design and Systems Engineering Elements II- Aircraft aerodynamic analysis - fundamentals, 2017.

[36] Tomas Melin. A vortex lattice MATLAB implementation for linear aerodynamic wing applications. *Master Thesis*, (Master Thesis), 2000.

[37] AircraftDesign-1_Aerodynamics.

[38] Ramón López Pereira. Validation of software for the calculation of aerodynamic coefficients w i th a focus on the software package Tornado. *Degree project*, page 55, 2010.

[39] T.G.H. Megson. *Aircraft Structures for Engineering Students*. Elsevier, fifth edition, 2012.

[40] Jonathan Lusk. *Wing and Fuselage Structural Optmization Considering Alternative Materials Systems*. PhD thesis, University of Kansas, 2008.

[41] Aldo Frediani. The Prandtl Wing. *VKI lectire series on Innivative Configurations and Advanced Concepts for Future Civil Aircraft*, pages 1–23, 2005.

[42] Ilhan Sen. Aircraft Fuselage Design Study - Parametric Modeling, Structural Analysis, Material Evaluation and Optimisation for an Aircraft Fuselage. page 180, 2010.

[43] Notes lecture 14 : Shear diffusion and large cut - outs. pages 1–26.

[44] Notes lecture 10: Crippling, Johnson - Euler parabola and buckling of a stiffened panel. pages 1–8.

[45] Prof Eberhard Gill. Verification and Validation for the Attitude and Orbit Control System. pages 1–51, 2018.

[46] Ludwig Prandtl. Induced Drag of Multiplanes. *Technische Berichte*, III(7):309–315, 1924.

[47] Aldo Frediani, Matteo Gasperini, Guido Saporito, and Andrea Rimondi. Development of a Prandtlplane aircraft configuration. *Proceedings of the 17th AIDAA Congress, Roma, Italy*, (1):2263–2276, 2003.

[48] D Schiktanz and D Scholz. Box Wing Fundamentals – an Aircraft Design Perspective. *DGLR: Deutscher Luft-und ...*, pages 601–615, 2011.

[49] Paul O Jemitola and John P Fielding. BOX WING AIRCRAFT CONCEPTUAL DESIGN.

[50] Aircraft aerodynamic analysis - Mobile surfaces on the wing.

[51] Mohamad Sadraey. Spoiler Design. (Figure 2):1–16.

[52] Mohammad Sadraey. *Aircraft Design: A Systems Engineering Approach*, volume 27. 2013.

[53] Daniel van Ginneken, Mark Voskuijl, Michel van Tooren, and Aldo Frediani. Automated Control Surface Design and Sizing for the Prandtl Plane. *51st AIAA/ASME/ASCE/AHS/ASC Structures, Structural Dynamics, and Materials Conference 18th AIAA/ASME/AHS Adaptive Structures Conference 12th*, (April):1–8, 2010.

[54] J.A. Mulder, W.H.J.J. van Staveren, J.C. van der Vaart, E. de Weerdt, C.C. de Visser, A.C. in 't Veld, and E. Mooij. *Flight Dynamics - Lecture Notes AE3202*. Delft University Press, Delft, 2013.

[55] Robert J Woodcock and David J. Moorhouse. Background Information and User Guide for MIL-F_8785C, Military Specification - Flying Qualities of Piloted Airplanes. Technical report, Air Force Systems Command, Ohio, 1982.

[56] Nihad E Daidzic. Jet engine thrust ratings. (September 2012), 2017.

[57] The Boeing Company. Boeing 777 Flight Crew Operations Manual - for Continental Airlines. 2002.

[58] Factors affecting Thrust.

[59] Sato Atsushi, Imamura Mitsuo, and Fujimura Tetsuji. Development of PW1100G-JM Turbofan Engine. *IHI Engineering Reviews*, 47(1):23–28, 2010.

[60] CFM. CFM LEAP Brochure. *CFM LEAP Brochure*, 2017.

[61] IHS MARKET. *Jane's Aero Engines*. IHS Market.

[62] Rolls Royce Trent XWB - Manufacturer Website.

[63] David Howie. High-Powered Trent XWB-97 Big Sister. *the magazine ISSUE 145*, (145):12–15, 2015.

[64] Rolls Royce. Rolls Royce Trent 7000 - Manufacturer Website.

[65] Derby De, Trent Xwb, Trent Xwb, Trent Xwb-b, and Trent Xwb. TYPE-CERTIFICATE For Trent XWB. (April):1–13, 2016.

[66] A. L. Mohd Tobi and A. E. Ismail. Development in Geared Turbofan Aeroengine. *IOP Conference Series: Materials Science and Engineering*, 131(1), 2016.

[67] B.T.C. Vos, R. Melkert, J.A. Zandbergen. 2 - Weight Estimation version 15-Feb-16.

[68] Dennis Huff. Technologies for Turbofan Noise Reduction New Technology Enables Aircraft To Meet Future Requirements. *Environmental Protection*, 2004.

[69] G.J.J. Ruijrok. *Element of Airplane Performane*. Delft University Press, Delft, 1990.

[70] Paul Olugbeji Jemitola. Conceptual Design and Optimization Methodology for Box Wing Aircraft. 2012.

[71] ICAO. *Annex 6 - Operation of Aircraft: Part I - International*. Number 9. 2010.

[72] Jan Roskam. Airplane Design Part III: Layout Design of Cockpit, Fuselage, Wing and Empennage: Cutaways and Inboard Profiles. 1989.

[73] J.A. Vos, R. Melkert. Wing and Propulsion System Design, 2018.

[74] L. Prandtl. Induced drag of multiplanes. Technical report, NACA, 1924.

[75] Emanuele Rizzo. *Optimization Methods Applied to the Preliminary Design of Innovative, Non COnventional Aircraft Configurations*. 2007.

[76] Jan Roskam. Airplane Design Part IV: Layout Design of Landing Gear and Systems. 1989.

[77] Mike Sinnett. Saving Fuel and Enhancing Operational Efficiencies. *Aero Quarterly*, pages 6–11, 2007.

[78] Jim Reed and Adam Eley. How safe is air quality on commercial planes?, jun 2015.

[79] J. D. Aplin. Primary flight computers for the Boeing 777. *Microprocessors and Microsystems*, 20(8):473–478, 1997.

[80] Karen Willcox. Aircraft Systems Cost Analysis. 2004.

[81] FAO. December 2017. *Rice Market Monitor*, 20(4):1–27, 2017.

[82] US Department of Commerce (2011). Sustainable Manufacturing Initiative website.

[83] Carbon Trust (2006). Energy Saving Fact Sheet: Energy Management.

[84] ohnson Controls Global WorkPlace Innovation (2010). Generation Y and the Workplace Annual Report 20.

[85] OECD. Start-up Guide: Seven Steps to Environmental Excellence. *OECD Sustainable Manufacturing Toolkit*, page 54, 2011.

[86] Gen Iii. Planned 2020 Gigafactory Production Exceeds 2013 Global Production ! Gigafactory Process Flow ! Raw Materials ! pages 0–5, 2015.

[87] Irene Kwan and Daniel Rutherford. Transatlantic Airline Fuel Efficiency Ranking, 2014. *Icct*, (November):43, 2015.

[88] Brandon Graver and Daniel Rutherford. Transpacific Airline Fuel Efficiency Ranking. (January):6–17, 2016.

[89] Sabre Airline Solutions. Efficient operations. page 28, 2013.

[90] Aluminum Association. Aluminum: The element of sustainability. *A North American Aluminum Industry Sustainability Report*, (September):70, 2011.

[91] Earl L. Wiener and Renwick E. Curry. Flight-deck automation: Promises and problems. *Ergonomics*, 23(10):995–1011, 1980.

[92] R.J. Hamann and M J L van Tooren. Systems Engineering {&} Technical Management Techniques. (1-2), 2006.

[93] Electric, Linear Motion, and Assembly Technologies. Lean Manufacturing : Principles , Tools and Methods Introduction : The 9 Principles of Lean Manufacturing. *Methods*, page 2, 2009.

[94] Oals Of, Wareness Of, and Mportance Of. Basic concepts of Lean Manufacturing The Goals of Lean Manufacturing. *Work*, pages 1–11.

[95] Dale Crane. *Dictionary of Aeronautical Terms, third edition*. Aviation Supplies & Academics, 1997.

[96] Sam Ro. Boeing's 787 Dreamliner Is Made Of Parts From All Over The World, 2013.

[97] Ken Stone, Vice President, and Project Executive. Aircraft Manufacturing Facility Design. pages 1–13, 1917.

[98] ZeFeng Wang, Jean-Luc Zarader, and Sylvain Argentieri. Aircraft Fault Diagnosis and Decision System based on Improved Artificial Neural Networks. *IEEE/ASME International Conference on Advanced Intelligent Mechatronics*, 2012.

[99] D. Jenkinson, L.R., Simpkin, P., Rhodes. Aircraft Cost Estimator. page 436, 2003.

[100] Quarterman Lee. Learning & Experience Curves In Manufacturing By. (October):1–15, 2014.

[101] Jan Roskam. Roskam VIII - Airplane Cost Estimation: Design, Developmet, Manufacturing and Operating, 1990.

[102] IATA Maintenance Cost Task Force. Labour Rate and Productivity Calculations For Commercial Aircraft Maintenance. *Iata*, 2013.

[103] Airline commerce. Can the 787 & A350 transform the economics of long-haul services ? *Airline commerce*, (39):23–30, 2005.

[104] Hamza Boukabache, Christophe Escriba, and Jean Yves Fourniols. Toward smart aerospace structures: Design of a piezoelectric sensor and its analog interface for flaw detection. *Sensors (Switzerland)*, 14(11):20543–20561, 2014.

[105] Alfredo Güemes. SHM Technologies and Applications in Aircraft Structures. *5th International Symposium on NDT in Aerospace*, (November):13–15, 2013.

[106] X. Zhao, W.J.C. Verhagen, and R. Curran. Aircraft bi-level life cycle cost estimation. *Advances in Transdisciplinary Engineering*, 2:110–121, 2015.

[107] S.W.A. Dekker. *On the other side of promise: what should we automate today?* Ahsgate, 2004.

[108] Don Harris. The influence of human factors on operational efficiency. *Aircraft Engineering and Aerospace Technology*, 78(1):20–25, 2006.

[109] Group Transport Studies University of WestminsterLondon. Aircraft crewing – marginal delay costs. (October), 2008.

[110] Robert C. Hendricks, David L. Daggett, Peter Anast, and Nathan Lowery. Future Fuel Scenarios and Their Potential Impact to Aviation. 2011.

[111] TYPE CERTIFICATE DATA SHEET A2NM, 2016.